A high resolution microscopy study of biological components for the incorporation in opto-electronic hybrid devices.

Benjamin Robinson. BSc

Submitted for the Degree of PhD

Department of Physics and Astronomy

May 2013

Supervisor: Dr Ashley Cadby

Declaration

I, the author, confirm that this thesis is a result of my own investigations at the University of Sheffield between September 2008 and June 2012. I confirm that this work has not previously been accepted in substance for any degree and is not being concurrently submitted in candidature for any degree.

Signed ..... (candidate)

Date .....

Abstract

Optical microscopy and scanning probe microscopy techniques have been utilised to acquire high resolution topography and fluorescence images of several biological samples. Applying these techniques to patterned samples and single molecules allow the optical properties of a sample to be investigated near to and below the diffraction limit, allowing emission properties to be correlated with those of topography. Optically active biological samples outside of their cellular environment are prone to photo-degredation and in measuring them a challenge is to ensure that optical measurements can be made before the onset of damage to the fluorophore.

In this study two forms of fluorescence microscope have been utilised with scanning probe techniques of AFM and SNOM. These techniques have been used alongside microcontact printed arrays of fluorescent proteins and photosynthetic light harvesting complexes to address the accuracy of the printing technique and it's applicablity to biological components for future bionanotechnological applications. Furthermore, the periodicity associated with the arrays has been applied to the techniques to address the relative resolutions of the microscopes as well as the samples being a drive behind implimenting biologically friendly components/techniques to the microscopes (such as liquid cells).

Larger structures from photosynthetic bacteria have also been addressed in this study in the form of chlorosomes which are model structures for light harvesting in low light conditions. Studies on the spectral properties of populations of 3 species have been conducted in this work with fluorescence microscopy and it has been shown that populations show small local variations in fluorescence. Furthermore it has been shown that the developed scanning fluorescence technique can be applied to photo senstitive samples successfully with only a small number of cases where spectral properties were affected by the measurement technique.

Using high resolution microscopy techniques this research shows the surface patterning techniques in conjunction with biological samples to have mixed success depending on the sample. It also shows spectral measurements on newly discovered chlorosomes with little photo degredation. It further shows the role that the microscopy techniques have in analysing biological systems in different configurations on substrates.

Acknowledgments

I would like to thank the support of the following people who made the process of completing this thesis more manageable even when at times, completion seemed like a unattainable task.

First and foremost I would like to thank my supervisor Dr. Ashley Cadby for giving me the opportunity to work on this project and for having the confidence in my abilities. Without his vital guidance, encouragement and support throughout my studies I am certain that I would not have been able to complete this work and for that I am truly grateful.

Throughout this work I have had the chance to work alongside many talented researchers within both Physics and Biology who have provided samples and discussion to overcome the adversities encountered when applying existing Physics experiments to Biology. I would like to thank Dr. Lin Wang in Physics for his input with optics in the optical microscope. I would also like to thank the members of the Hunter Group in MBB who made this work possible, Dr. John Olsen, Dr. Jaimey Tucker and Prof. Neil Hunter. The most thanks for the Hunter group however go to Dr. Cvetelin Vasilev for the endless supply of micropatterned biological samples and Dr. Peter Adams for the chlorosome samples and help refining the single molecule measurements to study these.

During my studies I have had the pleasure of being a part of a research group that has been both social and professional. Many of the talented researchers in this group have helped my work through discussion and technical knowledge. On top of this the regular friday night drinks, numerous BBQs and out-of-work group events have established friendships that have made my time working towards this thesis enjoyable. I extend my thanks to Jon, Darren, Andrew, Dave C, Dave M, Kieran, Charlotte, Nick, Jose, Adam. I finally thank Francesca for the friendly competition to be the first of Ashley's students to complete a Ph.D, for the many discussions about experiments or life in general and for many gifts of coffee.

For their support at times throughout my studies I would like to thank many of my friends. I would like to thank the many friends from Nottingham (Pink, Sandi, Al, Craig, Chris, Fiona, Laura G, Laura M, Ben, Rob etc.) whose support and friendship through my undergraduate degree ensured that I reached the point of starting my PhD. I would also like to thank the friends made in Sheffield; Chris, Lori and Maria definitely made moving to Sheffield and my time spent working here more enjoyable. Finally I thank James, Janine and Danny for the ability to play and write music outside of work as well as their friendship, the ability to play loud music definitely had a calming effect when frustration was high from problems in the lab.

For their endless support and encouragement I would like to thank my family. Their belief in my abilities has ensured that I have reached where I am today and I am sure that their support in me will continue to help me reach my goals.

Last but not least, I would like to thank my partner Tabby for her unrelenting support and belief in my abilities. I would like to thank her for always being there for me when things didn't seem to be going right with my studies and suffering me kindly when deadlines and stress levels were running high at times. Although she may not realise she helped me understand many concepts in my work by listening to me reel off information about a technique/theory I had been reading about on certain days so again I say thank you (and sorry as it must have been dull at times!).

Contents

List of Figures

Chapter 1

Introduction

1.1 Life, biology and light

Biological systems utilise light in a variety of different ways for applications such as, camouflage [1], mating and energy production[2]. Due to the variety of light conditions that arise in different environments, biological organisms have had to evolve in a number of ways to survive.

In this work, light interacting biological samples are used as a means to investigate how the natural world utilises light. By using spectroscopy, optical microscopy and scannning probe microscopy, structural integrity and fluorescent properties have been analysed. With regards to the potential use of these fluorescent proteins in future bio nanotechnogy applications, this work has applied microcontact printing (μCP) techniques to fluorescent proteins and light harvesting complexes from photosynthetic bacteria allowing an analysis to be made into how the biological samples are affected by the patterning technique which may be a way of preparing substrates in a configuration to promote energy transfer for the future applications. Analysis of other biological structures such as Chlorosomes that are present in some green photosynthetic bacteria and have the ability to efficiently harvest photons in very low light conditions, ideas from which could be applied to future light harvesting technologies.

In recent years, attention has shifted towards biological systems to inspire a new wave of nano electronics and to improve existing light dependent technologies, such as photovoltaics and photonics. One system that has had it's fluorescent properties studied in depth is that of the Green Fluorescent Protein (GFP) originally isolated from the jellyfish *Aequorea Victoria* [3]. Observations of the jellyfish emitting light whilst under UV illumination lead to the quest to successfully isolate the protein in order to study the protein's structure and to discover how to retain photostability and emission properties in the isolated protein. Research into the development of GFP led to a palette of different emission wavelengths whilst stability increased significantly in the early 1990s after GFP was used to highlight sensory neurons in nematode worms by *Chalfie et al.* [4]. After this demonstration, the increased interest in GFP as a biolological marker lead to the development of a range of colours by *R.Tsien* [5, 6]from cyan to blue to yellow, with red derivatives being developed much later. High stability fluorescent emission and the ability to insert GFP into the DNA of cells makes fluorescent proteins a desirable material for biological markers but also for potential use in biological nanoelectronics using proteins patterned on a surface to direct energy.

Photosynthetic organisms (plants and bacteria) are very effective at maximising energy production from the environment with quantum yields on the order of 90% [7, 8] observed in measurements and models. Photosynthetic organisms have evolved in such ways to absorb light at wavelengths that match the peak intensity in the solar spectrum, this differs in environments that are underwater and on land. In extremely low light conditions, where only a small number of photons are incident on a particular region, certain photosynthetic bacteria have evolved to form structures containing high numbers of light harvesting bacteriochlorophyll (BChl) which ensure the trapping of any incident photons.

Certain photosynthetic bacteria have developed large structures known as Chlorosomes to aid the harvesting of the small number of photons present in the environment. Chlorosome structures contain a large number of BChl, which increase the potential for the trapping of photons. These allow bacteria to thrive in conditions deep underwater for example, where only a small number of low energy photons penetrate. These structures also

ensure fast and efficient transfer of energy to the bacterial reaction centre to drive charge separation after light harvesting.

1.2 Optical microscopy and the diffraction limit

Optical microscopy has been used to investigate structures on the micron scale for centuries. As optics for use in optical microscopy have been developed, an increase in the attainable resolution has been achievable. This has allowed more to be learnt about samples using optical microscopy due to better observation of the micro world down to single molecule processes. It has been a beneficial tool for studying biological samples on the cellular level and has been used to reveal cellular interactions and processes. The optical microscope is useful on the cellular scale however, users desiring detail on increasingly small scales reach a limit imposed by the optics in the system, the diffraction limit.

Modifications have been made to the basic design of the optical microscope to combat the $\frac{\lambda}{2}$ limitation imposed by the diffraction limit. One such modification has been the development of fluorescence microscopy to look at samples that hold fluorescent properties (from naturally occurring fluorescence or from fluorescent markers). Fluorescence microscopy is a frequently used technique in biology and the life sciences allowing sub cellular information to be revealed whilst at the same time remaining a non invasive technique (e.g. unlike scanning probe microscopy techniques). Structures ranging in size from whole cells to DNA are detectable when fluorescence microscopy is combined with immunofluorescence labelling, which targets specific cells for measurement in box fixed and living samples. Slightly higher resolutions can be achieved with fluorescence microscope techniques in comparison to bright field techniques as bright objects are observed against a dark background compared to dark objects on a bright field which can lead to high signal masking some objects. The ability to stain specific regions at specific concentrations allow single fluorescent regions to be isolated for identification and measurement compared to that in the brightfield techniques.

Even though fluorescence microscopy allows individual components to be observed on

the cellular level, the resolution is ultimately restricted by the diffraction limit and the conditions imposed by the Rayleigh criterion. The Rayleigh criterion states that it is possible to increase resolution by using short wavelength excitation sources and by increasing the numerical aperture of the objective lens which thus increases the area over which the objective collects light from the sample. This however does reach a limit in experiments when the length scale of a sample reaches around $200 - 300$ nm, in line with the $\frac{\lambda}{2}$ limit.

1.3 High resolution microscopy

Due to the resolution limitations imposed on optical microscopy by the diffraction limit, other forms of microscopy are required to probe structures and obtain resolutions to below 300 nm. One such technique is that of scanning probe microscopy which can measure both surface topography and properties on the atomic scales [9]. One of the most useful and largely utilised forms of scanning probe microscope used in recent years has been the Atomic Force Microscope (AFM). Continued research into AFM has lead to the development of additional features that may be used to investigate various sample properties that otherwise wouldn't be accessible. Other than standard topography these modifications have allowed AFMs to be used to analyse electrical properties [10] and magnetic properties [11], to name a few. With modifications it is also possible to analyse force curves to reveal properties such as adhesion, energy dissipation and deformation [12] which alongside topography are used to further chracterise the surface of samples. The AFM has proved to be a useful tool for probing biological samples at the cellular level [13], the ability to conduct AFM measurements in a liquid environment [14] as well as air means that biological samples can be observed in an environment that is similar to that which is experienced in nature. The combination of AFM and fluorescence microscopy is a powerful technique for characterising specific areas of a cell's structure through the combination of site specific immunofluorescent tagging to find the area in question after which the AFM is used to probe past the diffraction limit.

It is possible to obtain optical data beyond the diffraction limit through the use of a

Scanning Near-field Optical Microscope (SNOM) [15] in conjunction with immunofluorescent labelling techniques [16] that are used in standard fluorescence microscopy making it another tool that is increasingly being used in biological research. Where SNOM differs from standard fluorescence microscopy is that it illuminates the sample from a source (a fibre optic probe) that is kept a constant but extrememly small distance from the sample surface, much less than a wavelength of the light used. Due to the small translational distances involved it is possible to detect and measure non-propagating waves, which means that the resolution is only limited by the illumination area and not by the wavelength of light used or the optics of the system [17].

1.4 Thesis Outline

The work presented in this thesis will draw on both optical and scanning probe microscopy techniques as well as spectroscopic techniques to investigate how biological systems interact with light and how they use it for energy transfer. Patterned arrays of green fluorescent proteins and samples using the photosynthetic bacterium *Rhodobacter Sphaeroides* have been investigated using optical microscopy with broadband and laser excitation sources, as well as, AFM and SNOM to address the success of fixing patterned proteins to surfaces for biologically inspired nano electronics. Patterned samples will also be used to contain energy propagation upon excitation to one dimension to create similar conditions to those that may be experienced in future bio-nano devices. Particularly in photosynthetic bacteria, the understanding of the energy transfer pathways can be understood from these experiments investigating this excitation transfer through excited state lifetime measurements combined with SNOM.

Single molecule/particle measurements have been used to study the large antenna complexes of the chlorosomes from photosynthetic bacteria. Scanning fluorescence techniques have been used to identify individual chlorosomes and measure their fluorescence properties using spectroscopy. These techniques have been used to characterise the structures from different species whilst developing the technique and ensuring that biological systems

can be measured with scanning fluorescence microscopy.

Chapter 2 focuses on the technology behind the microscopy techniques employed in this work, both scanning probe technologies and the classical optical microscope. The inception and development of the classical microscope as a vital tool in cell biology will be addressed. Modifications and techniques differing from the original design such as immunofluorescent labelling of cells and liquid immersion objectives have allowed the optical microscope to attain resolutions approaching the diffraction limit however this is still a major limitation to optical microscopy therefore the physics and concepts relating to this in optical microscopy will be addressed here. To obtain sample information at resolutions below the diffraction limit scanning probe microscopy techniques are needed and thus the development of the two types of SPM used in this work will be addressed. AFM has the ability to reach sub nanometre resolution, however it also has the flexibility to include many other ways of measuring material properties. Alongside the principles relating to the diffraction limit, light propagation will also be introduced here to explain some of the advantages of incorporating near field optics into microscopy methods. SNOM takes advantage of these near field effects to obtain sub diffraction limit optical resolutions alongside topography measurements. Similarly to the combined AFM and fluorescence systems, SNOM allows measurements to be made of both topography and fluorescence simultaneously allowing regions of fluorescence to be correlated with regions of greater topography (a major difference of SNOM being the attainable sub-diffraction limit resolution). The use of coated optical fiber based probes allow the evanescent waves to be enhanced so that they can be detected, it will be shown how this allows SNOM to detect non-propagating light confined to the sample surface as well as how the sub-wavelength apertures can be used to achieve high optical resolutions.

Chapter 3 outlines the relevant aspects of biology that are required for understanding the work in this thesis, as well as the photophysics relating to these areas (such as fluorescence). The samples used in this thesis; photosynthetic bacteria and fluorescent proteins will be addressed in detail, discussing the history behind them as well as the development of the original material into forms that are more useful for optical applications, such as the

development of GFP to incorporate more spectral wavelengths and to be more stable for immunofluorescent tagging. Alongside this, the applicable photophysics (fluorescence) will be addressed in detail looking at the concepts relating to these processes, such as those that will explain why these samples can be so fragile under measurement. In describing how the photosynthetic bacterial systems work, principles relating to the transfer of energy (such as Fluorescent Resonance Energy Transfer, FRET) will be addressed as this concept is important in these samples and one that may show how they can be used in future technological applications. Techniques that are relevant for the preparation of biological samples for high resolution imaging in this work will also be introduced and discussed. This will focus on the standard preparation of fluorescent proteins and photosynthetic bacteria in relation to growth and purification as well as the methods employed for patterning these proteins and bacteria onto a multitude of substrates, be this through particular types of surface chemistry technique or through contact printing techniques.

Even though the general aspects of sample preparation for the cultivation and purification of bacteria and proteins will be addressed in Chapter 3 the specific sample preparation techniques used in this work will be explained in Chapter 4. These methods will outline the specific purification techniques and the solutions used in order to preserve samples for surface fixation and measurements (similar solutions will also have a hand in preserving biological samples when microscopy measurements are undertaken). Sample preparations for photosynthetic bacteria and fluorescent proteins are similar along with the patterning process. Chlorosome purification is similar to photosynthetic bacteria purification with a different process of substrate preparation and sample deposition.

Chapter 5 investigates patterning of fluorescent proteins on a substrate using the different microscopy techniques that are at hand. These techniques are used to address the success of μCP techniques by measuring the reproducibility of patterned deposition and to measure the efficiency of the technique at achieving even deposition across the stamp region. Comparitive studies relating to the relative resolutions of the microscopy techniques can be made on the linear arrays of GFP in these patterned samples to ensure that the attainable resolutions can work with samples in the latter chapters and are optimised for

fluorescence work. Studies of the fluorescence made with the scanning probe microscope and that of the static fluorescence microscope can confirm whether the optical properties of a sample have been damaged in the patterning process, this can be through the comparisons of the spectra against that from the literature or solution prior to patterning. Confirmation of no shifts in the fluorescence spectrum shows that the chromophore hasn't de-natured, this can further be confirmed by changing the wavelengths where emission is detected with the scanning fluorescence microscope.

Chapter 6 builds on the measurements made on the patterned fluorescent proteins after it was shown that they are not damaged by the printing process. In this chapter the same sample preparation techniques are used to pattern linear arrays of light harvesting complexes from photosynthetic bacteria. By using the microscopy techniques the success of the patterning process with these samples can be addressed and degredation can be measured, which may arise from a shift in the emission wavelength or by reductions in the intensity of emission. Furthermore, by using pulsed laser excitation with the SNOM it is possible to measure energy transfer along the arrays of light harvesting complexes. The defined regions that contain complexes can also be used to obtain high resolution information regarding the concentration of biological material and the dimensions of the material that relate to different fluorescent properties.

Chapter 7 relates to the chlorosome structures which aid light harvesting in some photosynthetic bacteria in low low light conditions through the presence of a large number of light harvesting BChl. Chlorosomes from 3 species will be analysed systematically to address how spectral properties vary between species. The single particle spectroscopy technique with the scanning fluorescence microscope will also be introduced and developed here to allow systematic measurement and analysis of individual chlorosomes in a region. Each chlorosome will be analysed for it's emission spectrum which can give an idea of the variation in the local environment of the chlorosome samples in comparison to the different species. It also allows any de-naturing of chlorosomes across sample regions to be addressed.

Chapter 8 brings the thesis to a conclusion, and discusses the findings of chapters $5, 6, 7$

and how they relate to previous understandings of this area of research. The success of this work and how it relates to future work and continuation of the experiments discussed will also be noted.

1.5 Bibliography

[1] Messenger. J. Reflecting elements in cephalopod skin and their importance for camouflage. *Journal of Zoology*, 174(3):387 – 395, 1974.

[2] R Blankenship. *Anoxygenic Photosythetic Bacteria*. Kluwer, 1995.

[3] O. Shimomura. The discovery of aequorin and green fluorescent protein. *Journal of Microscopy*, 217(1):3–15, 2005.

[4] M. Chalfie, Y. Tu, G. Euskirchen, W.W. Ward, D.C. Prasher, et al. Green fluorescent protein as a marker for gene expression. *Science*, 263(5148):802–805, 1994.

[5] R. Heim, R. Tsien. Engineering green fluorescent protein for improved brightness, longer wavelengths and fluorescence resonance energy transfer. *Current Biology*, 6:178–182, 1996.

[6] G. Davidson M. Shaner, N. Patterson. Advances in fluorescent protein technology. *Journal of Cell Science*, 120(24):4247–4259, 2007.

[7] J. Timney J. Qian P. Vassilev C. Hunter C.N Olsen, J. Tucker. The organisation of LH2 complexes in membranes from *Rhodobacter Sphaeroides*. *The Journal of Biological Chemistry*, 283(45):30772–30779, 2008.

[8] J. Olsen J. Hunter C.N. Niederman R Sturgis, J. Tucker. Atomic force microscopy studies of Native Photosynthetic Membranes. *Biochemtistry*, 48(17):3679–3697, 2009.

[9] E. Bottomley L. King W. Oroudjev E. Hansma H Poggi, M. Gadsby. Scanning probe microscopy. *Anal. Chem*, 76:3429–3444, 2004.

[10] Oliver. R. Advances in AFM for the electrical characterization of semiconductors. *Reports on progress in physics*, 71:1–37, 2008.

[11] Zhukov. A Hendrych. A, Kubinek. R. The magnetic force microscopy and it's capability for nanomagnetic studies - The short compndium. *Modern Research and Educational Topics in Microscopy*, 2:805–811, 2007.

[12] Attard. P. Friction, Adhesion and Deformation: Dynamic measurements with the Atomic Force Microscope. *Journal of Adhesion Science and Technology*, 16:753–791, 2002.

[13] Scheuring. S Casuso. I, Rico. F. Biological AFM: where we come from - where we are - where we may go. *Journal of molecular recognition*, 24:406–413, 2011.

[14] K. de Grooth B. van Hulst N. Greve J Putman, C. van de Werf. Tapping mode atomic force microscopy in liquid. *Applied Physics Letters*, 64:2454–2456, 1994.

[15] D Heinzelmann, H. Pohl. Scanning near-field optical microscopy. *Applied Physics A*, 59:89–101, 1994.

[16] P. Nativel L. Gall-Borrut P. Costa L. Salehzada T. Bisba C Mathieu-Williame, L. Falgayrettes. Near-field microscopy and fluorescence spectroscopy: application to chromosomes labelled with different fluorophores. *Journal of Microscopy*, 238(1):36–43, 2010.

[17] M. Harootunian A. Muray A Lewis, A. Isaacson. Development of a 500 angstrom spatial resolution light microscope: I. Light is efficiently transmitted through lambda/16 diameter apertures. *Ultramicroscopy*, 13(3):227–231, 1984.

Chapter 2

Microscopy Techniques

Microscopy has been a vital tool for studying materials in science on length scales that are not naturally accessible with the naked eye. Optical microscopy has been at the forefront of scientific research in a variety of disciplines, being used in applications ranging from the imaging of living cells in their natural environment [1] to synthetic ceramic superconductors [2]. The design of modern optical microscopes and their operation have remained roughly the same for over half a century with the only major modifications arising from improvements in optics to eradicate aberrations and to improve light collection. The past decades however have seen several different techniques associated with optical microscopy arise in the quest to overcome, or get close to the resolution limit imposed by the nature of light, the diffraction limit. One such technique combined with immunofluorescent labelling of samples has been fluorescence microscopy which, alongside obtaining excitation/emission information, has been accompanied by vast improvements to resolution in optical microscopy through developments made to the optics used and in most cases, the excitation of one wavelength removes any interference from the other wavelengths in broadband sources. However, due to the nature of light the diffraction limit means the highest resolution attainable with optical microscopes is $200-300$ nm, around half the wavelength of visible light [3] which restricts the usefullness of conventional light microscopy for investigation on bacterial and polymeric systems which generally have length scales below 200

nm.

In 1982 the development of the Scanning Tunneling Microscope (STM) [4] meant that for the first time, measurements of the surface of materials could be conducted at a resolution far surpassing the diffraction limit of light. STM uses the quantum mechanical tunneling effect by applying a small voltage bias to overlapping tip-surface wavefunctions to record height variations of the probe when raster scanned across a surface [5]. The requirement of an electrically conducting sample limits the materials STM could measure, however, the principle of a controlled interaction being used to generate a surface image was not limited to electrical feedback and could be applied to atomic forces leading to the Atomic Force Microscope's inception in the late 1980s [6]. In the case of the AFM, a sharp probe on a cantilever is scanned across a surface with a correction voltage applied to move the tip in the z-axis in order to maintain a constant force, the voltage can be used to measure the contours of a sample [7]. The nature of AFM allows both repulsive and attractive aspects of the atomic force to be measured as well as a number of other sample properties such as magnetic fields [8], friction gradients [9] and current flow [10] (when specific equipment modifications are made).

The AFM allowed sub-diffraction imaging with an ability to measure a multitude of other material properties, however it gave no optical information which had been possible with the process of immunofluorescent labelling with fluorescence microscopy. The Scanning Near-field Optical Microscope (SNOM) was developed to produce both topographic information relating to the surface of a sample and sub-diffraction limit imaging (with visible light, microwaves or fluorescent signal). Building on a concept first theorised by the Irish scientist *E. Synge* [11] on the detection of sub-diffraction limit evanescent waves, through the use of a subwavelength imaging aperture. The SNOM was built with the intention to detect these non-propagating wave components before diffraction effects became an issue (discussed in 2.2.3.3). The ability to control tip-sample distances had already been displayed with the SPM techniques it was therefore possible to build a device which could maintain a distance smaller than the wavelength of light and excite the sample, in turn the fluorescence could be recorded at the same time as the contour and on the same

length scale. In this case the optical resolution is not limited by the wavelength of light but the diameter tip's aperture, this has lead to it being an important tool in the life sciences [12][13].

2.1 Optical microscopy

The compound microscope is believed to have first been created around the beginning of the seventeenth century with the instrument by *Van Leeuwenhoek* designed to count threads in cloth. With the quality of magnification achieved the early microscope was applied to biological applications to understand bacteria and yeast for example. *Hooke* [14] took the original concepts for the microscope shown by *Van Leeuwenhoek* with the intention to improve on the design through the optics and mechanical operation [15]. The instrument he built however was mostly used for demonstration purposes due to the nature at the time to use single lenses to achieve resolutions down to a micron [16]. Optical aberrations hampered images on early compound microscopes therefore it wasn't until the mid-nineteenth century, once these were partially corrected that focus shifted back to compound microscopes as a method for studying samples [2] (mostly in the cell biology world). As developments to improve aberration effects, the resolving power of lenses and methods of illumination occurred over the following century the use of the microscope in the sciences greatly increased and developed into an important instrument.

2.1.1 Resolution

2.1.1.1 Optical resolution

Optical microscopes are ultimately limited by their resolution, the smallest distance at which two parallel lines can be resolved. In 1873 *Ernst Abbé* realised this as not just a technical limit in the manufacture of optics/microscopes but it has a physical limit, the diffraction limit. According to *Abbé*, the limiting spot size resolution that can be achieved by a microscope is given below.

$$r \geq \frac{\lambda}{2NA} \tag{2.1.1}$$

Where λ is the illumination wavelength of light, NA is the numerical aperture of the objective where $NA = n \sin \alpha$: n is the refractive index of the material and α is half the angle of acceptance of the lens, the maximum critical angle defined by the the lens and focused light.

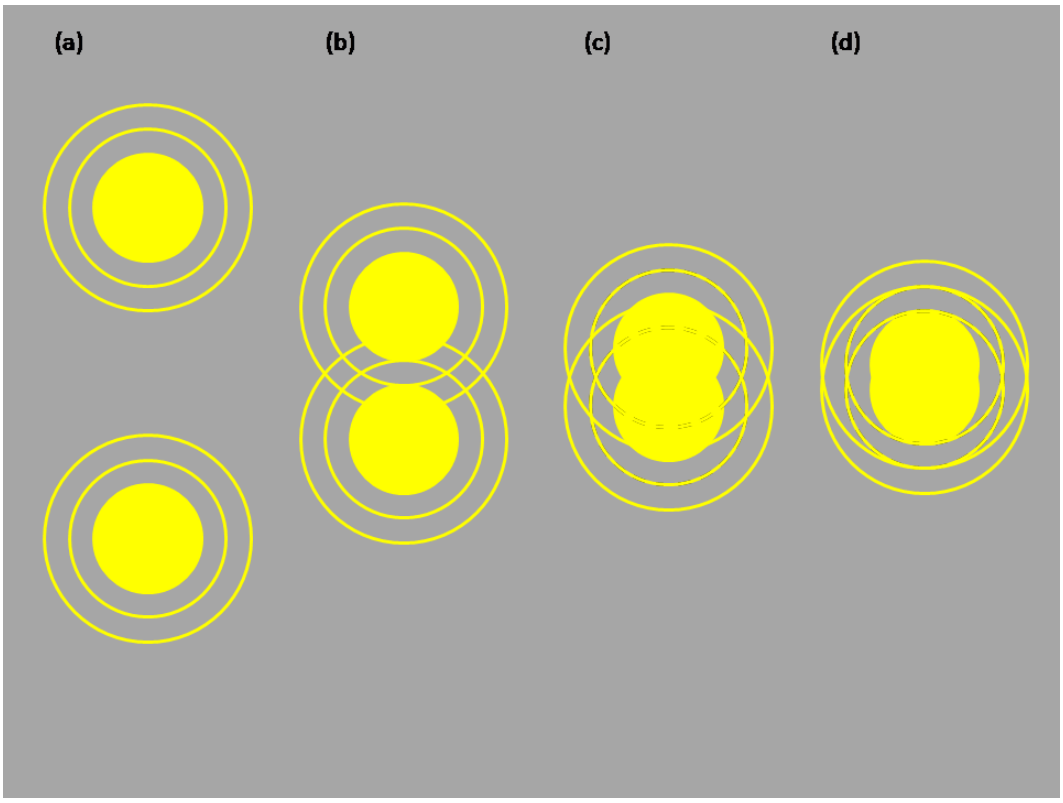

Figure 2.1.1: Examples of Airy disks of 2 point sources in the vicinity of one another where (a) the sources are separated by a large distance (b) a smaller separation distance but resolvable (c) the Rayleigh criterion where they are just resolvable (d) where they are unresolvable.

The limit to resolution was redefined and built on by *Lord Rayleigh*, initially in relation to astronomical sources of light [3]. The astronomer royal, *George Biddell Airy* had derived

the Airy disk for high irradience points of light (astronomical sources) [17]. Airy disks formed from the diffraction limited points of light show the best focused spots under conditions imposed by the optics and the nature of light. The disks display a central maximum of high irradiance surrounded by the subsequent dark and bright rings of the diffaction pattern of a point (shown in Fig. 2.1.1) whose positions are dependent on the wavelength of light and the numerical aperture or aperture size of the lens. The relation between the Airy disks and the resolving ability of the aperture can be shown with two sources in the vicinity of one another, shown by image (a) in Fig. 2.1.1. Each of these sources have an Airy disk associated with itself which spread over an angular distance of $\Delta\theta$ which is dependent on the equation:

$$\Delta\varphi_{min} = \triangle\theta = \frac{1.22\lambda}{D} \tag{2.1.2}$$

where λ is the wavelength of light from the source and D the diameter of the aperture (this also relates to the diameter of the acceptance cone of an objective which is equivalent to twice the numerical aperture).

Where two point sources are a distance apart ($\Delta\varphi$), where $\Delta\varphi \gg \Delta\theta$, the sources are easily resolvable. As the separation distance of the two points are reduced the Airy disks begin to overlap, 2.1.1 image (b), with the Rayleigh criterion conditions apply where these points are just resolvable when the centre of one Airy disk falls on the first minimum of the Airy pattern of the other point source image (c) Fig. 2.1.1 the minimum separation distance of which is depicted in 2.1.2 with $\Delta\varphi_{min}$ being equal to $\Delta\theta$.

At the point where the 2 sources progress beyond the conditions that are explained by the Rayleigh criterion (image (d) Fig. 2.1.1) they can no longer be resolved as separate entities and thus appear to be one larger point source. Fig. 2.1.2 represents the conditions between the Airy disks of the two point sources shown in 2.1.1, as cross-sections where the peaks represent regions of higher intensity. The plot shown in image (a) in Fig. 2.1.2 represents the point where the two disks begin to overlap (image (b) 2.1.1) which shows that

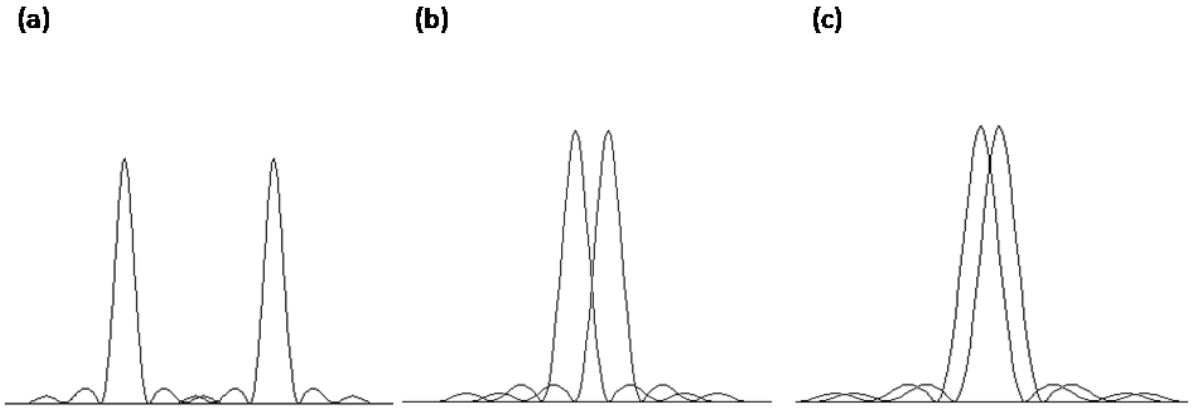

Figure 2.1.2: Cross-sectional representation of the airy disks of two point sources as they approach, (a) represents the point of overlap of the sources, (b) represents the point where the Rayleigh Criterion is observed and (c) represents where the two points are no longer resolvable.

the separation between the peaks is significant enough to resolve the 2 sources. The plot in image (b) in Fig. 2.1.2 on the other hand shows the separation distance that applies to the Rayleigh criterion (Fig. 2.1.1 image (c)) where the central points of maximum intensity correspond with the first minima of the rings surrounding and thus are resolvable which is also seen as the central maxima do not overlap significantly. The plot in image (c) Fig. 2.1.2 shows the point where the sources are too close together to be resolved (image (d) Fig. 2.1.1) and only one source is observed. From the cross-section it can be seen that a large portion of the central maxima overlap explaining the inability to distinguish between the two points of light.

In the cases of maximum resolution applying to both point sources and lines it can be seen that the resolution can be improved by using a shorter wavelength of light for observations or by using an objective with a higher NA. It is worth noting with NA being related to the refractive index of a material, resolution can be improved by increasing the refractive index of a lensing material, this principle is applied in both solid immersion lenses and oil immersion lenses. These factors improve the resolution of an objective small amounts, however the maximum resolution in practice is still limited to the *Abbé* limit of resolution, around 0.2 μm.

2.1.1.2 Detector resolution

With modern optical microscopy (e.g. fluorescence microscopy) CCD cameras tend to be used to see low level fluorescence and to obtain images of the samples being investigated. Equations 2.1.1-2.1.2 divuldge information on what the optics of the system can resolve, the detector however is subject to different criterion. The *Nyquist* criterion defines the resolution of a detector in relation to the sampling frequency of the digitiser, it requires a sampling interval that is equal to twice the highest specimin spatial frequency to preserve the spatial resolution in the resulting digital image.

In 2.1.3 Fig.1(a) the sampling of the digitiser happens at a frequency similar to the maximum resolution of the optics in the system. At this frequency 2 point sources are located in adjacent pixels, the resulting image in this case is shown and it can be seen that on the detector the point sources cannot be resolved separately. However, as shown in image (b), by sampling at double the rate on the digitiser, both point sources can be resolved as there is a pixel of zero value between the point source containing pixels.

The pixel resolution of a detector differs from that of the Rayleigh criterion with its dependence not being on the wavelength of light used or the numerical aperture of the objective.

$$Resolution = \left(\frac{Pixel\,Size}{Magnification}\right) \times 2.3 \tag{2.1.3}$$

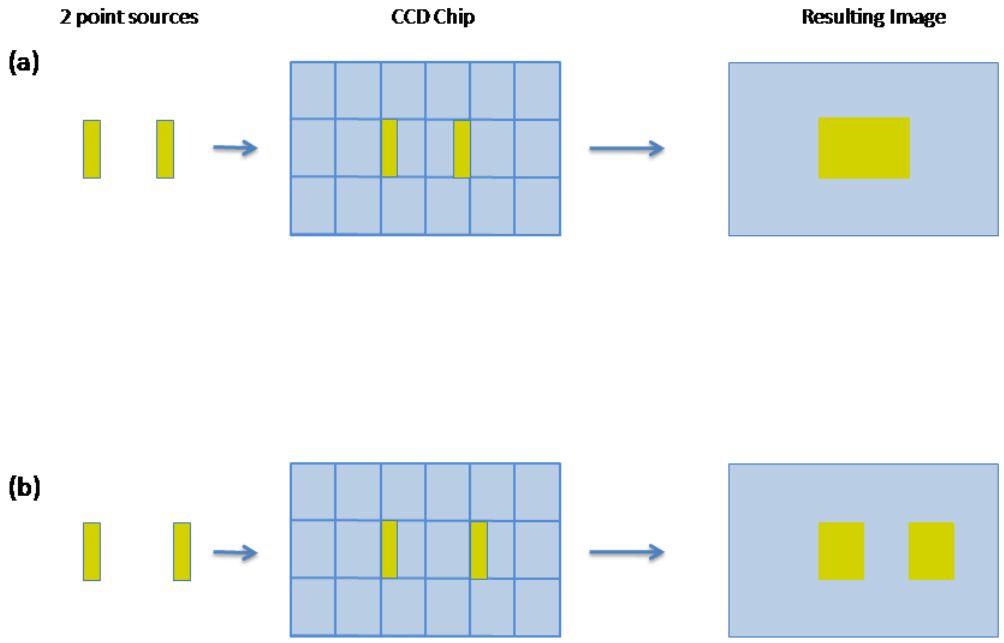

Figure 2.1.3: Images shown display the effects of Nyquist sampling on images comprising of sources of interest close to one another. Where two sources are close they are seen as a single point in (a) due to adjacent pixels being excited compared to (b) at twice the sampling rate observing two separate sources.

It can be seen that the pixel resolution of the camera relies on the pixel size in the object space (the initial part of the equation) which varies with objective power and Nyquist sampling interval. The sampling interval will have to be the minimum pixel size achievable in the object space therefore a multiplication factor of 2.3 gives the maximum resolution achievable by the detector.

The dynamic range of the CCD also can play a significant role in determining the resolution of a detector. The dynamic range associated with pixels on the CCD chip relate to the number of electrons that need to be liberated to register a single analog-to-digital unit (ADU). Fig. 2.1.4 shows two examples where no gain is applied in image (a) and where a 4X gain is applied in image (b). For example, in some cases full well capacity can be $16,000$ electrons, where the bit depth of the A/D converter is 4095 on ADU is equivalent to 4 electrons. However, when applying gain the full well is lowered as shown in Fig. 2.1.4 where a 4X gain is applied, instead of 4 electrons contributing to a single

ADU now 1 electron is equal to an ADU. Where the ADUs relate to grayscale values it can be seen that a higher number of ADUs will be detected when the intensity required for one is reduced. This allows lower signals to be detected however, it can also be seen how this increases the significance of noise where small signals adding to noise can manifest themselves as significant values after gain and thus making it difficult to detect weakly radiating points on a sample [18].

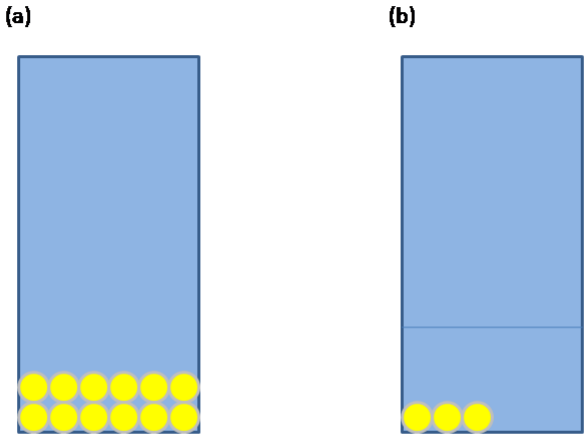

Figure 2.1.4: Camera gain affects the full well capacities of pixels on a CCD chip changing the number of electrons required to produce 1 ADU, (a) shows a pixel at full well capacity where as (b) shows it when 4X gain is applied.

2.1.1.3 Noise and aberration effects

Optical microsopy is subject to effects that can limit resolution, this can originate from effects in the system's optics or through effects relating to the CCD detector. Both microscopes and telescopes have been subject to aberration effects since 'traditional' lenses have been used in these instruments. One of these aberration effects is that of chromatic aberration which forms as coloured fringes around an image. This originates from different

path lengths for different wavelengths of light travelling through a material of a certain refractive index where different colours converge at different points. Although this has a greater effect on photography and in bright-field imaging, measuring samples with two or more markers of different emission wavelength attached to them will be subject to these issues if the lens in question hasn't had chromatic aberration corrected for (e.g. refocusing for different colours will have to be made due to the variation in where different coloured light converges). To get around the effects of chromatic aberration, compound lenses have been formed from materials with differing dispersive qualities to reduce the level of dispersion encountered by different wavelengths of light. Spherical aberration is another source of aberration effect/noise present with objectives and lenses. Spherical aberration can manifest itself as a reduction in sharpness of an image that occurs due to an increased refraction of light rays at the edge of a lens compared to the centre. The phenomenon of spherical aberration causes light rays to converge at different focal points depending on where on the lens they are incident, the further from the central point of the lens the greater curvature is seen on the lens and as a result rays here converge at a much shorter distance from the lens. Aspheric lenses with complex surface profiles can be employed to dramatically reduce the amount of spherical aberration observed in some systems due to their non-standard shape [19].

CCD detectors used in conjunction with optical microscopes introduce greater noise and uncertainties into a system. A source of noise is dark current which produces a distribution of signal occurring across a CCD chip due to heat and cosmic rays which varies between CCD chips and increases with exposure time. Signals can form from cosmic rays in a way similar to incident photons on the CCD chip (although resulting in a smaller quantity of excited electrons/pixels) resulting in sharp, intense excited pixels at specific points in time. Heat can also form a signal across the CCD due to the Maxwell-Boltzmann distribution in which the high velocity region of the distribution can lead to the liberation of an electron resulting in a broad background signal. Heating across the CCD is a more frequently occurring event than incident cosmic rays, therefore dark current can be reduced by cooling the CCD chip. It is possible to take a reading of the dark current, a subtraction

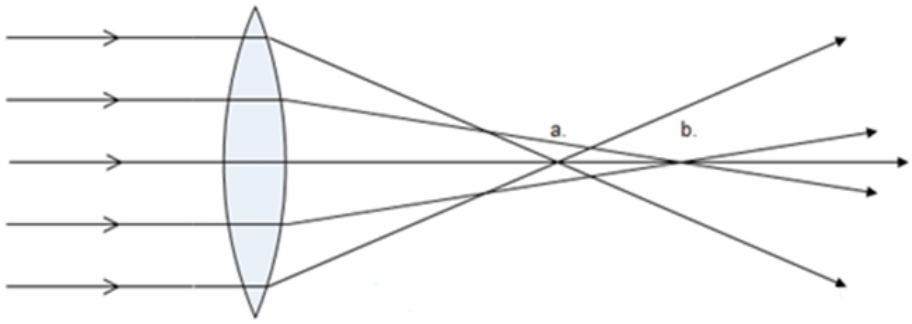

Figure 2.1.5: Spherical aberration occurring due to light incident at the edges of a lens being bent to a greater degree and converging at a position closer to the lens (a) than light that travels through a point closer to the centre of the lens (b).

of this can be applied to the optical signal to try and remove an average value for the effect. Another major noise source associated with CCD detectors is that of photon shot noise, arising purely from the detection of an optical signal. Shot noise manifests itself as an intensity fluctuation arising from uncertainties present as a result of the poisson distribution which describes the occurrence of individual random events, in this case photons from a source [20]. The shot noise scales as the square root of the incident number of photons, it can therefore be seen that with higher intensity light sources the shot noise (and thus uncertainty) has less of an effect on the signal. However, with lower intensity signals that typically arise in fluorescence microscopy, shot noise becomes more significant thus making it a lot harder to measure the true fluorescent signal from a sample. An on chip source of CCD noise is that of read noise which is present in all CCD devices, regardless of additional camera technology. Read noise refers to an uncertainty present in the process of quantifying an electronic signal on the CCD, this mostly arises from the on chip pre-amplifier. Read

noise from electrons in the pre-amplifier are additive and present independent of exposure time therefore it is possible to correct for this by taking an exposure of a dark CCD with a very short exposure time tending towards 0 seconds and subtracting the read noise value.

So far CCD detectors have been discussed, complementary metal-oxide semiconductor (CMOS) image sensors offer a different method of image acquisition that has both advantages and disadvantages over the CCD technique. CMOS image sensors are a technology that is as old as CCD, the potential use for optical imaging however wasn't realised until 1992. Similar to CCD, CMOS technology incorporates an array of light sensitive pixels to collect an image, all of the digitisation is completed at the pixel point rather than needing to read the signal and then digitise (reducing on some of the read noise). CMOS image sensors have been used in mobile phone imaging, brightfield imaging and industrial inspection, the lower power requirement than CCD (100X less) and faster imaging times make them ideal for these applications as well as for future high speed fluorescent imaging of samples. Even though CMOS offers higher imaging speeds compared to CCD, this comes at a cost with the technology and much more noise can be seen in CMOS technologies. Each pixel point has three or more transistors associated with it, this leads to picture noise where it is highly likely for incident light to fall on the transistors rather than the photodiode. CMOS sensors also function at very low gains which has an effect on sensivity and the ability to detect incident photons over noise.

2.1.2 Development of optical microscopy

The twentieth century saw a great improvement of objectives used with optical microscopes, with the developments reducing the effects that optical aberrations had on imaging. However, even with the vast improvements in manufacturing optics, imaging is still limited by diffraction and the resolving power of objectives, so new, novel techniques are required.

2.1.2.1 New optics

Far field optical microscope systems are ultimately limited by the diffraction limit however, different objective lenses have been developed to reach resolutions nearer to this limit. It is evident from the Rayleigh criterion in 2.1.1.1 that the resolution can be improved by changing the wavelength of incident light to a shorter one or by increasing the numerical aperture, which is a property relating to the shape and material properties of a lens, given by:

$$NA = n \sin \alpha \tag{2.1.4}$$

Where n is the refractive index of the objective material and α is one half of the acceptance angle of the objective. From this it can be seen that the numerical aperture of the lens is directly proportional to the refractive index therefore, the resolution of an objective can be improved by increasing the refractive index of the material used in the lens. It can be seen in Figure 2.1.6 on page 26 how increasing the NA of the lens material can lead to much greater light collection by an objective in relation to the acceptance angle of the lens. The image in (a) shows a lower NA objective, here the working distance of the objective is observed as quite long however, the radius of the light cone is small and thus the objective has a small collection angle. This means that the objective collects less of the signal as only the lower diffraction orders will be collected. In comparison, the objective shown in (b) has a much larger NA and thus the acceptance angle is much wider. Through this, the objective is able to collect light from the higher diffraction orders which leads to a greater signal intensity that is favourable in fluorescence microscopy for example when distinguishing between sample and background signal.

The principle of the oil immersion objective resides in the properties of refraction at a boundary between two materials of differing refractive index. In the case of a standard objective, light travels from the high refractive index medium of the glass coverslip into the relatively lower medium of air, at this boundary the light refracts away from the normal. As mentioned the NA relates to the acceptance angle of an objective, in this case some of

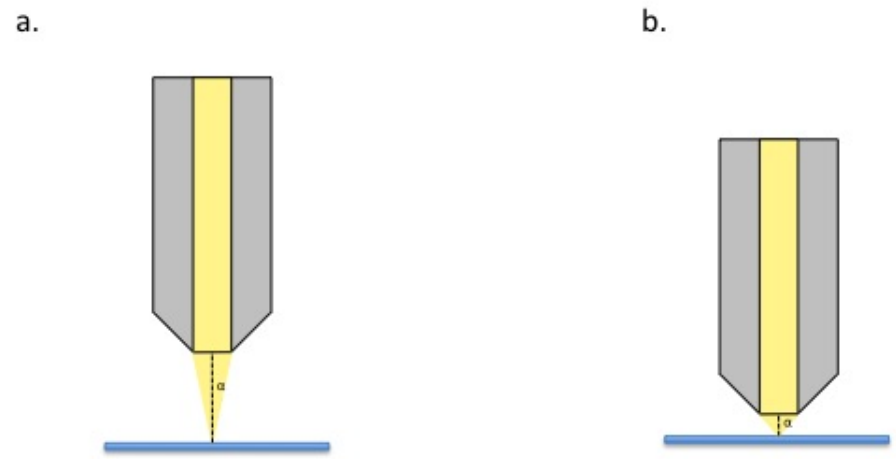

Figure 2.1.6: A comparison of the acceptance angles of light in two objectives of varying NA, a) lower NA b) higher NA

the light is refracted at an angle that puts it outside of the acceptance cone and some of the light is lost. However, the introduction of a material with higher refractive index than air (and thus approaching the refractive index of glass) leads to a smaller angle of refraction from the normal and most of the light being collected by the objectives acceptance cone. With immersion oils that have refractive index values on average of around 1.5 (on par with that of glass) it is possible to achieve NA values up to 1.6 [2].

Solid immersion lenses (SIL) operate on similar principles as the oil immersion lens, instead of a liquid medium being introduced to aid light collection a small solid lens is introduced between the sample and the objective. The solid immersion lens allows collection of light that is of higher spatial frequencies to be collected and thus those representing smaller surface structures, this is achieved through reducing the critical angle for total internal reflection allowing more light to be directed from the sample surface back to the excitation objective. SILs are fabricated from high refractive index materials into spherical or hemispherical lenses. The spherical nature of SILs follow from concepts described by

Born and Wolf [19] stating that two points of a spherical lens/SIL experience minimal aberration effects, one of these points is the centre of the sphere hence the use of hemispherical lenses. The other point is at a distance of $z_0 = (n_1/n_o)R$ from the centre of the sphere, R being the radius, n_0 and n_1 being the refractive index of the sphere and air respectively [21]. In this case the SIL uses a virtual focus which has greater magnification properties compared to the SIL with a focus in the centre, hence the use of both types. SILs may be fabricated from glass, silicon, GaAs or Sapphire with the possibility of achieving NA values in excess of 2 [22].

2.1.2.2 Fluorescence microscopy

The use of the fluorescence microscope in research and lab based applications has increased significantly alongside the development of fluorescent markers and the technique of immunofluorescent labelling. The combination of the fluorescence microscope and labelling has been highly beneficial to cell biology, allowing increased resolution and increased detail to be obtained on the cellular level. It is possible with fluorescence microscopy to get down to the resolution of individual molecules e.g. by using low concentrations of fluorescent material and more than one type of coloured fluorescent marker.

Fluorescence microscopy is designed to separate a re-radiating emissive component of light from a much stronger excitation component through the filtering of specific wavelengths. In fluorescence microscopy, instead of collecting all wavelengths of light only a small section of the visible light spectrum is collected allowing specific areas of a sample to be mapped with greater confidence. The fluorescence microscope still can not probe samples below the diffraction limit, however it can reveal the presence of fluorescing molecules on length scales below this (viewed as diffraction limited spots).

By changing the excitation source it is possible to improve the resolution of the fluorescence microscope (above the diffraction limit). By using a focused laser source, resolution can be increased due to the smaller excitation area this reduced excitation area of the laser means that a high excitation power can be delivered and emission received from a similar sized area. By having the excitation/emission confined to an area the size of the laser spot

spatial resolution is improved compared to that of other illumination mechanisms such as a lamp/broadband source which, can be subject to erroneous fluorescence (noise) across a larger sample area.

2.2 Scanning Probe Microscopy

Scanning probe microscopy is a technique that can be applied when features/regions of interest of a sample are on length scales that tend to that below the diffraction limit. Scanning probe techniques measure surface topography by maintaining a constant distance from the sample, a voltage response is applied to maintain this and these voltages variations are converted into a height image. Due to piezo controls the length scales in the x, y and z-axis can be on the sub nanometre scale, far exceeding standard microscopy techniques.

2.2.1 Atomic Force Microscope

Since its introduction in the late 1980s the Atomic Force Microscope (AFM) has been a valuable tool for measuring extremely small forces and for recording images of sample surfaces on the atomic scale. The AFM developed from the principles of other scanning probe techniques, such as the Scanning Tunneling Microscope (STM). The STM has one main limitation, that the sample must be conductive, however AFM doesn't rely on this property to obtain surface information and can record both attractive and repulsive forces at the surface making it a very powerful technique for surface characterisation [7].

2.2.1.1 Operation

To produce an image of the sample surface, the AFM uses a probing tip (often with a radius around 10 nm) attached to a spring-like cantilever which records deflections and digitises them to formulate an output image as the cantilever is scanned across the surface.

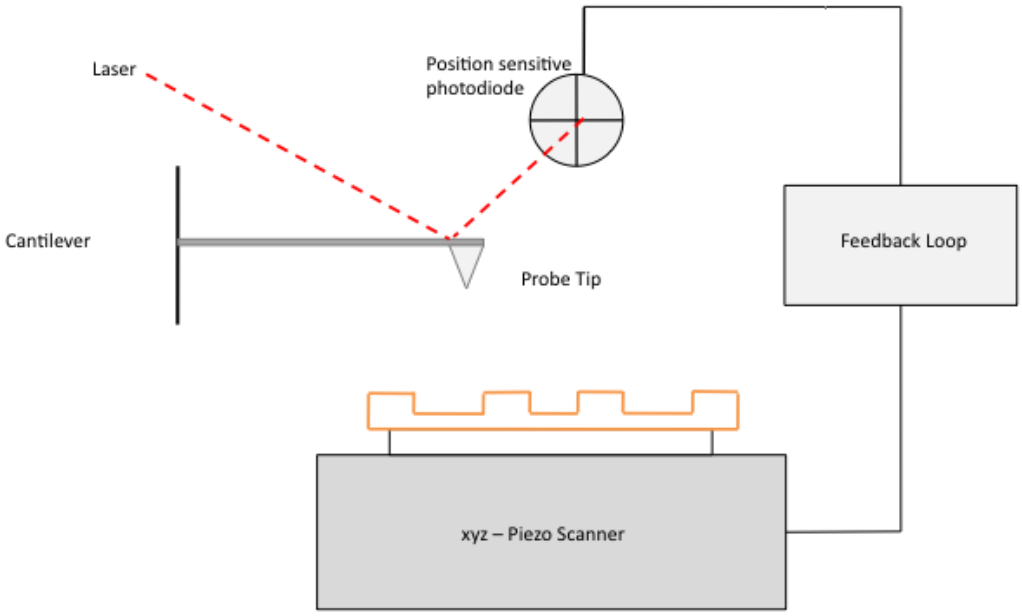

Figure 2.2.1: Schematic depicting the basic principle of AFM operation, modified from [24]

In the AFM the most important element is the tip which is formed from silicon or silicon nitride beams of $100 - 500$ μm in length [23], with a sharp tip mounted at the end for force sensing. A laser beam is reflected off the back of the cantilever to a position sensitive photodiode, the position variation of the laser spot recorded whilst maintaining a constant force, is read as a voltage pertaining to height variations.

In standard topographic measurements of sample surfaces the AFM can operate in two modes, the static DC-mode known as contact mode or the dynamic AC-mode known as non-contact mode AFM [24] (also referred to as Tapping Mode™ (*Veeco Instruments*)). Contact mode is the original mode for AFM imaging that developed from the probe scanning

techniques of previous scanning probe microscopes (e.g. STM). In contact mode AFM, variation of the tip-sample distance maintains a constant force on the sample, the voltage applied to the cantilever in doing so is measured to form a topographic image of the sample. As this measurement is conducted with the tip always in the attractive force region, both repulsive and attractive components can be measured.

Tapping mode AFM on the other hand is an intermittent contact technique where the cantilever is oscillated vertically at it's resonant frequency, in this case the feedback circuit maintains the oscillation at a constant amplitude. The amplitude of the cantilever oscillation is typically around $100-200$ nm [25], as a result of forces acting on the cantilever close to the surface such as van der Waals forces, electrostatic interaction and dipole-dipole interaction the cantilever is affected in such a way that the oscillation decreases as it gets closer to the surface. In maintaining a constant cantilever oscillation the piezoelectric actuator moves the tip in the z-axis to change the height which in turn is read as the variation in height of the sample.

Tapping mode AFM operation is less intrusive and lends itself to measurements of biological systems and more delicate samples due to the far smaller contact time between the probe and the sample compared to contact mode AFM which sees the probe constantly on the surface. As the force acting on the cantilever can be measured in conjunction with the distance from the sample, information regarding the type of force acting on it can be deduced from force-distance curves.

2.2.1.2 Scanning environment

Fig. 2.2.1 shows AFM operation in its standard environment using dry samples in air, it is however possible to conduct AFM measurements of samples in other environments. With most AFM systems it is possible to obtain enclosed cells to house the sample and hence to conduct other dry measurements such as changing the gas in the atmosphere e.g. nitrogen. Measurement of biological samples under liquid conditions increases the sensitivity of the equipment as well as allowing greater force control in the measurements due to the removal of the wetting layer, a layer with a high level of adhesion. Being kept under physiological

conditions in liquid allows biological samples to maintain a more natural and rigid structure which, even without reduced contact forces, is more durable and resilient under contact from the AFM probe with less denaturation occurring. Liquid AFM can be applied to both tapping mode and contact mode scanning techniques, due to the increased durability of samples under liquid however, in contact mode, samples are still subject to potentially destructive lateral forces [26] hence non-contact mode AFM under liquid is favourable for such samples. Within reason, for liquid AFM it is possible to use any liquid, for example one could use water or a buffer solution with varying pH for the study of samples in specific environments. The principles of liquid and dry environments can be applied to specifically designed AFM systems to vary the humidity of an environment by allowing different amounts of water to evaporate in an enclosed system (this can also be applied to other liquid chemicals) [27], once again this can favour biological systems in AFM as it improves their durability and observations can also be made in how they survive in these various conditions.

2.2.2 Atomic Force Microscope developments

On top of the standard AFM operation outlined in 2.2.1.1 (including that in different environments), the AFM has been developed to measure other specific sample properties. Fluorescence measurements have been incorporated with the AFM to locate specific fluorescent particles on a surface with optical measurements and then probe below the diffraction limit to obtain much higher detail about the structure of that specific area of the sample. Development of the AFM has also allowed other properties of samples to be measured on the nanometric scale like, adhesion properties (and other mechanical properties), electrical properties and magnetic properties.

2.2.2.1 Fluorescence Atomic Force Microscopy

The combination of AFMs and optical fluorescence microscopes has lead to the introduction of the Atomic Force Fluorescence Microscope (AFFM) which has proven to be a highly

beneficial technique in biology to the observe cells. As previously mentioned in 2.1.2.2 the use of immunofluorescent labelling and fluorescence microscopy has vastly improved studies of cellular processes and structure, understandably the combination of this and the higher resolution capabilities of AFM can be used to understand even more about the sub micron world. An AFM can be combined with an inverted microscope for fluorescence imaging capabilities where excitation of the sample and emission detection can be conducted through the bottom of the sample [28]. In this situation a broadband or laser source can be used to excite the sample, however to increase resolution in the fluorescence microscope confocal conditions can be employed to get as close to AFM resolution as the optics will allow. In this case excitation is through a laser source and collection of the fluorescence signal is only across a small band of wavelengths around the expected emission, this eliminates any erroneous light from being collected by the detector [29] in turn providing a signal that is purely from the emission of the sample. The presence of a pin hole in the collection optics of the confocal microscope also aid the enhancement of the images, collected as it eliminates out of focus light from the sample resulting in a much sharper image. The combination of fluorescence microscopy with AFM can be used to characterise the topographic properties measured in terms of their spectra as well as their intensity, e.g. this allows any correlation of sample thickness and fluorescence intensity to be deduced. With the use of immunofluorescent labelling, topographic information can be correlated with fluorescent information to relate specific proteins that have been produced with the fluorescent label to where they are in the cell, thus allowing greater understanding about specific areas of cells to higher resolution. Spectral imaging can be also used with samples containing 2 or more fluorescent dyes to distinguish areas of the cell from each other or the varying amounts of each labelled protein in the sample.

2.2.2.2 Conductive Atomic Force Microscopy

Conductive Atomic force Microscopy (C-AFM) is a technique similar to that of the STM from which the AFM and other scanning probe techniques developed. In STM, a sharpened probe is brought to within a few nanometres of the surface, at this distance a tunneling

current is produced which upon detection is pased through a current amplifier and converted to a voltage. The voltage generated is compared against a reference value and used to drive the z-piezo, in turn producing a topographical image of the sample [30]. In c-AFM on the other hand, topographic features of a sample are detected using standard contact mode AFM. A DC bias is applied to the AFM tip whilst the sample is held at ground and scanned, with this detection a current image is obtained alongside the topography image. As well as the ability to collect an image of the variations in the current across a sample the c-AFM can also be placed at any point of the surface to obtain I-V characteristics which has been useful in studying many properties of material systems such as solar cells [31], crystalline thins films of silicon [32] and the effect of dopant concentrations on the I-V characteristics of semiconductors [33]. Understandably this technique is only useful on samples that are conductive so this technique may be useful for semiconductor systems for example but not biological systems which are not conductive on the same scale.

2.2.2.3 Magnetic Force Microscopy

The Magnetic Force Microscope (MFM) has proved to be a useful tool for the investigation of arrangements of nanoparticles [34], thin films and in the optimisation of materials for use in magnetic tape devices [35], such as hard disk drives and recording devices. On top of research into materials for recording media, the MFM technique has also been used in superconductor research to image flux lines at low and high temperatures and the technique has also been stretched to investigate local magnetic interactions, eddy currents and magnetic dissipation phenomena [36]. Much like the c-AFM previously mentioned in 2.2.2.2 measurements of the magnetic properties of a sample can be made in conjunction and on the scale of the AFM probe, allowing specific magnetic properties to be directly related to topographical features on nanometre length scales determined by the AFM probe. For MFM measurements the tapping mode technique is used on an initial line scan of the sample to detect height information, a second scan of the the same line is conducted in order to obtain magnetic force information from the sample. The second scan of the sample, unlike the height measurement, isn't conducted in contact with the sample. The

cantilever is displaced a pre-determined z-distance so that it still feels the magnetic force, it retraces the path of the surface with any magnetic force causing a deflection of the cantilever which is converted to a value for the magnetic force [37]. Understandably AFM probes used in MFM are magnetic, unlike most standard probes.

2.2.2.4 Measurement of mechanical properties

The previously mentioned AFM developments have required samples to have a certain property, such as conductance, however other developments have been obtained through monitoring the forces present on the tip and as a result mechanical properties of samples can be measured. Analysis of the forces present on the tip have allowed topographical images to be obtained alongside information like the adhesion properties of the surface, energy dissipation across the sample and the deformation of the surface from contact with the tip [38]. The principles behind measuring these mechanical properties of the surface reside in force-distance measurements between the tip and the sample. Force-distance measurements plot the force acting on the AFM probe (in both repulsive and attractive regimes) in relation to the tip-sample separation, and how these between approach and withdrawl of a tapping mode tip divuldges some of the mechanical properties of a sample.

With the approach curve, as the tip-sample distance reduces to a point that is near to the surface the force dips below the zero point and into the adhesion regime. At this point the tip interacts with the surface and the attractive force of the surface becomes much greater than the spring constant of the cantilever, this pull down force varies in different environments (e.g. liquid) manifesting itself differently in the force-distance curve. The piezo continues to drive the tip into the surface until a point of maximum force [39] is reached where it reverses and withdraws. It can be seen from the withdrawl curve that there is some difference to the approach, removal of the tip leads to an increase in the adhesive force until it comes away from the surface, this minimum force value gives information relating to the adhesive properties at each point across the sample surface [40]. Adhesion is not the only property that can be obtained from the force distance graphs, energy dissipation (in electron volts) can be worked out from integrating over one period

of vibration of the cantilever indicated by the area between the approach and withdraw curves. With this in mind, a larger hysteresis between approach and withdraw curves represents much greater energy dissipation to sample [41]. In turn this can be related to the adhesion effects of the sample which lead to greater attractive forces on the withdraw curve indicating larger energy dissipation on more adhesive samples [42]. From the force-distance plots it is also possible to measure the deformation of a sample as a result of tip contact (with known tip size it is also possible to convert this to the hardness of the sample). The maximum sample deformation is measured in the approach curves of the AFM probe and relates to the distance between where the force of the tip is zero, and that where it is experiencing maximum force (peak force), errors in the measurement of deformation can arise however from the initial contact being at the 'jump on' distance and not the zero force point on the curve [40].

2.2.3 Scanning Near-field Optical Microscopy

It has been shown in 2.2.1 that with the application of scanning probe techniques it has been plausible for samples to be investigated on length scales far exceeding the diffraction limit present in optical microscopy techniques. The Scanning Near-field Optical Microscope (SNOM) combines the scanning probe microscopy techniques with optical microscopy to obtain simultaneous topography and optical information on these length scales that are below the diffraction limit. Through excitation and collection in the near field (nanometre regime) SNOM is able to utilise the non-propagating component of light (evanescent waves) emanating from fluorescence/reflection of a sample, collection of this light occurs on such a small length scale that it is detected before diffraction occurs therefore the resolution is dependent solely on the diameter of the excitation probe.

2.2.3.1 Principles of SNOM

The basic principles of SNOM come from theory relating to the diffraction of electromagnetic radiation by a sub wavelength aperture as well as the concepts relating to propagating

and non-propagating components of light, as discussed by Newton in his work on TIR [43]. Initially, the concept of using a sub-wavelength aperture for imaging on a scale that is smaller than the diffraction limit was theoretically proposed in 1928 by *Synge* [11], this was later theoretically addressed by *Bethe* in 1944 [44]. The properties of light relating to standard far-field apertures can be described by diffraction theory however, in explaining the concepts for the diffraction by a sub-wavelength aperture electromagnetic theory has to be employed. *Bethe* addressed this in his work applying specific boundary conditions to Maxwell's equations, these were found to be incorrect and was refined by *Bouwkamp* [45]. The work of *Synge, Bethe and Bouwkamp* realised that the near-field regime can be accessed when a subwavelength aperture is held close to the sample surface (distance less than the aperture diameter). When held at this distance the illumination area is determined by the size of the aperture and the distance from the sample. The near-field regime operates through the detection of non-propagating evanescent waves which due to the inverse decay of light from the source, are only detectable at distances that are less than the wavelength of light. Formation of these non-propagating components arise through scattering by nanometre structures. In comparison the far field operates on distance in excess of two wavelengths, detection in this regime often comes as a result of scattering by structures larger than the wavelength of light. Due to the lack of diffraction effects in this region the resolution is essentially only limited by the spot size/aperture diameter, this is the phenomena that the SNOM employs to reach resolutions in the region of 50 nm.

Regarding the interaction of evanescent waves upon limited (sub-wavelength) objects, *Wolf* and *Nieto-Vesperinas* showed how the evanescent waves are scattered into both a propagating and non-propagating component upon interaction with the limited surface [46]. Propagating waves are subject to standard diffraction effects however, non-propagating components are confined to the sample surface unless, as it was proposed, a sharp limited object (nanometre sized probe) was in the vicinity to turn non-propagating waves into a propagating and a non-propagating component. This principle in turn highlights the importance of a sharp limited probe in SNOM to be in close vicinity of a sample in order to beat the diffraction limit.

Aperture SNOM is a popular method of SNOM which employs a light-emitting probe consisting of a metal clad, tapered optical fibre the end of which, is uncoated to form a narrow aperture. Conditions for working in the optical near-field require the probe to be scanned in close proximity to the sample surface, at a distance which is smaller than the wavelength of light. The aperture must be much smaller than the wavelength of light used otherwise far-field microscopy is more effective for these conditions. As the probe is scanned across the surface the transmitted radiation is recorded at each point with the resolution being dependent on the size of the aperture. With the probe in the near-field and at a proximity that is less than the wavelength of light, diffraction effects don't pose a problem as the light is transmitted before these effects can take place, the only thing that can pose a limit on the resolution and the operation of the technique is low light throughput resulting in low transmission.

2.2.3.2 Development of SNOM

The ideas of *Synge* at the time were not put into practice due to the technical barriers present to produce subwavelength apertures that could be placed nanometres from a sample surface. With advances in the manufacture of sub micron structures, these technological barriers could be overcome and, the ideas proposed in the 1920s be put into practice. In a 1972 experiment by *Ash* and *Nicholls* [47] sub-wavelength resolution was displayed for 3 cm microwaves which, after passing through a small aperture translated to a $\lambda/60$ spatial resolution. This demonstration of sub wavelength resolution saw a renewed interest in trying to achieve similar results with that of visible light.

A little over a decade after the demonstration of sub-wavelength resolution with microwaves, two groups independently demonstrated SNOM in a guise that is similar to how it is used today. The groups of *Pohl et al.* [48] working at IBM in Zurich, Switzerland and *Lewis et al.* [49] working at Cornell University in the USA both used a sharp dielectric probe coated with metal containing, a sub-wavelength aperture which was held at a distance of nanometres from sample. Similarly to AFM, the STM proved to be an important piece of equipment for the development of the SNOM, due to piezoelectronics the probe

can be held at a distance from the sample that is within the near-field regime and the tip can be scanned across the sample at nanometre distances. Through monitoring with an attached tuning fork, a feedback loop controlled the tip-sample separation holding it in the near field regime for the purposes of the SNOM measurements, a technique that is still employed.

The significance of the incarnations of SNOM by these two groups was that they demonstrated sub wavelength resolution through an aperture with visible light, more useful for uses with fluorescent markers and naturally fluorescing samples. Using a metal coated quartz rod, *Pohl et al.* achieved sub-wavelength resolution with laser light at 488 nm demonstrating the potential for sub-wavelength imaging with a nanometre aperture. *Lewis et al.* achieved a resolution of 50 nm using light at 500 nm for excitation. The realisation that sub-wavelength resolution, dependent on aperture size could be achieved paved the way for SNOM to be an accomplished scanning probe microscopy technique.

2.2.3.3 Properties of the near field

In the theory and practice of *Synge's* [11] sub-wavelength aperture by *Pohl et al.* [48] and *Lewis et al.* [49] the key principle required to be achieved was that of being able to measure propagating and non-propagating (evanescent waves) in the near-field created at the tip-sample interface. Evanescent waves, a term coined by *Newton* upon their discovery in his work on total internal reflection, are non-propagating components of light. Unlike propagating components that can penetrate the far-field region, evanescent waves are confined to the surface of a sample allowing them to propagate in the x and y dimensions, however as they are a result of the presence of matter they decay exponentially in the z-direction [43]. The decay length can be calculated to be on the size of around 10 nm [50], thus showing the requirement of the SNOM to be able to keep tip-sample distances consistently in the nanometre regime.

Newton realised whilst investigating the chromatic nature of light that if the angle of incidence of a beam of light on a prism was larger than a critical angle, then the beam could be totally reflected within the prism even though the surface was not metalised. Introducing

a second, slightly convex prism to the surface of the first prism he intended to observe the behaviour of the field in the (x,y) plane, expecting light to only be transmitted at the point of contact between the two prisms. *Newton* however, recorded a larger transmission cross-sectional area than the contact area, inconsistent with what was expected. In coupling to a second prism the evanescent field is still present with an (x,y) component and a decaying amplitude with distance however, the second prism introduces an effect that 'converts' the non-propagating component into propagating waves, an effect known as photon tunneling.

The behaviour of the evanescent field can be described by the equation:

$$U(x,y,z) = A(x,y,z)\exp -i(k_x x + k_y y)\exp(-\alpha z)\exp i(\omega t) \tag{2.2.1}$$

Eq. 2.2.1 detailed by *Courjon* [43]shows the evanescent field to be dependent on both spatial co-ordinates and time where, A in the first term relates to the amplitude at a point (x,y,z), the second term relates to the propagation of the wave on the surface in (x,y). The third term relates to the exponential decay of the field along the z-axis where the coefficient α depends on the material properties and also the spatial properties. It has been shown that with decreasing surface structures the coefficient increases, relating to a larger confinement of the field over the sample surface. The final component applies to the time dependence of the field. This equation outlines the surface confinement of evanescent waves in the (x,y) plane and the necessity to introduce a probe in order to obtain sub-wavelength information.

Aspects of the diffraction limit and justifications for sub-wavelength resolution can be drawn from how the near-field relates to the Heisenberg uncertainty principle. The image of an object can be represented by considering a field U(x,y,z) at a position P(x,y,z) [19]. A field can be described by an amplitude at this point as well as a propagation vector k(x,y,z) originating at the point P and acting in the direction of propagation. The propagation vector is connected to the wavelength of the light by the relation

$$k = \frac{2n\pi}{\lambda} \tag{2.2.2}$$

where n is the refractive index of the medium through which the wave propagates.

Field intensity varies and as a result is not necessarily the same at any 2 points therefore by treating these points for which the change in field intensity can be measured in one dimension (x or y) allows the ultimate resolution of the system to be determined. If uncertainty of the position P is denoted as being $\Delta x, \Delta y, \Delta z$ and uncertainty on the propagation vector k described by $\Delta k_x, \Delta k_y, \Delta k_z$, then the application of the Heisenberg uncertainty relation states that

$$\Delta x \Delta k_x \geq 2\pi \tag{2.2.3}$$

which is also applicable in the y and z-directions. To minimise the Δx and thus give the smallest distance between two points, it is required for Δk_x to be large, in other words for the field to be varying greatly and there to be a large uncertainty in the direction of light propagation. Increasing the aperture of an objective to improve resolution is used in practice to collect largely scattered light (Δk_x) in order to reduce (Δx). Taking the projection vector in one dimension (in this case x), one can deduce the largest value expected for k_x as

$$k_x = |k| \sin\theta \tag{2.2.4}$$

where θ is the angle of projection of k on the x-axis. It can be seen that k_x vector will be smaller than the modulus of k and is dependent on it. By taking the range of variation in k_x to be $\Delta k_x = 2k_{xMax}$ where k_{xMax} is the largest value that k_x can take, then eq. 2.2.3 can be rewritten as

$$\Delta x = \frac{\lambda}{2n \sin\theta} \tag{2.2.5}$$

thus reaching the *Abbé* limit for resolution outlined in 2.1.1.1.

It is possible for k_x to not be dependent on $|k|$ due to the relation

$$|k_x| = \sqrt{|k|^2 - (k_y)^2 - (k_z)^2} \tag{2.2.6}$$

when either the k_y or k_z component is a complex number. If one of these components take the form of an imaginary number then k_x becomes large thus when applied to the uncertainty principle the value of Δx decreases and allows subwavelength resolution to be obtained. In the case of the near field when k_z takes an imaginary value, the other two components are real and the field propagation applies in the (x,y) plane, confining it to the surface.

2.2.3.4 Operation

Experimental set up for SNOM (like in AFM techniques) varies and strongly depends on the required measurements and the sample being studied, for example SNOM can be applied to both air and liquid environments, it can be used alongside Raman spectroscopy, it can be applied to fluorescence and fluorescence lifetime detection and it has also been applied to measurements of biological samples. The basic operating set up of a SNOM for fluorescence detection is shown in Fig. 2.2.2.

In SNOM a probe is brought to within a few nanometres of the sample surface and light from a laser source is coupled into the probe for illumination of the sample. The SNOM probe is scanned across the sample illuminating the sample surface and mapping topography and fluorescence signal, detected by the objectives, as a function of probe position. Laser light can be removed from the detected signal through using specific filters so that only fluorescence signal is measured by the SNOM.

SNOM can also operate in an apertureless configuration where differences to aperture SNOM lie in the probes used to investigate the near-field and detect non-propagating evanescent waves. The apertureless configuration scatters light to detect information from the near-field regime. Instead of the probes used in aperture SNOM, sharp tips such as those from AFM are used in this scattering technique. The tip is illuminated by an external source which acts as a highly localised source of light where strong electromagnetic fields are confined to the surface which result in enhancement of the region at the tip. This

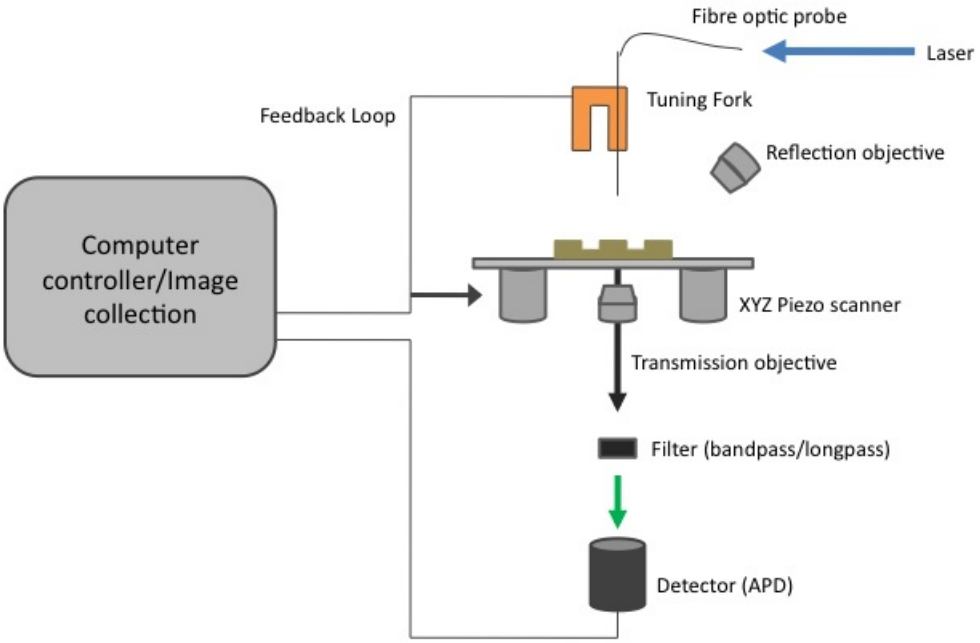

Figure 2.2.2: A schematic representation of the basic SNOM mode which was used in this work with the capabilities to conduct both transmission and reflection measurements.

acts as a sub-diffraction limit source in which the localised light can be detected by an objective, here resolution is again limited by the tip size.

2.2.3.5 Scanning technique

Due to the exponential decay of the near field in the z-axis, it is required in measurement of the surface, the SNOM probe maintains a separation from the sample that remains in the near-field regime for evanescent wave detection, delivery of constant power to the sample and that it does not succumb to tip damage. A shear-force mechanism is used to maintain a constant tip-sample separation whilst the tip is raster scanned across the surface. The tip is oscillated via a dither piezo at resonance parallel to the surface as it is brought towards the surface, distance between the tip and sample decreases and the oscillations of the tip are damped. A constant separation distance is achieved by monitoring the amplitude of this oscillation as it is affected by shear forces. This is maintained through a feedback signal that is used to move the tip to a height position where the oscillation amplitude remains the same across the sample, movement on the z-axis to maintain this is read out to produce the height map.

Due to the low intensity of evanescent waves and the weakening of intensity as a function of distance, it is preferable to have a detector with low noise or high quantum efficiency. Alongside detectors with these properties, maximising detection of fluorescence can be achieved through the use of collection objectives with high numerical aperture as well as external achromatic optics. To ensure that the detected fluorescence signal is maximised and a high signal-to-noise is achieved, filters are used to extract any stray light resulting from reflections or emission from different components of a sample as well as any signal arising from the delivery optics. To measure the fluorescence signal an avalanche photo diode (APD) is often used due to its ability to detect low light signals and low background noise. It is possible to couple SNOM with other detectors, e.g. CCD cameras and photo multiplier tubes, which allow spectroscopy measurements as well as those of just fluorescence at a specific wavelengths determined by filters.

2.2.3.6 SNOM probes

The modes of SNOM operation rely on the type of probe used and this can therefore lead to the techniques of apertureless SNOM and the more popularly used aperture mode SNOM. Aperture SNOM (based on the experiments at IBM and Cornell University in 2.2.3.2) has been the most successful mode of operation using the probe for illumination, collection and for both of these simultaneously. In illumination mode, light from an external source is supplied to the probe and as it passes through the tip end it is converted to an evanescent wave which in turn is used to illuminate the sample in the sub-wavelength regime [51]. Coupling of the evanescent wave with the sample can lead to propagating components of light (as addressed in 2.2.3.3) which can be collected by an objective depending on the sample used and whether they are predominantly transmissive or opaque. Illumination mode favours photosensitive samples as transmission of light through the aperture is in the region of 10^{-3} to 10^{-6}, governed by the relation $(d/\lambda)^4$ [44, 45] where d is the probe diameter, however this relatively low throughput can also hamper the output signal power. It is also possible to use the SNOM probe for light collection when the sample is illuminated in the far-field or if the sample is optically active. In collection mode the probe tip is brought to within 20 nm of the surface [52], the introduction of the limited, sub-wavelength probe to the near-field results in non-propagating evanescent waves being disrupted and achieving a propagation component as mentioned in 2.2.3.1. The propagating component of light can be detected by the aperture, again achieving sub-wavelength resolutions dependent on the tip size. The aperture SNOM technique can also be used for the significantly more difficult technique of illuminating the sample and collecting the the optical signal with the same probe, which requires highly reflective or optically active samples similar to those used in collection mode. This technique requires a probe to have a high collection efficiency that is on par with a high NA objective [53].

Apertureless SNOM (which incorporates scatter-type SNOM), is a much less frequently used SNOM technique although it has been increasing in popularity due to its potential to achieve resolutions higher than aperture SNOM techniques. In an apertureless SNOM system it is possible to use sharp tips (such as those used in AFM) instead of a probe with

an aperture. The sharp tip is illuminated via an external source which allows the tip to be used as a highly localised light source that scatters evanescent waves as opposed to the probes in aperture mode which act as a waveguide for the evanescent light. The potential resolution of an apertureless system is determined by the dimensions of the tip which as a result of using AFM tips allows potential resolutions to reach 10 nm [54]. Due to external illumination of the tip a large area of the sample is also illuminated at the same time, this leads to a very high background signal which with weakly emitting regions of interest can be highly detrimental to measurements. The issue of the large background contribution makes this a less favorable SNOM technique compared to aperture SNOM for most SNOM measurements however with the apertureless system it is possible to do such tip enhanced techniques like Raman spectroscopy and infrared spectroscopy which, due to the nature of aperture probes is not possible.

Due to the nature of their operation, SNOM probes have 2 main requirements: they should be sharp enough to accurately measure surface topography and they should contain a sub-wavelength aperture. SNOM probes used in the original measurements by *Pohl* and *Lewis* in the 1980s were fabricated by etching quartz crystals or by pulled micropipettes. These techniques suffered from poor reproducibility and low light throughput, a more successful method for fabricating SNOM probes was introduced by *Betzig et al.*[55] regarding coated tapered waveguides, a technique predominantly still used to make probes. These tips are manufactured from an optical fibre and by using a heating-pulling technique they can be used to form a tapered tip. Optical fibres are placed in a micropipette puller under tension, this is then heated using a CO_2 laser. As the fibre is heated and viscosity decreases the fibre is drawn out into a long taper until it reaches a required length where the laser is turned off and a stronger force is applied, fracturing the glass and forming the tip. A number of parameters can be varied in the heating-pulling technique that can affect the probe dimensions and their properties, these are: the amount of energy supplied to the glass (laser power), the laser spot size, delay between laser turn off and external force and the magnitude of the external force applied. This method of probe fabrication allows for large scale reproducibilty of SNOM apertures.

In order to confine light and form an aperture the sides of the probe are coated with an opaque metal. Aluminium is most commonly used (although it may be mixed with other metals to aid adhesion to the glass fibre) due to its low skin depth in the visible light regime meaning that only a thin layer of metal (15 nm @ 500 nm) is needed in order to obtain optical opacity. In depositing thin layers of aluminium on the probe, evaporative techniques tend to be used whilst the tip is rotated at a fixed angle from the source with the end of the probe in shadow so the metal coating is far less at this point ensuring higher light throughput at the tip. Thermal evaporation is a favoured coating technique (over other techniques like sputtering) as it ensures probes with minimal deficiences. With thermal evaporation there is a lower chance of oxide formation due to it being a relatively fast technique, it is also a technique that allows an even coverage of metal which in turn reduces the chance of 'pin hole' formation in the coating that causes increased background signal from light leakage.

It can often be found due to graining imperfections in the aluminium coating that the end of the probe may close over the aperture formed by the optical fibre, it can also affect the tip with grains of aluminium making it uneven for imaging. Often with the coating technique the fibre can be located a distance inside the probe from the tip-sample interface resulting in a reduced light throughput, by changing the manufacture process it has been possible to get around this through the use of focused ion beam (FIB) etching of the tip. The initial manufacture of probes through this process doesn't differ from those mentioned, tapered tips are formed through heating-pulling technique and coated with aluminium. Where this process differs however is that the aperture is milled using the FIB which fabricates an aperture of bespoke size through raster scanning of the beam at the end of the tip allowing highly reproducible tips to be formed.

2.2.4 Summary

Since the realisation of the optical microscope, resolution has always been limited by the basic properties of light. As a result, novel ideas have been applied to the microscope

in an attempt to get as close to the diffraction limit as possible, such as the techniques of fluorescence microscopy and the advent of immersion lenses. The scanning probe microscopy techniques of STM and AFM have developed as a way to beat the diffraction limit through accurate measurement of the surface on the order of nanometres. The AFM has also developed as a way to measure specific material properties of a sample that cannot be measured with optical microscopy. It has been possible to combine AFM and optical microscopy however, these optical measurements are still subject to the diffraction limit, therefore the technique of SNOM has developed as a way to beat the diffraction whilst measuring optical properties. Building on *Synge's* theory of light from a sub-wavelength aperture the SNOM was formed, utilising the near-field to obtain subwavelength information. All of these techniques have been used for numerous applications in different fields of research.

This section has introduced the principles behind optical microscopy techniques, AFM and SNOM. Limitations on resolution due to optics have been addressed as well as ways to improve the existing microscope technologies, principles of light in the near-field and how to utilise this with SNOM have also been addressed. Typical setups behind all three techniques have also been outlined, addressing ways to improve resolution, image samples of varying properties and all the instrumentation behind them (probes, tips).

The success of these reside in the ability of them to be applied to different types of samples and to measure many different properties from the mechanical to the optical. These microscopy techniques can successfully be applied to biological samples to reveal simultaneous topographical and optical information (be this from tagged samples or naturally light interacting) below the diffraction limit whilst not being largely invasive like electron microscopy thus, making them ideal for the work carried out in this thesis.

2.3 Bibliography

[1] V. Stephens, D. Allan. Light Microscopy Techniques for Live Cell Imaging. *Science*, 300:82–86, 2003.

[2] M Davidson, M. Abramowitz. Optical Microscopy Online PDF resource, 1999.

[3] Rayleigh. Investigations in optics, with special reference to the spectroscope. *Philosophical magazine series*, 8:261–274, 1879.

[4] H. Binning, G. Rohrer. Scanning Tunneling Microscopy. *Surface Science*, 126:236–244, 1983.

[5] A. Barnes J. O'Shea S Welland, M. McKinnon. Scanning probe microscopy. *Engineering science and education journal*, 1(5):203–210, 1992.

[6] C. Gerber C. Binning, G. Quate. Atomic force microscope. *Physical Review Letters*, 56(9):930–933, 1986.

[7] G Binning. Atomic Force Microscopy. *Physica Scripta*, 19:53–54, 1987.

[8] H. Guethner P. Lambert S. Stern J. McFadyen I. Yogi T. Rugar, D. Mamin. Magnetic force microscopy: General principles and application to longitudinal recording media . *Applied Physics*, 68:1169–1183, 1990.

[9] G. Erlandsson R. Chiang S. Mate, C.M. McClelland. Atomic-Scale friction of a Tungsten Tip on a Graphite Surface. *Physical rev. letters*, 59(17):1942–1945, 1987.

[10] J. Koetse M. Alexeev, A. Loos. Nanoscale electrical characterization of semiconducting polymer blends by conductive atomic force microscopy (C-AFM). *Ultramicroscopy*, 106:191–199, 2006.

[11] EH Synge. A suggested method for extending microscopic resolution into the ultramicroscopic region. *Phil. Mag*, 6(356-362):1, 1928.

[12] A. Huijbens R. Bakker B. Rensen W. Garcia-Parajo M. Hulst N. Figdor C. Lange, F. Cambi. Cell biology beyond the diffraction limit: near-field scanning optical microscopy. *Cell Science*, 114:4153–4160, 2001.

[13] K. Huckabay H. Livanee P. Dunn R. Dickensen, N. Armendariz. Near-field scanning optical microscopy: a tool for nanometric exploration of biological membranes. *Analytical and bioanalytical chemistry*, 396(1):31–43, 2010.

[14] R Hooke. *Micrographia, or, Some physiological descriptions of minute bodies by magnifying glasses, with observations and inquiries thereupon.* 1665.

[15] H. Gest. The discovery of microorganisms by Robert Hooke and Antoni van Leeuwenhoek, Fellows of the Royal Society. *Notes and Records of the Royal Society*, 58:187–201, 2004.

[16] B Amos. Lessons from the history of light microscopy. *Nature Cell Biology*, 2:151–152, 2000.

[17] G. Airy. On the diffraction of an object-glass with circular aperture. *Transactions of the Cambridge Philosophical Society*, 5:283–291, 1834.

[18] T. Nayar, S.K. Mitsunaga. High dynamic range imaging: spatially varying pixel exposures. *Computer Vision and Pattern Recognition*, 1:472 – 479, 2000.

[19] E. Born, M. Wolf. Principles of Optics. *Cambridge University Press*, 2002.

[20] M. Beenakker, C. Patra. Photon Shot Noise. *Modern Physics Letters B*, 13:337–348, 1999.

[21] E. Dalgarno P. Gerardot B. Hadfield R. Warburton-R. Reid D Serrels, A. Ramsay. Solid Immersion lens applications for nanophotonic devices. *Journal of Nanophotonics*, 2, 2008.

[22] G. Grober R. Wu, Q. Feke. Realisation of numerical aperture 2.0 using gallium phosphide solid immeraion lens. *Applied physics letters*, 75(26):4064–4066, 1999.

[23] W.H. Alsonso, J.L. Goldmann. Feeling the forces: atomic force microscopy in cell biology. *Life Sciences*, 72:2553 – 2560, 2003.

[24] E. Meyer. Atomic Force Microscopy. *Progress in Surface Science*, 41:3 – 49, 1992.

[25] R. Garcia, R. Perez. Dynamic atomic force microscopy methods. *Surface Science Reports*, 47:197 – 301, 2002.

[26] S. Muller S. Engel A. Muller D. Fotiadis, F. Scheuring. Imaging and manipulation of biological structures with AFM. *Micron*, 33(4):385 – 397, 2002.

[27] S. Magonov. Atomic Force Microscopy studies in different environments. *Agilent technologies Application Note*, 2010.

[28] S. Schutz G. Hinterdorfer P. Kada G Madl, J. Rhode. Simultaneous AFM/Fluorescence Imaging of Living Cells - Fluorescence-guided Force Spectroscopy. *Agilent technologies Application Note*, 2007.

[29] O. Lenferink A. Hunter CN. Olsen-J. Subramaniam V. Otto C Kassies, R. Van der Werf. Combined AFM and confocal fluorescence microscope for applications in bio-nanotechnology. *Journal of Microscopy*, 217(1):109–116, 2005.

[30] C.J. Chen. *Introduction to Scanning Tunneling Microscopy*. Oxford University Press, 2008.

[31] R. Jiang C. Al-Jassim M. Kazmerski L. Moutinho, H. Dhere. Conductive Atomic Force Microscopy applied to CDTe/CdS solar Solar Cells. *19th European PV Solar Energy Conference and Exhibition*, 2004.

[32] J. Fejfar A. Kocha-J Rezek, B. Stuchlik. Microcrystalline silicon thin films studied by atomic force microscopy with electrical current detection . *Journal of Applied Physics*, 92(1):587–593, 2002.

[33] M. Garno J. Kleiman-R Richter, S. Geva. Metal-insulator-semiconductor tunneling microscope: two-dimensional dopant profiling of semiconductors with conducting atomic-force microscopy. *Applied Physics Letters*, 77(3):456–458, 2000.

[34] P. Aruguete D. Bastus-N. Alivisatos A. Puntes, V. Gorostiza. Collective behaviour in two-dimensional cobalt nanoparticle assemblies observed by magnetic force microscopy. *Nature Materials*, 3:263–268, 2004.

[35] L. Loddet C. Porthun, S. Abelmann. Magnetic force microscopy of thin film media for high density magnetic recording. *Journal of Manetsim and Magnetic materials*, 182:238–273, 1998.

[36] U Hartmann. Magnetic Force Microscopy. *Materials Science*, 29:53–87, 1999.

[37] A Yaminsky, I. Tishin. Magnetic Force Microscopy. *Russian Chemical Reviews*, 68(3):165–170, 1999.

[38] Bruker. Scanning Probe Microscopy Modes - Online Resource, 2010.

[39] B Santner, E. Stegemann. Adhesion measurements by AFM a gateway to the basics of friction. *Federal Institute for materials research and testing.*

[40] N. Su C Pittenger, B. Erina. Quantitative mechanical property mapping at the nanoscale with peakforce qnm, 2010.

[41] B. Fuchs H. Cleveland-J. Elings V Anczykowski, B. Gotsmann. How to measure energy dissipation in dynamic mode atomic force microscopy. *Applied Surface Science*, 140:376–382, 1999.

[42] S. Pethica J. Ozer-H. Oral A Hoffmann, P. Jeffery. Energy Dissipation in Atomic Force Microscopy and Atomic Loss Processes. *Physical Review Letters*, 87(26), 2001.

[43] C Courjon, D. Bainier. Near field microsocpy and near field optics. *Reports on Progress in Physics*, 57:989–1028, 1994.

[44] H Bethe. Theory of Diffraction by Small Holes. *The Physical Review*, 66(7):163–182, 1944.

[45] C. Bouwkamp. Diffraction Theory. *Reports on Progress in Physics*, 17(1):35–100, 1954.

[46] M Wolf, E. Nieto-Vesperinas. Analyticity of the angular spectrum amplitude of scattered fields and some of its consequences. *Journal of the Optical Society of America A- Optics and image science*, 2(6):886–889, 1985.

[47] G Ash, E. A. Nicholls. Super-resolution aperture scanning microscope. *Nature*, 237:510–512, 1972.

[48] W. Lanz M Pohl, D. Denk. Optical stethoscopy: Image recording with resolution lambda /20. *Applied Physics Letters*, 44(7):651–653, 1984.

[49] M. Harootunian A. Muray-A Lewis, A. Isaacson. Development of a 500 angstrom spatial resolution light microscope: I. Light is efficiently transmitted through lambda/16 diameter apertures. *Ultramicroscopy*, 13(3):227–231, 1984.

[50] R Greffet, J. Carminati. Image formation in near-field optics. *Progress in surface science*, 56(3):133–237, 1997.

[51] K Kim, J. Song. Recent progress of nano-technology with NSOM. *Micron*, 38:409–426, 2007.

[52] M. Lewis A Betzig, E. Isaacson. Collection mode near-field scanning optical microscopy. *Applied Physics Letters*, 51(25):2088–2090, 1987.

[53] T Hosaka, N. Saiki. Near-field fluorescence imaging of single molecules with a resolution in the range of 10 nm. *Journal of Microscopy*, 202(2):362–364, 2001.

[54] S. Lahrech A. Aigouy-L. Rivoal J. Boccara-A. Gresillon, S. Ducourtieux. Nanometer scale apertureless near field microscopy. *Applied Surface Science*, 164:118–123, 2000.

[55] J. Harris T. Weiner-J. Kostelak R Betzig, E. Trautman. Breaking the Diffraction Barrier: Optical Microscopy on the Nanometric Scale. *Science*, 251(22):1468–1470, 1991.

Chapter 3

Light and biology

Light plays an important role in many of the biological processes that occur in nature. Many organisms utilise light in complex and highly efficient ways for energy production [1], camouflage [2] and signaling [3]. Interest in these mechanisms has increased greatly with the realisation that they may be able to play a role in future bio-inspired technologies. This work deals with photosynthetic bacteria, fluorescent proteins and Bragg reflecting elements of animal skin, all of which use light, but in different ways and for different applications.

Organisms using light have had to adapt in ways to deal with the variation in the properties of light across the Earth's surface. For example, the solar spectrum varies as it passes through different media, due to the absorption of specific wavelengths by the media or by other organisms in the same ecosystem. The variation of the wavelength in the incident spectrum can be seen to affect organisms living in such an environment that they absorb light at these wavelengths and are easily damaged at wavelengths inherent to different environments. This can be seen with the photosynthetic bacteria *Rhodobacter Sphaeroides* which residen within lakes in the absence of high levels of oxygen. These bacteria reside at a depth where infrared wavlengths have been absorbed and thus photons at near-infrared (NIR) wavelengths are present which are favourable to higher intensity bluer photons that are potentially damaging to the bacteria. Due to environment the photosynthetic bacteria can succumb to damage in oxygenated environments which it doesn't naturally encounter

at depth within lakes. Not only are shifts in the wavelengths of incident radiation observed in differing environments, the intensity of light can vary significantly. Certain photosynthetic bacteria for example have developed highly efficient light harvesting components (*Chlorosomes*) that contain hundreds of thousands of light harvesting *bacteriochlorophyll* (BChl) designed to increase the chances of absorbing any photon that reaches the depths they are found at, essentially increasing a complexes absorption cross-section.

Biological systems interact with light in different ways, photosynthetic organisms predominantly use light for energy, some organisms use fluorescent proteins which use light for emission at different wavelengths to name a couple examples. Photosynthetic systems are of interest due to the high quantum efficiencies that they have displayed, up to 95 % [4]. These systems employ several components that absorb incident light and efficiently transfer it to a reaction centre where charge separation can occur for energy production. Fluorescent proteins on the other hand were found to be used in the jellyfish *Aequorea Victoria* (*A. victoria*) for such reasons as predator evasion and signaling to other animals. The discovery of these proteins lead to much research surrounding their photostability and fluorescent properties as it was realised that they could have application in labelling of cells and could be highly beneficial in biology due to the higher resolution associated with fluorescence microscopy [5]. These systems will be addressed and introduce in this chapter as well as principles relating to their photophysics for the samples investigated in this work.

3.1 Fluorescent Proteins

3.1.1 History

Green fluorescent protein (GFP) and it's derivatives have been highly beneficial to the biological sciences since their discovery in the mid twentieth century, so much so that, *O.Shimomura, M. Chalfie* and *R.Tsien* received the 2008 nobel prize for chemistry for the discovery and development of GFP as a tool for research [6].

The mechanism of bioluminescence to produce energy from chemical reactions for the purpose of photon emission was initially recorded by *Davenport* and *Nichol* in a number

of marine animals, including *A. victoria* and other jellyfish [7]. They saw that, when stimulated with UV light certain cells on the bodies of the jellyfish would emit a green light, a discovery which lead to interest in the bioluminescence mechanism. *Shimomura* [8] was able to investigate the bioluminescence of the jelly fish *A.victoria* in great detail, carrying out investigations of samples in their native environment. From these investigations the active components of GFP were identified and two components relating to the bioluminescence were isolated. *Aequorin* was one of the proteins attributed to the fluorescence in these animals however, unlike the emission observed *in vivo*, this protein was recorded as being fluorescent in the blue at a wavelength of 470 nm. However, a second component isolated by *Shimomura et al.* showed the distinctive green fluorescence at 510 nm that was more familiar with *A. victoria* and thus was labelled GFP [9]. Continued work by *Shimomura* on GFP lead to discoveries on how GFP played a part in fluorescence energy transfer in *Aequorea*, as well as characterising its chemical structure and how the fluorescence varied under different physiological conditions.

At the time of discovery it wasn't realised how GFP could be applied to microscopy and biological investigations however, the work of *Shimomura* provided the information that was needed for the initial work to be carried out so that fluorescent proteins could be applied as biological markers. Successful cloning of the genes responsible for aequorin and GFP provided a basis to the work of *Chalfie* [10] to express these bioluminescent proteins in other organisms to be used as a versatile genetic marker. It was shown that after expression in *E.coli* the proteins maintained their fluorescent properties and as a result the expression of fluorescent proteins was conducted on complex organisms such as the nematode worm, *C. elegans* with the proteins expressed in the touch receptors to illuminate cell processes in the nervous system of the animal. The use of GFP as a biological marker has been realised as being a powerful tool for biological research with it's application to many more organisms from yeast to mamalian cells to fruit flies, in order to observe cell structures.

The discovery in the early 1990s that GFP could be used to label cells fluorescently, led to a period of heightened interest in fluorescent proteins leading to many developments to ensure they were even more suited to biological applications. Many variants of GFP

have been developed, with the chemical structure being altered in such a way to allow the excitation and emission wavelengths of the protein to be shifted, this has allowed a palette of colours to be developed with varying brightnesses and photostability that range from cyan (CFP) to the far-red (mPlum) [11]. Blue and cyan variants were the first to come from the *A. victoria* GFP and as a result have been developed significantly to yield greater brightness however, yellow fluorescent derivatives have displayed the greatest light yields of all the fluorescent proteins making it the most favorable of the proteins to use. Red variants although available, are relatively new and brightnesses are inferior to those of other colours. The development of different coloured fluorescent protein derivatives has been useful in allowing multicolour investigations to be carried out on cells by expressing different proteins in different areas of a cell. Designing brighter and more stable derivatives has allowed fluorescent studies to be carried out for longer before photobleaching of the proteins and to allow measurements to be conducted on most optical microscope systems.

3.1.2 Fluorescent mechanism

The bioluminescence mentioned in 3.1.1 is a mechanism that is important for animal survival which uses a chemical reaction to stimulate the emission of photons. Bioluminescent organisms employ an oxidation reaction for light production where a substrate (*luciferin*) is oxidised by an enzyme (*luciferase*), with oxygen normally acting as the oxidant. Isolation of the bioluminescent components of *A. victoria* revealed that two proteins were responsible for the characteristic green fluorescence, *aequorin* and GFP. Initial experiments by *Shimomura et al.* isolated *aequorin*, a protein that upon excitation emitted blue light whereas another fluorescent protein (that of GFP) accounts for the green fluorescence observed.

Light production by the *aequorin* protein differs to that of many other bioluminescent systems that employ the previously mentioned substrate-enzyme reaction using *luciferin* and *luciferase*. A major difference is that light is mediated through the presence of Ca^{2+} where the intensity of emission is dependent on the amount of Ca^{2+} present [12]. *Aequorin* in the presence of calcium has two distinct excitation peaks in the UV region of light at

280 nm and 350 nm, with a greater absorption at 280 nm [9]. Photon emission when excited at these wavelengths is detected at 465 nm. *Aequorin* is composed of two main units that of an apoprotein and coelenterazine which acts as a luciferin. Spontaneous reconstitution causes these two components to form a functional protein with 3 binding sites for Ca^{2+}, when calcium is bound to these sites under excitation, oxidation introduces a conformational change that turns coelenterazine into coelenteramide. The coelenteramide is also in an excited state which, upon relaxation emits a blue photon giving the protein its characteristic colour. *Aequorin* tends to be used as a calcium indicator in biological applications, not a fluorescent marker like GFP due to its lower emission intensities and stability.

GFP however is the dominant protein for bioluminescent colour in the native bioluminescent mechanism in *A. victoria*. The GFP protein contains a β barrel structure with a chromophore in the centre, a structure which helps to protect it from any fluorescence quenching induced by water. The absorption spectrum of GFP has two distinct peaks, one maximum peak at 398 nm and a smaller peak at 475 nm which although both having the same ground state arise due to differences in chromophore charge where a neutral form results in the maximum peak and an anionic form results in the lower intensity, longer wavelength peak [13]. Regardless of their absorption peaks, excitation of an electron in the chromophore leads to the emission of a photon at 510 nm. This chromophore is relatively stable and resistant to photobleaching when kept under the appropriate illumination conditions; where the 475 nm absorption peak is used for illumination (398 nm leads to rapid photobleaching), where temperatures are not high and where the pH is kept at a constant neutral value. The emission wavelengths and intensities can vary significantly under different conditions or when the protein is modified, it has been observed under low oxygen conditions that the emission peak of GFP shifts significantly to the red. Changes to the structure of GFP, such as those arising from denaturation lead to a loss of fluorescence this could be understood by rapid photobleaching or quenching of the chromophore by water when the protective structure is not present.

The presence of a blue light emitting protein in the green bioluminescent component of

the organism indicates that there is a specific interaction occurring between the two proteins. It is found that the blue luminescence from *aequorin* matches the longer wavelength peak in the excitation spectrum of GFP around 470 nm, with the green emission of GFP matching that of *A.victoria*'s bioluminescence. Spectral overlap between these two proteins indicates that there is energy transfer occurring between the two proteins. Energy transfer occurs through a non-radiative fluorescence resonance energy transfer (FRET) mechanism where the excited electronic dipole in the aequorin chromophore transfers energy to the GFP acceptor dipole in close proximity (around 10 nm), which relaxes to the ground state and emitting green light in the process.

3.1.3 Principles of fluoresence

Fluorescence techniques are valuable to the biological and life sciences as they have allowed naturally fluorescent systems and those tagged with fluorescent materials (e.g GFP) to be measured by spectroscopy or by fluorescent microscopy techniques, the latter revealing information about structure and processes present in cells and other biological systems. When understanding how fluorescent materials allow techniques such as fluorescent microscopy to be applied to biological systems it is necessary to understand the mechanisms and principles that give rise to the optical properties of fluorescence.

3.1.3.1 Photoluminescence

Luminescence is the process by which a photon is emitted by relaxation of an electron from an excited state. The situation where an electron is promoted to the excited state through the absorption of a photon is known as photoluminescence. Fluorescence is a form of photoluminescence where an optically excited electron undergoes internal energy transitions prior to relaxation to the ground state.

The mechanism involved in the absorption and emission of light are depicted in fig. 3.1.1. An incident photon, $h\nu_1$ is absorbed by the system and where the energy of the incident photon is sufficient then an electron from the ground state S_0 can be excited to a

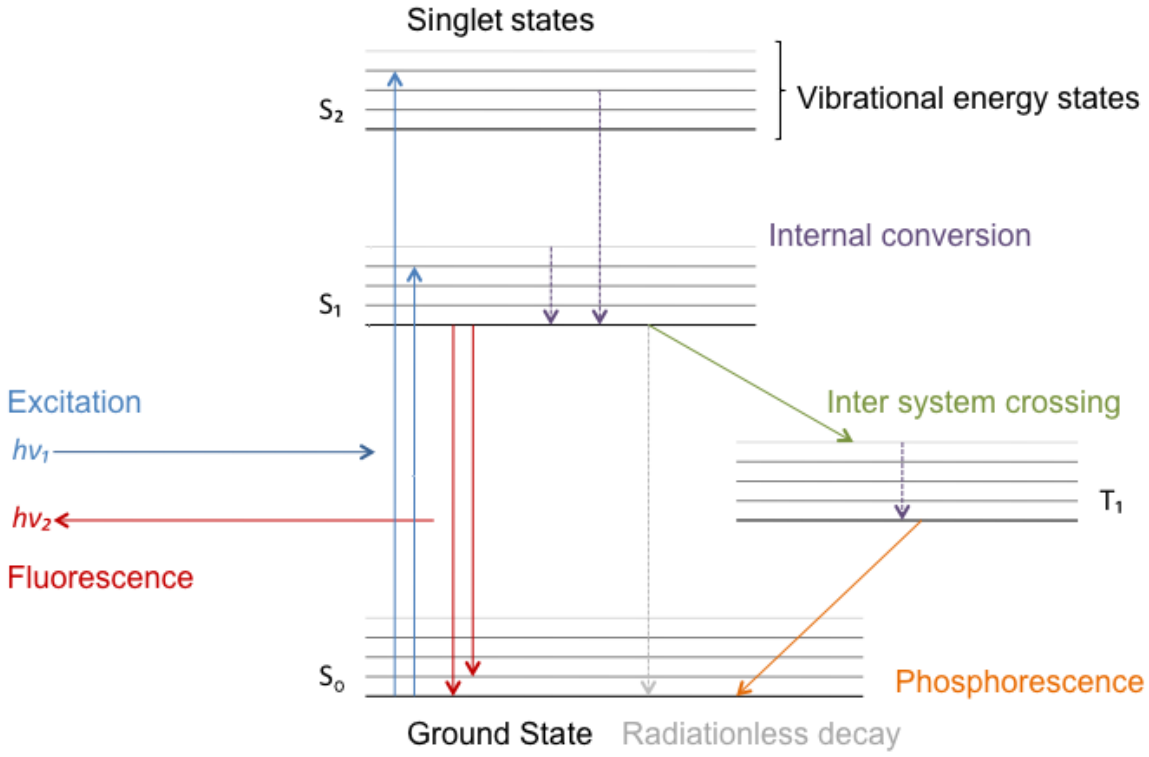

Figure 3.1.1: The Jablonski diagram showing the available energy states within a molecule as well as the available electronic transition pathways between the states.

higher energy orbital state $S_1, S_2 \ldots etc$, dependent on the excitation energy. An excited electron can occupy a number of different rotational and vibrational states within the higher energy states. Following excitation an electron usually occupies a higher vibrational level of the excited state followed by a rapid relaxation to the lowest vibrational level a process known as internal conversion, which is a non-radiative process as any excess energy is dissipated through molecular vibrations.

Photoluminescence can be divided into two types as a result of the nature of the excited states. Where an electron in an excited state has the opposite spin to one in the lower (ground) state they are deemed as paired, in this case the excited state-ground state transition is allowed and a photon is emitted, this being the process of fluorescence. Due to the internal conversion of the electron between vibrational states, the emitted photon $h\nu_2$ is of a longer wavelength than the absorbed photon $h\nu_1$. Internal conversion generally

occurs on the timescale of a picosecond and is complete before a photon is emitted due to the timescale of the fluorescence process being on the order of 10 nsec (typically, for most fluorophores).

Upon excitation by an incident photon there is a possibility that it may be converted to a parallel spin state (the triplet state T_1) by intersystem crossing which is a process forbidden by quantum theory (however it does occur) . In this case the two electrons are unpaired and share the same spin orientation forbidding them from sharing the same state due to the Pauli exclusion principle. To return to the ground state from the triplet state an electron must undergo a forbidden transition leading to emission of a photon by the process of phosphoresence. Due to the nature of forbidden transitions the rate constant of phosphoresence is magnitudes slower than that of fluorescence, on the order of milliseconds and shifted to much longer wavelengths making it unfavourable compared to the more frequently occurring process of fluorescence.

3.1.3.2 Spectra

The excitation/absorption spectrum of a fluorescent sample can be used to determine the energies required to raise the fluorophore to an excited state. The maximum absorption peak in a spectrum corresponds to the wavelength at which it is most effective to excite fluorophores to an excited state where the greatest number of photons can be absorbed and thus from where the greatest fluorescence intensity can be achieved. The minimum energy of an incident photon required to excite a fluorophore is that of the energy difference between the S_0 and S_1 energy states, this is represented in an excitation spectrum by a strong cut off to the spectrum when it is observed at longer wavelengths. The vibrational and rotational modes outlined in 3.1.3.1 are also observed in the excitation spectrum like that shown in Figure. 3.1.2 by a series of peaks and troughs relating to the small energy differences between the ground state and the different modes of S_1 (seen here in the high energy regime).

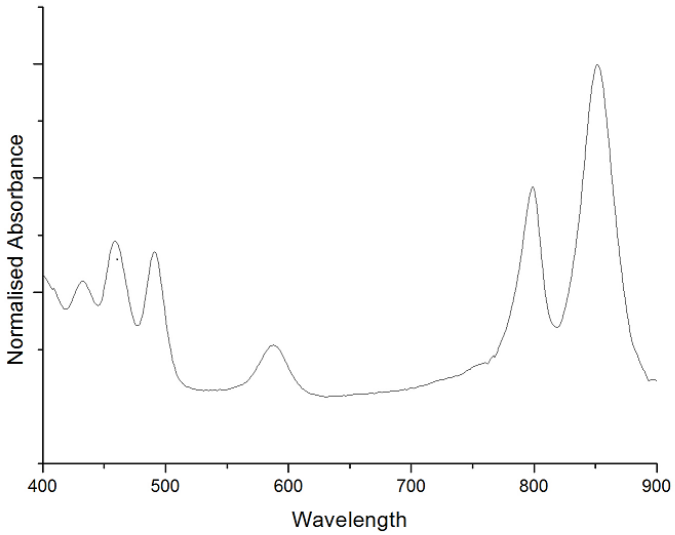

Figure 3.1.2: An absorption spectrum from LH2 isolated from *Rhodobacter Sphaeroides*. The main absorption peaks are displayed around 800 nm and 850 nm representing the BChl rings. The series of peaks between 400-600 nm a shown to represent a number of different vibrational modes in relation to the carotenoids.

Like the excitation spectrum, the emission spectrum can take a range of wavelengths relating to the energy differences of relaxation from S_1 to the various vibrational modes in S_0. However due to the internal conversion that takes place between the modes in the excited state the emitted photon tends to be of a lower energy than that of the initial absorbed photon. *G. Stokes* first recorded this phenomenon in 1852 which is thus referred to as the Stokes shift. Stokes shifts are observed in most fluorescent systems except when in a vapour phase, in these cases there is sometimes no shift due to the low gas concentrations. Collisions between molecules is a relaxation mechanism that is mediated through the vibrational modes, in the vapour case collisions occur infrequently removing this source of relaxation. In practice, samples with large Stokes shifts are desirable so that the fluorescence signal can be distinguished from the illumination source to prevent inaccuracies in the measurement. In cases where the electron occupies a higher vibrational mode in S_0 prior to excitation with a subsequent relaxation to the lowest state in S_0, the photon

emitted is of higher energy than that which was absorbed. This is known as anti-Stokes, which can explain any overlap in the excitation and emission spectra.

3.1.3.3 Photobleaching

In fluorescence imaging photobleaching is a highly detrimental effect when a fluorophore loses the ability to fluoresce due to structural damage occurring. Even though a fluorophore may go through many excitation/emission cycles photobleaching can occur as a result of prolonged light exposure as well as the excitation source being to high an energy/intensity. The precise method of photobleaching is not completely understood however it is believed to be associated with the formation of triplet states. Where triplet states are formed, the excited state lifetime is increased thus increasing the time in which a potential chemical reaction may occur (e.g. with oxygen) causing irreversible structural damage to the fluorophore.

3.1.3.4 Quenching

Quenching is another process that may reduce the intensity of the detected fluorescent signal however unlike photobleaching, quenching is a reversible process that doesn't occur due to sample damage. The process of quenching decreases the fluorescence intensity (and the fluorescent lifetime) of a substance by acting as a competing non-radiative excited state relaxation process. Quenching is an undesireable process when using fluorescent samples due to the reduction of the fluorescent intensity however, due to it being a reversible process it has applications to detect the presence of quencher molecules (e.g. molecular oxygen), the diffusion rates of quenchers in solvents of varying viscosity and to measure the permeability of cells to quenchers where fluorophores are localised within a protein/cell membrane.

Quenching may happen through different mechanisms the most common being collisional quenching and static quenching. Collisional quenching originates from a diffusive

encounter of a quencher with the fluorophore. Where an interaction occurs within the excited state lifetime of a fluorophore, the fluorophore experiences an induced non-radiative relaxation. The collisional quenching processes only affect the excited state of the fluorophore therefore, there is no affect on the absorption spectrum of the sample, only the emission. In the static quenching processes a non-fluorescent complex is formed between the fluorophore and the quencher, this complex absorbs light and immediately relaxes to the ground state; without the emission of a photon the energy from the non-fluorescent component can lead to effects such as heating and structural change in the complex. Static quenching can inflict changes on the absorption spectrum due to the formation of the non-fluorescent complexes in the ground state [14].

3.1.3.5 Fluorescence lifetimes

The fluorescent lifetime of a sample relates to the average time that an electron resides in the excited state prior to the emission of a photon. The fluorescence intensity of a fluorophore is directly proportional to the number of molecules located in the excited state that are available to emit photons therefore, by measuring the fluorescence intensity of a sample after excitation one can reveal the lifetime of fluorescence. The time it takes for an excited molecule to return to the ground state follows an exponential dependence which is given by:

$$I\left(t\right) = I_o\, e^{-t/\tau} \tag{3.1.1}$$

where $I(t)$ is the intensity which is a function of time t, I_0 is the fluorescence intensity at $t = 0$ and τ is the fluorescence lifetime [14].

As previously mentioned in 3.1.3.4 fluorescence competes with a number of different non radiative pathways therefore, with fluorescence lifetime being a measure of the average time a molecule remains in it's excited state, both decay processes must be taken into

account. The decay rate of both fluorescent and non radiative processes are represented in the fluorescent lifetime,

$$\tau = \frac{1}{\kappa_f + \kappa_{nr}} \tag{3.1.2}$$

where κ_f and κ_{nr} are the decay rates of the fluorescent and non radiative processes respectively.

3.1.3.6 Quantum yield

The quantum yield of a fluorophore is represented by a ratio between the number of photons absorbed by a fluorophore and the number emitted. As a result the quantum yield measures the number of incident photons that yield an emission and represent the emission efficiency of a fluorophore, given by:

$$\phi = \frac{number\,of\,emitted\,photons}{number\,of\,absorbed\,photons} \tag{3.1.3}$$

Quantum yields can vary across a large range from 0 to just under 1, with some biological systems reaching values that approach 1. The numer of absorbed photons is a value that encompasses the fluorescent and non-radiative process occurring within a sample and can affect the number of photons emitted. As mentioned in 3.1.3.4 for example, the environment can affect the emission of photons and thus the quantum yield of a sample can vary dependingly. The quantum yield of a sample could also be reduced by an increased occurrence of intersystem crossing and phosphorescence, a high quantum yield suggests that the level of intersystem crossing is kept low as are the potentially destructive processes due to increased excited state lifetimes (such as photobleaching).

3.1.3.7 Förster Resonance Energy Transfer

It has been mentioned in 3.1.3.6 and 3.1.3.4 that there are a number of non-radiative pathways that an excited fluorophore can employ to return to its ground state. One method is that of Förster resonance energy transfer (FRET) which often occurs in biological systems, e.g in photosynthetic systems to transfer energy to the reaction centre. Energy transfer in a FRET system occurs without the emission of a photon and is primarily the result of dipole-dipole interactions between a donor-acceptor pair. Interactions between the acceptor and donor dipoles come from dipole coupling the resonant frequencies of these being similar.

The rate of energy transfer in FRET is dependent on properties relating to the dipoles like the separation distance of the pair, the overlap of the donor emission spectrum and the absorption of the acceptor and the relative orientations of the dipoles. The rate at which energy is transferred between the donor and acceptor (κ_T) is defined as:

$$\kappa_\tau = \frac{1}{\tau_d}\left(\frac{R_0}{r}\right)^6 \tag{3.1.4}$$

where the lifetime of the donor in the absence of an acceptor is given by τ_d, r is the distance between the two dipoles and R_0 is a characteristic distance usually between $2-10$ nm, this is known as the Förster Radius where transfer efficiencies are 50 %. The dependence of the transfer efficiency (E) in respect to the distance can be shown by:

$$E = \frac{R_0^6}{R_0^6 + r^6} \tag{3.1.5}$$

One can see that when the radius is equal to the Förster Radius then the efficiency is 50 % of that observed in the absence of an acceptor, which is a small length scale as determined by the r^6 dependence.

The strong dependence of FRET on the distance between donor-acceptor pairs makes it a useful tool for determining distances between pairs, for example, it has been used to estimate distances between protein binding sites and the distances between chromophoric groups of proteins [15]. For these applications FRET can be detected where there are changes to donor fluorescent lifetimes, increases in the acceptor fluorescence intensities and changes to the polarisation of emitted light. A way to use FRET to conduct such measurements is to measure photobleaching of the acceptor where, the acceptor molecule is bleached in a way that the only fluorescent signal comes from the donor. In this case, the donor molecule can be excited and the emission from the two measured simultaneously of each other. Comparison of the fluorescence intensities can allow a transfer efficiency to be obtained that can be applied to the FRET calculations previously mentioned.

3.1.4 Applications of fluorescent proteins

Since their discovery fluorescent proteins have found application in many aspects of biology, particularly when applied to microscopy and cell biology. However, fluorescent proteins have also been applied to to other processes to show energy transfer pathways, as biological lasers, in medical research and for pharmaceutical applications.

3.1.4.1 Immunofluorescent labeling

The most important application of fluorescent proteins has been to use them in conjunction with fluorescence microscopy to label cells in a number of organisms in order to record cell structures and processes. The first noted example of this technique was that by *Chalfie,* as previously mentioned in 3.1.1, on the nematode worm *C.elegans*. After realising biological GFP would be favourable for cell labelling, *Chalfie* managed to successfully label the touch receptors of the nematode and through excitation of the GFP was able to pinpoint where they were located through fluorescence microscopy analysis. By positioning the GFP gene behind a protomer that is active in the nematode's touch receptor neurons, this could be injected into the sexual organs and is passed onto the eggs produced by the hermaphroditic

worm. This gene is therefore present in all cells of the new generation and can fluoresce when illuminated with ultraviolet light (or blue light).

As well as being applied to cellular processes in organisms such as *C. elegans,* fluorescent proteins have been applied to other organisms such as yeast. Differing from the work of *Chalfie* that used a gene switch to label cells, GFP has been used to identify localised regions containing unknown proteins found in the gene sequence of yeast. GFP has also been used in yeast species to study intracellular transport processes [16], metabolism [17] and cell cycle progression [35]. The rapid growth of yeast makes it desireable to study and use in modelling these processes.

Similar to that in the nematode flat worms, GFP has been used in mammalian cells to analyse protein dynamics and the function of living cells. Unlike previous methods of characterising protein/cell localisation which required fixation and thus a modification to samples to gain information from techniques such as electron microscopy. The introduction of GFP chimeras into a cell allow measurements to be conducted through photoactivation techniques whilst the cell remains unperturbed. This has been used to measure protein dynamics where specific GFP chimera populations (that may differ slightly in spectral qualities) can be activated or photobleached to study the movement of these throughout a body or across certain boundaries [18]. Furthermore, GFP has also been used to study mammalian cells by incorporating GFP into the nucleus of a cell to study nuclear behaviour and to study aspects of the cytoskeleton.

3.1.4.2 FRET pairs

Fluorescent proteins are often used as donor-acceptor pairs to quantify molecular dynamics when conducting FRET studies of biological samples. The CFP and YFP varients of GFP are most commonly used, acting as donor and acceptor respectively. Introduction of these fluorescent proteins to molecules and cells can be combined with FRET to measure such properties as diffusion across specific boundaries and to measure how labelled molecules mix [19]. Conformational properties of proteins can also be measured using fluorescent proteins combined with FRET by attaching the donor and acceptor at two different loci.

As the protein undergoes conformational change the distance between these change which is reflected by a change in the rate of energy transfer. The ability to introduce fluorescent proteins into a host via genetic engineering makes using them favourable over organic fluorescent dyes that require purification and chemical engineering.

3.1.4.3 Biological lasers

Recent studies of fluorescent proteins have realised their potential as single cell biological lasers. *Gather et al.* managed to induce laser action in a single mammalian cell that had be transfected with a mutant form of GFP [20]. The mammalian muscle cell (containing GFP) was suspended within a resonator cavity constructed from 2 highly reflective distributed Bragg reflectors and pumped with a nanosecond laser inducing lasing from the GFP in the $510 - 520$ nm range. Throughout the lasing process minimal photobleaching occurs to the active cell due to regeneration of the protein. Although this is a relatively new application for GFP it's future applications may reside in 3-dimensional imaging of cells.

3.1.4.4 Pharmaceutical applications

GFP and its variants are in widespread use in the pharmaceutical industry within the early phases of drug discovery. One type of drug screening is that designed for the discovery of molecules that have activity when interacting with a particular protein [21]. Proteins of interest can be investigated with fluorescence microscopy by labelling them with fluorescent proteins. The protein can then be imaged with high precision whilst a molecule of interest interacts with it, for example this can be used to see how a molecule can slow cell division. This process allows drug companies to determine whether a molecule affects a cell in the same way as a specific disease. Specific proteins maybe also be labelled with fluorescent proteins to see how they interact under specific stimuli, for example this may be the introduction of a disease or drug.

3.2 Photosynthetic bacteria

Light incident on the surface of the Earth is converted through photosynthesis into chemical energy by plants, algae and photosynthetic bacteria. The latter are investigated in this study and can be split into two groups, that of cyanobacteria (green photosynthetic bacteria) which carries out oxygenic photosynthesis in air and that of purple photosynthetic bacteria which carries out anoxygenic photosynthesis where molecules other than water are oxidised in the energy production process. In this thesis the anoxygenic photosynthetic bacteria are of interest and are addressed and used.

3.2.1 History

One of the first types of photosynthetic bacteria to be discovered was that of purple anoxygenic bacteria which have sulfur as a byproduct and not oxygen. This was noticed in the early 1900s with the discovery of two types of phototrophic bacteria that formed globules of elemental sulfer within the cells, it was later noted that purple bacteria actually formed sulfur on the outside of the cell.

3.2.2 The Photosynthetic Unit (PSU)

The bacterial PSU is designed in such a way that it will absorb light and efficiently transfer it to a reaction centre where charge separation takes place. Photosynthetic bacteria is arranged so that light harvesting antenna complexes are used to increase the absorption area of the bacterium. A bacterium normally has more than one light harvesting complex to absorb light as well as the ability to transfer energy between complexes through non-radiative energy transfer.

3.2.2.1 Light Harvesting Complex 2 (LH2)

The function of antenna complexes in photosynthetic bacteria is to absorb photons in order to direct energy to the reaction centre. For this work complexes from the bacterium

Rhodobacter Sphaeroides will be used and therefore addressed accordingly. The main light absorbing pigments present in light harvesting antenna complexes are those of bacteriochlorophyll (BChl) *a*, *b* (BChl with varying structure and as a result optical properties) and the carotenoids. The arrangement and binding of these determine the absorption wavelengths which distinguishes between LH1 and LH2.

The structure of LH2 unit, shown in Figure. 3.2.1, is based on a heterodimer of two short peptides, the α-apoprotein and β-apoprotein, these two helices arrange into a dimer binding both BChl and the carotenoids to it. Several of these heterodimer pairs arrange to form larger oligomer structures varying in size between species of anoxygenic bacteria. The structure of LH2 is that of an $\alpha_9\beta_9$ nonamer that forms a cylindrical structure where the inner walls are formed from a ring of 9 α-apoprotein α helices and the outer walls formed from 9 β-apoprotein α helices, with dimensions where, the inner wall has a radius of 18 Å and the outer of radius 34 Å. This cylindrical structure has both a closed top and bottom due to the folding of the α helices at the N- and C- termini [22].

All the pigments that are responsible for the function of the LH2 complex reside between the inner and outer walls of the α helix cylinder. The BChl-*a* molecules are arranged into two specific groups that can be primarily distinguished between by their spectral qualities. Positioned towards the cytoplasmic side of the complex (N-terminal) is a ring of 9 monomeric BChl-*a* molecules, one per apoprotein pair separated by a centre to centre distance of 21.2 Å. These molecules named the B800 molecules absorb light at a wavelength of 800 nm, as their name suggests, and lie flat in the plane of the complex (perpendicular to the α helices) [23].

A second ring positioned towards the periplasmic face of the complex contains the 850 nm absorbing B850, BChl-*a* molecules. These tightly coupled BChl-*a* molecules form a ring of 18 molecules with 2 molecules assigned to each apoprotein pair. The two B850 molecules assigned at each apoprotein pair are separated by 9.5 Å with the separation between B850 pairs being 8.2 Å. In contrast to the B800 ring, the B850 ring lies parallel to the α helices, vertical in the plane of the complex [23].

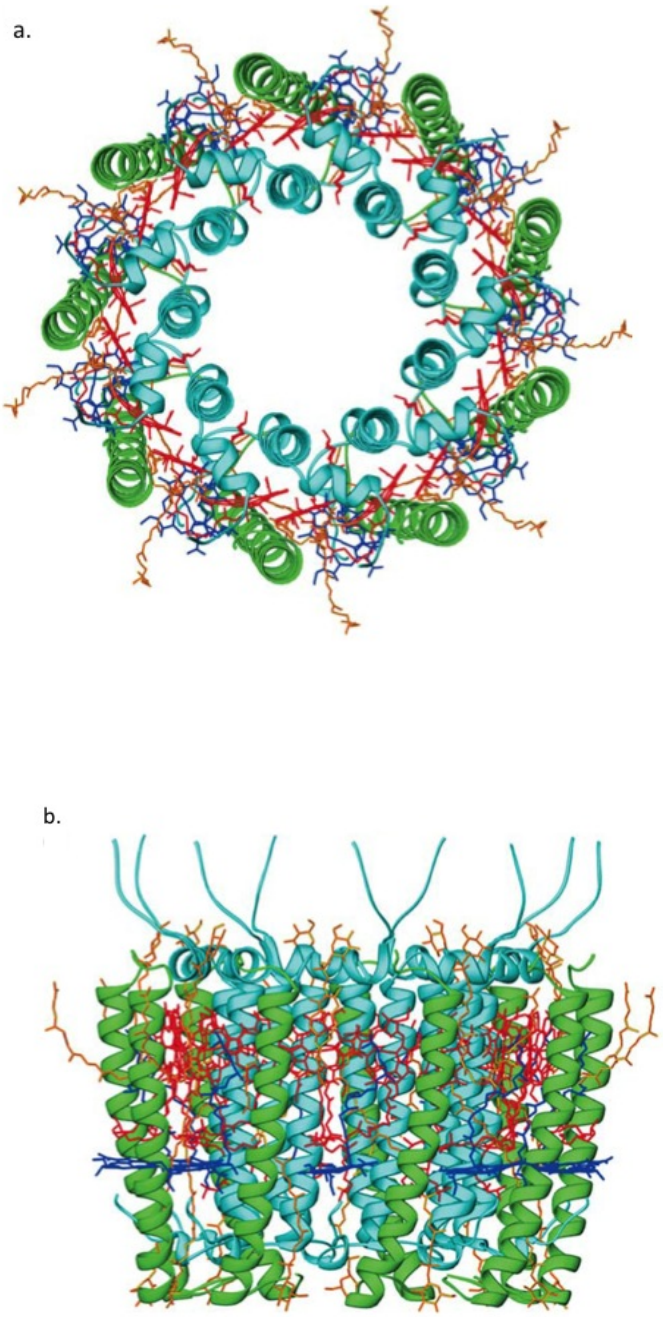

Figure 3.2.1: Structure of the LH2 complex (a) normal to the membrane plane (b) perpendicular to the membrane plane. Green and cyan represent α,β apoproteins respectively, red - B850 BChl-a, dark blue - B800 BChl-a and brown - carotenoids.

In the LH2 complex two carotenoid molecules are found per apoprotein pair which aid light harvesting by increasing the range of the absorption spectrum by, protecting the BChl molecules from photoxidation and playing a structural role in the complex. One carotenoid spans the complex starting at the cytoplasmic side of the complex in one apoprotein pair, passing via van der Waals contact with the edge of the B800 ring before proceeding to cross over to the next apoprotein pair where again it comes into van der Waals contact as it passes over the face of the B850 ring. This carotenoid essentially bolts the apoprotein pairs together playing a major structural role, which has been shown in mutants of LH2 lacking carotenoids. In these mutants the LH2 complex fails to assemble due to the lack of binding between apoprotein pairs. A second carotenoid is found associated with each apoprotein pair that lies along the outside of each apoprotein pair [24].

3.2.2.2 Light Harvesting Complex 1 (LH1)

The LH1 structure, shown in Figure. is one that is closely tied with the reaction centre of the photosynthetic unit (PSU). Similarly to the structure of LH2, LH1 forms a ring of repeating of heterodimer with a 16-fold repetition of $\alpha\beta$-apoprotein pairs arranged to form a hollow cylindrical structure with the α-apoproteins forming the inner wall and the β-apoproteins forming the outer wall. The LH1 complex is larger than that of LH2 with the inner ring of helices forming with a diameter of 78 Å and the outer ring forming a ring with a diameter of 108 Å [22].

Each apoprotein pair contains 2 BChl-a molecules, that are bound between the helices and are orientated along the vertical axis of the complex (perpendicular to the plane of the membrane). These BChls overlap similar to those of the LH2 ring so that the orientation of BChl in the LH1 ring means that they absorb light further into the near infrared region at 875 nm. The LH1 complex also contains a carotenoid molecule bound to each apoprotein pair, unlike that of LH2 however the carotenoid molecule at each point in LH1 has a major role in the light absorption and photoprotection and a much smaller role when it comes to aiding the structure of the ring [22].

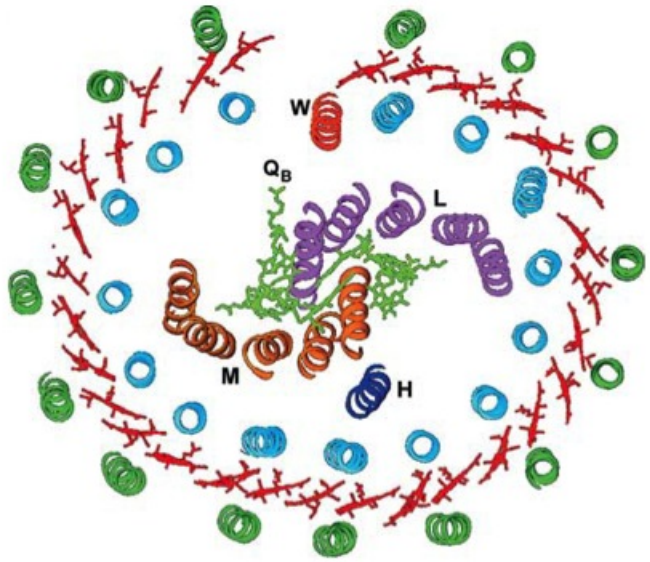

Figure 3.2.2: An example structure of the RC-LH1 from *Rhodopseudomonas palustrls* differing from *Rhodobacter Sphaeroides* with a 15 fold apoprotein structure. Viewed perpendicular to the plane of the membrane, green - β-apoprotein, cyan - α-apoprotein, red - B875 BChl-a, mauve - RC L-subunit, brown - RC M-subunit, light green - RC pigments and light red - protein 'W'. [36]

It has been shown in studies of the LH1 complex ring that the central diameter was of a similar size to the reaction centre which had been measured through x-ray measurements. This led to the theory that the LH1 ring housed the reaction centre in the middle of the cylindrical structure, which was later confirmed in similar measurements on wild type bacteria. The presence of the reaction centre explains the major difference in the function of carotenoids in the two light-harvesting complexes. The LH1 ring is bound to the reaction centre that it forms around therefore, this has the largest affect on the shape of the ring, where it has been shown in experiments where the reaction centre has been removed. Here rings may form due to carotenoid aided structure however, the rings are flexible and without

a reaction centre they form a multitude of shapes from circles to ellipses to horseshoes.

3.2.2.3 The Reaction Centre (RC)

In photosynthesis the reaction centre is important for the conversion of energy from an incident photon into chemical energy through charge separation. The reaction centre contains 3 protein subunits known as the light, medium and heavy subunits (L, M, H respectively) with multiple pigment molecules bound to the L and M units which arrange symmetrically into two branches (A and B). To each of these branches a BChl is attached forming a strongly interacting dimer known as the 'special pair', two more BChl are also found in close proximity to this pair. As well as BChl the reaction centre also houses 2 bacteriopheophytins and a pair of quinones located on two branches that also house the special pair [25].

3.2.2.4 The PSU *in vivo*

In vivo studies of the PSU have allowed the the arrangement of antenna complexes and the reaction centre to be visualised allowing for an increased understanding into how the photosynthetic bacterium can successfully absorb and transfer energy at high efficiencies. The size of the PSU and the arrangement of complexes within it contains some heterogeneity, the degree of which varies with the growth conditions. Variations in the intensity of light and temperature have an immediate effect on the growth of the PSU. The complexes are arranged in a way so that a large number of LH2 complexes surround that of the LH1 which houses the reaction centre to maximise energy transfer from this peripheral antenna complex to the reaction centre which are within a distance that maximises FRET [26].

3.2.2.5 Excitation transfer in the PSU

Light harvesting and excitational energy transfer are mediated by the BChl and carotenoid chromophores, other proteins in the structure of the PSU's light harvesting components serve purely as the structural scaffold. The chromophores in each component of the PSU

have developed to form a hierarchy of excitational and interacting energy states which efficiently funnel energy from incident photons from LH2 through LH1 and to the reaction centre. The excitation transfer present in the PSU occurs through the non-radiative Förster mechanism described in 3.1.3.7.

In LH2 complexes, the B800 BChl ring plays a role in maximising the absorption cross-section and thus the number of photons that the PSU can utilise for energy production. The B800 chromophores also maximise the absorption cross-section through their orientation which is perpendicular to that of both B850 and B875 BChls. Upon photon absorption fast efficient excitation transfer can occur between individual B800 BChl and the B850 ring. By looking at the absorption and emission spectra of the different BChl species it becomes apparent that this can occur through the Förster mechanism. There is a large degree of spectral overlap between the emission of the B800 BChls and the excitation peak of the B850 ring allowing non-radiative transfer to occur between them (the rate of transfer determined by the distances between the two). Transfer between different LH2 complexes may also be observed in these systems as shown in studies of LH2 only membranes. Excitation energy is transferred from the BChls in the B800 ring to those in the B850 ring where the energy is rapidly delocalised around the ring. The delocalisation of the energy around the ring allows fast and efficient transfer to the LH1, so that the orientation and location of complexes in the PSU do not affect the ability to harvest energy. In a standard PSU there is an abundance of LH1 to accept the energy however, in a system where there is a much greater abundance of LH2 than LH1 it is not always possible for the B850 ring to transfer energy to the BChls in LH1 if it is already in an excited state and waiting to transfer energy to the reaction centre. In this case excited B800 molecules may transfer excitation energy to a different LH2 complex if its B850 ring is already in an excited state and thus long range energy transfer has been observed in linear arrays containing only LH2 by *Escalante et al* [27].

Calculations have shown that transfer between LH2 and LH1 occurs on a timescale that is slower than the LH2 B800-B850 transfer arising from the larger length scales involved between the two. Energy transfer to LH1 complexes originates from several exciton states

in the LH2 B850 ring and like in the B800 ring, energy that is transferred to the LH1 BChl ring is rapidly delocalised [28]. The rapid delocalisation in these two BChl rings acts to allow excitation transfer from any point thus maximising the chance of transfer along the PSU chain. The final energy transfer process between the LH1 B875 ring and the reaction centre takes the longest, the greater distance between the B875 ring and the RC special BChl pair than any other transfer step present in the PSU means that transfer at this point takes place on the scale of tens of picoseconds [1].

The absorption and transfer of excitation energy in the bacterial PSU is not solely dependent on the BChl molecules/rings but is also reliant on the carotenoids to aid absorption. Carotenoids are able to absorb radiation in the visible region of the electromagnetic spectrum, a region that is inaccessible to BChls which absorb in the near infrared regime. Variations to the absorbing S_2 energy level is seen in different species of photosynthetic bacteria an effect that arises as a result of differences in the number of conjugated bonds present in the carotenoid. In carotenoids the incident photon excites the electron into the S_2 which procedes to relax via internal conversion to the optically forbidden S_1 lower energy state. Energy transfer occurs (predominantely to the B800 BChls) due to the S_2 and S_1 energy states of the carotenoids being similar to that of the Q_x and Q_y excited states in the BChls. As a result two energy pathways occur, that of $S_2 \rightarrow Q_x$ and that of $S_1 \rightarrow Q_y$, the former via the Förster mechanism and the latter through a coulomb mechanism. Transfer from the S_2 state is the favorable carotenoid to BChl energy pathway due to less excitation energy loss, however both pathways are important in maximising energy absorption and transfer across the incident electromagnetic spectrum.

3.2.3 Photodamage

The PSU can suffer due to a number of damaging effects which can contribute to a reduction in the unit's ability to efficiently transfer excitational energy and convert it to chemical energy in the reaction centre. One damaging effect is that to do with heating in the PSU which can cause damage to proteins in the system, particularly the light harvesting pro-

teins. Even though light is important for energy production in photosynthetic organisms, high intensity light absorbed by the chromophore can cause photoactive proteins in the vicinity to heat up to temperatures around 200 °C in a matter of microseconds [29]. From this it can be seen that continued excitation from high intensity light can have a severely damaging effect on proteins.

A key source of damage to the PSU occurs due to the formation of singlet oxygen a powerful oxidising agent that, upon contact with a cell or cell components can cause irreversible damage which inhibits the PSU's ability to harvest, transfer or convert excitational energy into chemical energy. Singlet oxygen is formed through a combination of light, oxygen and excited BChl molecules:

$$\begin{aligned} BChl + h\nu &\rightarrow {}^1BChl^* \\ {}^1BChl^* &\rightarrow {}^3BChl^* \\ {}^3BChl^* + O_2 &\rightarrow {}^1\Delta_g O_2^* + BChl \end{aligned} \tag{3.2.1}$$

Eq. 3.2.1 shows the process by which singlet oxygen is produced in photosynthetic bacteria [30]. BChls excited into their singlet state undergo intersystem crossing placing them into the triplet state, this longer lived state allows a greater amount of time for molecular oxygen to come into contact with the BChl where the occurrence of this creates singlet oxygen and relaxes the BChl. Damage due to oxidation is reduced by the presence of carotenoids as well as having both structural and light harvesting roles, they also provide photoprotection against singlet oxygen effects. The photoprotection properties of carotenoids are achieved through two processes, that of quenching singlet oxygen directly

$$\begin{aligned} {}^1\Delta_g O_2^* + Car &\rightarrow {}^3Car^* + {}^3O_2 \\ {}^3Car^* &\rightarrow Car + heat \end{aligned} \tag{3.2.2}$$

or by quenching the triplet state BChl

$$^3BChl^* + Car \rightarrow {}^3Car^* + BChl$$
$$^3Car^* \rightarrow Car + heat \tag{3.2.3}$$

In both of these cases the carotenoid provides a relaxation pathway for the excitation energy. In the process of quenching the singlet oxygen the carotenoid is promoted to the triplet state whilst reducing the energy of the singlet oxygen thus converting it to its triplet state which isn't harmful to the PSU. The dominant BChl quenching reaction allowing relaxation of the BChl triplet state by promoting the carotenoid to its triplet state, this reaction occurs on the timescale of nanoseconds, 3 orders of magnitude faster than the timescale of singlet oxygen formation and it has therefore been speculated that under physiological conditions singlet oxygen isn't generated [24, 31].

3.2.4 Variations/Evolution

Like most other organisms, there are different species of anoxygenic photosynthetic bacteria that vary in a number of different ways between one another. There are several types of anoxygenic bacteria that contain a similar PSU structure in regards to light harvesting antenna complexes which funnel light to the reaction centre, it is however the difference between these that lead to the difference in species. One difference is that some species of photosynthetic bacteria contain a third light harvesting complex (LH3). Variants of the species *Rhodopseudomonas acidophilia* and *Rhodosprillum molischianum* contain this third complex, its presence is determined by the growth conditions and the ambient light conditions present at this time [32]. The LH3 complex's BChls absorb at 800 and 820 nm [33], similiar to that of LH2 and like the relation between LH2 and LH1 excitation energy is funelled down from it through the other complexes to the reaction centre. Some species also show a variation in the structure of the light harvesting complexes. The structure of LH2 in *Rhodobacter Sphaeroides* has been addressed in 3.2.2.1, however a difference to

the nonamer structure can be seen in the LH2 complex in *Rhodosprillum molischianum* which has a ring based on an octamer arrangement of apoproteins [34]. This species also displays a different arrangement of the LH1 ring following a hexadecamer arrangement of apoprotein pairs not the 16-fold arrangement that is inherent in *Rhodobacter Sphaeroides*.

3.3 Chlorosomes

The evolution of photosynthetic bacteria in different environments has led to the development of additional light harvesting antenna systems which aid light harvesting and maximise the number of photons in an environment that are available to be funneled to the reaction centre for charge separation. Chlorosomes are organelles associated with the green sulfur variant of photosynthetic bacteria and not the afore mentioned purple anoxygenic bacteria. Further to them being associated with green photosynthetic bacteria, chlorosomes are also found in some filamentous anoxygenic phototrophs (known as green non-sulfer bacteria) and in some aerobic phototrophs.

3.3.1 Structure

Chlorosomes are the largest antenna structures known in nature and their structure allows them to efficiently harvest incident photons under low light conditions. Chlorosomes are zeppelin shaped sacks which can hold anywhere up to hundreds of thousands of BChl molecules. Where *Rhodobacter sphaeroides* contained BChl-a molecules in the light harvesting complexes, chlorosomes contain several types of BChl with the c, d and e varieties. The type of BChl and the number of each variety depends on the species of bacteria that the chlorosomes reside within. Depending on the species, chlorosomes typically contain the three types of BChl mentioned in differing concentrations which is reflected in the small spectral differences observed between chlorosome species. On average a single chlorosome can contain around $200,000$ to $250,000$ BChl-c and d molecules (determined by species) as well as $2,500$ BChl-a molecules. Further to this, single chlorosomes can

contain around 20,000 light harvesting and photoprotective carotenoid molecules, 18,000 quinone molecules and 20,000 lipid molecules. The majority of pigment-proteins present in the chlorosomes are arranged through self-assembly similarly to other photosynthetic bacteria and unlike green plants which require a protein scaffold for assembly. The self-assembly of the chlorosomes see them arrange into elongated tube like vesicle structures that have lengths between 100 and 200 nm and widths between 40 and 60 nm, on average. The sizes of chlorosomes have been recorded since their discovery in *Chlorobium thiosulphatophilum* by *Cohen-Bazire et al.* as well as with the discovery of chlorosome presence in other bacterial species such as *Chlorobaculum tepidum* and the filamentous bacterium *Chloroflexus aurantiacus.* In the measurement of these chlorosomes with such techniques as electron microscopy it has been possible to observe variations between species such as the overall volume of some chlorosomes varying by a factor of 5 and the overall shape of the chlorosomes which may take the mentioned zeppelin form as well as conically shaped forms and irregular forms.

The location of chlorosomes in the bacterial PSU is such that incident photons that are harvested by the BChl are quickly and efficiently directed towards a reaction centre, similar to the process that is seen in the PSU of the purple photosynthetic bacteria previously mentioned. The chlorosomal envelope is attached to the cytoplasmic membrane by a baseplate containing BChl-*a* which provides a pathway for the excitation energy harvested by the BChl present in the chlorosomes to be transferred to the reaction centre housed within the cytoplasm. Most of the BChl-*a* molecules that are present in the chlorosomes in these species of green sulfer bacteria are located within the baseplate and act to mediate energy transfer between the chlorosome envelope and the reaction centre.

3.3.2 Light Harvesting

Chlorosome structure and its position within the PSU is mentioned in 3.3.1, properties that are associated with the structure play a role in the light harvesting process and allow efficient energy transfer of incident photons to the reaction centre so that the small number

of photons present in the bacteria's natural environment can be utilised. The process of light harvesting and energy transfer draw similarities with the processes involved in the photosynthetic bacteria previously mentioned in 3.2, where light is collected by BChl and directed through other components to the reaction centre.

Chlorosomes species contain populations of hundreds of thousands of BChl molecules, the variety of BChls depending on the species of bacteria that they reside within. The concentrations of the different BChl molecules in the environment of the chlorosome contribute to the variations in the absorption wavelength of the different species. Although the BChl when aggregated in the chlorosomes provide different absorption properties for each type the absorption wavelengths are located in the 700-750 nm regime with chlorosomes absorbing photons close to the NIR region of the electromagnetic spectrum. The aggregated states of the BChls differ significantly to their monomeric states with large redshifts observed due to strong excitonic interactions present within the chlorosomal structure. The strong coupling strengths between nearest-neighbour pigments allow rapid delocalisation of the excitations from incident photons across tens of pigments with transfer times between pigments on the order of tens of femtoseconds. As a result of the rapid delocalisations the excitations are able to travel extremely fast throughout the chlorosomes. The organisation of the pigments in the chlorosomes may also affect the excitation energy transfer throughout the chlorosome through slight variations in the distances between pigments.

In the transfer of excitation energy from BChl light harvesting in the chlorosomes to the RC a BChl-*a* containing baseplate is employed. The excitation energy in the chlorosome flows through the BChl molecules and a small CsmA protein embedded within the baseplate. The presence of this BChl-*a* containing baseplate which absorbs at longer wavelengths than the BChl contained within the chlorosome envelope improves the transfer efficiency to the reaction centre significantly. The baseplate, although not containing as many BChls still contains a large number of BChl-*a*. The large number of BChl present in the baseplate which have excited state energy levels below those of the BChls present in the chlorosomes leads to a fast excited state population in the baseplate. The presence of the baseplate allows the transfer between the chlorosomes to be largely increased. The transfer

between the baseplate and the RC is around 50 times faster than that which would occur directly between the BChl in the chlorosome and the RC, this occurs due to a number of reasons relating to the difference in the number of BChl in the chlorosome and baseplate as well as properties of the overlapping donor and acceptor spectra and relative orientations of the transition dipole moments. The energy is transferred to the RC which acts similarly to that present in purple bacteria where the BChl-*a* acts as a donor to the RC which with the excitational energy is able to initiate energy production through charge separation.

3.3.3 Spectral Properties

The spectral properties of the chlorosomes, as mentioned, are dependent on the populations of the different types of BChl present which each have varying spectral properties in monomeric and aggregated states. Due to the number of BChl present in the chlorosomes being much greater than that in the baseplate, the spectral properties mostly depend on the populations in the chlorosomal envelope. The maximum absorption of chlorosomes reside between 700-750 nm with slight variations in the species arising through BChl populations and small environmental differences in the chlorosomal envelope pertaining to orientations of BChls induced by packing. It has been documented that chlorosomes containing mostly BChl-*c* have an absorption maximum around 740 nm whereas chlorosomes that contain higher proportions of BChl-*d* or *e* have maximum absorption peaks around 725 nm and 712 nm respectively. Further to the absorption peaks that can be attributed to the presence of BChl further absorption peaks can be observed which like in the spectra with LH2 previously mentioned can be attributed to the presence of carotenoids. Carotenoid peaks are observed in the 400-550 nm region, similar to this seen in the purple photosynthetic bacteria previously mentioned in this work. The presence of the carotenoids in this region allow singlet oxygen quenching and prevention to occur as well as increasing the absorption wavelength cross section for the chlorosomes thus allowing light towards the blue end of the spectrum to be harvested and transferred to the BChls and thus onto the reaction centre. Excitation spectra from chlorosome species may also show evidence of the BChl-*a*

pigments which reside in the baseplate, this leads to the observation of absorption peaks around 820 nm however, as mentioned previously this peak if present in the excitation spectra of the chlorosome species is small due to the relatively low number of BChl-*a* in the baseplate compared to BChl-*d* and *e* in the chlorosomes.

3.4 Summary

This chapter outlines the large body of research and the mechanisms by which the biological samples in this work interact with light for roles associated with energy production and camouflage/colouration in nature. Emphasis has been drawn to the energy transfer pathways specific for the studies on patterned proteins for light harvesting and fluorescent mechanisms. Emphasis has also been placed on chlorosome structures that aid light harvesting in photosynthetic bacteria.

This chapter has also introduced the principles behind the physics related to these samples such as properties surrounding fluorescence and the transfer of excitation energy. It has also been demonstrated how some of these samples such as, those of fluorescent proteins have been applied to cell biology to study many different biological organisms without causing any damage from inorganic molecular tags.

Initial principles regarding the sensitivity of samples to photo-oxidative effects have also been introduced for consideration of the experimental techniques undertaken in this work.

3.5 Bibliography

[1] N. Howard T. McLuskey K. Fraser N. Prince S. Cogdell, R. Isaacs. How Photosynthetic Bacteria Harvest Solar Energy. *Journal of Bacteriology*, 181(13):3869–3879, 1999.

[2] J. McCarthy, B. Guthrie. Living colour and it's application. *Review of progress in coloration and related topics*, 30(1):1–, 2000.

[3] Hanlon. R Mathger. L, Shashar. N. Do cephalopods communicate using polarised light reflections from their skin? *The journal of Experimental Biology*, 212:2133–2140, 2009.

[4] T. Damjanovic A. Autenrieth F. Schulten K Hu, X. Ritz. Photosynthetic apparatus of purple bacteria. *Quarterly Reviews of Biophysics*, 35:1–62, 2002.

[5] R. Heim, R. Tsien. Engineering green fluorescent protein for improved brightness, longer wavelengths and fluorescence resonance energy transfer. *Current Biology*, 6:178–182, 1996.

[6] The Royal Swedish Academy of Sciences. Scientific Background on the Nobel Prize in Chemistry 2008. The green fluorescent protein: discovery, expression and development., 2008.

[7] J. Davenport, D. Nichol. Luminescence in Hydromedusae. *Proceedings of the Royal society*, 144:399–411, 1955.

[8] O Shimomura. The discovery of aequorin and green fluorescent protein. *Journal of Microscopy*, 217(1):3–15, 2005.

[9] O. Saiga Y. Gershman L. Reynolds G. Waters J Johnson, F. Shimomura. Quantum efficiency of Cypridina luminescence with a note on that of Aequorin . *Journal of cellular and comparative physiology*, 60(1):85–103, 1962.

[10] M. Chalfie, Y. Tu, G. Euskirchen, W.W. Ward, D.C. Prasher, et al. Green fluorescent protein as a marker for gene expression. *Science*, 263(5148):802–805, 1994.

[11] G. Davidson M. Shaner, N. Patterson. Advances in fluorescent protein technology. *Journal of Cell Science*, 120(24):4247–4259, 2007.

[12] F. Saiga Y Shimomura, O. Johnson. Microdetermination of Calcium by Aequorin Luminescence. *Science*, 140(3573):1339–1340, 1963.

[13] R Tsien. The Green Fluorescent Protein. *Annual Reviews in Biochemistry*, 67:509–544, 1998.

[14] J Lakowicz. *Principles of Fluorescence Spectroscopy*. Plenum Press, 1986.

[15] E. Kenworthy A Lippincott-Schwartz, J. Snapp. Studying protein dynamics in living cells. *Nature Reviews: Molecular Cell Biology*, 2:444–456, 2001.

[16] L. Johnston M. Hegemann J Niedenthal, R. Riles. Green Fluorescent Protein as a Marker for Gene Expression and Subcellular Localisation in Budding Yeast. *Yeast*, 12:773–786, 1996.

[17] H Kitagaki, H. Shimoi. Mitochondrial Dynamics of Yeast during Sake Brewing. *Journal of Bioscience and Bioengineering*, 104(3):227–230, 2007.

[18] E White, J. Stelzer. Photobleaching GFP reveals protein dynamics inside live cells. *Trends in Cell Biology*, 9(2):61–65, 1999.

[19] M Kendall, J. Badminton. Aequorea Victoria bioluminescence moves into an exciting new era. *Trends in Biotechnology*, 16:216–224, 1998.

[20] S Gather, M. Yun. Single-cell biological lasers. *Nature Photonics*, 5:406–410, 2011.

[21] R Rudin, M. Weissleder. Molecular Imaging in drug Discovery and Development. *Nature Reviews: Drug Discovery*, 2:123–131, 2003.

[22] R Blankenship. *Anoxygenic Photosythetic Bacteria*. Kluwer, 1995.

[23] P. Barrett S. Prince S. Freer A. Isaacs N. McGlynn P. Hunter C.N Cogdell, R. Fyfe. The Purple Bacterial Photosynthetic Unit. *Photosynthesis Research*, 48:55–63, 1996.

[24] H. Cogdell R Fraser, N. Hashimoto. Carotenoids and bacterial photosynthesis: The story so far... *Photosynthesis Research*, 70:249–256, 2001.

[25] G. Buchanan S. Michel H Ermler, U. Fritzsch. Structure of the photosynthetic reaction centre from Rhodobacter Sphaeroides at 2.65 A resolution: cofactors and protein cofactor interactions. *Structure*, 2(10):925–936, 1994.

[26] A. Schulten K Ritz, T. Damjanovic. The Quantum Physics of Photosynthesis. *ChemPhysChem*, 3(3):243–248, 2002.

[27] A. Zhao Y. Tas N. Huskens J. Hunter N. Subramaniam V. Otto C Escalante, M. Lenferink. Long-Range Energy Propagation in Nanometer Arrays of Light Harvesting Antenna Complexes. *Nano letters*, 10:1450–1457, 2010.

[28] W. Nagarajan, V. Parson. Excitation Energy Transfer between the B80 and B875 Antenna Complexes of Rhodobacter Sphaeroides. *Biochemistry*, 36:2300–2306, 1997.

[29] W. Hoff W. Matthijs H. Mur L. van Rotterdam B Hellingwerf, K. Crielaard. Photobiology of Bacteria. *Antonie van Leeuwenhoek*, 65:331–347, 1994.

[30] H Cogdell, R. Frank. How carotenoids function in photosynthetic bacteria. *Biochimica et Biophysica Acta.*, 895:63–79, 1987.

[31] T. Bittl R. Schlodder E. Geisenheimer I. Lubitz W Cogdell, R. Howard. How carotenoids protect bacterial photosynthesis. *Philosophical transactions of the royal society B.*, 355:1345–1349, 2000.

[32] R. Takaichi S Gardiner, A. Cogdell. The effect of growth conditions on the light-harvesting apparatus in Rhodopseudomonas acidophila. *Photosynthesis Research*, 38:159–167, 1993.

[33] S. Cogdell R. Isaacs N McLuskey, K. Prince. The Crysallographic structure of the B800-B820 LH3 Light-Harvesting Complex from the Purple Bacteria Rhodopseudomonas Acidophila Strain 7050. *Biochemistry*, 40:8783–8789, 2001.

[34] L. van den Broek J. Schubert D. Michel H Kleinekofort, W. Germeroth. The light harvesting complex II (B800/850) from Rhodospirillum molischianum is an octamer. *Biochemica et Biophysica Acta*, 1140:102–104, 1992.

[35] Beavis. A Kalejta. R, Shenk. T. Use of a membrane-localised Green Fluorescent Protein allows simultaneous identification of transfected cells and cell cycle analysis by flow cytometry. *Cytometry*, 29:286–291, 1997.

[36] Roszak. A Law. C Southall. J Isaacs. N Cogdell. R, Gardiner. A. Rings, ellipses and horseshoes : how purple bacteria harvest solar energy. *Photosynthesis Research*, 81:207–214, 2004.

Chapter 4

Experimental Procedures

4.1 Preparation of biological samples

4.1.1 Rhodobacter Sphaeroides

Growth and purification of the photosynthetic bacterium *Rhodobacter Sphaeroides* for microscopy measurements was carried out in the department of Molecular Biology and Biotechnology (MBB). Due to the nature of the measurements one of the main requirements for the samples was for them to be fluorescent therefore, individual light harvesting complexes were used for measurements not complete PSUs which funnel light to the reaction centre and are non-radiative systems. To achieve samples of one type of light harvesting complex deletion strains of the bacterium were grown where the genes responsible for one of the light harvesting complexes were removed and and inert streptomycin cassette was inserted in its place. Through this process the DPF2 protein deletion strain containing only LH2 and the DBCΩ deletion strain only containing LH1-RC complexes could be grown (separation of the LH1 and RC could be achieved by a double deletion and an insertion of the LH1 genes). Mutant strains of *Rhodobacter Sphaeroides* were grown in low light/dark conditions at 34 °C to ensure maximum growth and minimal photodamage to the PSU.

Purification of the deletion strain bacteria after growth required a pre-treatment with DNase and lysozyme. The addition of these aided the disruption process employed to break the cell walls with a French press at a pressure of 20,000 psi, which was repeated to ensure maximum lysis. The lysate from this was loaded onto a 15 %/40 % (wt/wt) sucrose step gradient and centrifuged at 20,000 g for 30 mins where the heavier cell wall remnants and other components would be separated from the lighter cell elements (such as LH2). This band of material at the interface of the step was then loaded onto a 5 %/10 %/20 %/40 %/50 % (wt/wt) sucrose gradient and centrifuged at 40,000 g for 2 hours to remove any heavier remnant cell components and to isolate the light harvesting complexes, of which were recognisable by their characteristic colours governed by the presence of the carotenoids.

Spectroscopy could be employed to collect the absorption profile to ensure that growth of the material had been successful and to confirm only one light harvesting component was present. It also allowed any photodamage to be identified at first and to confirm material collected from the gradient was the light harvesting complexes. Samples diluted in 20 mM HEPES, pH 7.5, 150 mM KCl, 25 mM $MgCl_2$, 0.5 mM $NiCl_2$ were deposited onto substrates either through microcontact printing (μCP) or dropcasting where, samples diluted to very low concentration were left to adsorb for an hour to adhere to the surface and were washed several times with 20 mM HEPES, pH 7.5, 100 mM KCl recording buffer to remove excess complexes that hadn't fixed to the surface of the substrate.

4.1.2 Fluorescent proteins

Fluorescent proteins, like the light harvesting complexes, were provided by collaborators in the MBB department within the University of Sheffield. The gene sequence of the fluorescent proteins were amplified through a polymerase chain reaction from pCS2-Venus vector, a multipurpose expression vector. The resulting Nde I/ Bam HI fragment was cloned into a pET14b expression vector (*Novagen*). By introducing specific mutations into the YFP gene it was possible to achieve enhanced GFP genes that have properties such as

higher stability and higher fluorescence intensity.

Both His_6-YFP and His_6-GFP proteins were produced by heterologoous expression in *E. coli* (BL21) and were grown at 37 ^{o}C to an optical density of 0.6. These cells were then induced using isopropyl-beta-D-thiogalactopyranoside (IPTG) (0.4 mM) for 12 hours at 25 ^{o}C. Pelleted cells were acquired through centrifugation at 19,000 g for 20 minutes, these were lysed through sonification and the resulting lysate was clarified by a further centifuge step at 33,000 g for 30 minutes. Both of the His-tagged fluorescent proteins were purified to homogeneity from clarified lysate using a Chelating Sepharose Fast Flow Ni-NTA gravity flow column (*GE Healthcare)* as detailed in the manufacturer's instructions, the protein purity was assessed by gel electrophoresis (SDS-PAGE).

4.2 Surface patterning

4.2.1 Microcontact printing

Microcontact Printing (μCP) is a useful technique for patterning biological systems [1, 2, 3] and in this work is primarily used to pattern substrates for measurement with several microscopy techniques. In μCP a soft polymer stamp is formed with PDMS using either a master mould or by etching. For this work the stamp contains a linear pattern with line thicknesses on the order of several microns and the line spacing a similar size. The protein of interest is deposited onto the stamp producing a layer (thickness dependent on concentration of protein) that may be brought into contact with the substrate for a short period of time to transfer the protein and print onto the surface. Protein transfer is relatively fast and takes only a matter of seconds, contact for any longer than this can lead to patterns that contain more erroneous material deposited on the surface [1]. The glass substrate to which the protein is stamped onto is cleaned in one of two ways, the substrate may be soaked in piranha solution or in a solution of ethanol and NaOH to remove any oils present on the substrate surface that may affect protein absorption. Substrates are then immersed in 0.01 % Poly-L-Lysine (PLL) until they are needed for protein patterning

where they are thoroughly rinsed in DI water before the μCP process takes place. Coating of the glass substrates with PLL raises the adhesion properties significantly due to its positive charge, ensuring minimal loss of proteins when the samples are rinsed after protein deposition.

4.2.2 Thin Films

For the characterisation and imaging of the chlorosome species from photosynthetic bacteria surfaces were prepared with a thin film of the biological sample of interest. Sample and surface preparations varied in this work depending on the measurement used e.g. spectral analysis or single molecule fluorescence measurements being conducted. The production of thin films for spectral analysis and single molecule measurements follow similar preparation techniques with the main variation arising in the concentration of the solution applied to the substrate surface.

The samples used were prepared on glass coverslips to produce an average thickness between 100-200 μm. To ensure that chlorosomes fully adhered to the coverslips the surfaces were coated with 0.01 % PLL diluted with DI water with a 20 μl dropcast to the surface of the coverslip. This was left to fix to the surface for 30 minutes to form a single layer of PLL on the surface and was washed with copious amounts of DI water to rinse any excess PLL off the coverslips. Deposition of chlorosomes onto the surface was achieved through dropcast techniques with 100 μl applied to the coated coverslips for 30 minutes to 1 hour to ensure chlorosomes fixed to the surface, after this the surfaces were washed with 20 mM HEPES, pH 7. buffer solution to wash off any chlorosomes that had not adhered to the surface. In the different applications of the samples, different concentrations of the chlorosome solution were used, diluted in the 20 mM HEPES, pH 7.5 buffer solution. For application with thin films for basic spectroscopic measurements the chlorosomes were diluted to a concentration of either 1 : 20 or 1 : 200 depending on whether the samples gave a strong fluorescent signal with the technique. For the single molecule measurements it was required that the chlorosomes were spaced with a few microns between therefore, through

the application of several test concentrations the final concentration for measurement was found to be 1 : 2000.

4.3 Fluorescence Microscope

All fluorescence microscopy measurements were conducted using an inverted *Zeiss AXI0* optical microscope however, the techniques employed to obtain fluorescent images varied between that of standard fluorescence microscopy and scanning laser fluorescence microscopy which could be combined with AFM measurements through the scanning stage fixed to the inverted microscope.

4.3.1 Fluorescence microscope configurations

4.3.1.1 "Standard" fluorescence microscope

In the case of the 'standard fluorescence microscope' the inverted microscope obtains a static image from an area dependant on the field of view of the objective and is static. An AFM scanning stage is mounted on the microscope for scanning and combined fluorescence/AFM purposes however, in this mode it is used in a static configuration and is only employed to move the field of view to different regions of the sample. 4.3.1 shows a schematic configuration of the fluorescence microscope in this mode.

The illumination source for this configuration can vary, the microscope has a potential to use either a halogen or mercury lamp (both of which are designed specifically for the microscope), an LED at 473 nm fixed to the microscope or diode lasers which can be coupled through the back of the microscope. In the case of the broadband sources filters can be placed in the illumination path so that a sample is only excited by a specific wavelength which can improve the clarity of the fluorescence image. In all cases emission filters are used to remove the excitation signal and ensure that only the wavelengths of interest are measured, these filters may be long pass filters or bandpass filters depending on the spectrum of emitted light.

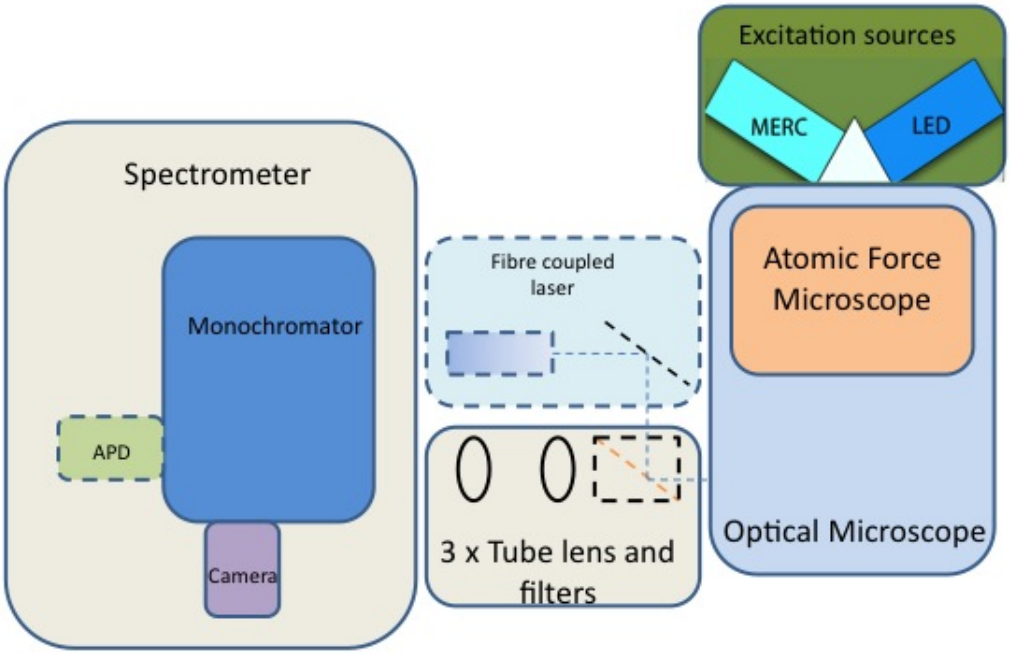

Figure 4.3.1: The fluorescence microscope system (solid lines) which houses the ability to use numerous objectives, excitation sources and excitation/emission filters. The external optics direct the emission to the monochromator and EMCCD camera. Additional components (broken lines) introduced to to the microscope system allowed for the scanning fluorescence microscope configuration.

As seen in Fig. 4.3.1 the emitted light is passed through external optics to collimate the light and to focus it to the monochromator which due to size restrictions is a set distance away. The caged system containing external optics consists of several lenses as well as a capability to add fluorescence filters, a necessary requirement when using diode lasers to illuminate the samples as it would otherwise have to pass through the emission filter prior to illuminating the sample and as a result be absorbed before reaching the sample. For

fluorescence measurements a 50 cm monochromator (*Princeton Instruments*) is coupled to an Electron Multiplied CCD (EMCCD) camera (*Princeton Instruments*) so that the system has a capability of either taking fluorescence images or recording the emission spectra through the use of the gratings in the monochromator. The back illuminated EMCCD in this system allows high resolution imaging with small integration times to reduce the background noise detected due to ambient light and also allows detection of low fluorescence signal through electron multiplication. It is also designed in such a way to minimise the effect of 'etaloning' where back illuminated CCDs become semi transparent in the near infrared. Light that has passed through a semi transparent is reflected between the front and back surfaces of these devices forming a resonant optical cavity where light and dark fringes occur due to constructive and destructive interference.

Image acquisition with the fluorescence microscope is conducted using the assigned software *Lightfield* (*Princeton Instruments*). Light that is collected from the sample and passed through the external optics and monochromator/EMCCD system is processed through this software which has the capabilities of analysing both fluorescent images and emission spectra in real time. The quality of images acquired using fluorescent microscopy depends on a number of predefined parameters as well as the system's ability to remove interference from ambient light. Ambient light has been removed from fluorescence microscope measurements in this work, by enclosing the whole microscope, external optics and detector. On top of enclosing the whole system, extra measures have been taken with the external optics by encasing the light path in tube lenses, preventing stray light from the excitation source and holes in the enclosure from affecting the light received at the detector. The software contains user defined parameters that can be used to optimise the system and obtain high quality images. The integration time of the images is a key parameter in the imaging process which allows both the imaging of weak fluorescent signals as well as those with a high fluorescent yield. Low integration times can be used with highly fluorescent samples to prevent saturation of the CCD chip (which can damage the detector) as well as reducing signal from potential background effects whilst higher integration times can be used with samples of lower fluorescence (in this work photosynthetic bacteria and single

fluorescent protein layers) to maximise the emission signal detected. This can increase the effect stray, ambient light has on the image and as a result leave the image with a much lower signal-to-noise therefore a trade-off has to be made between the intensity of the emission collected from a sample and the level of backgound that may affect the image. As well as taking images the software allows real time imaging to be used, this coupled with low integration times is ideal for focusing on a samples fluorescence and finding regions of fluorescence which is used in conjunction with the AFM sample stage to obtain ideal images of a sample.

When dealing with weakly emitting samples more than just the integration time can be changed to optimise the signal from the fluorescence microscope. The gain of the CCD is a parameter than can be adjusted by the user which increases the number of electrons that constitute one grey scale value which lowers the well depth of the pixel. The gain therefore increases the intensity of one grey scale value relative to the well, in low signals this can improve the observed signal and allow smaller integration times than those that would cause an increased background signal or damage to the sample. Another key feature of the software, useful for the imaging process, is the region of interest which allows the user to select specific areas of the sample. This can be used for fluorescence images to separate a fluorophore of interest from others however it is mostly used in this work to obtain emission spectra of the fluorescent regions. Used in conjunction with monochromator control in the software, which allows the user to reduce the slit width when the emitter of interest is centred to minimise areas of the sample that are not relevant to the signal required from contributing to the measured signal. Once the slits are reduced the region around the emitter can be selected and the gratings changed, this process ensures that when the emission is taken the data is from a single source and not a number of sources that could manifest itself as a broader emission instead of a defined peak of interest.

4.3.1.2 Scanning fluorescence microscope

As previously mentioned the scanning fluorescence microscope utilises the same microscope but the illumination method, external optics and image acquisition method vary in relation

to that of the standard system. As it is shown in Fig. 4.3.1 the microscope and the AFM sample stage are still used to house the sample and contain the excitation filters however additional components are added (depicted with broken lines). The illumination source is a laser and is directed to the sample through the same side port that the emission is collected from, therefore to separate these signals an emission filter is placed in the external optics before light enters the monochromator (the laser is at a wavelength that is absorbed by the emission filter, which it would have to pass through to reach the sample). The external optics remain the same in this version of the system with the only variation being the position of the emission filter in the external system.

Scanning fluorescence measurements exploit the AFM scanning stage present with the inverted optical microscope. By using the AFM sample stage it is possible to 'false engage' the AFM (scan without a tip touching the sample) and scan across the defined sample area in the same manner. This is possible as image formation in AFM uses a moving sample (courtesy of the sample stage) and not a moving tip. The diffraction limited laser spot is scanned across the sample surface in this method through the movement of the AFM scanning stage. The resulting fluorescence intensity is recorded at each pixel through the use of an avalanche photodiode (APD) that has its output signal connected to the AFM controller and this signal is compiled into a fluorescence image in the AFM software. This configuration uses similar principles to that which are used when taking spectra and images of individual fluorophores in Section 4.3.1.1. The EMCCD is used for focusing of the laser spot on the sample, using the external optics and by moving the objective, the diffraction limited laser spot can be detected and positioned in the centre of the image. The external system can be used to ensure that the spot formed is not undergoing any scatter in the system and isn't entering the optics at an angle, thus maximising the excitation power delivered to the sample. To ensure that only light from the excitation region (laser spot) is detected in the emission the monochromator slit width can be reduced to only surround the spot, the emission passes through the monochromator for the measurements in the scanning system however, a different exit port is utilised to which the APD is attached. The signal from the APD is detected by a custom Labview (*National Instruments*) program

which prior to scanning is used to ensure that the focus of the laser spot hasn't shifted, ensuring that the intensity measured is as high as possible. Finally in order to observe fluorescence whilst scanning, the APD signal is fed into an input port in the AFM driver which once scanning allows the user to collect an intensity map of the sample.

As image acquisition is reliant on the scanning method in this configuration, the parameters that can be altered by the user to optimise fluorescence images are similar to those that can be used in AFM. For example, one adjustable parameter that is similar to that utilised in AFM is the scan size, which can be adjusted between several microns (any lower and diffraction effects cause a problem as the laser is diffraction limit) up to a maximum of 100 μm. This allows a range of samples to be investigated in this work from large linear arrays formed by μCP down to samples that measure upto a μm (chlorosomes). A key advantage of the adjustable scan size in this method is for comparisons of the different microscopy methods used on samples in this work, similar regions can be measured on the same length scales and key information on resolution and function drawn. The pixel size of the fluorescence image is also defined by the user, similar to the methods in AFM it is determined by the number of lines scanned on the sample which at different resolutions on the same size scan region results in varying pixel size. The integration time per pixel can also be controlled through the scan stage as the scan rate (lines per second) can be modified in the AFM software, by going slower with this rate the length of time the laser illuminates a pixel increases. Much like the methods of SNOM and static fluorescence microscopy this time needs to be optimised to reduce any collection of background noise in longer scans and to not spend too much time on a sample region, increasing the chance of photo-oxidative effects occurring. It is possible for the user to use the monochromator control to optimise the system too by utilising the gratings to reduce noise and effects from wavelengths that are not of interest. This work has used the ability to select specific wavelengths of interest with the monochromator to reduce the effects of background/stray light and also to control the peak wavelength at which an image is taken. This second use has allowed intensity mapping at different wavelengths to be used to reconstruct emission spectra using this system.

4.3.2 Resolution

Due to the size of the samples used in this work, resolution is a key consideration in the measurement of fluorescent samples. The microscope used in the acquisition of fluorescent images has the ability to facilitate a number of different objectives, initial measurements on the samples were carried out with standard objectives with numerical apertures (NA) ranging up to 0.7. Although these give a resolution that approaches the diffraction limit, it was difficult to observe weakly emitting samples due to poor light collection. Standard microscope objectives however were useful for the verification of fluorescence from samples, the large field of view meant that regions of interest could be found and more powerful objectives used for higher resolution fluorescence imaging. The configuration of the sample stage and the standard thickness of coverslips used in the sample preparation allows for oil immersion lenses to be used when fluorescence imaging, with NA values of 1.4 and the resolution only limited by the diffraction limit. With this ability to achieve high resolution, oil objectives were favoured for fluorescent imaging in this work, for both far-field fluorescence microscopy and SNOM.

The resolution of the two different fluorescence microscopy techniques used in this work varied depending on the detector as well as the illumination source. In the case of the static imaging technique, the EMCCD camera in conjunction with the microscope optics is responsible for the maximum achievable resolution. The combination of the two determine the observable field of view which varies for the different objectives used. For example, by using Eq.4.3.1 the observable field of view with a 50X magnification, 0.7 NA objective is 57.3 μm compared to that of an oil immersion objective of 63X magnification, 1.4 N A which yields 45.5 μm (with the magnification power taking into account the 3X magnification in the external optics).

$$F.O.V(x,y) = \left(\frac{Pixel\,size}{Magnification\,power}\right) X\, Number\, of\, pixels \tag{4.3.1}$$

Furthermore the pixel size and therefore the obervable resolution attainable by the camera varies with the objective power due to the magnification onto the 512 x 512 pixel

CCD chip. For this work an extra 3X magnification factor was present in the external optics of the microscope which allowed the pixel resolution to reach a comparable size to the resolution of the oil immersion objective (0.172 μm) and the diffraction limit, achieving the highest resolution attainable by a far-field system.

The scanning system's resolution on the other hand is dependent on the excitation source and the scanning stage. High powered objectives ensure that the laser spot was on the scale of the diffraction limit which ultimately provided a limit in the excitation area and the emission area at each point of the sample. Whilst the static system is limited to the field of view the excitation/emission area (resolution) can be achieved at each point in any scan size determined by the sample stage. With resolution the scanning stage and the AFM program also play a part in determining the resolution of the microscope configuration in this work, where as, the laser spot illuminates a determined area of the sample the emission is collected and transferred into an image with a resolution determined by the software. Ideally a higher number of lines in a scan size can achieve resolution on the scale of that associated with the laser spot size, however this equates to longer scan lengths unless the scan rate is significantly increased. This trade off has resulted in some measurements in this work being conducted with higher line scan values at small scan size to reduce pixel size where as others have been conducted on large areas with higher scan rates (achievable with the false engaged AFM as there is no tip contact present).

4.3.3 Biological considerations

The biological samples used in this work are highly susceptible to photo-oxidative damage, therefore specific considerations have to be taken into account when applying fluorescence microscopy to them. As addressed in 3.2.3, high intensity light conditions can cause serious damage to light harvesting complexes and fluorophores in biological samples. To reduce the level of photodamage occurring in measurements of the biological samples, modifications to the illumination mechanisms and the methods behind obtaining images were made. For illumination in the static configuration, broadband lamps and single wavelength LEDs

were used, these mechanisms of illuminating the sample allowed the intensity to be varied, reducing the light intensity and optimising the optics detect maximum fluorescence from the sample limited the amount of induced photodamage. This allowed samples to be illuminated for longer periods of time either at the same region or with a number of separate measurements. Neutral density filters could also be used in the excitation path to reduce the intensity of light incident on the sample, preventing photo-oxidative damage whilst ensuring the light source was run at full/high power to reduce any significant intensity fluctuations arising from variations such as heat. Similar measures were introduced for the excitation of samples in the scanning configuration fluorescence microscope. Reducing the power of the laser exciting the sample in this configuration is a necessity as the power density at the sample is on a scale that could cause instantaneous damage, eliminating its fluorescent properties. To reduce irrepairable damage to the samples a number of neutral density filters were added to the external optics for the laser path, a variable neutral density filter was also introduced to control the laser power and to optimise a level at which the intensity is significant for fluorescence but not of a value that will damage the sample.

The period of time that the samples were illuminated for was another imaging property that had to be taken into account when considering the biological samples in this work. Initial measurements were conducted with one of the illumination sources constantly on, this was also the case when aligning the sample and finding regions of interest on the surface. Although this method did allow some images to be obtained, having the sample constantly illuminated resulted in a reduced lifetime due to the increased amount of time for photo-oxidative events to occur [4]. To reduce the effects caused by constant excitation by the light source, they were switched off between alignment and image acquisition, as well as between imaging events. By turning off the illumination source, the lifetime of samples under measurement by fluorescence microscopy were increased however, with the enclosed system this could increase the time involved in the imaging process. To reduce the time involved in the imaging process and realignment (reducing the length of time samples were illuminated) a custom Labview (*National Instruments*) program was developed so that with the scanning fluorescence technique the laser could be controlled remotely without

opening the enclosure. This was desirable as the power density of the laser can cause damage so the ability to immediately turn it off once an image had been acquired could reduce the damage caused to the sample. Integration times of the detectors was another factor to be taken into consideration for biological samples in this work. As the samples weren't illuminated between measurements the integration time of images was the main value that determined how long a sample would be illuminated for and thus the time where photo-oxidative effects could take place. Similarly to optical measurements in 4.5 a balance has to be found between integrating long enough for a significant fluorescence signal to be detected and not so long that the signal-to-noise is reduced/photodamage occurs. In this work it was found that in measurements on the static configuration ideal integration times were between 200 ms to 2 s however in the case of the scanning system integration times applied to each pixel depended on the scan parameters so in this case photo-oxidation was seen alongside higher resolution images (around $2-3$ s per line).

The environment that the biological samples are in is very important in preventing damage to the sample, reduction of the amount of oxygen present whilst under illumination aids in preventing photodamge from occurring. It was possible to conduct measurements in different sample environments in two ways, both of which are applicable in AFM as well as with this fluorescence microscope configuration. Where the sample was deposited on a glass slide a drop of imaging buffer may be deposited on the top of the cover slip with the surface tension being significant enough to prevent it being lost off the edges of the sample, this method allowed samples to be imaged under liquid conditions in both microscope configurations. The other method that was used to image samples under physiological conditions was to use the profusion cell supplied with the AFM in conjunction with a petri dish to hold the sample. Depending on which objective was used the working distance varied therefore, it was possible to mount a sample containing cover slip into the petri dish with lower NA lenses although when it came to achieving maximum resolution with the oil immersion objective it was required that biological material be affixed to the petri dish. In this case petri dishes were prepared via the same method outlined for coverslips in 4.2.1. The use of petri dishes and the profusion cell allowed a larger volume of buffer to

be used which rectified some of the issues that arose with the drop method where smaller volumes evaporated whilst measurements were taking place thus protecting the sample for longer. It also allowed nitrogen to be introduced around the sample as an extra protective measure to remove as much oxygen as possible from the system.

4.3.4 Image acquisition/processing

Image acquisition in the two configurations in this work differ due to their static and dynamic nature. The use of the EMCCD and the static system allowed a number of parameters to be adjusted within the associated software to facilitate high resolution fluorescence imaging. With the correct filters in the system fluorescence from the sample can be aligned and focused using the eye pieces in conjunction with the camera. In the imaging process the camera software allows the shutter to be closed and dark, background readings to be obtained which can then be subtracted from acquired fluorescent images to improve the signal-to-noise relationship, in this case taking thermal effects into account. The user also has control over parameters such as, the threshold of the image in the display, the gain applied to the EMCCD and binning all of which can improve imaging from samples that have a low fluorescent intensity. The ability to adjust the contrast of the image alongside the integration time allows real-time imaging of a sample for alignment purposes which can then be altered for single image acquisition. Where fluorescent regions are weak compared to other regions on the sample, specific actions can be taken and parameters set to ensure that only emission from that region is collected at the detector. Regions of interest may be selected within the software which only display the specfic number of pixels selected by the user, effectively ignoring all other regions of the sample. This process may be used with weakly fluorescing regions but it can also speed up the frame rate of a series of images, if only a small number of pixels are used the rest of the CCD can essentially be discarded and a new image taken thus reducing the readout time.

The recording of emission spectra with the EMCCD detector requires a number of parameters to differ to that used when taking fluorescence images. Much like the method

used in obtaining fluorescence images, the system is aligned and regions of interest selected whilst imaging the sample in real time. The emitting region of interest can be centred and through control of the monochromator the slit width can be reduced to prevent broadening in the emission spectrum. The monochromator used in this work had the option of two gratings of 300 g/mm and 150 g/mm with respective resolutions at 473 nm of 0.208 nm and 0.418 nm (although these are also dependent on the entrance slit width on the monochromator). The different gratings could be selected for imaging the emission spectra from samples which after selection of a central wavelength for the emission spectrum could be obtained using the assigned software. The EMCCD collects a spectrum for each line in the region of interest which means for analysis, selection of the appropriate line for the emitting region has to be made information of which can be obtained from the alignment images. The emission spectra could be refocused in the real time imaging to maximise the emission peak, this could be carried out where the emission weakens due to misalignment and not sample damage, to ensure that accurate spectra are obtained.

The acquisition of fluorescent images with the scanning fluorescent microscope draws parallels with the methods behind spectra measurements with the EMCCD. The quality of images obtained with the scanning fluorescence microscope largely depend on a number of parameters determined by the user that can be applied at the monochromator and with the AFM scanning stage. The alignment of the laser for scanning measurements uses the EMCCD and real-time imaging to ensure a good quality laser spot, the monochromator may also be used with the software (using the internal mirror as opposed to gratings) to measure the full width half maximum of the spot and therefore its size. Similarly to the measurement of emission spectra, it is required with scanning fluorescence microscopy that only the region where the laser is present (and therefore maximum emission intensity) on the APD therefore, slit widths of the monochromator are adjusted accordingly to reduce any effects of background light. Due to slight differences in the path length between the EMCCD and the APD, an extra alignment step is undertaken to ensure the signal present on the APD is maximised. As the alignment of the APD is a manual process using an x-y stage, some alignment issues can arise if the stage is knocked, for example. To ensure that

the signal is maximised in relation to the background whilst the enclosure is open, extra care is taken to block stray light with extra tube lens. The fluorescent image with this system is obtained through movement of the AFM sample stage after a false engage where parameters such as the scan size, scan rate and line resolution can be adjusted to ensure the image acquired is at the highest resolution attainable with the optical limitations. The APD measures the number of counts per pixel to build up an image and as a result doesn't have the capabilities to produce an emission spectrum however, on top of using an emission filter the gratings in the monochromator can be used in such away to measure emission intensities from the sample at specific wavelengths to obtain information about the fluorescence from a sample at across the visible spectrum.

The image processing carried out following acquisition of fluorescence images was dependent on the imaging method as different image file types were delivered by the two and as a result required different software for post processing however, minimal image processing was applied to the images and where it was it was used for aesthetic value. Images obtained with the EMCCD/static microscope system had levelling performed on them to account for uneven illumination that was observed in the fluorescence image, this was often due to effects from the light path or due to effects of pixel response across the CCD. To account for this tilt, 3 point levelling was used on regions where no sample was present, levelling in relation to the defined points. Further enhancement to the definition of the image can be achieved through modification of the contrast through the software's histogram function. Emission spectra obtained were analysed in a compatible analytical software such as Origin or Excel (*Microsoft)* after exporting from lightfield. Minimal processing was required in this software to improve the clarity of the spectrum however analytical methods such as profile fitting could be applied to the spectrum for further analysis.

Images from the scanning fluorescence microscope were processed and analysed in a similar way to those obtained from SNOM measurements. The 3 point levelling analysis was applied across the sample to account for any tilt in the optical data across the sample due to the light path or any variation in laser intensity. The histogram feature was used to improve the clarity of the images so that regions of interest could be observed for

cross-sections to analyse the image for example. Fourier transfers could also be applied to these images to confirm repeating structural properties in images that were unclear in the analysed images. Images obtained through the scanning fluorescence microscope used in this work only divulged fluorescent intensity across the image, however it was possible to use several images of the same region of a sample obtained at different monochromator wavelengths to get a fluorescence intensity at a specific point for each wavelength. Obtaining this from the software allowed the user to use graphical software (Origin 8) to recombine the emission spectrum to confirm no damage had been caused to the sample.

4.4 Atomic Force Microscope

AFM measurements were primarily obtained using a BioScope Catalyst AFM (Bruker). This AFM was favoured due to its configuration which has a removable head allowing the the unit, containing the tip, photodiode and laser to be removed from the scanning stage for easier access to the sample and the ability to use samples that are prepared on most substrates, even on petri dishes (used for liquid measurements). For the samples studied in this work SNL-10 cantilevers (*Bruker*) were used which allowed samples to be measured both in air and in liquid environments. The multi tip layout of these probes facilitate their use with any environment as well as with most samples due to the cantilevers being of varying sizes and of varying spring constants which allow for smaller lateral forces to be applied to the biological systems which are susceptible to damage from some tips. The cantilevers attached to these probes and used in this work had spring constants varying between 0.06 N/m and 0.35 N/m, and resonant frequencies between 18 kHz and 65 kHz allowing AFM measurements to be made in air and liquid.

In the AFM system a level of noise reduction has been utilised to maximise the attainable resolutions and to obtain as much sample data as possible. With the nature of AFM image acquisition a main source of noise can be that of erroneous vibrations that can originate through thermal fluctuation or mechanical noise for example. To reduce the effect of mechanical noise the AFM scanning stage and head were mounted on an isolation

bench which used compressed air to damp vibrations [5]. The AFM controller, computer and associated power supplies were mounted off of the bench so that mechanical noise originating from the fans in these pieces of equipment didn't interfere with the AFM. The AFM was housed in the enclosure that also held the optics for the fluorescence microscope, this however brings issues regarding thermal noise to light. Moving power supplies with cooling fans to the outside of the blackout box reduces this along with vibrational noise however, some electronics still remain which cause heating/vibration therefore regulation can be achieved by removing the front access panel between measurements/samples to allow for the temperature to equalise (although not possible for combined AFM/fluorescence measurements).

4.4.1 Image acquisition

The amount of information that can be obtained from an image relies on the image quality which in the case of AFM depends on the scanning parameters and matching the mode of operation to the properties of the sample. For the samples used in this work non-contact mode AFM has been used as when dealing with biological samples, this is preferred over other modes such as contact mode as it is less destructive to the sample due to the smaller interaction times, allowing more accurate measurements to be taken with less deformation occurring to the soft samples. It also doesn't lead to as many collisions with the edge of a sample feature which can lead to the sample being pushed along with the tip and thus not measured, an issue that can occur with contact modes.

Many parameters can be adjusted in the scanning process to maximise the resolution of an image such as the proportional and integral gains relating to the feedback loop which may be optimised to reduce noise and improve how the tip tracks along the surface. The scan rate and tip velocities can also be adjusted to ensure that the probe has enough time to react to the topography changes and doesn't risk damaging the sample or causing damage to the tip, which may be degraded from to dirt sticking to it or blunting it and thus reducing the maximum attainable resolution. In the software the scan size and the

number of lines that make up the image can also be adjusted which in turn can improve the resolution of an image due to reductions in pixel sizes displayed on the screen, for example with a 20 μm scan size with 256 lines the pixel size is 78 nm, however at a resolution of 512 it is half this at 39 nm allowing for smaller objects to be resolved.

Another aspect of the image acquisition process that can be modified is the type of image that can be obtained by the AFM. Alongside the standard topography image the BioScope Catalyst has the ability to obtain images divulging more information than just the height by using the controller to obtain information from the force-distance curves using the peak force quantitative nanomechanical property mapping (QNM) mode. In this mode images can be built up from obtaining information regarding deformation, adhesion and modulus from the force-distance curves, this extra information allows the user to classify samples even more. Other image types such as amplitude (relating to the oscillation of the cantilever), phase and z-error can be obtained to show how the feedback mechanism deals with a sample.

4.4.2 Biological considerations

To facilitate the measurement of biological samples a number of considerations were taken into account and modifications were made to the imaging technique to reduce the damage caused whilst observing the sample. A key consideration taken was that of keeping the sample in a configuration that maximised its stability whilst under forces induced by the tip. To keep the biological samples stable and their structure intact, samples could be kept under physiological conditions like those experienced when in the native cell configurations. Physiological conditions could be emulated in this case by immersing the samples in an imaging buffer and using liquid AFM techniques to acquire images. The liquid environment reduced some of the lateral forces acting on the samples, due to the AFM technique being operated at slower tip velocities and lower set point ultimately allowing the tip to interact with the sample gently.

On top of keeping the sample structurally stable, liquid conditions were also used to

account for some of the issues that arising due to the laser used for the operation of the AFM. The laser from the AFM head partially illuminated the samples constantly whilst images were obtained, when large and high resolution images were taken this time increased and the chances of photo-oxidative reactions thus increased (when in air). Keeping the samples in buffer solution, as well as with the presence of nitrogen blown across the sample, allowed most of the oxygen to be removed from the system and reduced photo-oxidative processes. This may lead to changes in the protein structure of the samples due to the stress induced from excitation processes therefore, measures were taken to obtain an accurate structural profile of the sample.

4.4.3 Image processing

Small adjustments were made to images acquired with the AFM to account for anomalies caused by the acquisition process or errors originating in the system. Images were processed using the image processing software Gwyddion which allowed minor corrections to be made in order to improve the image but also allowed specific measurements to be made to analyse the samples.

Sample tilt is a recurrent problem in AFM topography images that manifests itself as an uneven zero value in the height scale across the sample. On top of clamping the sample down on the scanning stage to reduce tilt, levelling can be performed on the image so that small features are revealed that were previously masked by the higher value of regions where there is no sample. Gwyddion can level images through automatic levelling where it takes an average across the sample and levels the data, it also allows levelling using 3 user defined points which can be used to select regions where there is no sample so that tilt can be corrected for by fitting these regions to one another.

When dealing with samples that contain features of varying size, smaller topographical features may be masked by automatic scaling due to the the larger features. During analysis this means smaller features may be overlooked, therefore the software's histogram function can be used to adjust maximum and minimum limits to the image scale allowing

the smaller features to be identified for analysis.

To analyse sample heights in detail the software allows the user to obtain a line profile which takes a cross-section of a defined line in a region. This is useful for samples such as the printed substrates used in this work as it allows the efficiency of the printing process to be observed. It allows the user to see weather a monolayer or more layers have adsorbed onto the surface. It also allows the user in this case to see whether a printed pattern is reproducible and the same across the stamp.

Another useful feature that can be incorporated into the analysis of AFM images is that of fourier transforms. These can be used either for identification of recurring features of samples or to realise recurrent noise in a system which in turn can be isolated and removed from the image through the fourier transforms. In the identification of repeating structures in an image like the recurrent linear arrays, fourier transforms are useful to identify the observable repetition or that which at first may not be observable without some image analysis/adjustment. In the case of noise reduction constant frequency noise such as that from a fan can be eradicated by using the fourier transform to isolate the frequency and omitting it from selection prior to an inverse fourier transform which recombines the image.

4.5 Scanning Near-field Optical Microscope

All SNOM measurements were conducted using an Aurora-3 Scanning Near-field Optical Microscope (*Veeco Instruments*). For the imaging of samples, laser light was coupled into aluminium coated fibre optics probes, these were either pre-mounted onto tuning forks (*Veeco Instruments*) or purchased and mounted onto tuning forks in the lab (*Jasco/NT-MDT*). All SNOM probes used had approximate aperture sizes of around $50 - 100$ nm in diameter and the resonant frequency of all tuning forks approximately between $80 - 110$ kHz. Several lasers were used with this SNOM depending on the optical properties of the samples used, these included a 20 mW, 488 nm Ar^+ laser (*Coherent*), a 20 mW, 473 nm diode laser (*Laser* 2000) and a 10 mW, 800/850 nm diode laser (*ThorLabs*). The SNOM was operated in transmission mode with light collected through a 100×1.3 NA

oil immersion objective and directed out through the side of the SNOM unit. Externally the light was directed through a tube lens and focused on the detector, additional filters could be added to the light path to omit stray light. Both long pass and band pass filters were utilised at this point depending on the fluorescence intensity from a sample and to maximise the signal.

The fluorescence signal collected from the sample is directed to and focused at the detector which in this system is an avalanche photodiode (APD). The quantum efficiency of the APD was such that signal from the different samples could be detected through the external optics, across the spectrum. The nature of the APD also allows very low signals to be detected due to the amplification of signals from single photons.

The SNOM system, with the external optics was enclosed within a custom built enclosure to ensure no stray light could enter the system. This also ensured that the APD wasn't subjected to ambient light which could cause damage to the detector. Signal-to-noise could also be vastly improved by enclosing the system and removing background light. To prevent damage to the SNOM probe and subsequent increase in the aperture size from damage, it was mounted on an anti-vibration table.

4.5.1 Modifications for imaging samples

A number of modifications were made to the standard SNOM set up so that biological samples could be accurately measured. Initial measurements of the samples in this work found that the original system suffered from low signal-to-noise, for example, in the case of patterned substrates of fluorescent proteins and *E.coli* labelled with GFP, the topography displayed the regions of interest but the optical image only showed recognisable fluorescence at very high laser power which for extended periods of time would cause photobleaching [6]. In the original setup the external optics enclosed within the SNOM were left open and therefore were open to ambient light. To reduce any small levels of ambient light that may enter the enclosure a tube lens was introduced to house these optics. The number of background counts detected by the APD in this case was reduced to around 1 count per

10 ms essentially eliminating the background signal previously detected. The collection objective used in the original system had a magnification of 50X and 0.7 NA, to improve upon this by increasing the collection angle and the amount of fluorescence collected, an oil immersion lens with a 63X magnification and 1.4 NA was introduced to the system. This vastly improved light collection negated the need to increase laser power to detect significant signal-to-noise, thus causing less damage and allowing the low light biological samples such as the light harvesting samples to still be measured.

Measures were taken in the sample preparation process to reduce the amount of photobleaching and photo-oxidative damage induced in the sample. Due to the nature of biological samples and the severe damage photo-oxidation can do to the light harvesting and fluorescent mechanisms, an extra enclosure was fitted around the SNOM head prior to scanning allowing a steady stream of nitrogen to be fed across the sample. Oxygen could be removed from the system by filling the enclosure with nitrogen and maintaining a steady stream whilst taking measurements. This allowed photo-oxidative reactions to be reduced and the sample to be active for much longer periods of time.

Another issue that may cause problems when measuring biological samples with SNOM is the regulation of the laser power at the tip. High intensity laser light at the tip can induce significant heating effects which can cause deformation of the tip, affecting both the topographic information that can be obtained as well as the amount of light that may be delivered to the sample [7]. High power densities at the tip can also cause a problem for photosensitive samples such as the ones used in this work therefore keeping this to a minimum is desireable when investigating samples. With these requirements in mind, the intensity of the incident laser was regulated through the use of a variable ND filter to ensure that minimal damage could be caused to the tip and the sample.

4.5.2 Photosensitivity

Considerations regarding the photosensitivity of biological were taken into account in relation to the SNOM technique and modifications made to it accordingly. To bring the SNOM

probe in close proximity to the sample prior to engaging and to position it on specific areas of the sample, it was necessary to illuminate the sample with an LED so that the probe can be viewed with a camera. This method caused the sample to be under illumination whilst the probe was being positioned which, due to the nature of the samples could impede the fluorescence properties of the samples. As these initial stages of the imaging process require sensitive positioning of the probe tip, illumination is essential and therefore removing the LED is not an option however, by using a variable power supply with the LED it was possible to reduce the intensity of incident light whilst it was also ensured in the operation that the LED was only illuminated for short periods of time in the alignment process to reduce the amount of potential photobleaching. Initial preparations also required accurate alignment of the optics and the APD to maximise the fluorescence observed, to achieve this a laser was used as a light source. As the alignment process isn't instantaneous the laser would be illuminating a surface constantly which, if conducted with the biological samples present could cause significant photobleaching and oxidation. Therefore for the alignment process the sample of interest was removed and replaced with a blank substrate of similar properties (thickness/optical density). In some cases it may have been possible align whilst the sample was present (much thicker films on a substrate), if this was the case then the laser was changed to lower energy red laser so that the incident light on the sample would be largely non-bleaching.

Samples under investigation in this study saw varying degrees of uniformity across the surface of the substrate which was dependent on the sample preparation technique. Drop casting of light harvesting complexes saw large areas of uniformity in sample density, however in some regions a very low sample density was observed. This was also the case with the μCP samples where biological samples were confined to patterned areas which are present in very specific regions as a result of the stamp size. As SNOM images take a long time to acquire, it is not ideal to take fluorescence images and to illuminate the sample whilst attempting to locate sample containing regions. The laser used to illuminate in this process can damage the sample and only a small number of scans can be conducted for each sample therefore, to locate the region of interest scans are conducted without the laser

present. It is possible with the SNOM to do this by taking topography measurements in the dark, these measurements show either the patterned regions or regions of high complex concentration where fluorescence images can later be obtained with the SNOM so that the illumination only occurs when the image is acquired. A measure taken to reduce the amount of time required to locate a region of interest was to mark stamped/dropcast regions with a scratch which further reduced the amount of time that the sample had to be illuminated with the LED for location on the camera, again reducing potential photo-oxidative effects. This approach (albeit a simple one) was highly successful in speeding up the identification of regions containing biological material, it was also an approach that could be applied to numerous different substrates with the only drawback being that on sufficiently thin substrates they could crack/break upon scratching.

4.5.3 Confirmation of fluorescence

With some biological samples in this work it was found that fluorescent properties were either different to that expected or non-existent, the reason for this could potentially be from the sample preparation or from photodamage. A further step was introduced in preparing the samples for SNOM measurements which was to use the fluorescence microscope to confirm fluorescence from the sample and what filter sets should be used based on their fluorescent properties. By using the fluorescence microscope with a standard halogen lamp/low power LED the intensity of light incident on the sample can be kept to a minimum to reduce photobleaching before SNOM measurements can be made. The microscope is coupled to a CCD and a monochromator therefore, standard fluorescence imaging can be used to confirm fluorescence is present and the spectra of this can be obtained to make sure the sample hasn't degraded (often shown as a blue shift) and that the correct filters are used for the SNOM.

4.5.4 Image acquisition

4.5.4.1 Scanning parameters

The amount of information that can be obtained from an image is dependent on the quality of the image which for SNOM, relies on the scanning parameters. The scanning parameters required to achieve high quality SNOM images vary from sample to sample depending on a number of properties associated with the surface such as, the height range, sudden variations in height and the general sizes of regions of interest. Apart from improving the quality of images and the resolution of the system, modifications to the scanning parameters are employed to prevent the probe tip sustaining any damage (as the probe takes a finite time to respond to sudden topography changes). In the case of the tip responding to surface changes, the gain settings that control the feedback mechanism can be modified which changes how the tip responds to the specific changes in topography.

The fine tuning of scanning parameters to improve topographic information acquired from a sample can be seen in the example of elongated *E. coli* cells in Fig. 4.5.1. The cells are cylindrical and posses diameters of several hundred nanometres which result in abrupt features at their edge which can make it difficult to obtain reliable topographic information. Dramatic changes in the height of these samples require changes to specific scanning parameters, one of these parameters being the scan speed. By slowing the scan speed of the probe tip the feedback mechanism has more time to adapt to the abrupt height changes which at higher speeds it would not be able to do, leading to tip damage from it crashing into the side of the structure. Slower tip velocities coupled with the gain settings can also be employed to prevent the reduction in height manifesting itself as an elongated curve edge as shown in the images (a) and (b).

Samples with small topographical features on the other hand also require values similar to those mentioned above for the large topographical features present with *E.coli*. In the example of the linear arrays of GFP from μCP, a low scan speed is also required. In the case of smaller topographies a high scan speed may result in the topography appearing flat or with large curvature in the edges in the peaks in the cross section due to the response

time of the feedback mechanism not being sufficient at those speeds to see a height change. Therefore, in the case of the GFP lines a better topography image is observed when the scan speeds are kept low and when the gain parameters are set at specific values to allow the tip-sample distance to be maintained at a very small value so that when moving back off a line of GFP the edge isn't seen as a smooth gradient but as an abrupt drop.

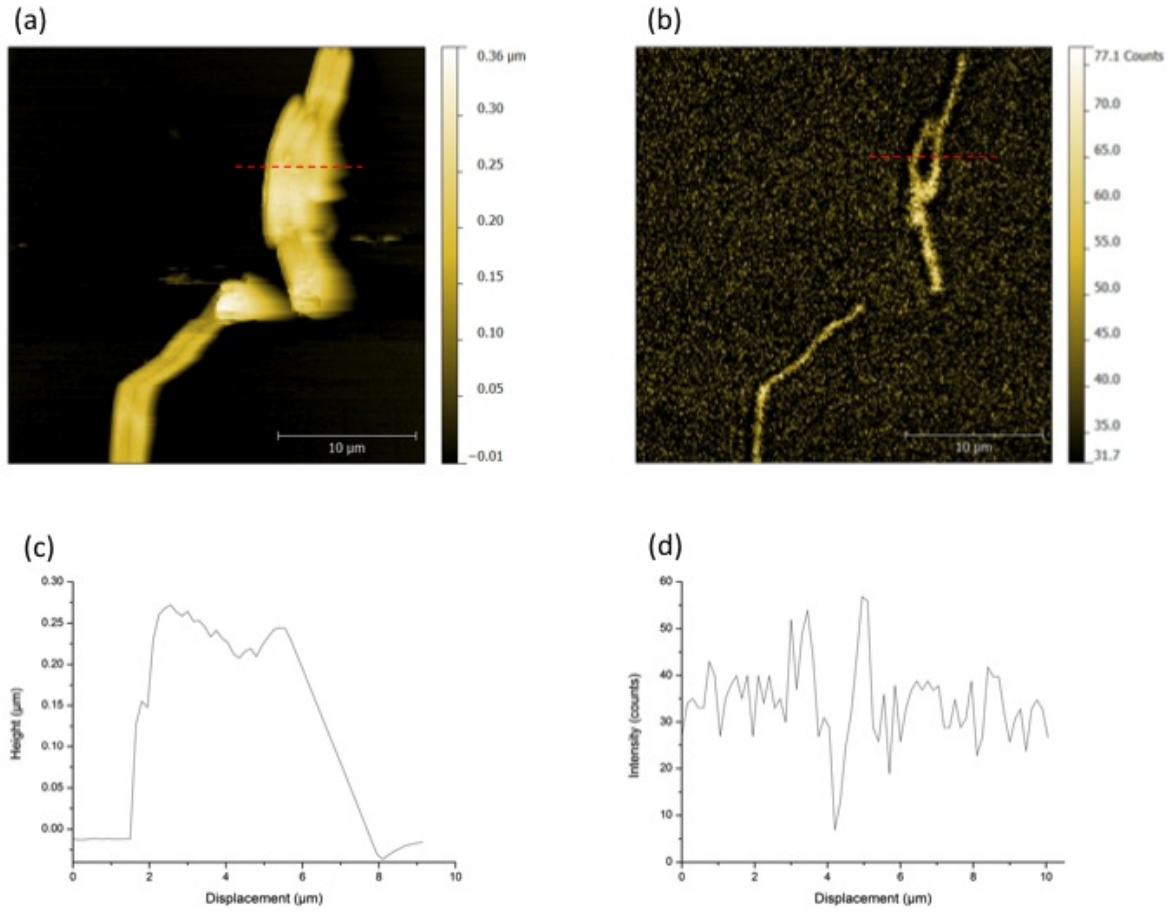

Figure 4.5.1: SNOM images acquired for YFP tagged *E. Coli* cells with mutations to prevent cell separation, showing in (a) 30 x 30 μm topography (b) line profile acquired for the highlighted region in topography (c) 30 x 30 μm fluorescence (d) line profile for highlighted region in fluorescence.

Resolution of images acquired with the SNOM (outside of the limit imposed by the tip) are defined by the user in the guise of the number of line scans that make up an image. This is highly beneficial for large images where at lower line resolutions a pixel

may represent several hundred nanometres. The greater resolution also aids optical image acquisition with the APD where each pixel again signifies smaller pixel areas that are on the scale of the maximum theoretical optical resolution. When optical images are taken alongside height images of a sample the scan speed is no longer dependent on that assigned by the user but that of the defined integration time of the APD at each pixel. In defining this parameter considerations have to be taken as to how long the integration time should be, too short will result in a low fluorescence intensity value, too long however will increase scan times thus increasing illumination time within which photo degredation can occur and depending on the sample, potentially result in more background signal being detected. In this work the integration time varied, for the fluorescent proteins with greater fluorescent intensities values of $20-30$ ms were used, however as the photosynthetic systems were less fluorescent the value would range between $20-50$ ms to achieve the optimum time for the sample.

4.5.4.2 Processing

Small adjustments were made to acquired SNOM images (topography and fluorescence) to account for anomalies due to the system. A main source of image processing was that to correct for sample tilt in topography. By performing levelling of the height image it was possible to get an accurate measurement for the sample, if this wasn't carried out in the patterned arrays, for example, across the sample it would be seen that the zero value is not constant and increases alongside the maximum thickness of the fluorescent proteins. Corrections were carried out in one of 2 ways in the image processing software, Gwyddion. One way was through automatic levelling included in the software although useful for fast image processing it was more inaccurate than using a 3-point levelling process that can be performed on areas specified by the user. The second allows 3 similarly flat regions (e.g. where there's no sample) to be used to flatten and match these regions of the image, the regions specified may look like they vary largely due to the sample tilt but can be matched to one another to provide an accurate depiction.

In fluorescence images acquired by the SNOM similar measures are taken so that the

image can be analysed. Fluorescence images are also subject to issues pertaining to sample tilt due to this, signal may be lower or higher depending on the variation in the distance that the evanescent wave travels relative to different parts of a sample (remembering that signal degrades with propagation distance). Applying a 3-point levelling process to these images allows similar regions of zero/low signal to be matched to one another and then corrected for any non-uniformities. This process can also be applied where varying intensities may be seen across the image due to the alignment of the transmission objective, if the fluorescence isn't focused centrally the resulting image may see a variation in the focal point and thus the maximum detectable fluorescence.

It was found when dealing with fluorescence from different samples and with varying APD integration times that signal-to-noise levels varied which could cause issues in distinguishing fluorescent signal for weakly emitting samples. In this case image mathematics could be applied in an attempt to improve the clarity of the fluorescent signal. Images in SNOM are recorded in both the forward and reverse configuration therefore two images are collected per scan and with this, the two fluorescent images that are collected can be added and an average taken. As the signal to noise ratio may vary in the two directions the signal can be observed to increase relative to the noise, this can also be applied to successive images of the same region if no photo-oxidative effects have occurred.

Another measure taken to enhance both topography and fluorescence SNOM images was to adjust the contrast of the images through the software's histogram function. Doing this allows the colour distribution across the sample to be controlled over the height range of interest by adjusting the minimum and maximum threshold values, allowing finer or weaker features to be resolved where they may have been previously masked by the height ranges of the original image.

4.6 AFM/Fluorescence

As the AFM used in this work was mounted on an inverted microscope, it was possible to obtain simultaneous fluorescence and AFM images.Due to the scanning nature of the

AFM only the scanning mode fluorescence can be utilised as the EMCCD microscope would result in blurred images of the field of view with the EMCCD camera. Another reason to not use the EMCCD is that the amount of vibration induced by the cooling fan for the CCD would yield very poor AFM images, this problem isn't encountered with the APD.

As the scanning fluorescence microscope imaging method works on the same principle as AFM (the only difference being the property being measured), modifications to the combined system are kept to a minimum compared to the individual techniques. The scanning fluorescence microscope can be aligned and focused through the method previously mentioned. To allow both AFM and fluorescence images to correlate to one another the EMCCD is used furthermore in the alignment process when used in real time imaging. By using the focus of the microscope it is possible to correlate the position of the tip with the laser. Preparation of the monochromator and APD then follow the same process with imaging starting when the AFM is engaged with the sample, the readout of the AFM giving data relevant to the topography/surface properties whilst also combining with the fluorescence obtained from the APD. Properties relating to both techniques are kept in the combined process allowing fluorescence imaging at different wavelengths through the monochromator to be correlated with specific regions in topography. Image processing of the two forms of image remain unchanged from the processing previously mentioned however, the software is used to obtain line profiles of the topography and the fluorescence of which the data can be plotted to correlate relative intensities with thickness.

For the AFM/fluorescence image process a number of considerations were taken into account to ensure high resolution imaging of the sample with both microscope components. The configuration of the equipment allowed measurements to be conducted under imaging in a petri dish whilst a light stream of nitrogen could be fed towards the sample via the AFM profusion cell thus ensuring that photo-oxidation was kept to a minimum to maintain the optical properties of the sample but also ensuring AFM of high resolution under physiological conditions which is ideal for the biological samples not to suffer structural damage. To obtain high resolution AFM images any vibration of the system had to be kept to a minimum so that the tip wouldn't crash and so that there is no noise from external

sources present on the topography. To achieve this the EMCCD detector was only used in the initial alignment of the optical properties of the system, the fan induces constant noise on the image with a periodic nature which is undesireable when dealing with samples containing periodic structures. It was also realised that the fan on the laser caused vibrational noise to the AFM images therefore the laser driver was located outside of the enclosure to ensure the attainable resolution wasn't comprimised. Optical measurements in this set up are marred by the laser used on the AFM to measure the deflection of the cantilever. To collect signal originating from fluorescence an 820 nm short pass filter was introduced into the optical path, in conjunction with the fluorescence filters this could be removed from images. With bandpass fluorescence filters this didn't cause a severe problem however, for samples with broad emission longpass filters were needed which could receieve signal from the laser on the AFM.

4.7 Summary

This chapter has outlined the instrumental setups used to examine biological samples of photosynthetic bacteria, fluorescent proteins and chlorosome light harvesting structures. The microscopy techniques required to measure fluorescence and topography of sample surfaces both in far-field and near-field regimes have been addressed in this chapter along with the considerations undertaken with each technique to facilitate the measurement of photosensitive biological samples. Even though these considerations have been undertaken in this work, they remain open for other researchers to develop for measurements using the same equipment on other sensitive biological samples, such as with other proteins and other light harvesting samples. The procedures that are utilised to purify proteins and isolate specific light harvesting components from photosynthetic bacteria have also been addressed. Surface preparation techniques also show the methods by which samples can be fixed to the surface by thin film techniques or by patterning techniques which may hold the key for future research into the further development and production of biological nanowires for bio-electronic applications.

4.8 Bibliography

[1] J. Michel B. Bosshard H. Delamarche E Bernard, A. Renault. Microcontact Printing of Proteins. *Advanced Materials*, 12(14):1067–1070, 2000.

[2] P. Bruinink C. van der Werf K. Olsen J. Timney J. Huskens J. Hunter C.N. Subramaniam V. Otto C Escalante, M. Maury. Directed assembly of functional light harvesting antenna complexes onto chemically patterned surfaces. *Nanotechnology*, 19:1–6, 2008.

[3] H. Stutz R. Delamarche E Foley, J. Schmid. Microcontact Printing of Proteins Inside Microstructures. *Langmuir*, 21:11296–11303, 2005.

[4] G Glaeser, J. Klug. Photo-oxidative stress in Rhodobacter Sphaeroides: protective role of carotenoids and expression of selected genes. *Microbiology*, 151:1927–1938, 2005.

[5] C Gittes, F. Schmidt. Thermal noise limitations on micromechanical experiments. *European Biophysics Journal*, 27(1):75–81, 1998.

[6] R Tsien. The Green Fluorescent Protein. *Annual Reviews in Biochemistry*, 67:509–544, 1998.

[7] A. Hallen H. Paesler M Yakobson, B. LaRosa. Thermal/Optical Effects in NSOM Probes. *Ultramicroscopy*, 61:179–185, 1995.

Chapter 5

Imaging of patterned biological material

5.1 Introduction

Optical microscopy techniques have been vital tools for probing samples at the micron scale in the life science . Significant amounts of information can however be lost in optical microscopy due to the diffraction limit and the restrictions that it imposes on spatial resolution. It is possible to overcome this optical limit by employing techniques such as SNOM which has the ability to exploit the properties of evanescent waves by utilising a nanoscale light source to achieve sub diffraction limit resolution.

To study samples formed from the μCP printing of fluorescent proteins (outlined in 4.2.1), far-field fluorescence microscope measurements have been conducted as well as near-field SNOM measurements. Through the acquisition of images with far-field and near-field fluorescence microscopy techniques alongside AFM images, it has been possible to draw a relative comparison of the resolutions attainable when these microscopy techniques are applied to ordered samples. The microscopy techniques used in this work have also allowed information to be obtained relating to the relationship between the topography of specific regions of interest and their fluorescence intensity and has allowed correlations between

the two to be drawn.

Sample preparation is a vital consideration for the possible future applications associated with these materials to ensure that deposition of light interacting proteins is uniform and of a significant density across the sample. The sample preparation is also vital to preserve structural detail in the patterning process ensuring that the background fluorescence signal is kept to a minimum so that high signal-to-noise can be achieved to allow high resolution fluorescence microscope images to be obtained. Reproducibility of the sample's structural and fluorescent properties is of high importance in this work and these microscopy techniques can act as a measure of this.

The fluorescence microscope techniques used in this study have acted as a method to analyse the structural integrity of patterned proteins on the surface as well as analysing the photostability of the proteins that have been transferred. Measurement of the fluorescent spectrum of the proteins as well as the fluorescence intensity over time allows any changes that occur to the protein's optical properties as a result of the patterning process to be observed. It also allows the effectiveness of the patterning process to be addressed by analysing the amount of material transferred to the surface as well as the optical properties. Fluorescent proteins can be analysed through fluorescent techniques that image by constantly illuminating the sample, which allows the lifetime and photostability of the sample to be addressed. The various microscopy techniques have allowed the lifetime and photostability of the fluorescent proteins to be addressed finding that GFP is a favorable fluorescent protein for μCP.

5.2 Spectroscopic properties of fluorescent samples

The main objectives of the measurements conducted on the patterned fluorescent proteins were to compare the microscopy techniques at hand and to analyse the merits of using μCP in the patterning of biological samples. Observing how the samples were affected by fluorescent measurements and seeing whether there was any degredation in their optical properties was of interest to see whether such techniques could be applied to other biological

samples from bacterial light harvesting complexes that are much more susceptible to photo-oxidative damage. It is desireable with the measurement techniques that changes to the sample are not induced which would cause optical properties to be significantly affected.

To address the success of protein patterning in retaining a sample's fluorescent properties, spectroscopic information was acquired and applied to see if the patterning process caused any significant changes to the protein's optical properties. The spectroscopic information could also be used to reference against samples which are illuminated for relatively long periods to address spectral changes with fluorescence microscopy analysis. Absorption and emission spectra of fluorescent proteins were obtained using a Fluoromax-4 spectrafluorometer (Jobin Yvon). Spectra obtained from bulk fluorescent material (as shown in 5.2.1) of YFP display the charactistic absorption peaks, in line with the literature at 470 nm and the fluorescence is also observed at 535 nm [1, 2]. Similar bulk spectral measurements on GFP (not shown) have also displayed no significant change when compared with the literature. These measurements show that, growth conditions employed for these fluorescent proteins don't affect the spectral properties when compared with those in the natural protein conditions and is therefore favorable for creating fluorescent material to be used in patterned structures.

Spectroscopy of the the bulk material was primarily employed to ensure that the purification process applied to the protein and the introduction of dilution buffer didn't cause significant changes to the spectral properties of the protein. Dilution of the fluorescent protein in 20 mM of HEPES buffer ensured that the fluorescent proteins were maintained at a constant pH of 7.5 to not cause damage to the fluorophore that may occur due to acidic or alkali environments and thus affect the spectral properties due to ionisation of phenol groups. This also ensures that the solution is maintained at a concentration where reabsorption of emitted photons doesn't occur in significant amounts. The spectra could also be compared to spectra from the fluorescent patterned samples to show if the purification caused specific changes or if the patterning process caused any changes to the fluorophore structurally or through photo-oxidation.

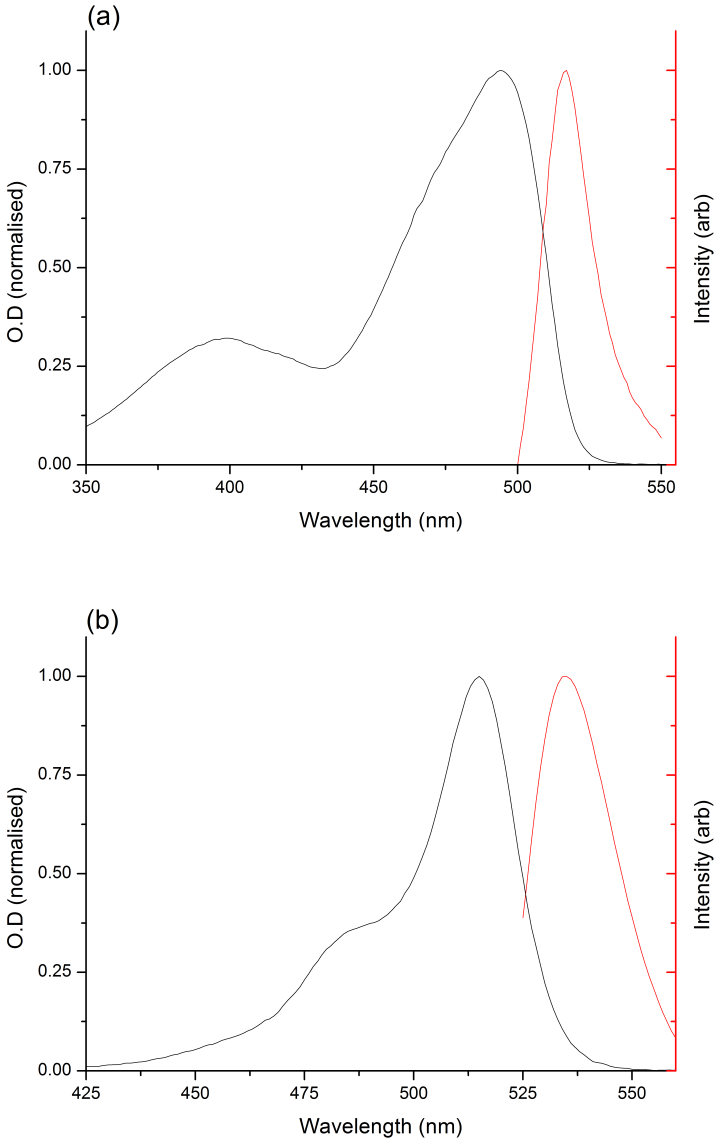

Figure 5.2.1: Bulk solution measurement of the absorption (black plot) and fluorescent emission (red plot) from (a) Green Fluorescent Protein, (b) Yellow Fluorescent Protein .

5.3 Fluorescent Microscopy of Patterned Fluorescent Proteins

5.3.1 Micropattern analysis

The high fluorescence intensity observed from GFP when measured with the fluorescence microscope allows images of samples to be obtained approaching the diffraction limit. The strong and stable fluorescence from GFP coupled with μCP on substrates facilitate investigations into the viability of the patterning process and into the relative resolutions of the microscopy techniques used to measure this.

Fig. 5.3.1 shows images of the patterned GFP samples obtained with the fluorescence microscope using the two different illumination sources. Excitation filters centred at 470 nm were used to excite the samples at their peak absorption maximum and thus achieve maximal fluorescence intensity. Image (a) sees some variation in fluorescence intensity across the different patterned areas which potentially arises from variations in the amount of fluorescent material present on the substrate (an effect that can be addressed later through combined scanning probe and fluorescent measurements). Within the field of view in image (a), the resolution isn't particularly high except for the more intense regions which can be put down to the objective used for the acquisition of the image. Illumination using an LED with a central wavelength of 470 nm allows much more to be revealed regarding the amount of GFP patterned on the surfaces, as seen in image (b). The higher intensity and more precise excitation source allows some of the weaker fluorescent regions to be detected with the fluorescence microscope with less erroneous light from the excitation source adding to the noise of the image.

It can be seen in both images from the halogen lamp and LED illumination that, the μCP fluorescent sample coverage can vary locally both in fluorescent intensity and the apparent amount of material fixed to the surface. The intensity of the lines vary across the surface, which can be seen in Fig. 5.3.2, with some regions having low fluorescence (point 1) or no fluorescence at all (point 2), arising either from a lack of fluorescence from material present or from very small amounts of fluorescent material being present and

thus contributing to signal. In comparision bands are seen where there is a much higher level of fluorescent intensity potentially arising from regions locally having a much higher concentration of fluorescent material. In these images some of the variation in fluorescent intensity along the patterns can be explained by effects resulting from the detector which may be due to uneven illumination of the detector or the sample. An example of this can be seen in Fig. 5.3.1 image (b) where the fluorescent intensity is seen to be higher in the top region of the image. Addressing this as possibly arising due to uneven illumination of the sample can explain the uneven fluorescence as either being a direct result of the excitation intensity leading to greater emission or reduced emission in regions where photo-oxidation may occur due to a relatively higher excitation intensity. The large variations observed in the intensity of the patterns can be best explained by variations arising from amounts of material applied to the substrate in the printing process. Non-uniformity in the material applied to the PDMS stamp has a direct effect on the uniformity of patterns transferred to the substrate. Similarly the amount of material fixed in regions in the stamping process can also be from uneven coverage of the Poly-L-Lysine (PLL) on the substrate.

Image (a) in Fig. 5.3.3 shows a 57 μm field of view from using a 50X 0.6 NA lens, however a vast improvement to the resolution can be observed in image (b) by changing the objective to an oil immersion lens. The oil immersion lens in this case has a magnification of 65X and 1.4 NA which also changes the field of view to 44 μm). A greater amount of fluorescence can be seen in the weaker regions due to the increased acceptance cone of the lens and area of collection for emitted light. Comparisons between these two lenses can be drawn from taking line profiles of similar regions in the images, this is shown in Fig. 5.3.4 and shows comparisons of emission intensity against that of the background. It can also be used to compare the physical dimensions pertaining to the width of the lines and draw information regarding the relative resolutions of the microscopy technique whilst using the different lenses. In this case it can be seen from the oil immersion objective that fluorescence intensity is increased in line with better NA properties, increased resolution is

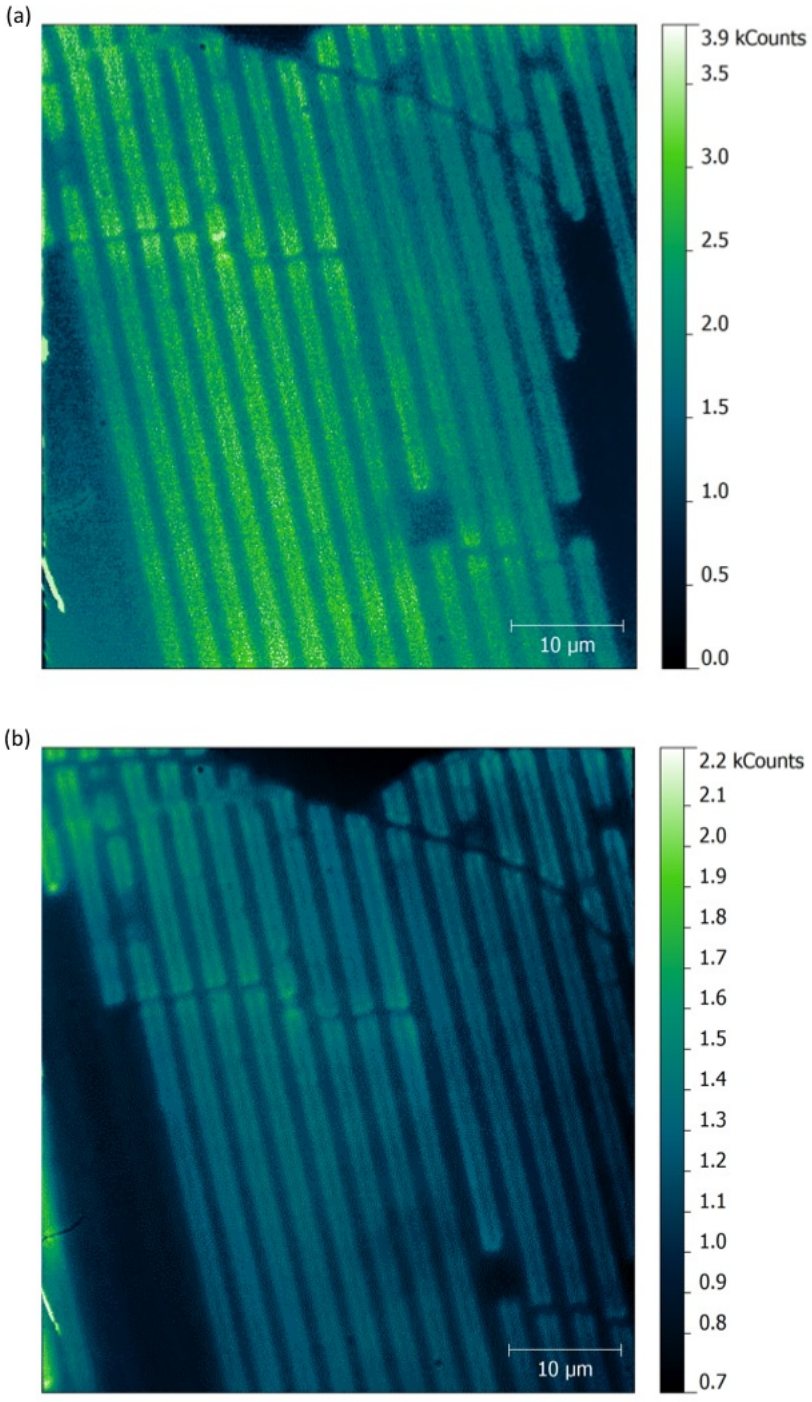

Figure 5.3.1: Images of patterned GFP acquired from fluorescence microscopy using two different illumination sources. (a) Illumination through halogen lamp with excitation filter (b) illumination through 473 nm LED.

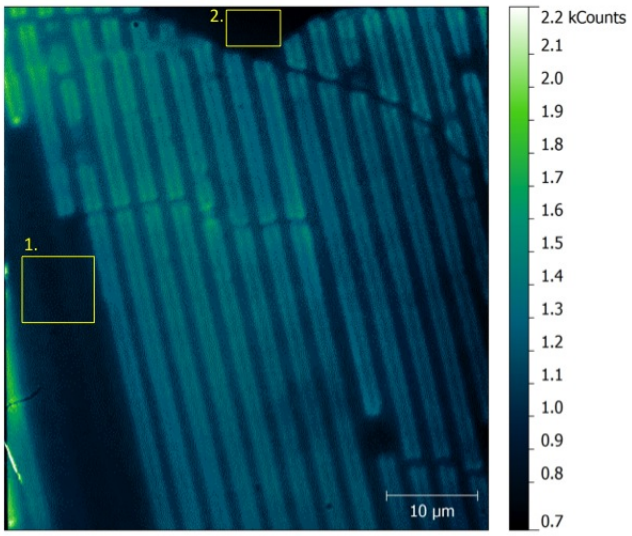

Figure 5.3.2: LED illumination image showing regions of varying pattern coverage with 1. a region of apparent low fluorescent intensity and 2. a region where no sample appears to be present.

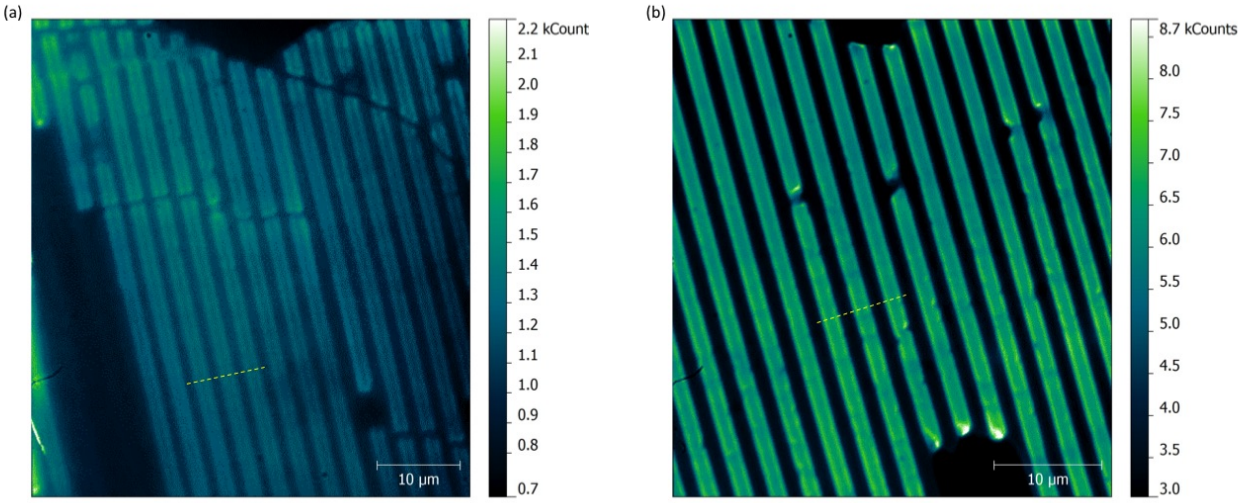

Figure 5.3.3: Comparison of the resolutions attainable with standard microscope lenses and oil immersion lenses. (a) fluorescence image of patterned GFP acquired with a 50X objective (b) patterned GFP acquired using a 63X oil immersion lens. Both images use a 473 nm LED as the illumination source.

also mirrored with the NA increase and magnification increase, as seen with the reduction of the line width in the line profiles.

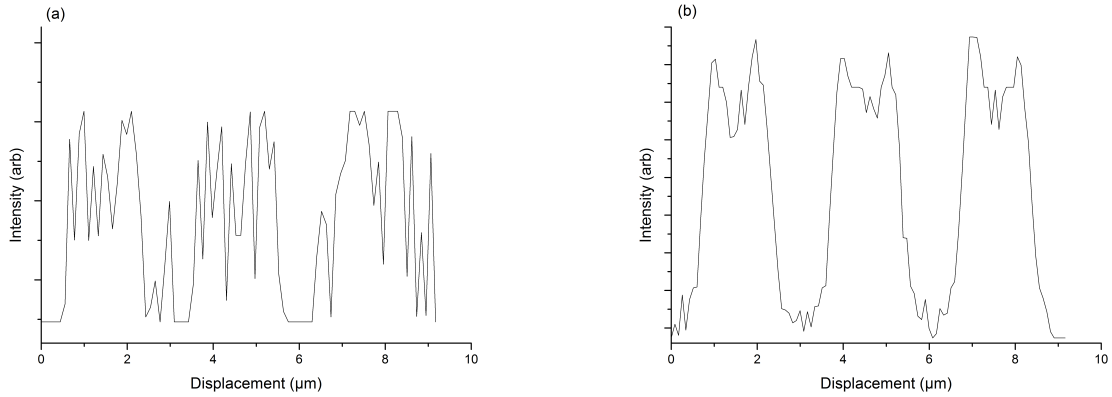

Figure 5.3.4: Comparison of cross-sections from regions highlighted in Fig. 2.1.6 with similar line widths using (a) standard objective (b) oil immersion objective.

5.3.2 Spectral analysis

Fluorescence microscopy is used on μCP samples in this work to analyse the efficiency of the printing process by investigating the uniformity of material on the surface or to analyse the optical properties of the patterned proteins to identify whether the patterning process induces any damage to the fluorophore. To improve fluorescent signal the optical microscope incorporates excitation filters to remove unwanted ambient wavelengths from the excitation source or ambient light from the environment. This is also combined with the selection of specific wavelength ranges with the monochromator for high signal-to-noise detection by the detector. The measurement of the emission spectrum is obtained from a small region of interest situated on one of the fluorescent lines, selection of a small region by opening the monochromator slits by 500 μm or less prevents the emission spectrum broadening due to bulk material and too much fluorescence signal. This process

is employed to keep the emission spectrum narrow and the uncertainty in the emission peak wavelength to a minimum.

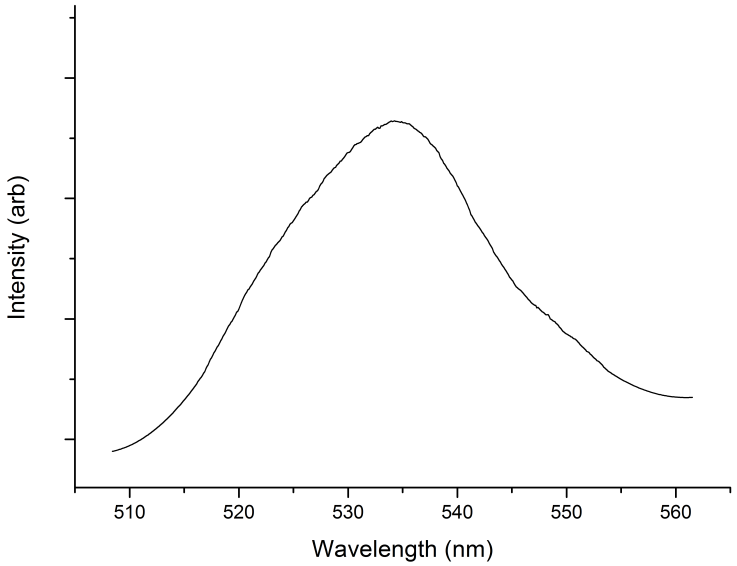

Figure 5.3.5: YFP spectrum measured with the optical microscope and EMCCD camera.

Fig. 5.3.5 shows the emission spectrum from the microcontact printed YFP sample. One can see from the spectrum that the printing process hasn't affected the optical properties of the protein in any significant way as the expected emission peak is still centred around 535 nm [3]. This implies that the absorption/emission properties are retained and thus damage to the chromophore hasn't occurred (e.g. spectral changes from pH). Accurately measuring the emission spectrum in this case is possible due to the reduction of light which is incident on the EMCCD where no significant spectral broadening occurs whereas this would be the case if the spectrum was acquired across a whole image like in Fig. 5.3.3. The emission spectrum here shows that this is a technique that may be applied to other proteins as the physical process of stamping proteins onto a pre-treated surface

doesn't induce chromophore damage and ensures that enough material is transferred to the surface to observe fluorescence.

5.4 AFM analysis

Due to the nature of scanning probe microscopy analysis of the μCP surfaces with AFM can reveal information about the sample regions which have low or no fluorescence activity when observed previously with fluorescence microscopy. The fluorescent microscope's optics allow the field of view of fluorescent images to be on the same scale as AFM scan regions therefore direct correlation can be drawn between images of the same region. The scanning probe technique can reveal if there is fluorescent material present in the regions where no fluorescent signal is detected.

Fig. 5.4.1 shows an AFM image from the micropatterned surfaces in which the greater resolution can be seen compared to similar images obtained with the optical microscope, this is shown with the more defined patterns and thus edges to the lines. The variation in the amount of material across the sample can be seen in the AFM image due to the image scaling which allows regions of varying topography to be seen. The images show that the printing technique causes more material to adhere to the surface in some regions than in others which may be a result of uneven deposition of fluorescent proteins on the Polydimethylsiloxane (PDMS) stamp. It may also be a case that when in contact with the PLL coated coverslips the stamp isn't level and thus the amount of contact/pressure applied to some regions is less than in others leading to greater contact forces to induce adhesion. Line profiles of these regions allow the amount of material present in the printed regions to be determined. With this it is possible to infer how many layers of protein are present on the surface as the dimensions of GFP have been well documented in the literature with the length of the proteins being 4.2 nm [4]. In this case it can be shown that a lot of material is deposited on the surface with at least 100 layers of protein units transferred to the surface.

Line profiles of the patterned regions divuldge information relating to the samples di-

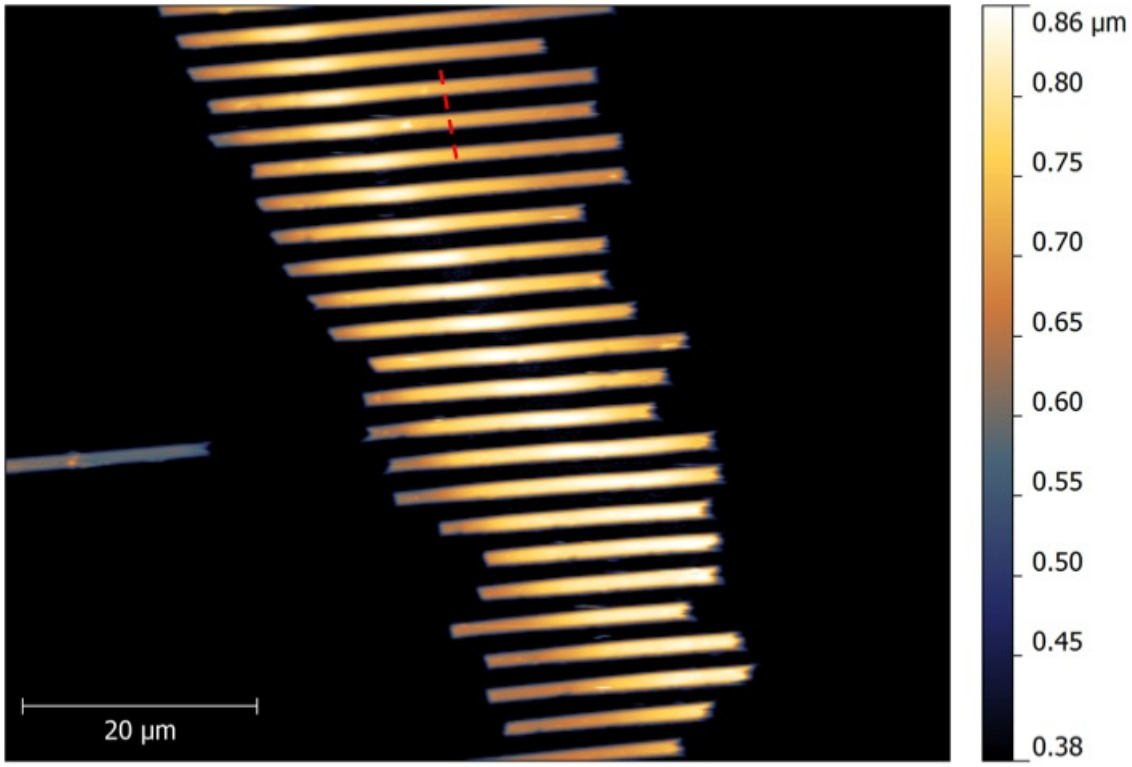

Figure 5.4.1: A 512 x 512 pixel resolution AFM image of patterned GFP.

mensions in the x/y and z-axis which is used to investigate the amount of protein deposited on the surface in local regions of the sample as well as the accuracy of depositing proteins in patterns on the surface. A line profile taken perpendicular to the direction of the linear array is used in Fig. 5.4.2 to obtain information regarding the reproducibilty of these lines in the μCP process. Measurement of the line widths across the x-axis of the line profile yield an average line width of μm, with the range of values varying between 1 μm and 1.2 μm. Observation sees the μCP technique as one that can produce a repeating pattern with only small variations to the pattern sizes (line profiles were also taken in other regions yielding similar results). Any variations that are observed in the width of the protein patterns can be a result of a variation in the physical size of the lines on the PDMS stamp or due to small variations in the protein coverage on the stamp prior to printing, in this case

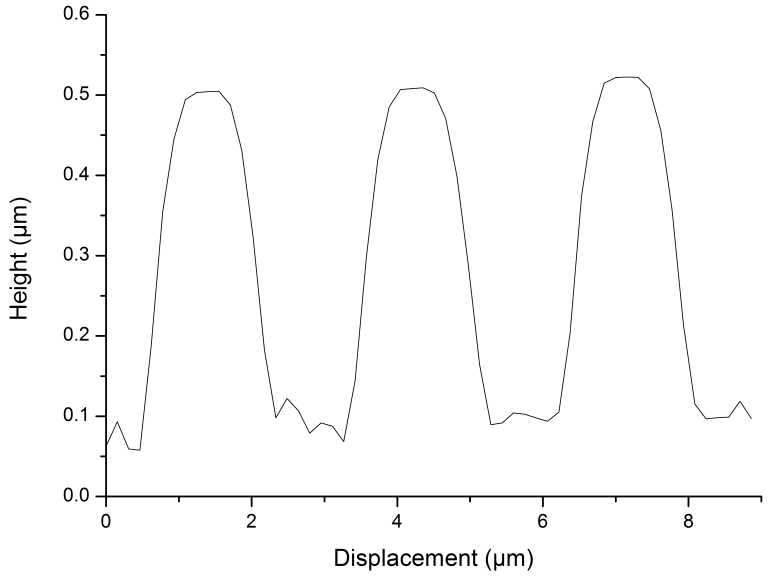

Figure 5.4.2: The image shows a line profile from the previously presented AFM image upon which analysis of the line widths can be made.

there may be some material on the edges of the lines that deposit material to the surface and thus this can be investigated by looking at the height of these regions, line profiles in Fig. 5.4.3 show the occurrence of this. All three lines represented in the line profile show peaks on the lines, the third line cross-section shows shows the afore mentioned effect of material gathering at the edge of the lines with large peaks on each side of the plateau.

5.5 Combined Fluorescence and AFM

The combination of fluorescence microscope and AFM techniques allow for fluorescently active patterns to be characterised in a way that allows correlations to be drawn between topography and fluorescence. Although it is not possible to achieve optical resolutions on the length scale of SNOM due to the diffraction limit of light, it still allows simultaneous

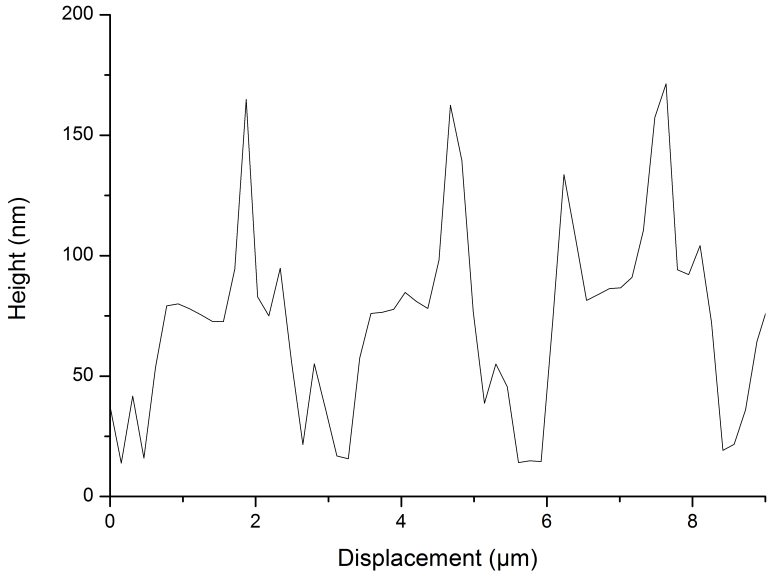

Figure 5.4.3: AFM line profile of a region where deposited material isn't uniform across the pattern.

acquisition of optical and topographic information about a sample whilst also operating on regions of interest up to 100 μm at a practical speed.

5.5.1 Pattern analysis

Images acquired with combined fluorescence/AFM allow regions of varying fluorescent intensity to be correlated with the topography changes present on the sample surface. Using this technique it can be identified whether differences in fluorescence arise from varying amounts of material on the pattern or whether this occurs due to damage caused from the patterning technique. The improvement in resolution obtained by using the oil immersion lens has been previously shown and as a result an oil immersion lens is used in this technique to ensure maximum optical resolution to compliment the high resolution AFM images. The excitation source for analysing the samples in this technique is a 473 nm laser, delivering more power than the LED/lamp. This also results in a 400 nm diameter laser spot and excitation region which aids resolution through a smaller background signal

at each pixel present in the scanning process. In comparison to the other fluorescence technique used, the detector in this case is an APD which has a significantly low noise count and counts photons at each pixel depicted by the scanning stage. In this case the image size can be dictated only by the scanning area set by the user.

Fig. 5.5.1 shows the AFM topography image and the corresponding fluorescence image which have been obtained simultaneously. The first thing to note with these images is that they don't overlap completely and there is some shift between the features on the two images, this is a result of the alignment between the AFM probe and the laser spot used for fluorescence. As the size of the AFM probe tip is smaller than the diffraction limit of light, there is an uncertainty to where the tip resides in x/y when viewed with the EMCCD in the alignment process. This uncertainty can lead to the two images being misaligned with one another on the scale of microns. Even with the translation of the image in Fig. 5.5.1 it is possible to see that for the samples both types of image can be obtained simultaneously and with high resolution following with what is expected, fluorescent signal is contained to the identifiable lines in the AFM image and regions of no signal can be attributed to where there is a lack of protein presence in the AFM image. In the displayed fluorescence image shown some fluorescent signal is observed in the regions between the protein lines where no material is expected. Background signal arises from reflections or filter leakage in the microscope system and not an inaccuracy in depositing material on the substrate as the comparisons made to the AFM image show that there is no indication of there being any features resulting from deposition of material in these regions.

As with the other microscopy techniques mentioned, line profiles are an important tool when analysing the images obtained for the patterned proteins to ascertain whether the variations of fluorescence intensity in different regions arise from varying material concentrations, as well as allowing analysis into the success of the μCP techniques in reproducing patterns on a substrate. Corrections are made with the image analysis software to account for the x/y translational differences seen between images ensuring that the line profiles taken are of the same region. Fig. 5.5.2 shows the region used for the line profile and corresponding line profiles, difference in resolution of the two techniques can

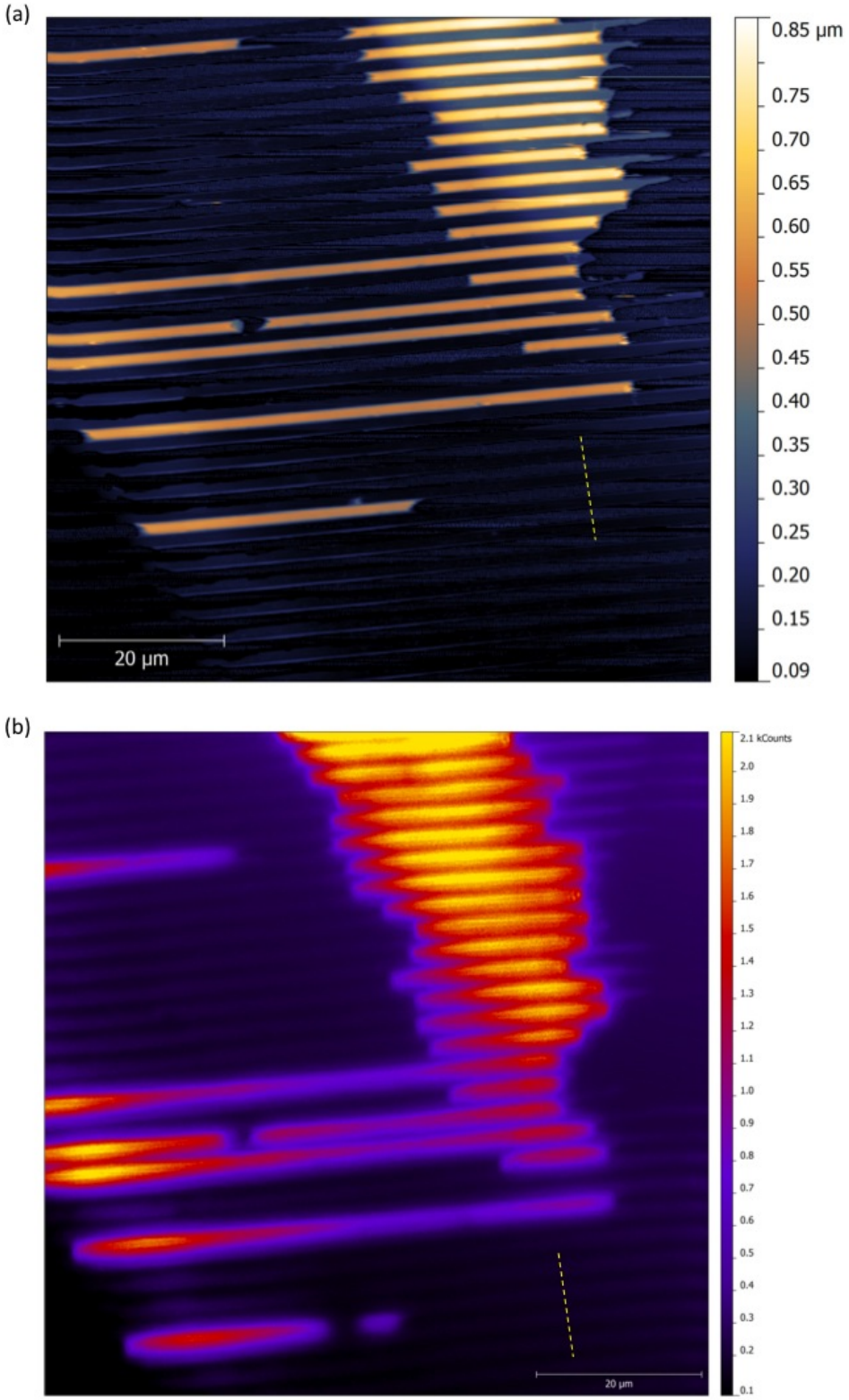

Figure 5.5.1: Combined AFM and fluorescence measurements. (a) a 512 x 512 pixel image of a 80 μm x 80 μm scan region with AFM. (b) the corresponding fluorescence image.

be noticed in these images with the more defined edges to the protein lines seen in the AFM image compared to the fluorescence image. Differences are also seen between the two when calculating the average width of the patterned lines with the fluorescence image yielding lines that are wider than that from the AFM. Direct comparisons show that the fluorescence intensity and topography increase simultaneously suggesting that the high fluorescent signal comes from regions with more bulk material. A variation is seen in the amount of material on the surface, showing that although the printing process is successful at attaching protein material to the surface of a substrate, there is a variation in the amount of material in local regions.

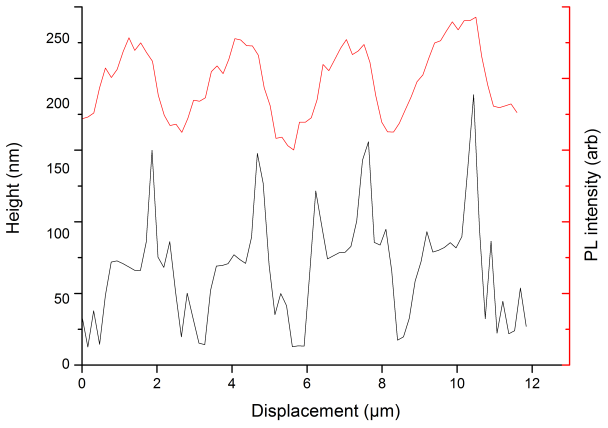

Figure 5.5.2: Line profiles could be used to analyse the patterned regions in the images obtained with the scanning fluorescence/AFM technique. The profiles shown correspond to the highlighted regions in 5.5.1 where the height profile (black) and fluorescence intensity profile (red) are shown.

5.5.2 Spectral Analysis

By using this combined AFM/fluorescence microscopy technique it is possible to obtain spectral information regarding the emission from the patterned proteins. With the spectral information, structural integrity can be probed to see whether the properties of the fluorophore are maintained both in the patterning process and when under measurement.

Use of a monochromator in the optical microscope makes it possible to specify the imaging wavelengths used for measurements, eliminating ambient light from the detector that arises from the microscope system or from the use of longpass filters.

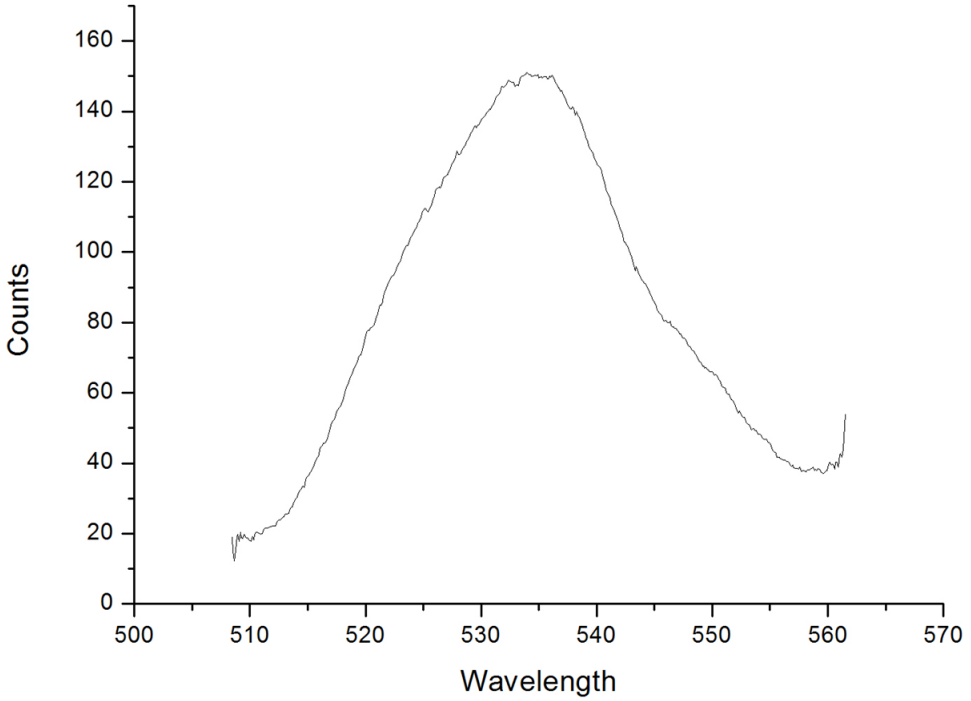

Figure 5.5.3: Recombinated emission spectrum from patterned YFP lines

By obtaining images whilst adjusting the monochromator wavelength across the expected wavelengths of the emission a number of images can be acquired which map the variation in peak fluorescent intensity at each wavelength. One can see a variation in the relative intensities through the wavelengths and by analysing the same point on a line in each image a value can be acquired for the intensity. Thus intensity can be plotted as an emission spectrum such as that shown in Fig. 5.5.3 where YFP has been used due to its higher stability with the constant high intensity excitation. Although this technique of acquiring an emission spectrum can take some time and increase the chances of photo-

damage due to the constant illumination, it can be used to ensure no structural changes have occurred in the patterning process.

5.6 Scanning Near-field Optical Microscope

Scanning probe techniques, like AFM, traditionally only allow topography information to be obtained from a sample, with modifications however it is possible for fluorescence information to be collected (like in this work) although this is still diffraction limited. SNOM on the other hand provides fluorescence/topography information below the diffraction limit which when measured simultaneously can allow correlation to be drawn from regions of varying topography and intensity. As well as probing dual properties of fluorescence emission and topography of the patterned protein samples, the SNOM used in this work provides another technique to draw comparisons between the different microscopy techniques applied to patterned samples. Measurement of the standard patterned fluorescent proteins with SNOM allows the comparatively higher resolution of the near-field optical technique to be utilised whilst at the same time complimenting techniques such as AFM that are often used for the acquisition of topography data.

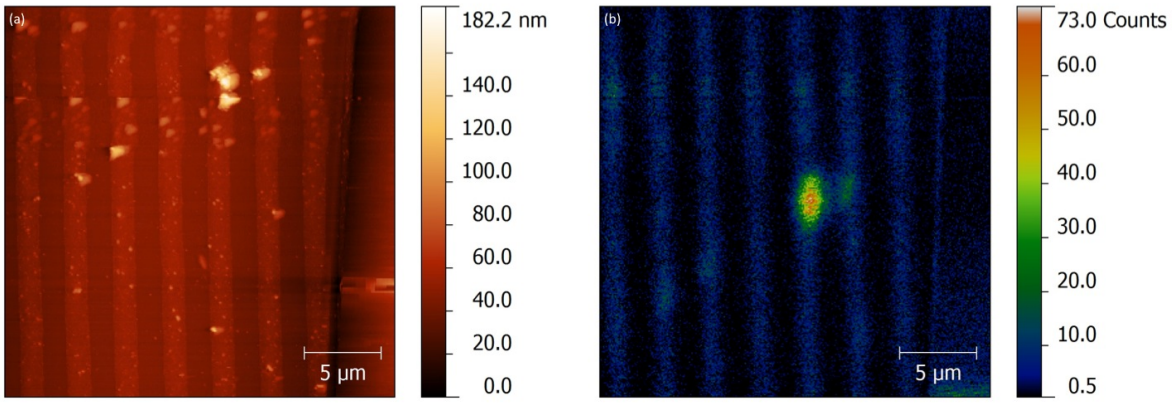

Figure 5.6.1: Topography and fluorescence with SNOM. (a) 20 μm topography image of GFP patterned lines, (b) corresponding fluorescence image.

Fig. 5.6.1 shows the fluorescent and topographical information obtained from linearly

patterned proteins of GFP; it is immediately possible to see differences between the two images that seem to contradict those previously displayed with patterned GFP proteins. The patterned proteins showed a much higher resolution in the scanning probe technique of AFM rather than that obtained by fluorescence microscopy. The topography image obtained through SNOM displays less defined edges to the patterned lines which appear to be much thicker than those shown in the fluorescence image. This difference can be placed with the poor topography resolution of the SNOM probe arising from its spatial size. In comparison to AFM, that has probes on the scale of nanometres, the SNOM probe has a tip that is on a length scale of hundreds of nanometres in diameter which, although it allows nanometre resolution in the z-axis, limits resolution in the x/y axes to the diameter of the probe. In comparison to the topography the fluorescence image shows much higher resolution and defined edges to the lines which display thicknesses in accordance with measurements from using the AFM. Although suffering from limited resolution due to the physical dimensions of the probe, the topography measured by the SNOM still contains essential information about the sample when combined with the fluorescence data. Using both the sub diffraction limit fluorescence images with the topography regions of varying height can be correlated with variations of fluorescence to either pinpoint regions and thus structures that are emitting the observed fluorescence or to find links between the thickness of a region with a higher or lower intensity fluorescence. In this second case simultaneous variation of the two properties can be interpreted as either a greater concentration of fluorescence material leading to an increase of fluorescence at that point on the surface or where there is more material and a decrease in fluorescence, a reduction in the sample's fluorescence due to bulk emission effects.

From line profiles of the same regions in the two types of image it is possible to see whether any increases in the fluorescence intensity that are attibuted to variation in thickness also follow the same degree of change in intensity or if it is a non-linear relation between the two properties. Line profiles can also be used to investigate whether any changes in the fluorescence intensity are a result of the small scale height variations in topography and thus a result of different protein complexes/regions being present within larger structures.

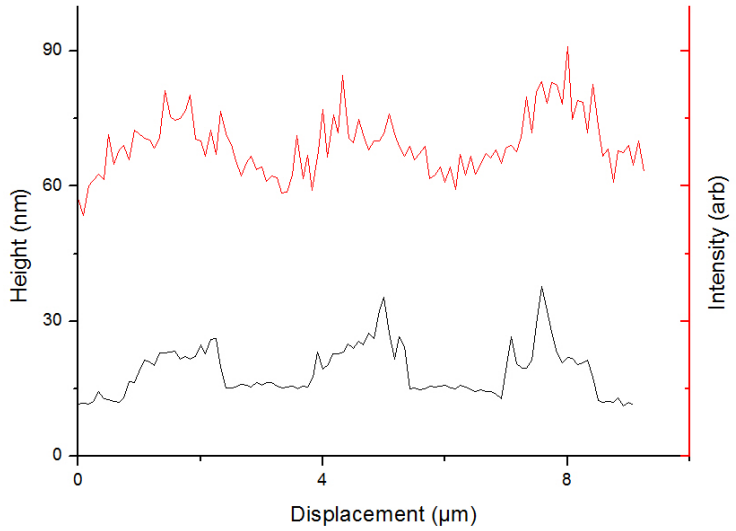

Figure 5.6.2: Line profile for patterned GFP with SNOM. The black profile shows the topography, red shows the corresponding fluorescence.

Line profiles of a region shown in topography and fluorescence images are displayed in Fig. 5.6.2 . These line profiles can immediately be used to analyse the relative resolutions of the two attainable properties from SNOM. Here it can be seen that the width of the lines in the topography image are seen to be larger than their fluorescent counterparts. As already mentioned the greater size of the lines in topography can be attributed to the resolution/size of the probe compared to the 50-100 nm aperture for excitation, however it could also be inferred that the smaller width of the lines in the fluorescence image could be a result of the active fluorescent material mostly being confined in the centre of the line (or if single proteins are damaged at the edge) then less fluorescence would be observed at the edges leading to the appearance of a smaller width. However if this was the case one would expect a tapering in the fluorescence signal at the edge as regions with less protein present suffer a greater amount of decay and the bulk survive, as this isn't seen here the difference in widths can be attributed to the relative resolutions of the measurements. The two line profiles also show a similar relationship between topography and fluorescence that are seen with the combined AFM/fluorescence data where greater fluorescence intensity is

seen in thicker regions of the sample.

The use of SNOM on these high stability fluorescent proteins can be seen to not cause any significant structural damage that can be a result of photo-oxidative effects. From these measurements, certain considerations can be taken, to deal with the photostability for less stable samples such as those of photosynthetic light harvesting complexes patterned in the same way. With the weaker samples nitrogen can be fed into the atmosphere in the SNOM to ensure that the samples remain photoactive for the length of time that it takes to acquire an image. Although the patterned fluorescent proteins are not completely photo-oxidised (lacking fluorescence) by SNOM measurements, continuous measurements carried out on the patterns do yield reductions in the fluorescence intensity of the samples and thus fluorescence decay. Fig. 5.6.3 shows several images of the same region that have been taken over continuous measurements of a patterned region. In these images one can see that the fluorescence intensity decreases with laser excitation due to some photo-oxidative effects, image (d) shows a larger scan area within which the other images had been contained. The photo oxidative effect can be observed in this image with the two distinct regions, one that has been excited and the other that hasn't (higher fluorescence intensity).

The lines seen in some of the fluorescence images obtained for the samples appeared widened similar to the topography, in contrast to that which was expected. This effect can be placed not with the patterns being wider but damage to the SNOM probe which may have led to an increased aperture size which can result in a lower resolution (where resolution in the near-field regime is limited only by the size of the subwavelength aperture). On top of the apparent widening of lines increased fluorescence signal in the regions where there should be no sample is also observed indicating that there may have been too much fluorescent material on the stamp prior to fixation on the substrate leading to an uncertainty in the patterned area. This may be overcome by reducing the amount of material on the stamp for printing to reduce the uncertainty of measurements and improve overall resolution of the patterned samples. This may also be a result of stray light in the system introduced by the tip being damaged and allowing too much light through.

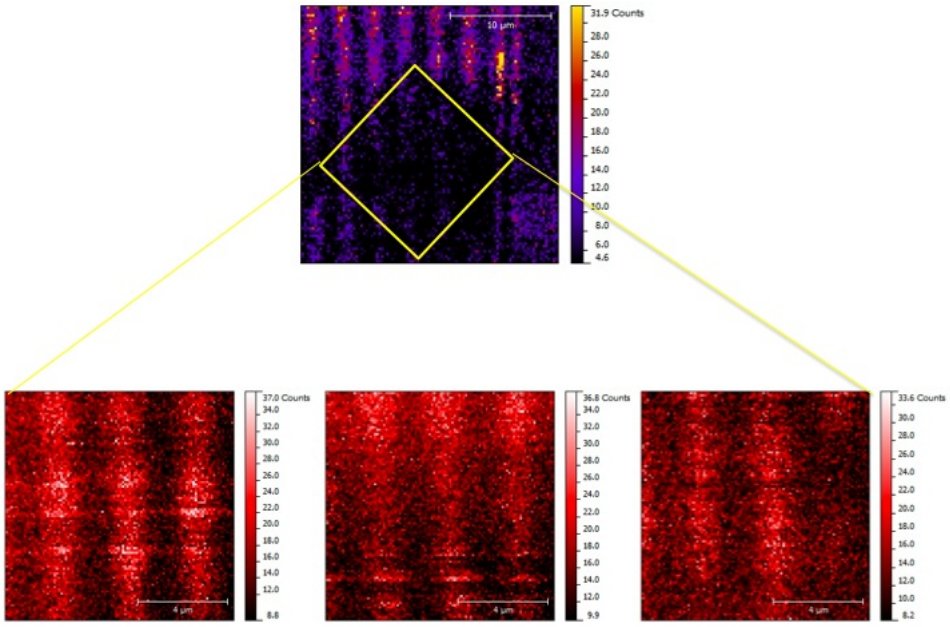

Figure 5.6.3: 25 μm scan of SNOM fluorescence displaying a 10 μm region that has been photo-oxidised through continuous measurement (above). The images below show the 10 μm region over time with the patterns becoming progressively more damaged (lower fluorescent and less well defined, left to right).

5.7 Resolution comparison

The reproducibility of the μCP technique makes the patterned fluorescent proteins ideal samples to compare the relative resolutions of the microscope techniques. With the techniques it is possible to image regions of similar size to draw direct comparisons between the techniques. Similar regions are compared by either setting the same scan area with the scanning probe/scanning optical techniques or by analysing similar regions of interest in the optical systems. In the scanning techniques some consideration has to be taken into account to compare the relative resolutions of the techniques as the scanning resolution can be changed through the software controlling the sample stage (pixel size as resolution). As it can be modified to significantly improve the resolution of the scanning technique, comparisons of the different microscope resolutions has been made with scanning resolutions set to values that are practical for the measurement of biological samples. The practicality of using higher resolutions is based on the length of time an image takes to acquire, in techniques such as SNOM this increases the illumination times involved and can lead to photo damage. The chances of photodamage with longer image acquisition times also affects the number of repeat images that can be acquired on each sample region therefore with this in mind, values used are not particularly high yet still yield pixel resolutions that are on the nanometre scale.

Fig. 5.7.1 shows three AFM images taken with varying line resolutions of 256 x 256, 512 x 512 and 1024 x 1024 obtained for a μCP sample of fluorescent proteins, due to the number of lines that make up the horizontal and vertical axis of these images the time it takes to acquire an image doubles with the increasing resolutions. Based on the time and resolution merits, subsequent images have been acquired with line values of 512, this can also be applied to the scanning laser optical microscope in an attempt to obtain similar pixel sizes in the imaging program. However with the SNOM technique, the time spent at each pixel is greater than that of the scanning stage involved with AFM/laser scanning, Fig. 5.7.2 shows different line resolutions for the SNOM technique. The image shows two resolutions of 100 and 200 pixels per axis these can be applied to any scan size to achieve

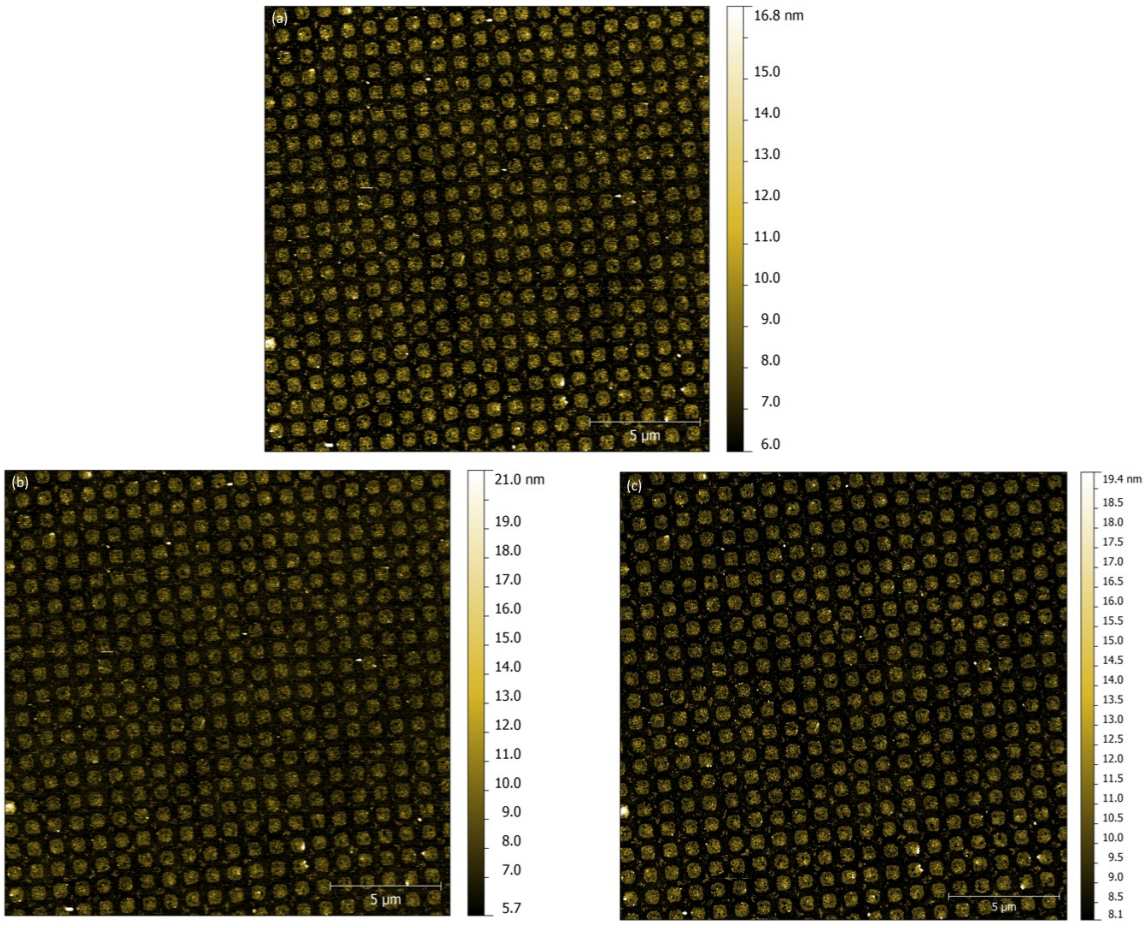

Figure 5.7.1: μCP grids of YFP measured with AFM at varying line resolution: (a)256 x 256 (b) 512 x 512 (c) 1024 x 1024 pixels

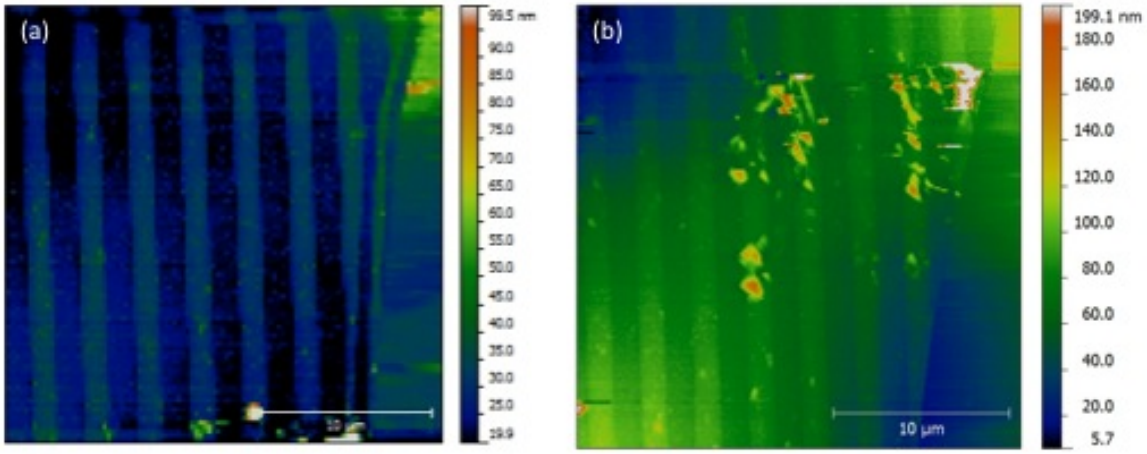

Figure 5.7.2: The images show 25 x 25 μm SNOM topography images obtained for micropatterned GFP with the x, y axes each comprising of (a) 100 lines (b) 200 lines.

adequate high resolution, increasing the resolution to values higher than this however begins to become impractical with the increased integration times at each pixel due to the optical measurements. Higher resolution values lead to much longer image aquisition times on the time scale of hours which, with the length of excitation of the sample can lead to photodamage over this time and lead to images that are non-uniform.

Fig. 5.7.3 shows images from the four microscopy techniques used in this work that of SNOM, AFM, far-field fluorescence microscopy and scanning fluorescence microscopy. Image (a) taken with the standard optical microscope has used the afore mentioned oil immersion lens to improve resolution resulting in a field of view around 45.5 μm. The field of view for the scanning optical microscope and AFM in image (b-c) has been set at 80 μm, they have also been acquired at a line resolution of 512. Image (d) is that acquired through SNOM, the field of view in this image is 25 μm determined by the maximum scan size of the technique. It is possible to observe some differences in the resolution of these images prior to obtaining line profiles from the apparent definition of the lines and the contrast differences at the boundary between the lines and the background region with no protein present. One can see in this case that the AFM and SNOM techniques offer the

most pronounced lines compared to the optical techniques, in line with expectations when the diffraction limit is taken into account. Line profiles of a number of lines in similar regions allow a greater analysis of the resolution of each technique to be obtained. With the average measured line widths obtained for each technique to compare them against one another and the expected line widths from the stamp used in the printing process, this information can also be used to address the success of depositing the sample on the substrate with the thickness of patterns and reproducibility.

Fig. 5.7.4 shows the line profiles obtained from the images in Fig.5.7.3. With the profiles on similar graphs it is possible to see how the definition of the line width (and thus resolution) varies between the microscope techniques. In this comparison one sees that the profiles from the scanning probe techniques yield a more pronounced edge to the fluorescent protein line and thus signifies the expected diffraction limit free, higher resolution properties of these techniques.

5.8 Pattern analysis

Where systems such as patterned fluorescent proteins are to be used as potential components in bionanotechnology it is important to address the success of the patterning technique to ascertain whether it accurately produces patterns that are uniform in their fluorescent properties and topography as well as being reproducible for use with a number of substrates. In this study the microscope techniques have been applied in ways to allow analysis of pattern uniformity to be conducted in the post processing. Fig. 5.8.1 compiles several of the previously encountered images of the patterned flourescent proteins with the lines highlighted on the images to be used as candidates for a measure of the pattern uniformity along the lines, this meaning that the lines have no visible uniformities (such as those seen with the very bright region in the SNOM image). By taking line profiles parallel to the pattern on the surface, the height variations on the protein lines can be compared to those where no sample is present on the substrate. Due to the differences in the size of the scanning regions of each technique, the height variations can be addressed on length

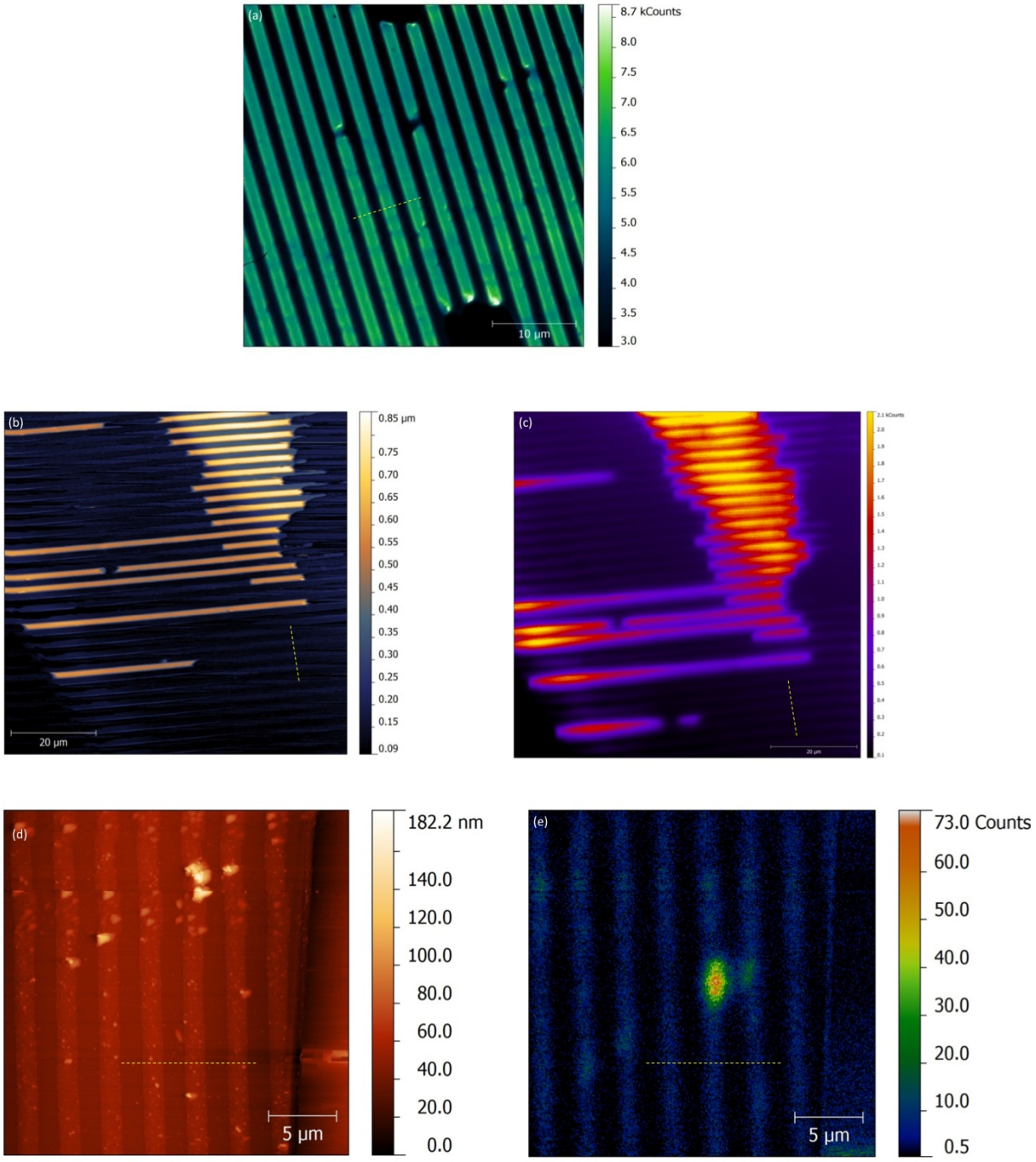

Figure 5.7.3: Images of μCP GFP obtained with the different microscope techniques, (a) standard fluorescence microscope (45 x 45 μm) (b) AFM (80 x 80 μm) (c) scanning fluorescence microscope (80 x 80 μm) (d) SNOM topography (25 x 25 μm) (e) SNOM fluorescence (25 x 25 μm).

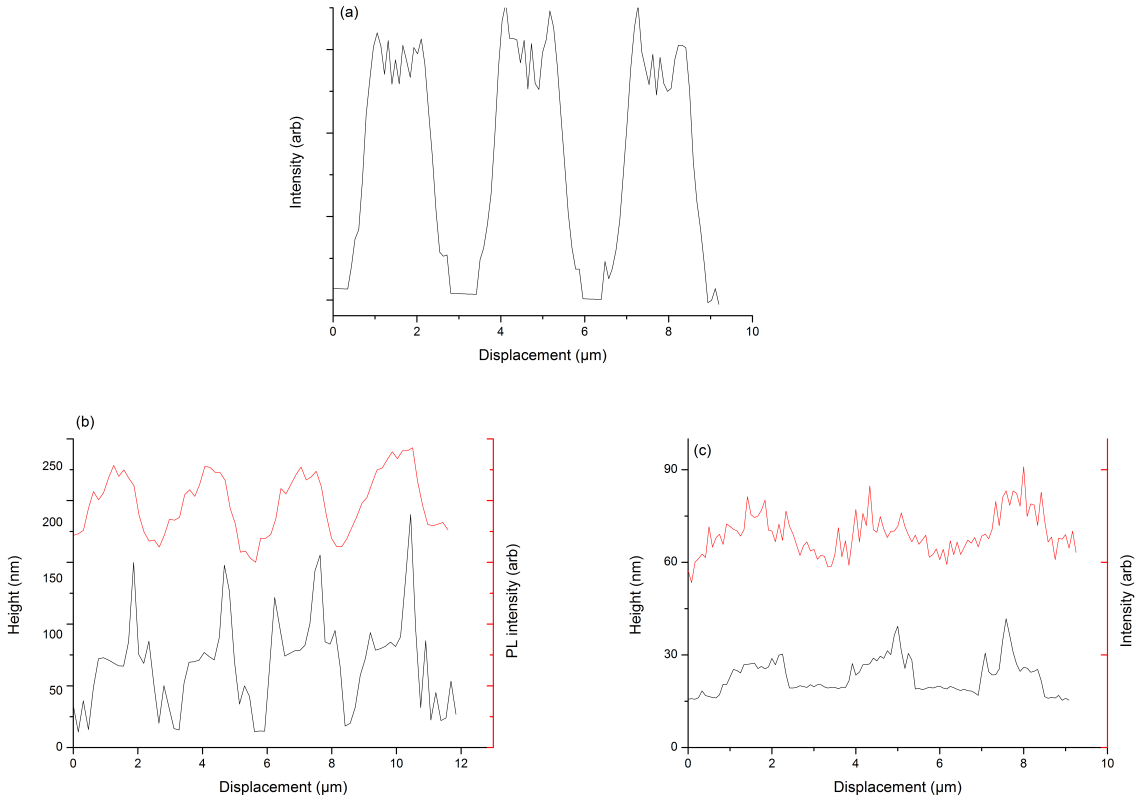

Figure 5.7.4: Line profiles corresponding to similar regions in the microscope images previously shown (a) line profile from fluorescence microscope (b) AFM line profile shown in black and scanning fluorescence in red (c) SNOM topography in black and fluorescence shown in red.

scales ranging from the sub micron to tens of μm.

Fig. 5.8.2 shows the line profiles corresponding to the regions highlighted in Fig. 5.8.1 . It can be seen in the optical images that the variation in pattern height along the sample varies small amounts similar to that also seen in the line profile of the blank substrate regions showing that in this low resolution case the patterning technique applied to fluorescent proteins can produce patterns that are mostly uniform and vary only with noise present due to the observing system. The AFM line profiles also show no major variations between the uniformity of the printed patterns and the background of the substrate, it can be noted that the roughness of the background line profile is less than the patterned profile which suggests that minimal material is transferred to regions that are meant to be blank. The scanning fluorescence microscope line profiles show a similar uniformity to the patterning when compared to the background signal, in this case the background fluorescence intensity is high compared to the pattern fluorescence. This can be attributed to ambient light leaking into these regions through reflections in the optical system or filter leakage, it may also be a result of some fluorescent protein being transferred to the background regions of the substrate. In images (d-e) line profiles are shown for the topography and fluorescence measurements made with SNOM. These line profiles show similar results that are seen in the other microscope techniques with the variation of the patterned protein topography/fluorescence observing low variations in line with the noise seen in the background measurements. This property furthermore suggests that sample uniformity is high along the patterned lines with variations in the sample thickness resulting in fluorescence variation predominantly being observed due to noise and not due to actual thickness differences (and example of a major difference in sample thickness being seen in the SNOM images with a thick region of a line pattern being detected).

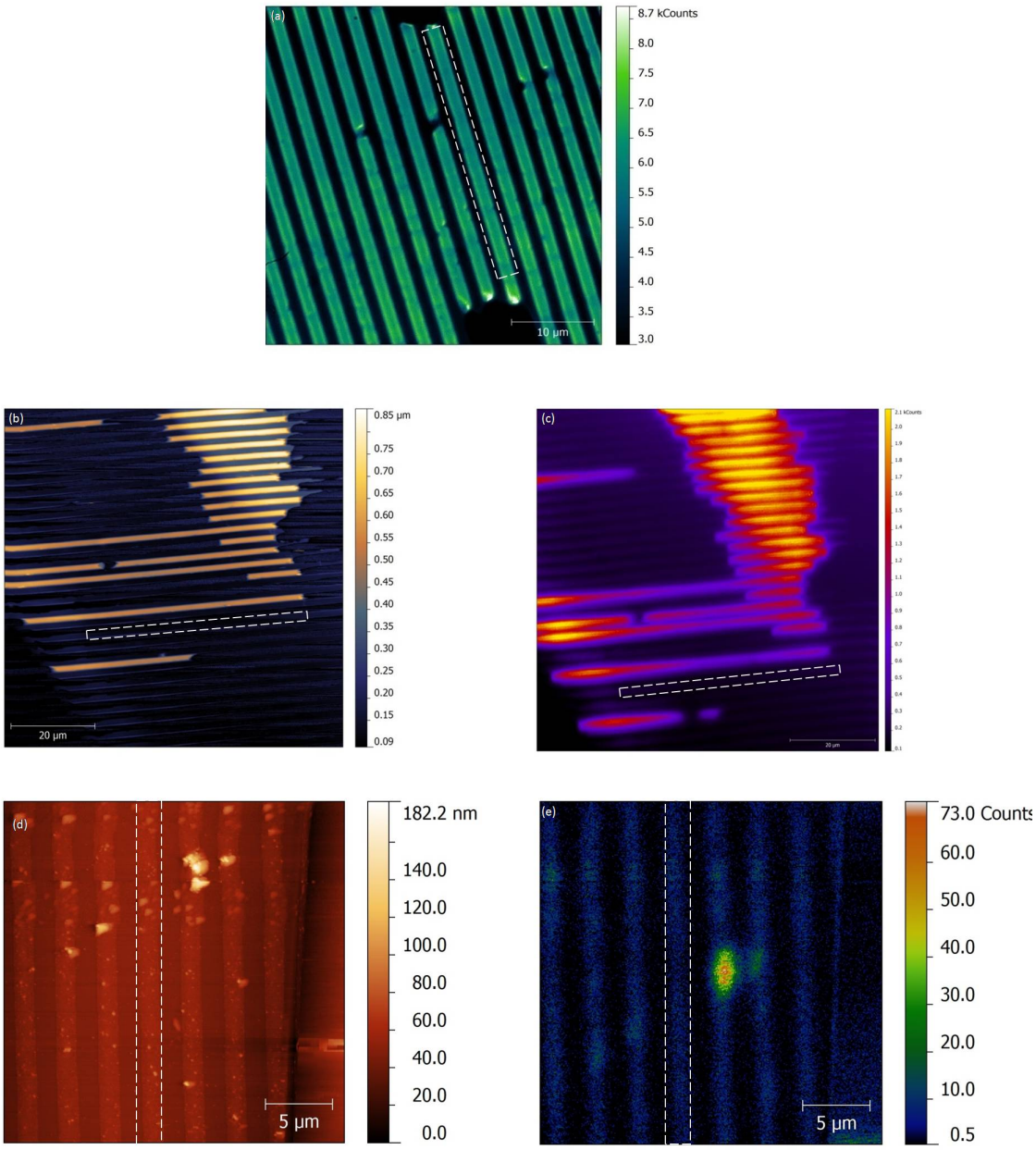

Figure 5.8.1: Images marked for pattern analysis into uniformity of the patterning process. (a) fluorescence microscope image (b) AFM (c) scanning fluorescence microscope (d) SNOM topography (e) SNOM fluorescence.

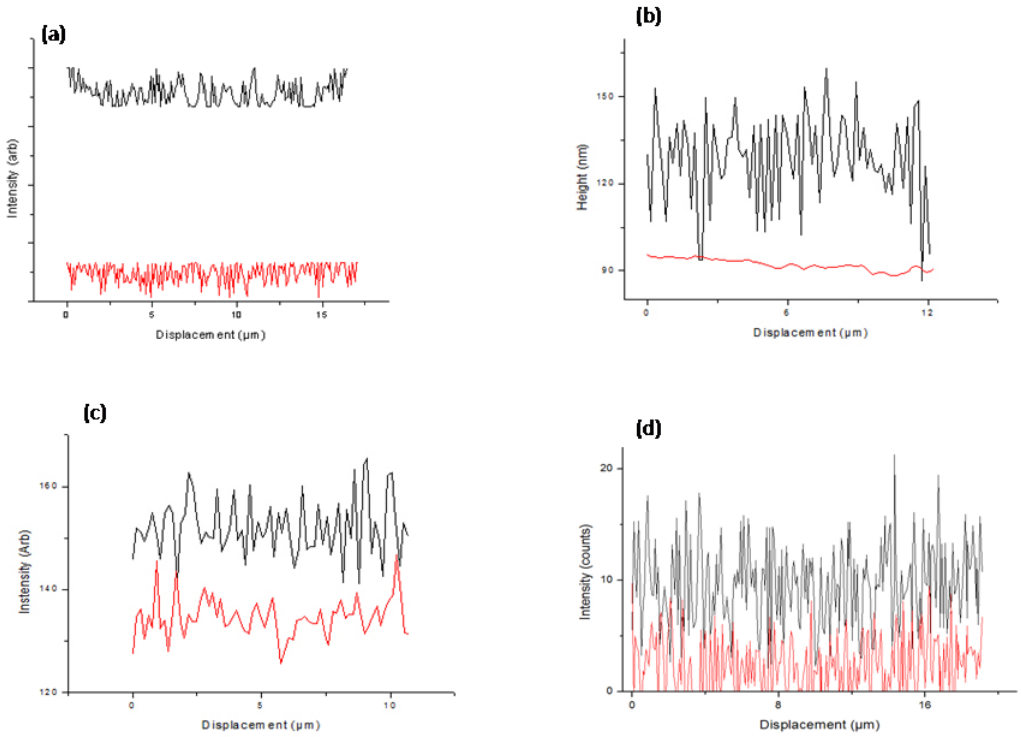

Figure 5.8.2: Line profiles analysing the uniformity of the patterned fluorescent proteins using (a) fluorescence microscope (b)AFM (c) scanning fluorescence microscope (d) SNOM topography (e) SNOM fluorescence.

5.9 Summary

Measurements on samples formed from μCP fluorescent proteins have shown the patterning technique to be successful when applied to the biological samples, with the fluorescent proteins being a stable sample to facilitate many measurements on a single sample. Overall the patterning process has been observed to produce linear arrays of fluorescent proteins that are reproducible and leading to uniform thickness of the arrays across the substrate. Fluorescence and scanning probe microscopes have been utilised to analyse the properties of the patterned samples to investigate sample thicknesses/protein coverage as well as the fluorescent properties. This can be used to interpret whether damage has occurred to the fluorophore either through the patterning process or by the imaging techniques. Using the different microscopes it was possible to show that overall sample coverage from the printing technique with the proteins was uniform, some thickness variations of the patterns were seen although these however were contained to local regions and could be inferred as resulting from variations of the amount of protein applied to the PDMS stamp prior to printing. Furthermore, it was shown with the techniques that the uniformity of the sample coverage along the lines varied with noise when compared with measurements made on blank regions of the substrate and not largely due to variations introduced due to the printing process.

Other than to address the success of the patterning technique using the different microscopes at hand, the patterned proteins with their specified periodicity were used to address the relative resolutions of the different microscope techniques as well as ensuring that the microscopes could successfully be applied to different biological samples for future measurements. Use of the different microscopes with the standard patterned samples displayed that which was expected in relation to the relative resolutions of the microscopes. The scanning probe techniques were seen to have much higher resolution than that of the standard fluorescence microscope technique, properties that were in line with theory. On the whole it was seen that the different microscope techniques didn't induce any significant damages to the samples in regards to the physical patterns however with the

techniques that employed laser excitation that some damage was induced to the sample. With these techniques use of the high intensity excitation for an extended period of time lead to some photo-degredation, this was low however and fluorescence was still present. It can be noted in regards to the SNOM technique that the photo-degredation was higher than that seen in the other techniques due to the length of time required to acquire an image. It can be concluded that the SNOM technique may be too slow compared to the AFM/fluorescence techniques to measure the samples of interest without damage being induced. Future measurements could incorporate biological considerations to reduce the small amounts of photo-damage caused, also resolution could be improved by making further modifications to the imaging techniques. Time correlated spectroscopy could also be applied to see whether any energy transfer processes occur with the patterned fluorescence proteins as with the high photostability properties they would be appropriate for future nanotechnology applications.

5.10 Bibliography

[1] Tsien. R Shaner. N, Steinbach. P. A guide to choosing fluorescent proteins. *Nature Methods*, 2(12):905–909, 2005.

[2] G. Davidson M. Shaner, N. Patterson. Advances in fluorescent protein technology. *Journal of Cell Science*, 120(24):4247–4259, 2007.

[3] R. Heim, R. Tsien. Engineering green fluorescent protein for improved brightness, longer wavelengths and fluorescence resonance energy transfer. *Current Biology*, 6:178–182, 1996.

[4] Kallio. K Gross. L Tsien. R Remington. S Ormo. M, Cubitt. A. Crystal Structure of the Aequorea vicoria Green Fluorescent Protein. *Science*, 273:1392–1395, 1996.

Chapter 6

Fluorescence studies of patterned bacteria.

6.1 Introduction

The investigation of light harvesting properties and the energy transfer/fluorescent properties of samples from biological systems introduces a number of difficulties both to measurements of these properties and in the sample patterning process. Whereas the use of components from photosynthetic bacteria introduces issues pertaining to photo-oxidation etc, the samples are extremely efficient and investigation into whether they can be fixed to surfaces whilst retaining optical properties is of interest for their potential application for biological components in nanotechnology.

Light harvesting antenna complex 2 (LH2) from the bacterium *Rhodobacter Sphaeroides* has been used in this work for all measurements of patterned material from photosynthetic organisms, the study of which has used both optical and scanning probe microscopy techniques, like those used in Chapter 5 to probe the optical properties of the patterned samples. Pattern properties and dimensions of μCP arrays are addressed in this chapter based on the optical techniques previously used. These are used to address the viability of accurately printing this biological system whilst allowing optical properties to be retained.

To analyse these patterned biological systems using high resolution microscopy techniques, sample preparation is vital to allow fluorescent properties to be retained and thus be detected with the optical techniques to indicate the stability of the fluorophore after patterning. Achieving high resolution images to analyse the patterns requires biological considerations to be taken into account and modifications to the microscopes/imaging process to be made to ensure that the process of observing the sample to investigate optical properties doesn't damage the fluorophore. This chapter focuses on some of the modifications made to imaging techniques in light of the different biological considerations required to allow successful measurement of sample properties.

This chapter also investigates the energy transfer properties of these light harvesting complexes in patterned structures, an understanding of which would be essential for any potential roles as biological nanowires for the future of nano technology. Modifications are made to the existing SNOM system to allow for time correlated spectroscopic measurements to be made of the excited state lifetimes of material in the arrays to see whether any lifetime increase/decreases occur which could suggest the presence of energy transfer processes.

6.2 Spectral Properties of *Rhodobacter Sphaeroides*

6.2.1 Absorption/Emission properties

It is favourable to have an understanding of the spectral properties of samples prior to conducting measurements with the microscopy techniques used in this work. This ensures with fluorescence analysis that the microscopes are set up so that the correct wavelengths are used for excitation and emission and that samples aren't wasted on time consuming measurements such as those that are not fully optimised.

The spectral properties of LH2 from *Rhodobacter Sphaeroides* has been documented in the literature [1]. Although the values stated in the literature for excitation peaks and emissions peaks of the complex could be used in the microscopes for these measurements, there is a chance that they may differ to those of the purified deletion strain LH2 grown

for this work. Differences in structural conformation from growth conditions or genetic properties can lead to differences in the wavelengths of light harvesting proteins in the complexes [2]. Accurately knowing the excitation and emission wavelengths allow for optical microscope measurements to be optimised with the spectra of bulk LH2 was made using a spectrofluorometer (*Horiba Scientific*). For the bulk measurements LH2 was diluted in 20 mM HEPES pH 7.5 buffer solution to ensure the physiological conditions for the samples under excitation were maintained and that accurate spectra were obtained with no reabsorption of light from the sample.

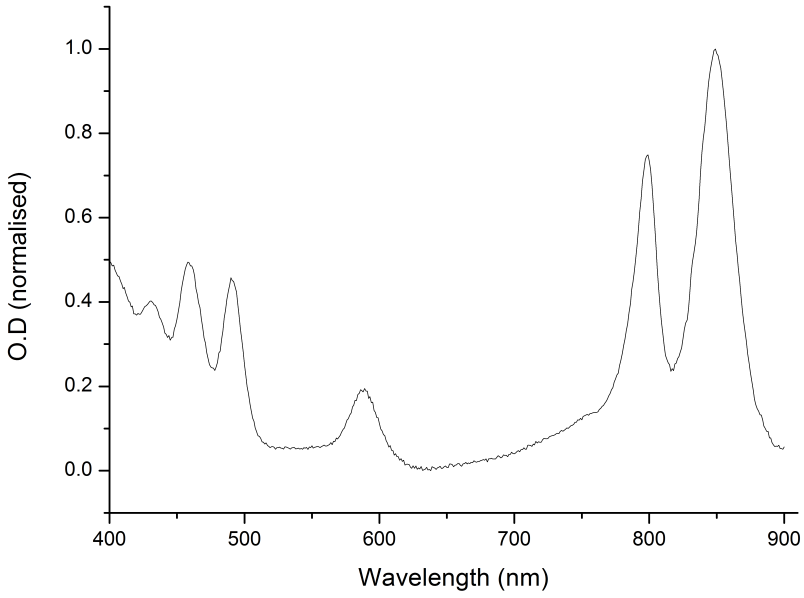

Figure 6.2.1: Absorption spectrum of purified LH2 complexes from the photosynthetic bacterium *Rhodobacter Sphaeroides*.

Fig. 6.2.1 shows the absorption spectrum acquired by measuring transmission of light through LH2 compared against a reference spectrum at each part of the spectrum through the equation:

$$O.D = -log_{10}\left(\frac{I}{I_0}\right) \tag{6.2.1}$$

where I is the intensity at a wavelength with the sample present and I_0 the intensity of the reference spectrum at the same point. From spectroscopic measurements made in the literature it is expected that peaks corresponding to the absorption of the bacteriochlorophyll rings in LH2 are seen at 800 and 850 nm with peaks also seen around $400 - 500$ nm corresponding to the carotenoids [3]. The peaks identified in Fig. 6.2.1 suggest that the complexes are not damaged or changed significantly in the growth and purification processes. This also means that measurements made later with the microscopes can be compared to other measurements previously made on the complexes from the same bacterium.

Fig. 6.2.2 shows the emission spectrum acquired for the bulk LH2 material where each single wavelength in the 800-950 nm range has been integrated for a second. In the acquisition of the emission spectrum shown here for LH2 some considerations were taken into account due to the constant illumination of photosensitive material. Excitation of either of the BChl rings at 800 nm or 850 nm should yield a high level of fluorescent emission due to the larger absorption cross-section at these points however, as mentioned in 3.2.3 (Eq. 3.2.1), BChl is prone to photo-oxidative decay through the formation of triplet states and singlet oxygen. With this in mind the carotenoids were used for excitation with the emission spectrum due to their ability to transfer excitation energy to the BChl through means of non-radiative energy transfer. Excitation of the carotenoids also allowed their photo-protective properties to be used to prevent formation of singlet oxygen and reduce the level of photo-oxidative decay induced in the sample. In this spectrum, emission is seen from the BChl rings at 850 nm, however the peaks around 900 nm corresponding to the B850 ring are not observed due to the spectral response of the photodetector. These differ slightly to those that are reported in the literature by around 20 nm, however this may be accounted for by the excitation of the carotenoids and subsequent transfer to a

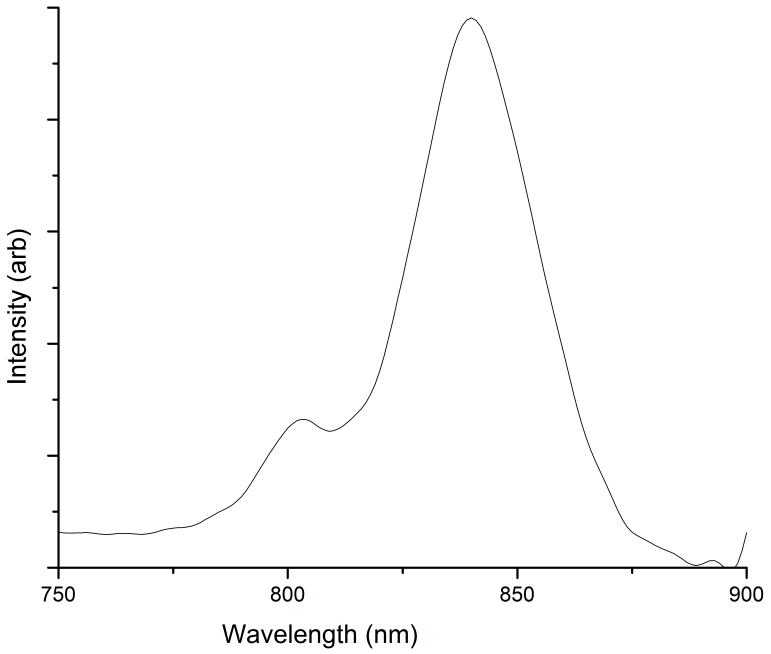

Figure 6.2.2: Emission spectrum obtained for purified LH2 from the *Rhodobacter Sphaeroides* bacterium with excitation at 473 nm and emission collected for the B800 BChl ring (determined by response of spectrometer).

vibrational state that is not the same as those used for direct excitation of the BChls. The presence of the carotenoids in the excitation may lead to immediate quenching of the BChls therefore allowing no time for energy transfer processes to occur within the vibrational states and they relax directly from the excited state. Furthermore the inconsistency in the measurement compared to the literature may be a result of conformational changes which have been reported to induce wavelength shifts [4].

Fig. 6.2.3 shows a photoluminescence excitation (PLE) spectrum of LH2 which allows the excitational properties of the emission to be analysed. Due to the quantum efficiency of the fluorometer's detectors in the near infrared regime the emission peak used in the PLE experiment above is that of the B800 ring (at 850 nm). Using the spectrometer, the PMT responsible for the detection of the emission is fixed to detect the intensity of emission only

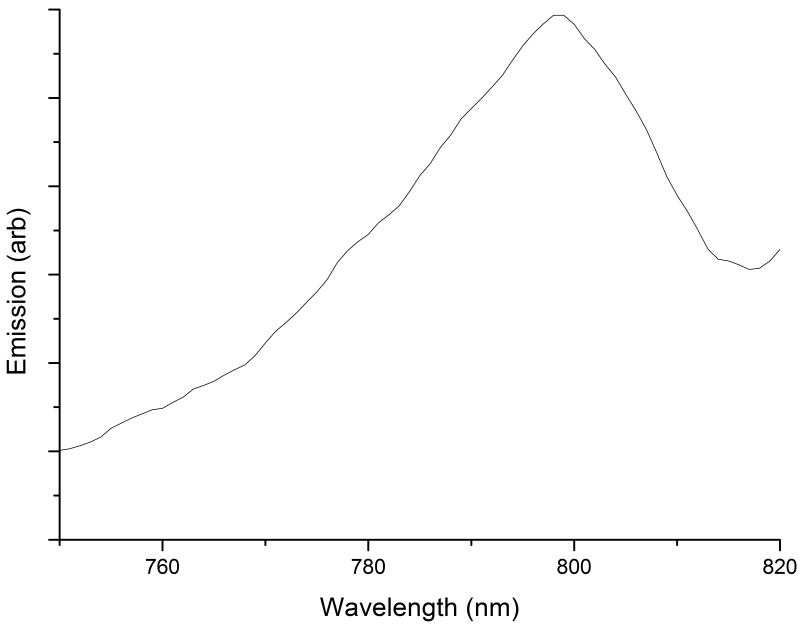

Figure 6.2.3: Photoluminescence excitation spectrum where emission intensity is measured at 850 nm for the purified LH2 complexes from *Rhodobacter Sphaeroides* across an excitation range.

at the previously specified wavelength. The excitation wavelength is progressed through the $750 - 820$ nm range which can be used to show how the intensity of the emission of the sample varies with excitation wavelength. The spectrum shown in Fig. 6.2.3 shows maximum fluorescence to be detected at an excitation wavelength of 800 nm, which is in line with that expected for fluorescence eminating from the B800 BChl ring.

6.2.2 Thin Films

As the light harvesting complexes are to be patterned on to glass substrates it is of interest to know whether depositing small layers of light harvesting complexes on substrates has an effect on the spectral properties of the biological material. The samples used for acquiring the thin film spectra are not μCP but formed from drop-casting techniques where small amounts (tens of μl) of diluted LH2 are deposited on a clean glass coverslip and left to

adsorb for an hour prior to rinsing with purified water. The result of this preparation technique is a thin layer of light harvesting complexes across the surface of the sample which may be measured with the previously mentioned spectroscopy techniques.

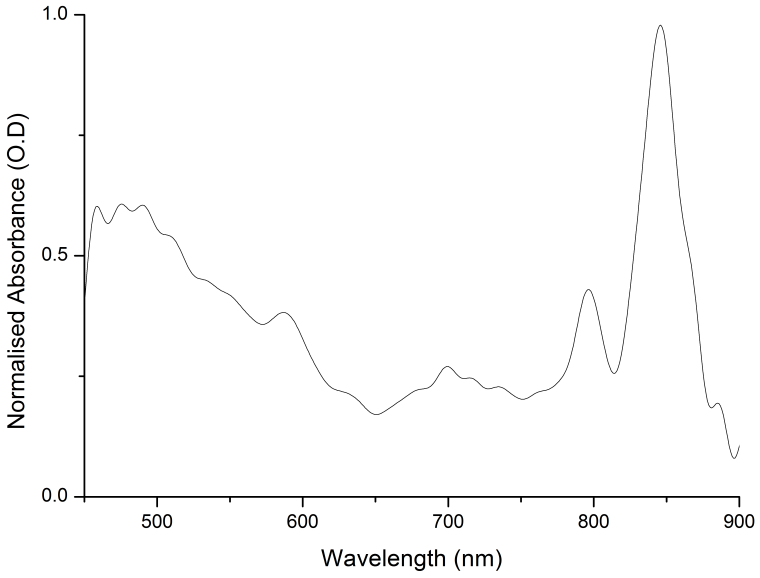

Figure 6.2.4: Absorption spectrum of LH2 dropcast into a thin film.

Fig. 6.2.4 shows the absorption spectrum obtained for the thin films of light harvesting complexes. Due to the smaller amount of material present on the substrate the integration times at each point of the spectrum are increased to 0.5 seconds to improve signal-to-noise. By using the absorption spectrum to address any conformational changes to the complexes it is possible to see that, when in a thin film on a substrate complex properties still hold. Similar to the bulk absorption measurements the band of carotenoids and the two BChl rings are observed in the expected regions.

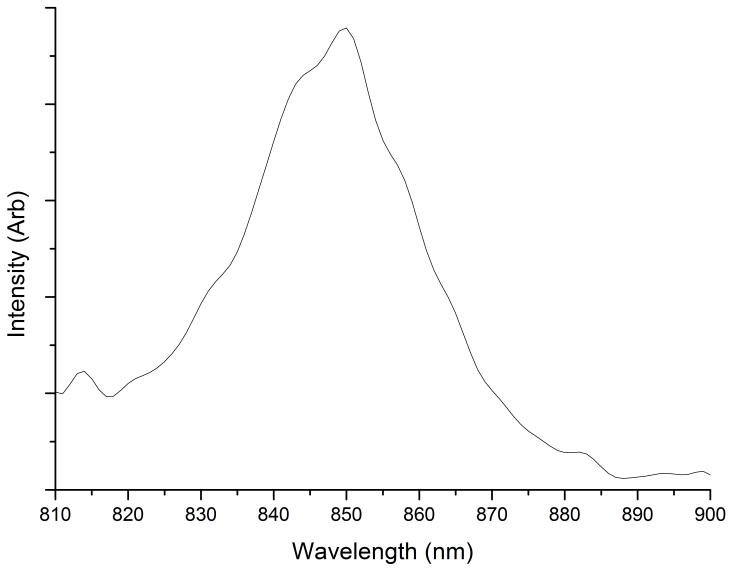

Figure 6.2.5: Emission spectrum for LH2 complexes from thin films of drop cast *Rhodobacter Sphaeroides* displaying the fluorescence observed from the B800 BChl*s*.

The emission spectrum shown in Fig. 6.2.5, like that of the absorption spectrum of the thin film light harvesting complexes required much longer integration times at each point of the spectrum to account for the smaller concentration of photoactive material present on the surface. When compared with the spectrum obtained for bulk LH2 it can be seen that the adsorption of the light harvesting material onto the substrate has no significant effect to the complexes and the emission properties. It is also worth noting that whilst the emission spectrum was obtained the amount of time the sample was under illumination was increased which also increased the potential effects of photodamage. Shifts in the emission peaks of the BChls are expected if the sample undergoes any photodamage and thus changes due to its structure however, no emission peak shifts are observed showing that outside of physiological conditions the sample remains stable and unaffected by these simple spectroscopic measurements.

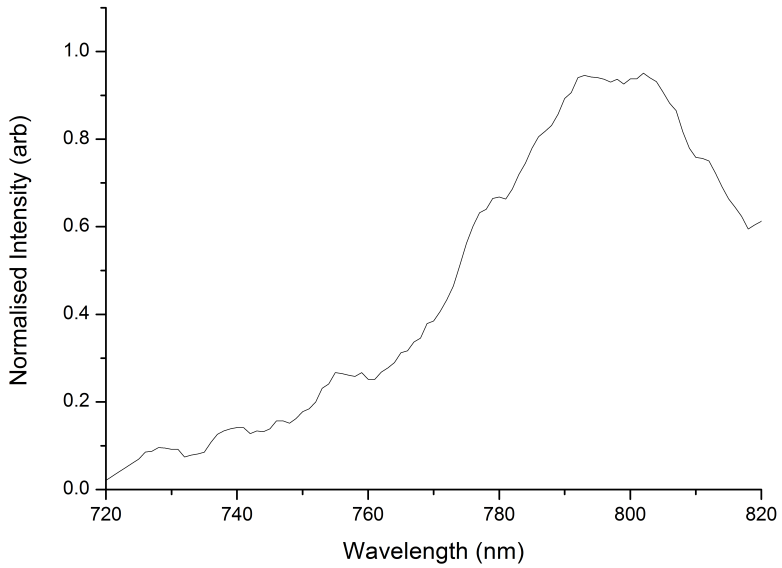

Figure 6.2.6: Photoluminescence excitation spectrum obtained from thin films of drop-cast LH2.

Like in the bulk measurements PLE spectra can be obtained to see from what components of the complex the emission peaks are coming from. In Fig. 6.2.6, again much like that of bulk measurements, in Fig. 6.2.3 one can see that the emission observed at 850 nm is characteristic of that from the B800 BChl ring.

6.3 Biological Considerations

It has been shown in 6.2 that the process of purifying LH2 does not cause any significant damage or changes to the spectral properties of the complexes, it has also been shown that when fixing the light harvesting complexes to a substrate no spectral changes are seen either. With this in mind it can be assumed that any significant damage or change in the spectral properties of these samples will be induced either by stamping the complexes on the substrate or through higher intensity illumination/interaction with force microscopes.

Several considerations pertaining to the sensitivity of the complexes from photosyn-

thetic samples were taken into account with the different microscopy techniques. Changes to the techniques were not needed with the patterned fluorescent proteins in chapter 5 due to the relatively higher photostabilty compared to photosynthetic complexes. As the scanning fluorescence microscope used in this work shared the AFM sample stage, a number of modifications can be made to aid with the preservation of the patterned samples whilst under illumination. The likelihood of photo-oxidation and thus damage occurring to the samples can be reduced by maintaining the samples in physiological conditions, achievable by measuring the sample in a liquid environment. Buffer solutions allow the sample to be kept at a constant pH to prevent damage to the light harvesting complexes whilst allowing sample structure in a hydrated environment to be retained. In this case the sample was kept under physiological conditions in two ways. One way employed to keep the sample under liquid was to directly deposit the buffer solution onto the sample, relying on the surface tension of the droplet to remain on the sample under measurement. This method was very successful for fluorescence measurements due to the non-contact nature of the technique. With the scanning fluorescence technique a better method to reduce the chance of disruption to the droplet by evaporation was to submerge the sample in a petri dish. The working distance of the oil immersion lens in this case meant that the sample had to be prepared directly to the petri dish (same cleaning and printing technique as with coverslips), the greater volume of liquid here also meant that there was no chance of the fluid evaporating which occurred where the droplet was under constant laser excitation. The combination of the petri dish and a profusion cell allowed for further measures to be taken to reduce photo damage through the formation of singlet oxygen and thus oxidation of the BChl. The potential for oxidation could be greatly reduced by removing most of the oxygen from the system through the introduction of nitrogen through the profusion cell. Nitrogen was blown across the surface of the buffer solution (within which the sample was fixed) to leave mostly nitrogen in the immediate vicinity of the sample and thus reducing the likelihood of singlet oxygen production. Measures were also taken regarding sample illumination to help reduce the chance of photo oxidative decay happening, by reducing the amount of time that the sample was illuminated when aligning the fluorescence micro-

scope. By turning the excitation source off between measurements the chances of sample degredation could be removed as no photons were incident on the sample.

The same considerations were taken into account with the SNOM, however similar modifications couldn't be made due to some limitations imposed by the system. The SNOM used in this work didn't have the ability to incorporate a petri dish or a profusion cell therefore measurements similar to those conducted with the scanning fluorescence system under buffer solution were not possible. Early measurements on patterned light harvesting complexes attempted to emulate the liquid measurements under a droplet of buffer solution however, a droplet had a significant height off the substrate to interfere with the tuning forks of the probes and thus had the potential to drastically affect the associated resonance. It was possible to reduce the amount of liquid on the surface to a level where the probe could engage without the tuning forks being affected, this was however an unsuccessful technique due to there being significantly less liquid on the surface which evaporated much faster than the time it took to acquire an image. Although samples could not be kept under physiological conditions in a buffer solution it was possible with modifications to conduct measurements with most of the oxygen removed from the system in order to reduce the chances of photo-oxidative reactions occurring. Like in the previously mentioned system with the fluorescence microscope and profusion cell, nitrogen was introduced into the environment through means of an enclosed hood placed over the SNOM head. To ensure oxygen was removed before measurements, the nitrogen was left for up to 30 minutes to reach a concentration where it exceeded that of oxygen around the sample. Similar to measures taken with the fluorescence microscope, reduction in the amount of time the sample was unnecessarily illuminated was vital to prevent photodamage, therefore when the probe was engaged with the surface the LED used to view the probe was switched off. Furthermore, when only topography measurements were being conducted or when no fluorescence measurements were occurring the laser used for excitation was turned off further reducing the stresses imposed on the sample.

6.4 High resolution microscopy of Light Harvesting Complexes

Samples of patterned photosynthetic light harvesting complexes were studied using fluorescence microscope techniques and the scanning probe technique of SNOM to address the success of the μCP of these samples. These methods allow analyses to be drawn focused on the optical properties of the samples. In this analysis topography data was obtained with the SNOM but not the AFM due to the damage induced by the AFM laser which was at a wavelength that intensely excited the sample (NIR excitation at 820 nm). The accuracy/reproducibility of the patterning technique, as well as the photo-stability of the samples after patterning could be addressed with the microscopy techniques used in a way similar to that in Chapter 5. Due to low light intensity and the emission wavelength of the samples being in excess of 800 nm wavelength the standard fluorescence microscope wasn't used due to the EMCCD response and low intensity however, the detector of the scanning laser microscope still allowed fluorescence measurements to be obtained.

6.4.1 Scanning fluorescence microscopy

Scanning fluorescence microscopy was a technique employed to analyse fluorescence information on imaging timescales less than that of SNOM. Doing so helped to prevent against photodamage as the samples were excited for a shorter amount of time per image acquired, compared to integration times at each pixel across each line in SNOM.

Fig. 6.4.1 shows a scanning fluorescence image obtained for the patterned light harvesting complexes. Excitation of the light harvesting complexes in this image has come from a 473 nm laser to take advantage of the carotenoids for their photo-protective properties to prevent photo-oxidation of BChls as well as their ability to transfer excitational energy to the BChls. Collection of the fluorescent signal is achieved through the use of a 800 nm long pass filter which enables a significant signal-to-noise to be achieved for analysis of the weakly fluorescing photosynthetic samples. Scanning fluorescence measurements on

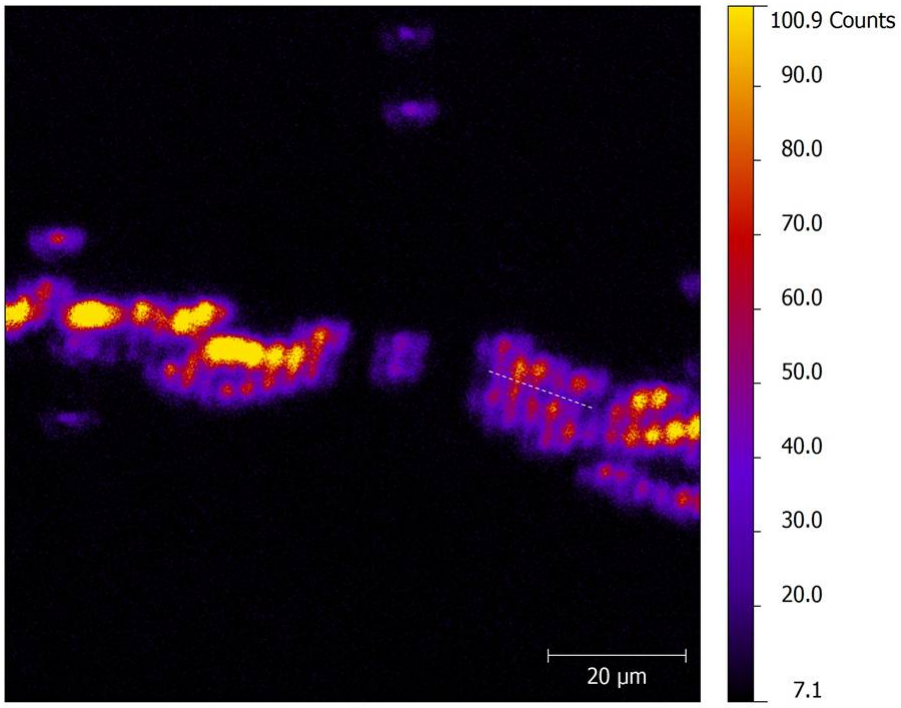

Figure 6.4.1: Scanning fluorescence microscope image of μCP LH2.

patterned light harvesting complexes have observed fluctuations in the intensity of fluorescence suggesting a variation in the amount of light harvesting complexes present similar to that seen in Chapter 5.

The patterned light harvesting complexes shown in Fig. 6.4.1 display an uneven deposition of biological material on the surface with significant variations in sample thickness occurring in local regions. Local effects are seen to vary more radically than variations seen across the sample which are more gradual and a result of uneven illumination or collection of fluorescence. The effect of these large local variations suggest that using μCP to pattern light harvesting complexes isn't ideal and the reproducibility of these patterns on the surface isn't optimised.

6.4.2 SNOM

SNOM allows the patterned LH2 to be investigated optically below the diffraction limit, identifying local variations in the biological sample potentially arising from photo-damage or the patterning process. This also provides a higher resolution analysis of the optical properties of the pattern structures and their photo properties. Fluorescent images of the samples taken with SNOM used a laser centred at 470 nm to excite the carotenoids in the sample to take advantage of the photo-protective properties that they hold.

Fig. 6.4.2 show the height images and corresponding fluorescence images observed for the patterned LH2 substrates. For these images it was necessary to increase the integration time of the detector compared to that with the fluorescent protein samples due to the relatively weaker fluorescent signal, a sample property and not an effect of photo-damage due to oxidation. Increasing the integration time at each pixel provided much lower scan speeds and thus rate. In earlier measurements of the sample with only the topography it was found that, the scan rate had to be reduced in order to provide a more accurate image. This can be seen in the topography in image (a), in as much that the height of the lines of photosynthetic material is quite large (near to a micron) and as the probe moves fast across the sample increasing the risk of the tip crashing into the side of the samples due to immediate height variations occurring faster than the reponse time of the z piezo. The opposite is when the probe leaves the plateau of the line and drops back to the background substrate. When running faster a large broadening of the line can be seen due to the z sensor again not responding fast enough over the large distance in the z-axis however, these measurements have been conducted at a scan rate that give the more accurate and defined images like that in Fig. 6.4.2.

It can be seen in the SNOM images that the patterning process isn't as successful with LH2 as it is with the fluorescent proteins. The uniformity of the patterned lines is very low with large variations seen across local regions with respect to the amount of material present on the surface. Similarly to that observed with the fluorescent protein samples, regions with a greater sample thickness (and thus concentration of material) observed as

greater fluorescence intensity. This suggested no significant quenching occurred due to minor bulk effects that may occur due to the amount of material present in these regions. Other regions and samples of the patterned LH2 show similar non uniformities in the linear arrays, with the lines on some samples not successfully forming and thus becoming disrupted, optical properties in these cases however still remain the same as expected.

Line profiles of the fluorescence images can be used to investigate whether the signal-to-noise is of a significant level to accurately measure the patterned arrays. This can mostly be used in initial measurements of the samples using SNOM to optimise the integration time of the detector. The signal-to-noise values can also be used to assess whether the sample is suffering from any degredation due to the high light intensity at the aperture, heating or the introduction of oxygen into the environment. It would be expected that the noise value becomes of greater significance relative to the signal as the fluorescence from the sample decreases through photo-induced sample degredation. Even with the measures taken to reduce photodamage to the light harvesting complexes, a significant amount of damage was still observed, limiting the time available to obtain images from a sample before the fluorescent signal fell to a level discernable from noise. Significant degredation to fluorescent signal was seen over 1 - 2 hour SNOM measurements regardless of laser excitation being present throughout, suggesting that ambient light or the length of time in a physiological environment which is also warm adds to sample decay. The time scale of fluorescence degredation observed placed limitations on the number of images obtainable with SNOM as each scan could take upto an hour with a 200 line resolution, with the time frames degredation across an image could also, potentially be observed and thus lead to the detection of uneven fluorescence signals.

6.5 Pattern Analysis

The images obtained with the different microscopes are used to analyse the LH2 patterns in terms of the efficiency of pattern coverage, patterning reproducibility, whether the patterning induces any structural damage in the light harvesting complexes and whether the

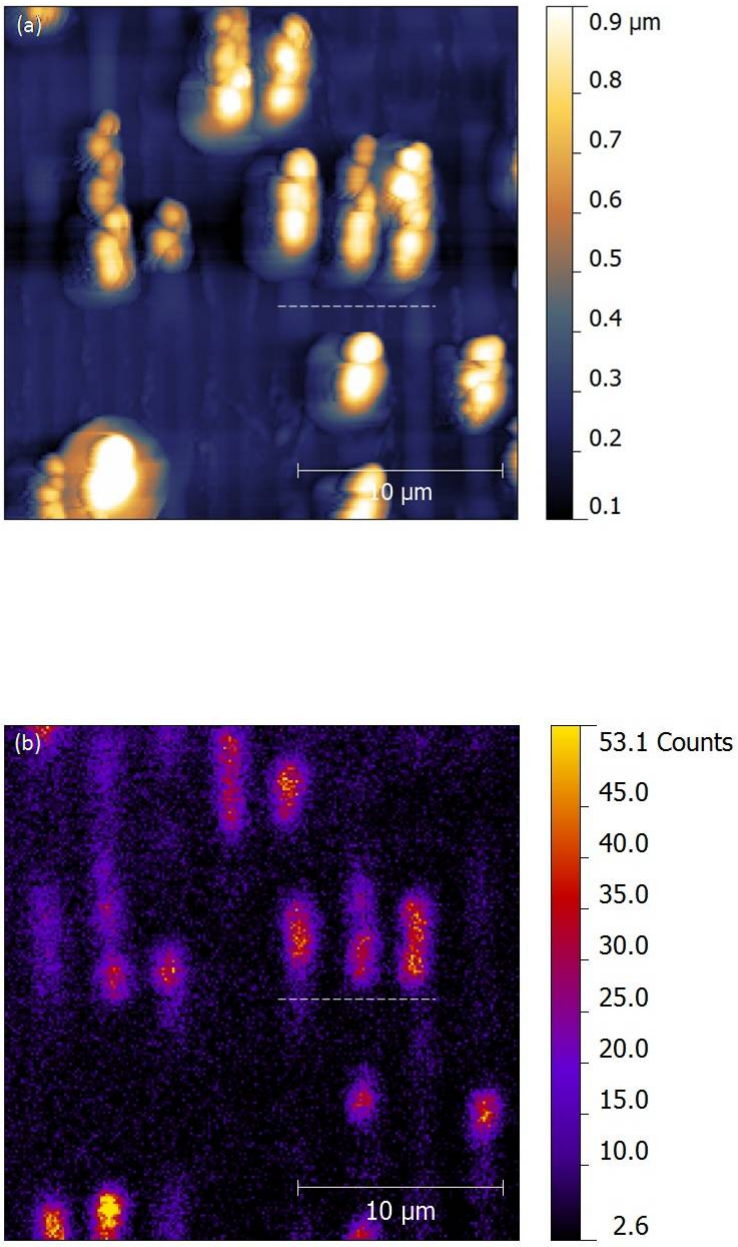

Figure 6.4.2: SNOM images of patterned arrays of LH2 from *Rhodobacter Sphaeroides*. Image (a) shows the topography image of the patterned sample with the corresponding fluorescence image shown in Image (b).

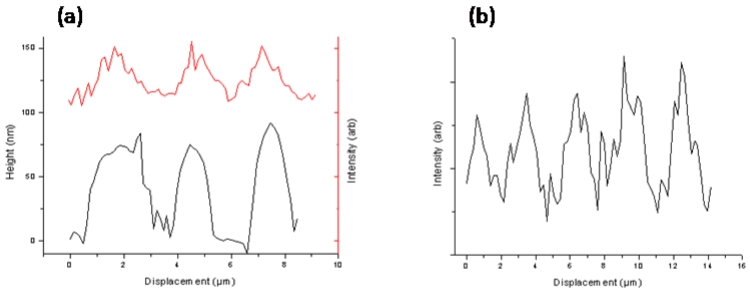

Figure 6.5.1: Line profiles of similar sample regions of microcontact printed LH2 obtained using (a) SNOM, black profile as topography, red as intensity (b) Scanning fluorescence microscope.

samples can remain photo-active to allow for a number of measurements with the help of the modifications made to the microscopes in light of the biological considerations taken into account.

6.5.1 Cross-section analysis

Line profiles were utilised in this study to analyse images obtained of patterned light harvesting complexes where they are used as a tool to further analyse the relative resolutions of the microscopes. By using the patterned surfaces as 'standard' samples, as well as being a tool to analyse the patterning process in terms of the reproducibility of the line dimensions, the accuracy of line patterning, uniformity of the material fluorescence in the patterned structures and analysing the degredation of samples under measurement.

To assess the relative resolutions of the microscopes used to measure these samples,

the line profiles shown in Fig. 6.5.1 have been acquired from similar sample regions in the different microscope fields of view. Basic levelling functions have been applied to the images to correct for sample tilt arising from the acquisition of an image which leads to background values having differing values depending where in the field of view investigations are made and thus in the line profiles gives a more accurate representation of the sample cross-section as the background value is near zero. It can be seen from the profiles that the resolutions of the different techniques vary. The edges of the lines in the fluorescence technique appear to be less defined show wider lines that that seen in the SNOM technique. The relatively higher resolution of the SNOM is apparent in the line profiles similarly to the comparisons made between fluorescence and AFM, the line edges are more defined at higher resolution and such the lines appear thinner.

So far, analysis of the line profiles have been made based on their appearance relative to one another, it is possible to quantify the measured line widths with the different techniques to compare their relative resolving powers. Each of the images contain several individual lines of patterned protein so it is possible to collect an average line width in the images from each technique. An issue arising in the measurement of line widths however relates to where on the line profile the edges of the structures should be defined. For these measurements the edges of the lines for the higher and lower limits seen in the x-axis were as the full width half maximum for each line which with the varying steepness of the edges leads to variations in the measured width in line with varying resolutions. Averaging over the lines shown in the images in Fig. 6.5.1 gives line widths of the fluorescence microscope as 1.61 μm the SNOM topography as 1.43 μm and SNOM fluorescence as 1.14 μm. The differences in the FWHM values of the lines observed here vary in accordance with the expected relative resolutions of the different microscopy techniques.

In this work, line profiles were also obtained along the y-axis to address the complex coverage along the line patterns to show whether variations in complex fluorescence in the z-axis is a result of small local noise or from local variations arising in the adhesion of samples. Applying line profiles to the y-axis can also be used to show the effectiveness of the microscope techniques at measuring LH complexes by seeing if the technique changes

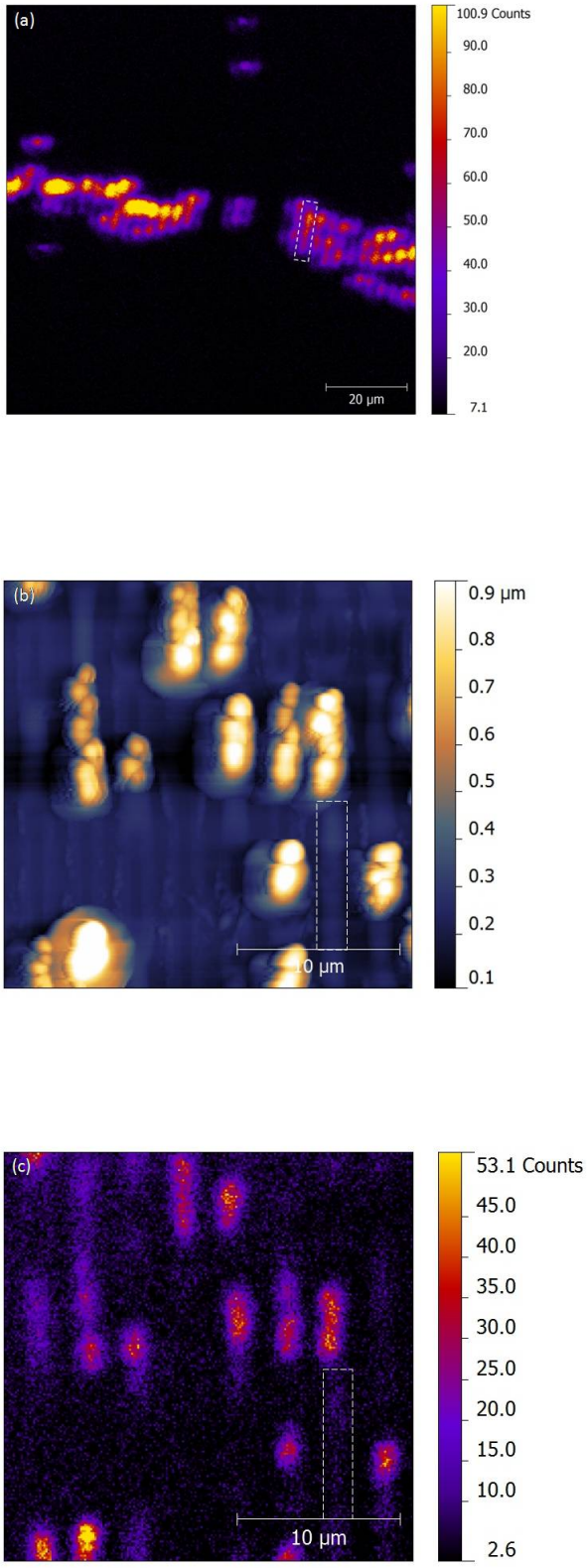

Figure 6.5.2: Candidate lines on patterned LH2 substrates to address the coverage of photosynthetic light harvesting complexes through the μCP process using (a) scanning fluorescence (b) SNOM (topography) (c) SNOM (fluorescence).

the complexes or can discern between the background and the sample. By comparing how rough the profile measured in the y-axis along the lines are to similar profiles along the regions with no signal, properties of the sample can be identified to be a result of successful patterning or from regular noise variation that would lead to small variations in the signal/measurement for on the lines of complexes. The line profiles in the y-axis can be used with the fluorescence measurements to address the average signal to noise values of the technique by comparing the intensity of the samples fluorescence against the intensity measured from the sample free region. Using the fluorescence images shown in Fig.6.4.2, lines that appeared to be unbroken or have any regions of concentrated material could be used for line profiles (two examples are highlighted in the Fig.6.5.2 images). The corresponding line profiles for these regions are shown in Fig. 6.5.3 where the line profile on the patterned lines displayed in black and the background in red. Albeit with different intensities, the fluorescent signal and that of the background show similar line profiles showing that in these regions the light harvesting sample is patterned evenly with variation only coming from random noise events that are inline with those experienced in the background signal. In the SNOM topography images it can be seen that the line profile taken on the patterned line varies drastically, this is however seen in the background line profiles as well. With this large variation occurring in both of the profiles it can be assumed that the variations don't occur due to patterning inconsistencies but due to variations across the image the whole image arising in the imaging process. With this in mind it can be inferred that the patterning technique on some of the lines has the ability to successfully attain uniform thickness that can be addressed both in fluorescence and topography.

6.5.2 Pattern Coverage/Reproducibility

The analyses of the patterned samples in this work are made with energy transfer processes in mind, as well as their applicability for bionanotechnology. The requirement of energy transfer leads to a number of properties that are desireable for the sample, such as patterned

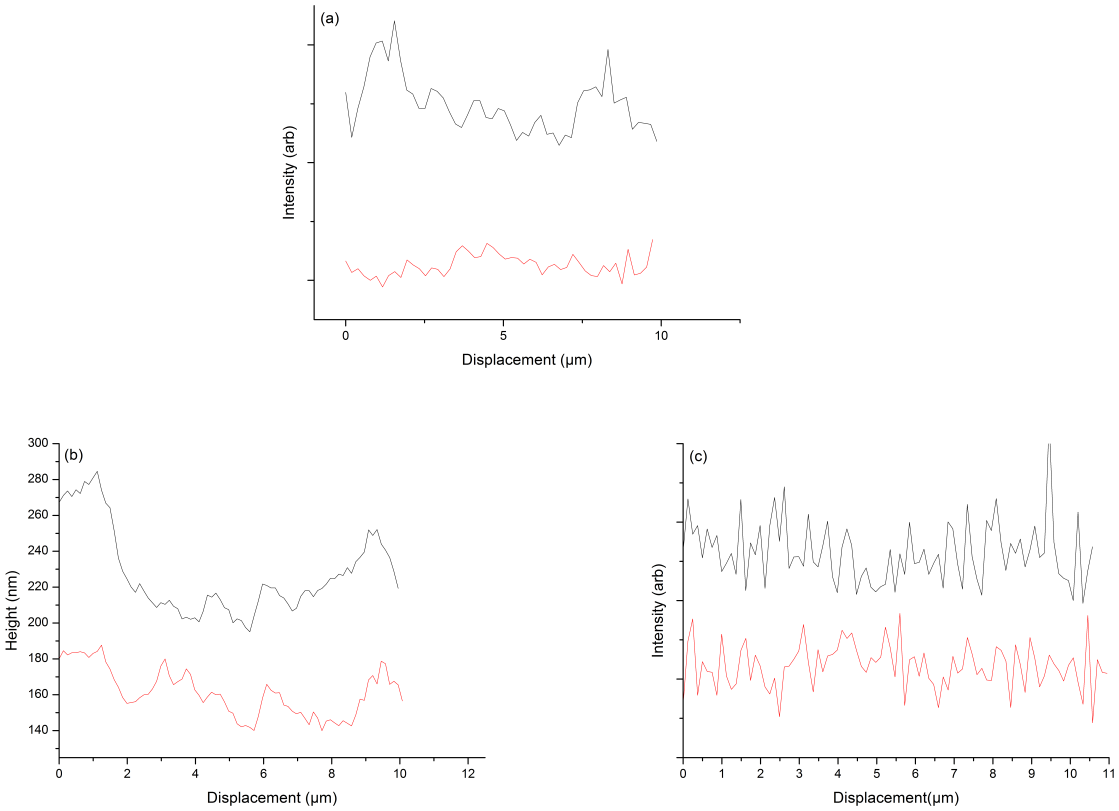

Figure 6.5.3: Line profiles acquired parallel to the μCP lines shown in Fig.6.5.2 using (a) scanning fluorescence microscope, (b) SNOM topography (c) SNOM fluorescence. Black profiles are obtained on the patterned complexes, red obtained for the background substrate.

lines being unbroken to ensure that energy can be transferred along a predetermined region. The reproducibility of patterned samples is a major consideration that needs to be fulfilled to ensure that standard energy transfer properties of these samples can be maintained.

It has been previously shown that there are regions of the patterned samples that are in line with the requirements of the patterned linear arrays, in such that there are a number of unbroken lines of light harvesting complexes attached to the substrate. Although there were some regions where the linear patterns had successfully adhered to the surface, the majority of the light harvesting complexes fixed to the surface with no discernible pattern. On top of a lack of linear patterns the lines were also found to be disrupted in

topography measurements and fluorescence measurements as well as also having varying material thicknesses along the lines.

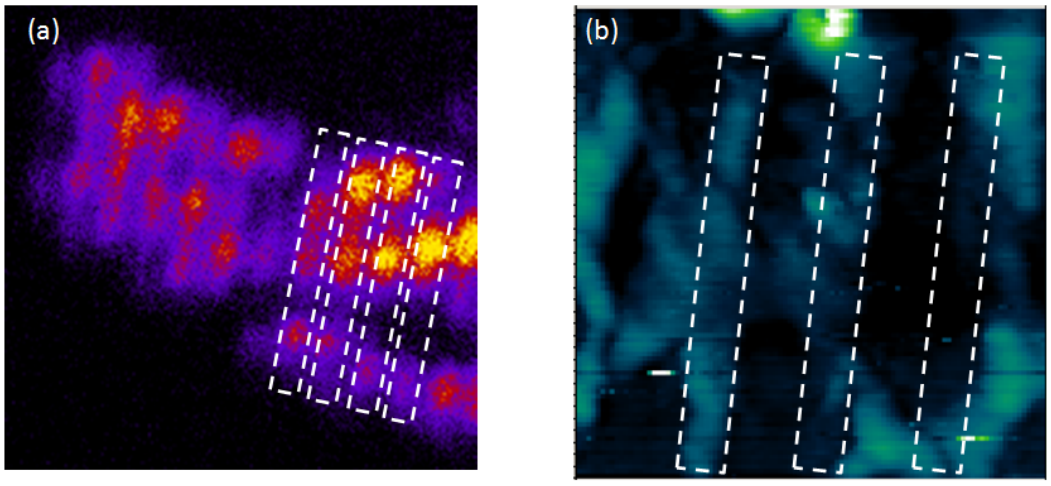

Figure 6.5.4: Images acquired with the different microscopes show inconsistencies in patterning where the patterns don't transfer accurately; this is shown in (a) Scanning fluorescence (b) SNOM topography where the highlighted regions show examples of where the pattern reproducibility is low (broken patterns, non-uniform coverage).

Fig. 6.5.4 shows examples of regions where reproducibility isn't fully achieved. When it comes to the linear arrays it can be seen that these vary from broken lines to regions where no discernible lines have actually adhered to specific regions of the substrate. Image (b) displays a SNOM topography measurement as an example of a region where the pattern

doesn't appear to have adhered to the surface. The broken line in the image shows an estimation of where the pattern was expected to be seen however, the material in this case appears to spread out from where it should have been deposited. The reason for this may be that in comparison to the fluorescent proteins, surface tension of the LH complex in comparison is lower and prior to samples adhering and drying onto the substrate they dry unevenly or are disrupted and spread out in the x/y-axes to form the variations observed. Disrupted patterning may also arise due to the substrate being used with the light harvesting complexes and as a result the printing method may be to blame for the problems seen. The technique is based on that used with the fluorescent proteins so that the differences in the sample's properties could affect the patterning technique and results. If the disruption observed is a result of the μCP process not being optimised to the LH2 samples there is a possibility that the contact time of the PDMS stamp or forces relating to the contact region of the stamp could lead to the disruption. If the stamp is only in contact with the substrate for a short time there is a chance that the material doesn't have enough time to fully adhere to the surface and thus with the removal of the stamp and any resulting forces, the surface tension of the sample can be disrupted in a way that causes the material to spread out and not form a linear array. Furthermore there may be a case with the contact time being too great that causes inaccurate patterning, a long contact time may allow biological material that has affixed to some areas in the stamp's troughs to flow onto the substrate causing extra undesirable 'patterning'.

Image (b) in Fig. 6.5.4 shows some of the issues with this sample arising from broken line patterns, another factor undesirable for the potential future applications of these samples. In regards to sample coverage it was seen that in some cases the amount of biological material located in some parts of the sample were greater than others. Both of these observations suggest that with the LH2 samples, it is much more difficult to produce patterns that are uniform in nature. With both of these issues it may be that the material initially deposited on to the PDMS stamp was not of uniform thickness, this would lead to the measured discrepencies observed on the sample surface. The angle of contact with the substrate can also account for some of the variations in thickness across the sample

where light contact with the surface only transfers a small amount of loosely bound complexes and the region of higher pressure and contact leads to transfer of a larger amount of material. In terms of the broken lines, this could follow a similar effect with either no sample being present on parts of a line or that areas of the sample may have dried due to the small amount of liquid on the stamp. It may also be possible that the stamp used for pattern had some damage which with small troughs on the raised regions caused by fractures on the stamp, could lead to no patterning of material.

It is desireable to have uniform coverage of the light harvesting complexes across the sample to ensure that light harvesting occurs equally across the sample and not just focused in specific regions. It is also desireable so that energy transfer is efficient and occurs evenly across all of the light harvesting complex arrays and that energy transfer occurs on similar time scales and doesn't become delayed in regions where there is a high density of light harvesting complexes. Inconsistent coverage was also observed in the patterned light harvesting complex samples in regards to the presence of the lines. Inaccurate patterning of the lines with these samples saw incomplete or broken lines, undesireable where the aim was to try and observe excitation energy transfer along lines of light interacting samples. Both of these sample coverage issues suggest that with μCP of light harvesting complexes it is of greater difficulty to achieve uniform sample coverage compared to those achievable with fluorescent proteins. The non-uniformity of the biological material deposited on the substrate may be a possible result of two factors in the μCP arrangement. Another factor that may affect the sample coverage could be that of the substrate. The Poly-L-Lysine (PLL) solution added to the glass coveslips was of a concentration that aided adsorption of the fluorescent proteins to the substrate however there is a chance that light harvesting complexes do not bond as strongly to the PLL like GFP/YFP and as a result the solution is not of a significant concentration to allow enough material to adhere to the surface unifomly. Potentially it is more likely that the patterning inconsistencies arise due to the PDMS stamp and the contact printing process. The varying line thicknesses may arise from some regions of the stamp being coated with more material than others which may lead to the variation of layer thickness from monolayers to other regions that are

comprised of several layers. The lack of some lines may also be an effect of the pattern coverage on the PDMS stamp, either from some lines on the stamp not being coated with light harvesting complexes or the LH2 solution evaporating in other regions and not successfully transferring to the substrate. Material coverage on the stamp can also account for local regions along a pattern where high concentrations of material has fixed too. This may be likely from aggregation of the light harvesting complexes prior to transfer to the stamp which upon printing are transferred to the stamps and lead to the large variations locally. Some sample coverage variation is seen across the substrate, for example in Fig. 6.5.4 one can see larger values in the height of the material contained in the lines towards the top of the image compared to that seen in the lines towards the bottom of the image. This can arise from more biological material 'pooling' at one end of the stamp allowing more material to potentially be transferred to a region. The pressure applied to the stamp in the printing process may be uneven and in the regions where there is greater pressure more material is applied to the surface compared to that in the regions of less pressure, this may also go towards explaining some of the previously mentioned issues regarding the lines where the patterns transferred aren't linear in nature and appear to spread across the surface.

6.6 Time Correlated Spectroscopy

Time correlated Spectroscopy (TCSPC) was a technique employed in this work, combined with SNOM, to investigate the excited state lifetime of the samples. The combination of the TCSPC technique, where an ultrafast laser is used to deliver excitation to a sample in laser pulses and the time resolved fluorescence emission detected, is combined with the SNOM. This allows high resolution with the optical measurements as well as providing a map of the fluorescence lifetime of the sample that can be compared to the topography also acquired by the SNOM. Probing the fluorescence lifetime of the light harvesting complexes in the patterns is of interest as it reveals potential energy transfer processes which may be identified by variations in the fluorescence lifetimes such as the lengthening of the lifetimes

where some of the excitation energy is being transferred to other complexes as opposed to relaxing of its own accord. This work shows the effect that patterning has on the light harvesting complexes and the ability they have for energy transfer.

6.6.1 Image Acquisition

The acquisition of high resolution TCSPC data was achievable by modifying the SNOM to accommodate time resolved fluorescence imaging. The standard operation of the SNOM incorporates a continuous wave (CW) mode laser to ensure that specific excitation is delivered to the sample surface at every pixel, this however is not a mode compatible with TCSPC measurements. To allow the excited state lifetime to be probed the SNOM is modified to include a 4W white light, ultrafast laser (*Fianium*) with a pulse length of picoseconds. The ultrafast laser is connected to the SNOM by an optical fibre in the same way as standard measurements, the laser is also connected to a computer control to operate the TCSPC photodetector allowing trigger pulses to be used from the laser driver to correlate pulse widths and detection times with the detector.

With the TCSPC photodetector a plot for the excited state lifetime can be obtained with each pulse from the laser. The settings used with the detector can be modified in a way to ensure that the fluorescence signal collected from the sample is optimised for the fluorescence intensity variations that can occur due to the differing emission properties of samples. The integration time of the detector can be modified in such a way to collect more light to produce the excited state fluorescence lifetime profile, the integration time of this measurement can be correlated with the SNOM system to apply to each pixel. In this system the counter settings applied are the same as for standard fluorescence with the value being roughly equal to that applied to the TCSPC lifetime acquisiton. A differing factor however is that instead of a fluorescence image being produced with the SNOM system/computer the counter settings applied at each pixel of the SNOM image act as a trigger for the TCSPC detector.

The method mentioned allows a lifetime plot to be acquired for each pixel, from this

it is possible to analyse the lifetime fit and the intensity of the fluorescence lifetime which in post processing can be used to produce an image of these values. Using a custom Labview program, the lifetime spectra (which can contain 625 to 2500 spectra) can be analysed with an exponential fit to find the lifetime of each point or the intensity and this value can be built into a corresponding intensity image or lifetime map. This map can be compared in relation to the topography image acquired simultaneously to identify whether the arrangement of the light harvesting complexes into linear arrays has an affect where energy transfer can be seen between complexes oriented in the line.

6.6.2 Lifetime Imaging

Imaging of the excited state lifetime with SNOM, like standard fluorescence SNOM on the light harvesting used laser excitation centered at 470 nm and to collect the emission at 850 nm a broad 870 nm bandpass filter of ~ 40 nm or an 850 nm longpass filter can be used As the measurements made here could vary significantly with photo damage occurring the laser power arriving on the sample was kept to a minimum so a balance could be maintained between fluorescence observed from the sample whilst damage to the sample induced by the laser was kept to a minimum. On top of the power of the laser being kept to a minimum the sample was also measured under nitrogen to remove oxygen from the system. It was essential to apply the modifications in line with the biological considerations as it was necessary to integrate each pixel for longer than standard SNOM, 3 seconds due to the lower intensity fluorescence. The number of pixels in 'low' resolution images (25 or 50 lines) can still be quite high ranging from 625 to 2500, where the integration time at each pixel is on the order of seconds the total image time can be longer than an hour. The length of time it takes may cause the sample to undergo photodamage whilst the measurements are being conducted as the timeframe within which such effects can happen is increased. The potential for photo-oxidative effects stresses the need for the inclusion of nitrogen in the sample region and the modifications for biological samples, especially in this case where excited state lifetimes are likely to be affected by these effects.

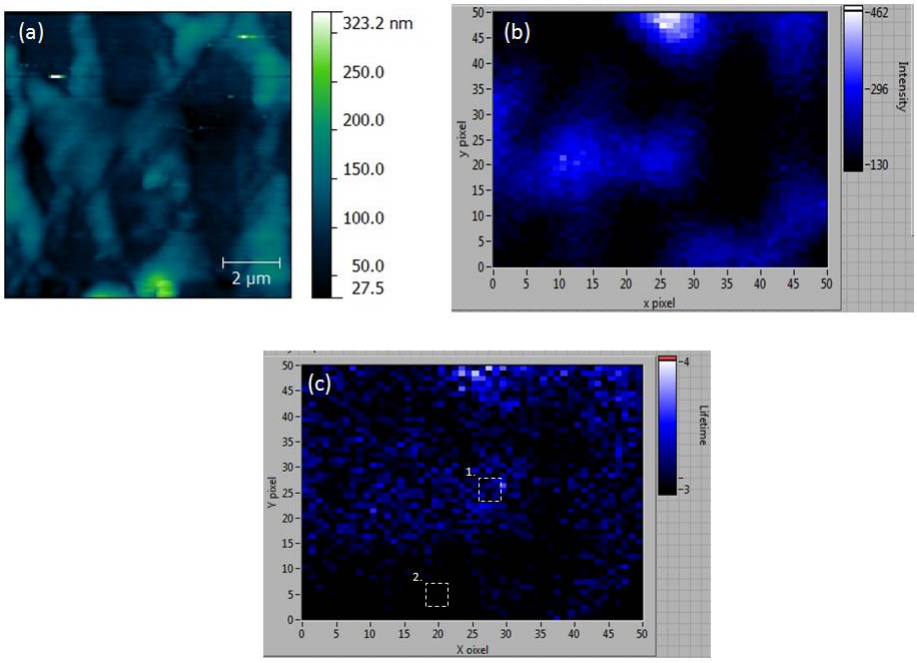

Figure 6.6.1: Data acquired with the SNOM/TCSPC combined system on LH2. Image (a) shows the topography image which corresponds to image (b) an intensity image of the lifetime spectra and image (c) a lifetime map of sample (scale in nanoseconds).

Fig. 6.6.1 shows data acquired with the combined SNOM and TCSPC configuration which allows the topography to be directly compared with the intensity of the fluorescence observed in the fluorescent lifetime data. Also shown is the ability to compare the pattern's topographic features with the fluorescent lifetime measured at each pixel of the sample. A key feature of the topography image is that the lines of patterned protein are not particularly well defined. Although some regions of the pattern appear to be arranged roughly linearly, overall it can be seen that the patterning process for LH complexes is not as efficient as when it is used with fluorescent proteins. Comparing the topography image with the intensity image obtained from the fluorescent lifetimes, the inaccuracies present in the printing process can be further observed. As expected when comparing the two, fluorescence intensity is seen where light harvesting complexes are present and no signal is seen where there is no sample showing a lack of erroneous fluorescence/light scatter that

could affect the measurements. It is also possible when comparing the topography and fluorescence image to, in this case, see differences in the resolution of the two types of image acquired with the SNOM. The physical dimensions of the SNOM probe can account for this due to the nature of the topography acquisition process with the SNOM probe being on the order of several hundred nm whereas the diameter of the aperture from which the laser is emitted is between 50 - 100 nm and is the only thing limiting optical resolution in the near field. As the probe size introduces a limit to the topographic resolution it is observed to be less defined and more 'spread out' than the optical image thus explaining the difference.

Image (c) in Fig.6.6.1 shows the fluorescence lifetime map acquired with the previously discussed images, from it one can again see the similar patterning that is observed in the topography image suggesting that the lifetimes observed are affected by the presence of sample and thus reveal information pertaining to the light harvesting complexes on the substrate. Although the lifetime map is the same resolution as the fluorescence and topography images (with 2500 pixels) the resolution appears to be much lower when taken at face value. The nature of the lifetime variations can account for the appearance of patterned regions with relatively short excited state lifetimes and other regions where it is longer with pixels that are close to one another. The fluorescence lifetimes vary only a small amount between regions where the sample is present and where there is no sample present and as a result the scaling of the image is modified as such to show this. The modifications to scaling however also accentuate the small variations that occur due to noise present from the laser or electronics and therefore the on pattern measurements can reveal 'breaks' where the variations in the lifetime of the sample show it to be different.

6.6.2.1 Image plotting/Spectra analysis

Analysis of the TCSPC spectra to create images of the fluorescence intensity and fluorescence lifetime of the sample was conducted through Labview (*National Instruments*)

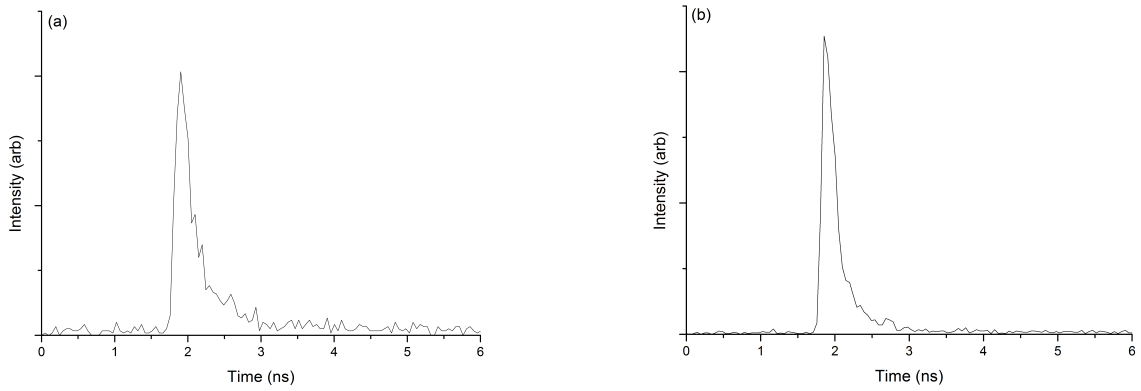

Figure 6.6.2: Image (a) and (b) show plots of the fluorescence lifetime obtained from the points (1.) and (2.) respectively in 6.6.1

allowing automation of the pixel plotting and spectra analysis. The custom built program allowed the number of spectra acquired in the SNOM/TCSPC process to to be loaded into the program and the values plotted on a graph in the software for analysis. Within the program it is necessary to set several parameters to ensure that the analysis is calibrated for the image, it is necessary to tell the software the number of spectra allowing it to know the pixel size of the image in the x/y-axes.

In line with the nature of the data, the intensity and time values are fit to the exponential:

$$F(t) = \alpha_1 + (\alpha_2 e^{(-t/\tau)}) \tag{6.6.1}$$

where $F(t)$ is the fluorescence intensity at time t, α_1 and α_2 are normalisation terms for the pre-exponential region and τ is the lifetime.

From the exponential it can be seen that several parameters may be represented in the plotted images due to the fit, the lifetime and intensity. The exponential also accounts for the rise in the intensity allowing the decay properties with time to be accurately analysed by the software. Running the program several times with several different values applied to the constants in the exponential allowed the fit to be more accurate as the values can best

match the ideal fit. Values such as the time constant can be modified, in turn improving the lifetime images that are produced by the software.

As with the analysis of images obtained with the other microscope methods the program designed in labview has the capabilities to modifiy the image scaling to allow variations in sample properties to be identified in the analysis process. The scaling allows small variations to be 'amplified' and therefore subtle differences in the lifetime properties of the printed samples to be identified and measured.

6.6.3 Pattern Analysis

The analysis of the fluorescence lifetime of the light harvesting complexes acts as another pathway through which the technique of μCP of biological components can be analysed as well as addressing the excitation energy processes in the printed samples. The combined TCSPC/SNOM data acquired can be applied in a way to identify energy transfer that is occurring in the sample as well as identifying whether the patterning technique causes any damage to the light harvesting properties of the photosynthetic components measured.

It has been shown through the intensity images as well as the fluorescence lifetime map produced from the TCSPC data that the patterning technique is once again deemed unsuccessful in producing reproducible linear μCP patterns with LH2. The images in Fig.6.6.1 show this and can be used in conjunction with the other techniques to identify two distinct regions of the sample with varying fluorescence lifetimes. The lifetime in Fig.6.6.1 show regions of shorter and longer lifetime that are separated significantly to allow them to be distinguished between one another. Combination of fluorescence intensity and lifetime in these regions allow for the two regions of the pattern to be analysed where sample is present and where the no sample region is seen, which is that of the substrate. Closer inspection of the opposing regions can analyse whether LH2 is present of pattern regions where it shouldn't be present and it can be deduced to what extent patterning was successful. Where material is being transferred to the regions between the arrays one would expect to observe a fluorescent signal, however in some cases an intensity signal may

be detected due to noise features such as cosmic rays, erroneous light etc. The inclusion of the lifetime data can allow the detected signal to be identified as that which comes from the sample's emission, based on its lifetime or if it is an erroneous effect in which the lifetime will match that of the substrate. These properties have been used to deduce from the patterns in Fig.6.6.1 that although the linear patterns do not print well with the light harvesting complexes, there is no significant transfer of light interacting material to the regions where there should only see the bare substrate.

The main merit of using the TCSPC method is to analyse the excited state of the photoactive complexes and to identify regions where variations in the excited state lifetime of the material can indicate occurences of energy transfer. With the measurements made in this work where the TCSPC is combined with SNOM measurements, results have been obtained regarding the different excited state lifetimes of regions across patterned samples. To accurately portray the lifetime of the sample for the lifetime map, parameters applied to the exponential used to find the best fit had to be refined. The processing of the data acquired in this work to form images found that the time parameter was the key value to achieve the best estimate for the fit. The image (c) shown in Fig.6.6.1 used a time value of 3 ns to achieve the best fit which is on the time scale of energy transfer reported in the literature for LH2. In some measurements (shown in Fig.6.6.3 image (a)) it was apparent that there was more than one lifetime present leading to discrepencies in the measurement of the plots. The presence of more than one lifetime may indicate that the detected fluorescence may arise from both the B800 and B850 BChl rings which would be constistent with the 850 nm longpass filter used that allows detection of the fluorescence from these rings at 850 nm and 910 nm. Modifications to the exponential by introducing a second time dependent parameter allowed this to be fit to accommodate for the second lifetime. The appearance of multiple lifetimes can be explained through the filters used and these combined with the optical properties of the light harvesting complexes. In 3.2.2.1 the structure of LH2 has been discussed and the BChl rings have been mentioned, both of these are active light harvesting structures that without LH1 or the reaction centre have the ability to fluoresce. In the optimisation of the TCSPC/SNOM technique different filters

were used to allow more fluorescent signal to reach the detector where the probe was not ideal or where excitation energies were low. Under physiological conditions the fluorescent lifetimes of these rings vary due to the transfer pathways in the physiological conditions of the photosynthetic unit, the intra complex transfer being faster than the inter complex lifetimes due to the relative differences in distance involved, the two lifetimes match the possibilities of the two BChl rings fluorescing. The reason this second lifetime is not seen in Fig. 6.6.3 image (b) however is that an 850 nm bandpass filter is incoporated into the set up which isolates the emission from the B800 BChl ring thus allowing analysis of only one light harvesting ring and one lifetime.

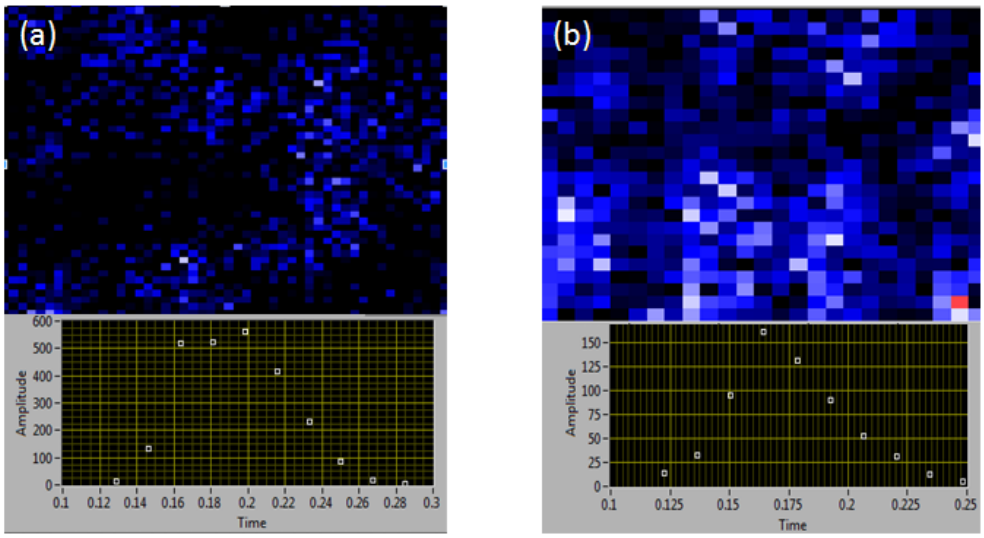

Figure 6.6.3: Shown is an example of regions measured with the SNOM/TCSPC method that detected multiple lifetimes, a property than can be identified from the Intensity vs. Time plot. Image (a) showing the presence of more than one lifetime peak and Image (b) showing a situation with only one peak.

Analysis of the lifetime image acquired for the patterned LH2 observes effects and results that weren't expected based on findings reported in the literature. Closer inspection of the topography image and the plot of the fluorescence lifetime instensity show that which is expected based on the previous measurements made in this work. Where patterned material is seen in the topography, the intensity of fluorescence varies with the height as well as there being no fluorescence present when material isn't present. The image of the calculated fluorescence lifetime seen in Fig.6.6.1 image (c) however appears to be the same with no lifetime where there is no sample however, based on the scale of the image these regions actually have a short lifetime value. This is counter intuitive to what is expected where the lifetime of the substrate would be assumed to be much longer than the bulk patterned material with the expectation that it remained excited until natural relaxation occurs over a period of time. The lifetime of the bulk material is longer than that of the background which although not what was expected shows that there could be some degree of interaction between the complexes arranged in the patterns which could suggest potential energy transfer. Although the patterned material is of a longer lifetime than the background substrate it still displays a shorter lifetime than that of bulk material measured in the literature [5]. These effects suggest that the patterning process or the arrangements of the material into dried patterns may have an effect on the fluorescent properties, not by causing shifts in the emission wavelengths but in the stability of the excited state, with decay of the excited state.

6.7 Summary

Measurements into the potential of light harvesting complexes patterned onto substrates for future bionanotechnology applications show it to contain both merits and failures. Overall the patterning process was unsuccessful with limited accurate linear pattern transfer which could cause issues if these samples were to be used as biological nanowires for example. Refinement of the sample/technique to increase the surface tension of the light harvesting

complex sample which may lead to it not spreading across the sample and forming the structures seen under the scanning microscopes. It may be that with these samples, μCP isn't an ideal method of patterning, unlike with the fluorescent proteins previously shown. With future work other methods like PEG fixation could be incorporated into the patterning process to direct light harvesting material to the patterned regions efficiently, the amount of material in regions could also be regulated in these regions with greater accuracy allowing monolayers, bilayers etc to be investigated in regards to fluorescent properties and energy transfer properties.

The other significant interest of the work into the patterning of light harvesting material was to investigate the fluorescent lifetime properties of the patterns and thus any transfer of excitational energy. It was possible to measure the lifetime properties using the TCSPC/SNOM setup without causing significant photo-degredation to the sample, however analysis of the data showed that the arrangement of the samples in the patterns could have an affect on the excited state properties of the sample. A reduction of the patterned material lifetime was seen in comparison to the bulk measurements suggesting something in the patterning process may have caused this to occur. At present it is believed that there may be some effects pertaining to excited state annihilation occurring which could cause this variation however further work into the samples with this technique need to be made to be sure of these effects. Future measurements may also benefit from better patterning as the inability to create lines could have an effect on the energy transfer properties observed leading to the unexpected variations in lifetimes observed.

6.8 Bibliography

[1] C.N. Grondelle R. Korenhof A. Amesz J. Dorssen, R. Hunter. Spectroscopic properties of antenna complexes of Rhodobacter sphaeroides in vivo. *Biochimica et Biophysica Acta*, 932:179–188, 1988.

[2] G. Gibson L. Grief G. Olsen J. Hunter C.N Jones, M. Fowler. Mutants of Rhodobacter Sphaeroides lacking one or more pigment protein complexes and complementation with rection centre, LH1 and LH2 genes. *Molecular Microbiology*, 6(9):1173–1184, 1992.

[3] H. Cogdell, R. Frank. How carotenoids function in photosynthetic bacteria. *Biochimica et Biophysica Acta.*, 895:63–79, 1987.

[4] M. Freer A. McDermott G. Hawnthornthwaite-Lawless A. Cogdell R. Isaacs N Prince, S. Papiz. Apoprotein Structure in the LH2 Complex from Rhodopseudomonas acidophila Strain 1000: Modular Assembly and Protein Pigment Interactions. *Journal of Molecular Biology*, 268:412–423, 1997.

[5] N. Howard T. McLuskey K. Fraser-N. Prince S. Cogdell, R. Isaacs. How Photosynthetic Bacteria Harvest Solar Energy. *Journal of Bacteriology*, 181(13):3869–3879, 1999.

Chapter 7

Results : Chlorosomes

7.1 Introduction

Chlorosomes are large antenna structures found in green sulphuric bacteria. They are the largest examples of antenna structures found in nature and a major source of light harvesting complexes for the bacterium [1]. The high density of BChl molecules in the antenna structures allow the bacteria they reside in to survive in extremely low light conditions and could act as model system for the development of light harvesting technologies for integration in low light regions of the Earth's surface [2].

In this work chlorosomes have been isolated from the green sulphur bacteria *Chloroflexus (Cfx.) aurantiacus, Chlorobaculum (Cb.) tepidum* and Candidatus Chloroacidobacterium (Cab.) thermophilum. This work compares the properties of these complexes from the differing bacteria using scanning optical microscopes and spectroscopy. Single particle analysis has also been shown using scanning fluorescence microscopy through which, identification of the photosynthetic complexes of interest can be made against other material deposited on the substrate. Spectroscopic properties can also be probed with the single particle configuration allowing comparison of the spectroscopic properties of the different complexes to be compared, as well as single particle spectroscopy to be compared against bulk measurements. Spectroscopy of the individual chlorosome complexes also allows the

variation in the optical properties (and physical dimensions) of different complexes in a population to be compared to show what degree of variation can occur across a sample due to changes to the structural properties of the chlorosomes, their orientation and damages that may occur to the samples.

The addition of the fluorescence microscope to the AFM scanning stage allows single particle measurements and comparisons to be made to investigate the chlorosome samples. The photostability of the chlorosome samples can be addressed through the technique's ability to probe the intensity and peak wavelength of individual complexes. This technique also allows the optical measurement techniques to be addressed for use with these samples to observe the amount of photodegredation induced due to the excitation process as well as acting as a measure to see whether the modifications made to the microscopes for the biological samples minimise effects of laser illumination.

7.2 Spectroscopy

In this work it is necessary to know the optical properties of samples in order to optimise the fluorescence microscope systems to aid the selection of light sources for excitation and to collect only the required emission wavelengths to ensure high resolution imaging. With this in mind it was essential to carry out characterisation of the different species of chlorosome used in this work to attain both their excitation and emission properties accurately. Acquisition of the spectra was conducted with a Fluoromax Spectrophotometer (*Horiba Scientific*) which allows both types of spectra to be obtained as well as offering the capabilities to carry out measurements on liquid bulk samples and thin films.

7.2.1 Bulk spectral properties

The spectroscopic properties of chlorosomes in bulk was of interest in this work as it could act as a measure to determine whether the adsorption of chlorosomes to the glass substrates induced changes to optical properties and thus damages. It could also be compared against

measurements made in the literature which was mostly with bulk samples and not thin films.

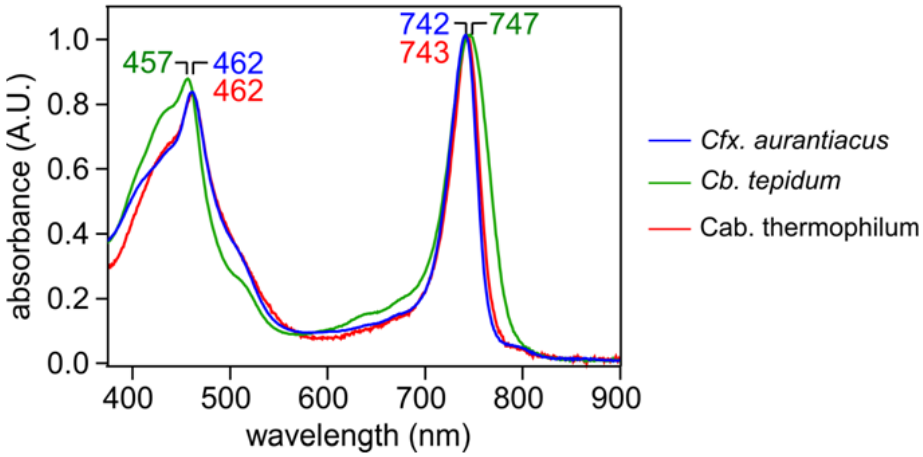

Figure 7.2.1: Absorption spectra from the species *Cfx. Aurantiacus, Cb. tepidum, Cab. thermophilum* diluted in HEPES buffer solution.

All three absorption spectra in Fig. 7.2.1 have been normalised for the purpose of comparison however, all of them were obtained with similar detector settings. To ensure that all of the individual components of the chlorosomes were included in the spectra obtained, the wavelength region observed was from 350 - 900 nm. Slit widths on the monochromator were kept to a minimum to ensure accurate absorption peaks with minimal broadening due to too much light, as this meant light intensities were reduced the integration times at

each wavelength were increased from the standard 0.1 seconds that have been used elsewhere in this work to 0.5 seconds. The main light harvesting components contained in the chlorosome antenna structures are displayed in this spectra with the broader, bluer peaks around 460 nm belonging to the photo-protective, light harvesting carotenoids and the near-IR peaks around 745 nm showing the absorption peaks for the BChl-*c* proteins that act as the main source of light harvesting. It is also possible to identify a small shoulder around 800 nm in the *Cfx. aurantiacus* and Cab. thermophilum representing the presence of BChl-*a* (similarly to the peaks seen in LH2 outlined in 3.2.2.1) in the baseplate from the chlorosomal structure [3]. Small variations are seen in the peak absorption maxima of the 3 chlorosome species which are marked at the corresponding peaks in Fig. 7.2.1. The variation seen in these absorption peaks arise through the differences in the structures of the different chlorosomes and how they aggregate and thus containing varying environments for the BChl-*c* in the chlorosomal envelope.

Alongside the small variations that are shown in the absorption spectra of the chlorosome species, the emission properties show small variations in the peak wavelength between the different chlorosome species. Due to the variations in the local environment and the internal structure of the samples, the different species of chlorosome show small variations in their peak wavelength which can differ by tens of nanometres, as shown in Fig. 7.2.2. As can be seen from the shown emission spectra, the *Cfx. aurantiacus* and Cab. thermophilum species show emission peaks that are very similar to one another at 748 nm and 750 nm respectively. *Cb. tepidum* species on the other hand shows a greater variation from the other chlorosome species with an emission peak at around 760 nm, these variations show the manifestation of the varying local environments in each chlorosome species. Differences in the local environments can arise from the populations of the different types of BChl which have slightly different absorption and emission properties, the orientation of these in the chlorosome structure can also allow variations in spectral properties.

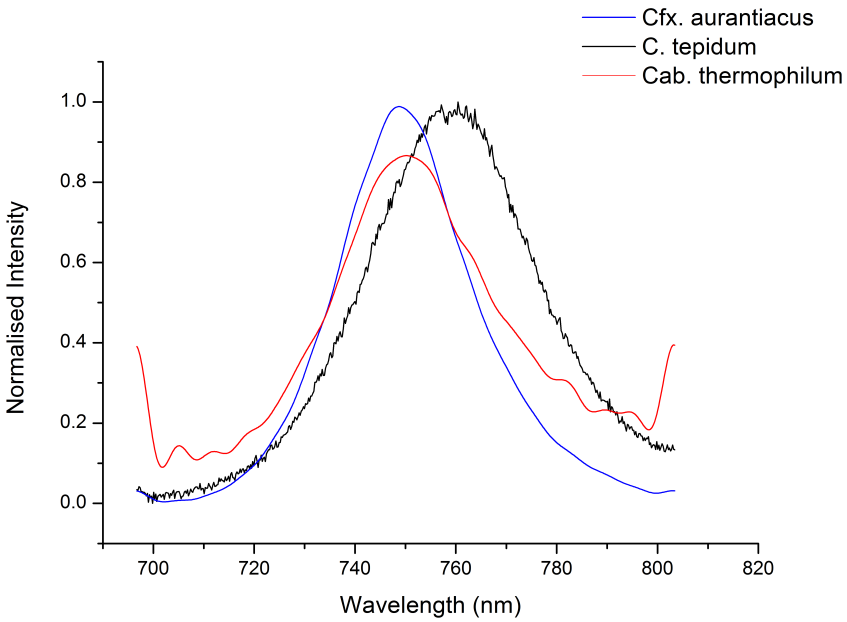

Figure 7.2.2: Emission properties from the species *Cfx. aurantiacus*, *Cb. tepidum*. *Cab. thermophilum* diluted in HEPES buffer solution.

7.2.1.1 Sample Preparation

To prepare the samples for spectroscopic measurments on bulk material, dilutions were required that were sufficient to allow measurements to be conducted without effects like the reabsorption of fluorescence occurring. It was also required that the optical density didn't significantly reduce the amount of light that can be detected by the spectrometer and thus limit the ability to produce accurate spectra. Samples were diluted significantly to produce accurate spectra and reduce the optical density with spectroscopy being done on samples at concentrations of 1 in 2000 of the chlorosomes to HEPES buffer pH 7.5. Dilution in HEPES buffer at pH 7.5 as to keep the samples in physiological conditions and to prevent damages that may arise from pH values that are too acid or alkali whilst under illumination. Measurements had also been conducted with samples diluted to 1 in 200, however with the optical density being higher less light was detected in the absorption measurements and some broadening was also observed in the measurements of fluorescence.

7.3 Biological Considerations

Due to the nature of biological samples to succumb to various levels of light induced damage, it was necessary to take into account a number of properties that may lead to complex damage and thus reduce the quality of images and the time over which a sample may be imaged for. Modifications for sample properties were applied to the microscopes to improve analysis of the complexes and not to damage them significantly whilst they were under observation.

Chlorosome damage induced by the excitation source was a major source of the photodegradation observed in the process of investigating samples using optical microscopy. Similar to the effects reported previously for LH2 and GFP, light sources incident on the sample with high excitation power have the ability to lead to high levels of photodegradation due to a greater number of photons being incident on the sample and thus a greater number of excitation events. Photodegradation is exacerbated in these measurements as well due to the higher intensity of the lasers used for the scanning optical arrangement compared to excitation with the LED/lamp. To observe and analyse these samples a 473 nm diode laser was used, allowing the natural properties of the chlorosomes in the sample to be exploited to prevent some of the light induced damage present in the imaging process. Illumination of the absorption peaks of the chlorosomes around 470 nm allowed excitation to occur through the carotenoids, the process of which aided photostability. Exploiting the carotenoids for excitation of the chlorosome complexes allowed the active lifetime of the samples to be increased as the excitation of BChl molecules can lead to the formation of singlet oxygen where the incidences of excitation are high. Using the carotenoids to transfer excitation energy to the BChls however, introduces a pathway to prevent singlet oxygen remaining in the system and less BChl directly excited with the light source. The presence of carotenoids to quench the excitation of the BChl states also prevents the formation of excess triplet excited states of the BChl molecules which lead to increased time periods where potential photo-oxidation processes can occur. With a large amount of excitational energy in the chlorosome system there is still a high chance for photodamage

to occur regardless of carotenoid excitation being used to protect the sample. Excitation of the carotenoids prevent some of the harmful photo-oxidative effects but not all of them and as a result the chlorosome samples are still likely to degrade whilst under constant illumination. A measure that has been taken to reduce the number of potentially harmful photo-oxidation events occurring with the chlorosome samples has been to regulate the power of the laser and to keep the intensity of laser light delivered to the sample to a minimum, thus reducing the number of high power photons incident on the chlorosomes. Furthermore several modifications were made to the measurement technique to reduce the chances of photo-oxidation occurring such as, when locating regions of the sample surface that were of interest for the scanning mode optical imaging a lower powered LED was used to reduce the intensity of light delivered to the sample to allow standard microscopy to be used. Between images the laser was diverted away from the surface to again reduce the high intensity laser light from causing damage to the sample, the reduction in the time of constant illumination allowed the samples to be imaged for longer where it is assumed that these measures lower the frequency of singlet oxygen and triplet state BChl formation.

As the chlorosome complexes were isolated from green photosynthetic bacteria they were removed from their native environment and were therefore removed from ideal physiological conditions associated with the native bacterium. This was a consideration that was addressed and applied to the imaging techniques in this work. To keep the chlorosomes under favorable conditions, they were imaged under buffer solution which allowed the samples to be hydrated similarly to the native environment preventing structural damage and allowing their pH to be kept neutral, protecting against damage arising from acidic and alkali conditions. Imaging under buffer solution allowed the environment to be maintained in such a way to further prevent photo-oxidative effects that lead to damaging effects in the chlorosomal complexes. Alongside the increased chances of photodamage due to high light intensity, the presence of high or natural levels of oxygen can lead to the formation of singlet oxygen which can lead to damage resulting in degredation of optical properties. To curb the damaging effects arising from the presence of singlet oxygen and light, several procedures were taken to adapt the sample environment. As already mentioned, the sam-

ple was imaged under buffer solution to keep it in a physiologically favorable environment as well as keeping it in an environment that had low levels of oxygen present to prevent singlet oxygen formation. On top of being under buffer solution samples fixed to petri dishes for analysis were held in a profusion cell designed for the AFM with which nitrogen could be passed across the top of the sample to remove oxygen from the system. Even with the modifications there was still the presence of photo-damage leading to sample degredation therefore, the buffer solution used to image the sample under was modified to include sodium dithionite, the addition of which helped to maintain a reducing environment and extend the lifetime of samples under fluorescence imaging. As well as the addition of sodium dithionite the buffer solutions were splarged with nitrogen for storage and prior to the addition to samples, to remove more oxygen and aid the lifetime of the buffer solutions that are also prone to degredation.

The measures taken to regulating the light intensity incident on the sample and the level of oxygen in the system were done so to prevent the degredation of the emission peaks of the chlorosomes and to eliminate the formation of a 670 nm emission peak, shown in Fig. . This unexpected peak in the emission spectra was observed in early measurements of chlorosomes with the fluorescence microscope system. It is believed that this peak may be a result of structural changes present in the chlorosomes under illumination which leads to the aggregated structures being disrupted in such a way to induce the 670 nm peak which is attributable to the presence of monomeric BChl-*c* [4].

7.4 Image Acquisition

7.4.1 Fluorescence Microscopy

Scanning fluorescence microscopy which combined the optical microscope with the scanning stage of the AFM allowed images to be acquired with varying fields of view that are determined solely by values set with the AFM scanning stage. In the fluorescence measurements conducted on the chlorosome samples it was possible to vary the scan size in a way

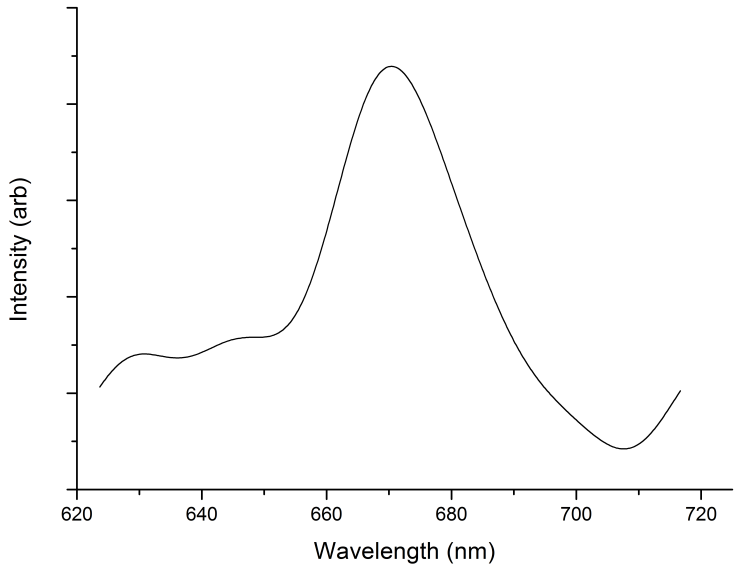

Figure 7.3.1: The emission spectrum obtained for the *Cfx. aurantiacus* depicting the 670 nm emission peak depicting structural damage to the chlorosomes whilst under measurement.

that was advantageous for different measurements. Large scan areas in excess of 20 μm could be applied to address the effects of different concentration chlorosome solutions applied to the substrates. The number of complexes adhered to the surface can be identified to address sample concentrations to see which concentration is the best to conduct single molecule fluorescence analysis. Smaller scan sizes can be used to accurately measure inter complex distances as well as progressively isolate a complex in the field of view to conduct single complex analysis to obtain emission spectra. To identify regions of interest for further measurements, 20 μm scan sizes were used, these were sufficient to identify single complexes and measure the distances between complexes. This scan size allowed a number of chlorosomes (up to 20) to be seen for the concentration and each of these could then be measured at smaller scan sizes to accurately measure the perceived distances between the complexes (scan sizes around 10 μm) as seen with optical microscopy. Scan sizes from 5 μm through to 1 μm can be applied to isolate the single chlorosomes prior to reducing the scan size to 0 μm and thus centring the laser spot/detector and achieving point source

excitation of the sample.

Fig.7.4.1 shows 10 μm regions obtained with the scanning fluorescence microscope for the 3 different chlorosome species. The chlorosomes in each fluorescent image manifest themselves as diffraction limited spots with average diameters of 300 - 400 nm which is in line with the theoretical resolution of the optics in the microscope arrangement. From these images, information regarding the arrangements of the chlorosomes can also be obtained. Where the diameters of fluorescent points are on the scale of the diffraction limit it can be inferred that single chlorosomes are seen, where points are of greater diameter it can furthermore be inferred that multiple chlorosomes are separated by small distances (below the resolution limit). Both of these chlorosome arrangements are expected from a random distribution of particles.

In these images one can also see that due to the random distribution of particles the inter-particle distances can vary quite significantly in a single image. The properties associated with the random distribution of particles are useful to physically identify the number of particles within a region that corresponds to the concentration of the solution cast on the substrate. The random distribution also allows the resolution of the microscope with these samples to be addressed by measuring the minimum distance observed between two point sources that can still be resolved from one another, the best resolution measured with these samples was estimated as $\sim$350 nm. The smallest resolutions measured in each individual image however varied due to the random nature of particle distribution, however for each species/sample an average distribution could be obtained which for the sample and concentration could act as a measure to predict how well the sample would be distributed on the surface and thus aid the sample preparation to ensure that particles were still resolvable when optical measurements were made and that for example, concentrations weren't too high so that aggregation of many chlorosomes occurred.

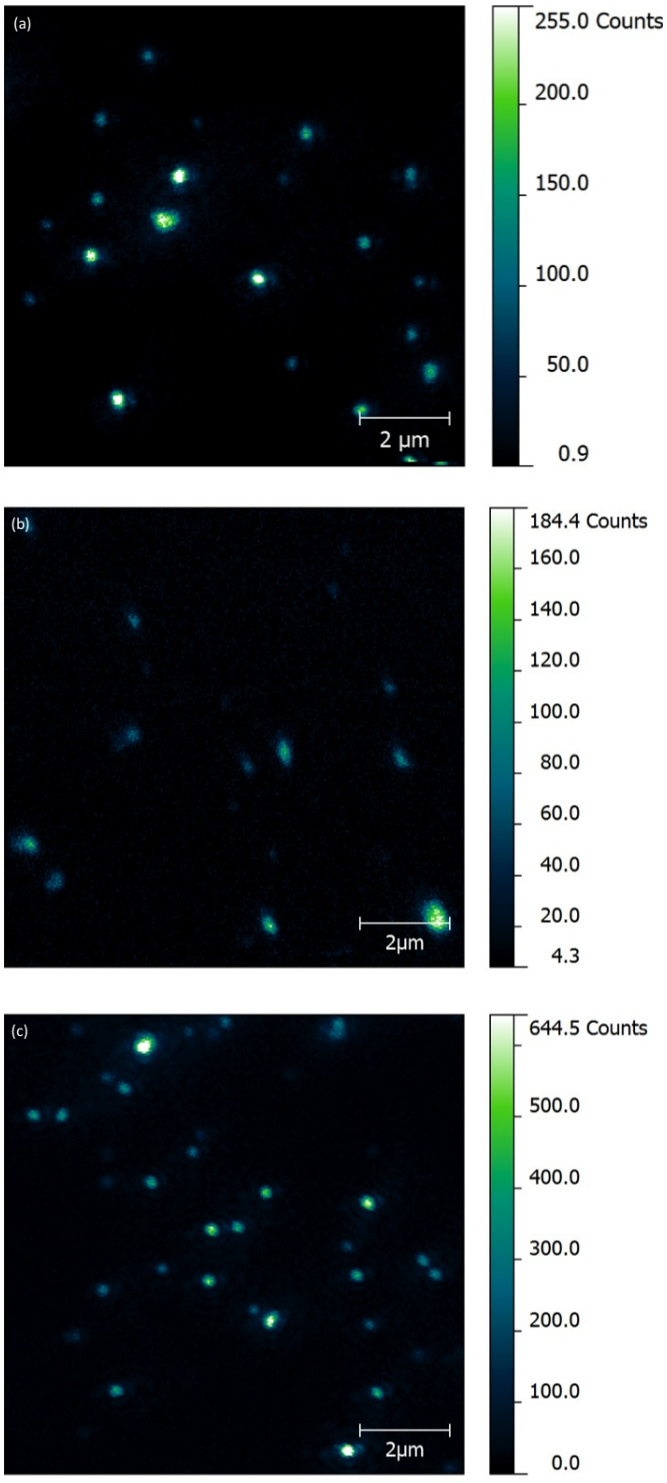

Figure 7.4.1: Scanning fluorescece microscopy is used to identify fluorescence from chlorosomes which could be used as candidates for characterisation. 3 species are shown (a) *Chlorobaculum tepidum* (b) *Chloroflexus aurantiacus* (c) Chloroacidobacterium thermophilum.

7.5 Single Particle Measurements

The combination of both scanning fluorescence microscopy and static fluorescence microscopy allowed measurements to be made that couldn't be achieved by only one of the microscopes. The high resolution of the laser scanning microscope could be used to obtain high resolution measurements of the chlorosome samples whilst at the same time the EMCCD camera could be utilised. The EMCCD can be used on the point source chlorosome particles to obtain emission spectra for each individual point source to compare how the chlorosome species vary between each other as well as measuring the heterogeneity of the emission across a sample from a single species.

By measuring the spectroscopic properties of individual chlorosomes the previously shown scan sizes and fluorescent image shown in Fig. 7.4.1 were used to identify regions of interest. Identification of a number of individual particles in a particular scan region allowed the versatility of the scanning stage to be utilised to navigate to each chlorosome in turn to conduct analysis of these. By offsetting the scanning stage to move the laser to each complex scan sizes could be reduced to zoom in on the individual complex. With the laser centered on a complex in a $1-2$ μm scan region the scan size can be reduced to 0 μm ensuring that the laser is centred at a single point above the chlorosome complex with no movement. Emission spectra could be obtained at this point by diverting fluorescent signal to the EMCCD attached to the monochromator with prior settings that reduce the slit width of the monochromator to prevent spectral broadening due to an excess of light both relating to the fluorescence intensity and background. Exposure settings also allow optimisation for the detection of both high and low intensity fluorescent signals for the chlorosomes. This prevents effects of broadening spectra by optimisation of signal relying on more factors than just an increase of exposure time, thus reducing an excess of light entering the detector.

Fig. 7.5.1 show the inverted fluorescence images of 10 μm regions for the different species where the edges have been highlighted in each image and single particles have been

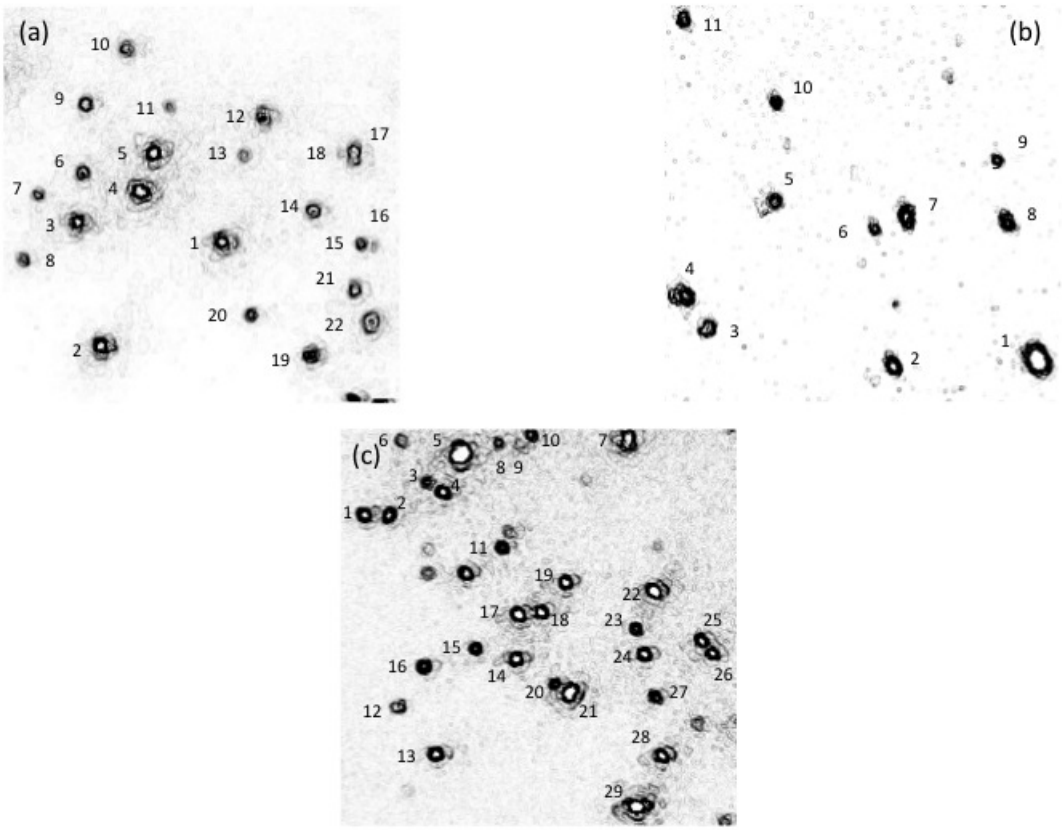

Figure 7.5.1: Fluorescence images allow point sources to be identified for spectroscopic measurements, individual chlorosome candidates are marked for (a) *Chlorobaculum tepidum* (b) *Chloroflexus aurantiacus* (c) Chloroacidobacterium thermophilum.

identified and numbered to correspond to spectra obtained for each point (shown in Fig. 7.5.2). The spectra obtained can be compared against fluorescence data in the literature to see whether damage had occurred to the sample in the imaging process or in the fixation of chlorosomes to the substrate (Cab. thermophilum could not be compared as no previous data is available for fluorescence in the literature). From image (a) in Fig. 7.5.2 an average emission value of 748 nm is seen for *Cfx. aurantiacus* with a deviation of ± 1.352 nm across the complexes, for *C. tepidum* in image (b) an average wavelength of 768 nm is observed with deviation of ± 1.276 nm and for Cab. thermophilum the peak wavelength is 751 nm with a deviation of ± 1.035 nm. With each of the emission spectra shown in Fig. 7.5.2 the variation in the intensity of the peak emission wavelength follows from the apparent brightness of the single complexes seen in the field of view in the image as expected.

7.6 Analysis

The spectra observed for the chlorosome species displays the variations in optical properties that can arise due to the formation of these large structures. Variations in the aggregation of BChl-*c* to form chlorosomes lead to the emission peaks being where they are, the variations between species that are observed in the measured spectra arise due to small structural differences. The aggregation of BChls to form different species leads to large variations in optical properties however, small variations are observed between individual chlorosomes in the fields of view measured in this work. The heterogeneity of the emission peaks in each species is significant enough to be seen with the greatest degree of variation observed in the chlorosome species *C. tepidum*. It is suggested that on top of the environment after aggregation having an effect large enough to be distinguished between different species, the heterogeneity that gives rise to the variations between single chlorosomes can be put down to slightly different environments occurring within the population. The heterogeneities within the populations may also give rise to the large FWHM observed

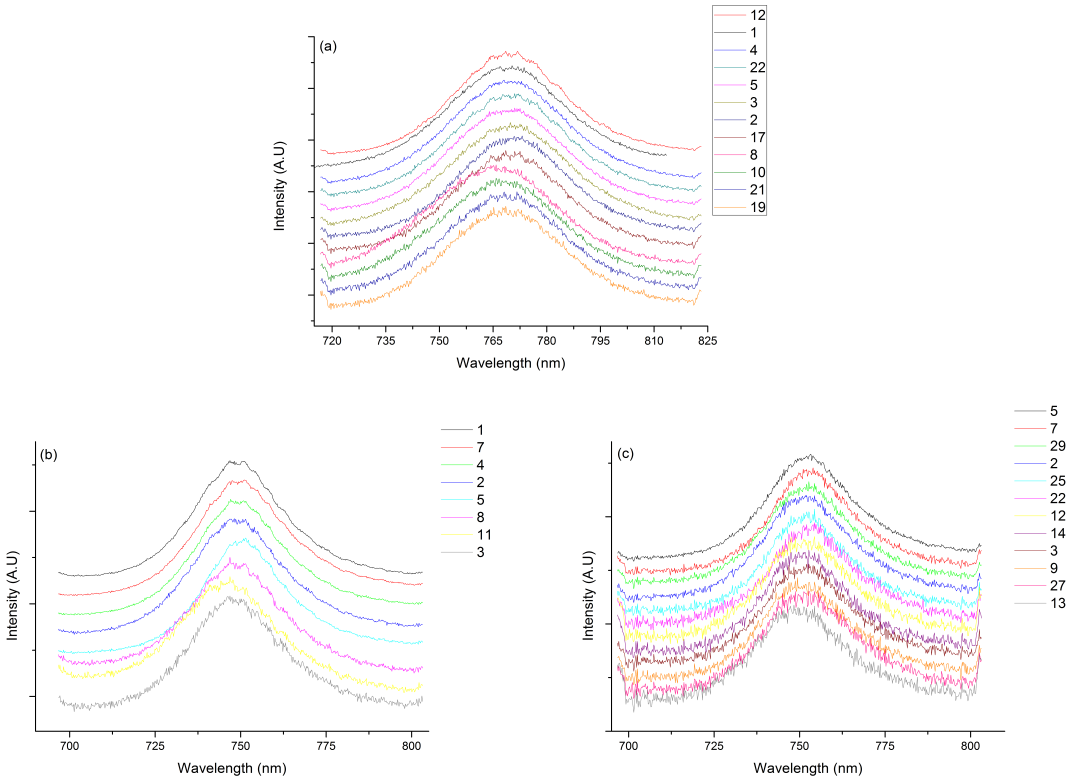

Figure 7.5.2: Emission spectra of individual chlorosomes highlighted in Fig. 7.5.1 see small variations about a specific species emission wavelength. The species (a) *C. tepidum* (b) *Cfx. aurantiacus* (c) Cab. thermophilum are shown above.

for the species in the bulk measurements compared to that of the single chlorosomes, this may also be applied to the point sources that were particularly large and bright that were deemed a result of multiple complexes closer to one another than the maximum resolution of the microscope arrangement. It can be seen in the spectra for *Cfx. aurantiacus* when comparing point no. 1 and point no. 5 that the emission spectrum measured at point no. 1 has a FWHM maximum greater than point no. 5, suggesting the presence of more than one complex with hetrogenous properties is can lead to a broadening of the emission peak where they combine.

With each chlorosome the emission spectra obtained and displayed in Fig. 7.5.2 is an average of 20 spectra taken in succession. Although emission spectra were obtained for each chlorosome in the fluorescence images, not all of them are displayed in Fig. 7.5.2 due to their accuracy (based on signal-to-noise) being compromised by the effects of photodegredation. With the constant illumination of individual chlorosomes over the time that it took to obtain the number of individual spectra the intensity of emission was seen to degrade, suggesting that the laser excitation was causing damage to the chlorosomes even with the modifications for biological measurements applied. The modifications made to ensure that the chlorosome samples were kept under physiological conditions without the presence of a significant amount of oxygen allowed the fluorescent properties of the whole sample to be maintained for much longer when the whole sample is being imaged. Across the whole sample the intensity within an area of the sample is low as energy is spread to other complexes however, with single particle measurements one chlorosome is subject to the high intensity light increasing the probabilites of photooxidation due to the higher number of high energy photons falling on the particle. The effect of degredation is most noticeable in the *cfx. aurantiacus* chlorosomes, in Fig. 7.6.1 single chlorosomes of similar fluorescence intensity, as measured by the EMCCD, have been used to look at the effects of constant illumintion under measurement. Assuming that the laser excitation is stable, the power delivered to chlorosomes is the same for each species therefore similar intensity single complexes can be used for comparison. The graphs in Fig. 7.6.1 show a plot of the time against the maximum fluorescence intensity at the peak of the spectra in each

accumulation. Although not an in depth analysis, the gradient of the slope associated with the change of fluorescence intensity over time can give a rate at which the single chlorosome particles degrade as well as also giving a time frame within which the samples degrade to a value which is too low to significantly distinguish from the background. It is apparent from the plots that the *cfx. aurantiacus* fluorescent signal decays at a much faster rate than with the other chlorosome species, the measured gradients show this with *cfx. aurantiacus* having a gradient 4 times greater than cab. thermophilum and *c.tepidum* at -84.1 compared to -14, -19.8 respectively. It may also be noted that when looking at the degredation of emission from a single chlorosome, changes are seen as the intensity of fluorescence decreases, changes are not seen significantly in the wavelength of the peak emission. This suggests that in the region where fluorescence observations take place the only variation seen is that the sample loses fluorescence which may be a result of the oxidation of BChl and thus damage that results in a loss of the fluorescence signal. However, what may also occur in this region could be to do with the previously mentioned 670 nm emission peak. Changes to the environment that the chlorosomes are in and the conformation of BChl complexes could lead to the disassociation of BChl-*c* from one another and lead to increasing amounts of monomeric BChl being present which is characteristic of the 670 nm peak. This would also account for the decrease in the peak around 760 nm for the chlorosomes as an increasing amount of the BChl contained within the chlorosome structures are being converted to the monomeric form.

7.7 Conclusion

Following on from the analytical microscopy techniques developed for the measurement of patterned biological material in chapters 5 and 6, the fluorescence microscopy techniques have been developed and refined to allow both the acquisition of high resolution fluorescence images and single particle emission spectra. In measuring 3 different species of chlorosomes, single particle techniques have been utilised to analyse fluorescent properties both in bulk

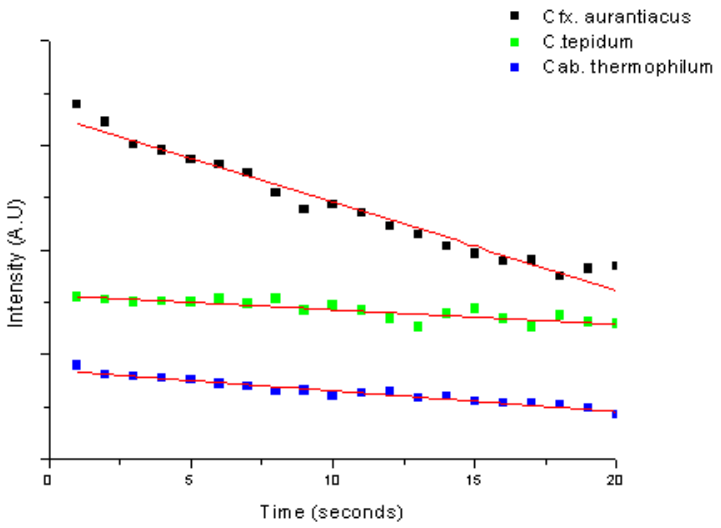

Figure 7.6.1: Decay of similar intensity chlorosomes from the 3 species are shown with normalised intensities. Linear fits are applied to address the rate of signal degredation.

measurements and single particle measurements. It has been possible to compare these fluorescent properties with those in the literature [5, 6] conducted on bulk material to address any differences whilst at the same time ensuring that complex damage was not a factor introduced through sample preparation or measurement. These measurements also showed some of the early research into the optical properties of the newly discovered Chlorobaculum thermophilum chlorosome.

In this study of the chlorosome species, *Cb. tepidum, Cfx. aurantiacus* and Cab. thermophilum, bulk measurements of the biological material have been utilised to check excitation/emission properties for the optimisation of the fluorescence microscopy method and to act as an indicator to whether damage or changes to the optical properties have occurred in the sample preparation process which would lead to a difference when compared to the properties reported in the literature. With the bulk measurements of the different species, the fluorescence microscope could be set up in a way so the correct excitation source was selected to attain optimal excitation/emission and that the emission filters and monochromator could be set in a way that irradicated stray light that was not from the

sample which was of no interest.

The 3 species were systematically analysed with fluorescence microscope techniques in this study to compare their coverage of substrate when at similar material concentrations, this was seen in the concentration of chlorosomes seen on the surface of the substrate after adhesion. The fluorescence technique was used to find candidate regions of each species where a number of individual chlorosomes could be identified from point sources of fluorescence due to their size and intensity (under this criteria regions of multiple chlorosomes could also be identified). Processing of indvidual chlorosomes in this work was conducted through the acquisition of multiple emission spectra for each chlorosome, through this, heterogeneity within species could be identified as well as the major optical differences present between species, both of which are believed to be a result of varying degrees of variation in the chlorosome environment.

A persistent issue with the measurement of the chlorosomes in this chapter (as well as other optically active biological material studied in this work) is that of photo-damage arising from the excitation of the sample. Early measurements of chlorosomes using the optical microscope observed very little to no fluorescence in the expected emission region around 760 nm but a large amount of emission observed around 670 nm, characteristic of the monomeric forms of BChl-*c* suggesting that the imaging process affects the chlorosome structure in such a way, either through the damage of single BChl in connected regions of the chlorosomes or by inducing conformational changes which cause changes to the arrangement of the BChl. Developments to the system were made to prevent the effects of photo-decay and allow correct acquisition of spectral properties to be observed within a population of single chlorosomes. By introducing imaging buffer solutions with reducing components and conducting all measurements under liquid, environments as close to physiological conditions as possible. The system was developed to allow higher accuracy measurements of the spectral properties of the chlorosome samples in question, as well as facilitating more repeat measurements to be made per sample as the time in which photodegredation times occurred was significantly reduced. With this is it was found that the variations observed in the emission wavelengths between complexes were a result of the

heterogeneity of chlorosomes in a population due to their environment and not a result of photo induced effects causing conformational changes and thus spectral changes to the BChl*s*.

7.8 Bibliography

[1] T. Remigy H. Tsiotis G Hauska, G. Schoedl. The reaction center of green sulfur bacteria. *Biochimica et biophysica acta*, 1507:260–277, 2001.

[2] J. Kuypers M. Overmann J. Manske, A. Glaeser. Physiology and Phylogeny of Green Sulfur Bacteria Forming a Monospecific Phototrophic Assemblage at a Depth of 100 Meters in the Black Sea. *Applied and Environmental Microbiology*, 71(12):8049–8060, 2005.

[3] H. Shibata Y. Itoh S. Saga, Y. Tamiaki. Excitation energy transfer in individual light-harvesting chlorosome from green photosynthetic bacterium Chloroflexus aurantiacus at cryogenic temperature. *Chemical Physics Letters*, 409:34–37, 2005.

[4] K. Suzuki M. Nakagawa H. Shikama Y. Konami H. Wang Z Nozawa, T. Ohtomo. Structures of chlorosomes and aggregated BChl c in Chlorobium tepidum from solid state high resolution CP/MAS C NMR. *Photosynthesis Research*, 41:211–223, 1994.

[5] R. Natarajan L. Dickinson L. Fuller R Betti, J. Blankenship. Antenna oranisation and evidence for the function of a new antenna pigment species in the green photosynthetic bacterium Chloroflexus Aurantiacus. *Biochimica et Biophysica Acta*, 680:194–201, 1982.

[6] Y. Tamiaki H. Saga, Y. Shibata. Spectral properties of single light-harvesting complexes in bacterial photosynthesis. *Journal of Photochemistry and Photobiology C: Photochemistry reviews*, 11:15–24, 2010.

Chapter 8

Conclusions

The work presented in this thesis has allowed for the development of experimental techniques with an understanding of biological properties which paves the way for future research projects to conduct high resolution investigations of biological components. The development of optical microscopy techniques and operational methods of scanning probe microscope techniques (such as SNOM) have allowed biological considerations to be taken into account and applied to microscopes to facilitate measurements of samples that easily succumb to photodamage. Variations in illumination techniques, the introduction of oil immersion objectives, the application of liquid measurements and modifications to operational techniques have been systematically outlined in this work to allow future work on easily damaged photosynthetic samples to be conducted to progress the application of such samples to biological nanotechnology. This work also displays fluorescent proteins as an ideal test system for the development of optical and scanning probe microscopy techniques and microcontact printing techniques with which photosynthetic samples could be applied to surfaces and measured. This work also displays preliminary research into the optical properties of chlorosomes from green sulfur bacteria with single chlorosome spectral measurements conducted using the developed scanning fluorescence microscope. These initial measurements are open for future measurements on other species or further spectral/microscopy investigations of these species; the biological considerations and

subsequent modifications made for the chlorosome species can also be taken into account for future experiments to ensure that photo-induced damage is kept to a minimum and protects the spectral properties of the samples of interest.

8.1 High Resolution Microscopy Techniques

Optical microscopes and the many variations of scanning probe microscopes have been vital tools used in the analysis of materials in the sciences. Both forms of microscopy allow varying properties to be measured as well as introducing a number of limitations and issues that may arise when introduced to samples across the fields of science. For increased characterisation of surfaces/samples in biological applications new imaging techniques are focusing on combinations of microscope techniques, such as those used to analyse both topographical and fluorescent properties of samples.

Part of this work has seen the development of existing microscope systems to facilitate measurements of biological samples and to allow more than one property of the sample to be measured simultaneously. Atomic Force Microscopy (AFM) has been combined with optical microscopy to allow large far-field fluorescent surface analysis to be made alongside AFM as well as allowing high resolution scanning fluorescence microscopy to be applied simultaneously with AFM so that variations in the two measurements to be correlated with one another.

Analysis of the varying samples has allowed the differences in resolution between the microscopes to be observed. In this work the microscopes have been developed to allow the smallest resolvable distances with optical microscopy to be around 300 nm, with the AFM on the scale of tens of nanometres and with the SNOM around 100 nm, all in line with theoretical expectations and those also seen in the literature [1, 2, 4, 3]. With this it has been possible to apply small modifications to the microscopes to allow greater resolution images to be attained or to allow a variety of different samples to be analysed. Furthermore, knowledge of the observed resolutions has been applicable in the sample preparation techniques to produce PDMS stamps in the μCP techniques to transfer optically active

biological material to a substrate that is patterned in such a way that lines of material are distinguishable from one another with all microscopes as the distance between them isn't lower than the resolution of the microsope. The theoretical resolutions have also been applied to the dilution of chlorosome samples to ensure that single chlorosomes can be distinguished from each other so that the samples are not too concentrated so that multiple fluorescent points don't merge to produce large areas of indistinguishable emission.

8.2 Patterned Biological Samples

μCP techniques have been applied to a number of different samples in the literature varying from inorganic to organic and to biological [5, 6, 7, 8]. With the potential future of nanotechnological devices leaning towards the inclusion of biological components, this study has displayed μCP as a method to pattern optically active biological samples for both the use in comparing relative merits of microscopes and to investigate the merits of this patterning technique. Furthermore, the patterning of these samples has also been used to investigate energy transfer processes which could be applicable for these as future structures for devices.

Patterned samples in this work were comprised of two different samples that had varying properties, those of fluorescent proteins derived from GFP and purified LH2 antenna complexes from the photosynthetic bacterium *Rhodobacter Sphaeroides*. GFP and its derivatives have been studied intensively in the literature and act as a system in this work that can be used to address the merits of the technique for patterning proteins through μCP. They also act as an ideal system to investigate resolutions of the microscope systems used and to address how applicable the techniques are with biological samples. LH2 on the other hand has been used in this work to investigate its optical properties through the use of the microscopy techniques at hand. Light harvesting and energy transfer are also properties of interest with the samples from photosynthetic bacteria and the patterning has been utilised in an attempt to measure the transfer of energy along the patterns formed with them.

The high fluorescence intensity and the photostability of the fluorescent proteins used meant that minimal modifications needed to be applied to the microscopes to prevent photodegredation and thus facilitate the measurement of these proteins. From the acquired images it was seen that the patterning technique with GFP and its derivatives was successful with defined lines transferred to the substrate. The samples were also seen to retain optical properties indicating that minimal damage occurred to the fluorophore, during the patterning process, furthermore it also indicated that measurement of the samples caused minimal damage to the fluorophore and the optical properties. Using the images acquired with the different microscopes in similar (or the same) regions of the sample, it was possible in the post processing to compare the relative resolutions of the techniques with the patterned GFP/YFP acting as standard samples due to their regularity on the surface and high fluorescence intensity. Line profiles of the regions display what is expected from theory that the scanning probe techniques show higher resolution in the form of more defined linear patterns when compared to the optical techniques which succumb to the limitations imposed by the diffraction limit. It was seen that the fluorescent proteins patterned well with the μCP technique however, not all regions were the same. Some regions saw thicknesses of material on the surface that varied significantly which affected the reproducibility of the patterns as well as the optical properties with fluorescence intensity scaling with sample thicknesses.

With the patterned LH2 samples analysis was carried out both with scanning probe techniques and optical techniques however, in comparison to the measurements made on GFP patterns the static optical microscope was not used for image acquisition due to the emission being located in the near infrared and the intensity being low for detection with the LED excitation source. In comparison to the patterns fromed from GFP, LH2 patterning was much less successful with only a small number of lines being formed on the surface, potentially due to the printing process or to do with sample properties such as surface tension of the solutions. When obtaining images the samples were measured under physiological environments with minimal oxygen presence and under liquid to prevent damage to the samples from excitation associated with the optical techniques. Although

the formation of patterns with this sample wasn't ideal the optical properties remained allowing imaging to be conducted with the scanning fluorescence microscope and the SNOM, all resolutions and perceived detail scaling with the different techniques. The nature of the light harvesting complexes is to direct excitation energy towards a reaction centre, due to this property TCSPC measurements were made using the SNOM to investigate the energy transfer properties in the LH2 patterns. Some energy transfer was seen from the lengthening of fluorescence lifetimes compared to those measured in the literature however, the results also suggested energy transfer occurring in the background signal from the substrate relative to the complexes. The potential reason for this may be an effect if excited state annihilation however this is an area open to further experiments.

8.3 Chlorosome Species

Several different chlorosome species were investigated in this work as systems that can efficiently harvest energy in low light conditions due to the high number of light harvesting molecules that they contain. These structures could in future act as model systems to mimic these properties or may be applicable in such devices that may be able to incorporate their optical properties.

This study looked at the optical properties of the chlorosomes allowing single particle techniques to be utilised with the microscope as well as characterising the properties of them. Two of the species used had previously been investigated in the literature with bulk optical measurements (*Cb. tepidum, Cfx. aurantiacus*) however these were some of the first measurements made into the emission properties of the Cab. thermophilum chlorosomes. Dilute samples on the substrate were investigated with the scanning optical technique to find a population of interest for each species where single chlorosomes were present. By combining the scanning stage and the EMCCD camera, individual chlorosomes could be investigated to record emission spectra.

Emission spectra of chlorosomes could be used to compare the variations in the optical properties of the different species due to the variations in the environment that lead to the

change in wavelength of tens of nanometres. Spectra were also obtained for chlorosomes within a population which in each different species showed that there were varying degrees of heterogeneity present. The measurement of single chlorosomes also showed the effect of high energy illumination with these samples in the way that even with modifications made to the microscope to reduce the effects of photo-oxidation, degradation in the fluorescence intensity was still observed.

8.4 Difficulties addressed

A major difficulty present with all of the microscopes used in this work as well as with each sample was the presence and influence of photo-oxidative effects. With each system it took time to optimise it for measurements on each type of biological sample with modifications such as oil immersion lenses being introduced to allow samples to be imaged for longer as the intensity of the emission decreased. Furthermore the introduction of oil immersion lenses allow samples with lower emission intensity to be imaged due to improved light collection. Where it was possible, the imaging environments were removed of oxygen either by introducing nitrogen into the atmosphere (SNOM) or by imaging samples under buffer solutions (AFM, fluorescence). These modifications were seen to vastly improve the imaging techniques used on the samples of interest. The effects however were not completely removed and some photodegradation was still observed, this occurred after several measurements of a particular sample had already been conducted.

The patterning technique was one difficulty present in the patterned samples. Although the patterning didn't directly affect optical properties in either of the samples used, the success of patterning wasn't completely reproducible which could lead to small variations in sample coverage relating to sample thicknesses and thus the intensity of regions with the GFP samples. It could also lead to the very uncertain patterning present with light harvesting complexes. This made investigations into optical properties difficult due to the variability of fluorescent signal, in the case of TCSPC measurements of light harvesting complexes it could lead to regions where no energy transfer could occur.

A further problem was that of low signal with some of the biological samples used, in particular photosynthetic bacteria. Bacteria have evolved to direct energy to a reaction centre quickly and efficiently which leads to them emitting only a small amount of light as most transfer is non radiative. Where the LH2 is isolated and no LH1 is present to transfer energy to, the emission intensity remains low. Modifications were made to the systems with oil immersion lenses to improve the collection of light/emission, the power of the light sources could also be adjusted (although this increases photodegredation). This did improve signal although it was still low when compared to GFP and polymers, which the equipment was intially set up to use therefore refinement of the systems was needed to allow successful imaging of these samples.

8.5 Future Work

Different microscopy techniques have been developed in this work to allow successful analysis of biological samples both patterned and deposited on the surface randomly. The study is on the most part complete however there were some areas of study that were not completed due to time constraints affected by the development of imaging processes. Proposed future work with these areas in mind are presented in this section.

- Analysis of energy transfer pathways using SNOM and TCSPC were briefly studied for LH2 with unexpected results. Further study would conduct a more in depth analysis of the excitation pathways of both patterned samples. This would be conducted using the same set up but requiring more samples to be investigated to see whether the effects observed were down to the one sample or the bacterium. This would also investigate GFP in the same way to see whether any energy transfer pathways exist between proteins.

- The μCP technique used was seen to be ideal for some samples but not for others, further work could apply the same analysis techniques to different patterning methods. Methods such as PEG tags [9, 10] and nanolithography [11] could be compared

for their applicability to the samples investigated. Furthermore in this work only patterened samples on the μm level have been investigated, other pattening techniques (and even the same stamping techniques) could be used to form nanopatterned substrates separated by differences greater than the optical microscope resolution.

- With the μCP technique the patterns rely heavily on the PDMS stamp, varying the stamps can allow different orientations of sample to be deposited on the surface. Using the microscopy techniques combined with the TCSPC measurements different patterns orientations can be addressed to investigate the effects they have on observing fluorescence and energy transfer present between different areas of the patterned samples. Expanding on the use of linear arrays, further investigations could vary the distances between parallel lines with fluorescence measurements using the laser focused on one line to see whether energy is transferred to the parallel line and thus observation of fluorescence occurring on the line that isn't excited. Varying the distances between the lines could allow an ideal distance for energy transfer to be found outside of the physiological environments. TCSPC measurements may also be incorporated into this analysis with the SNOM which could allow fluorescence lifetimes to be measured at the edges of lines to assess whether excitation energy is transferred between lines. Other patterns may be used such as those shown in Fig. 8.5.1 where the stamps and patterns have been formed from moulds made from AFM calibration grids. These can be used to successfully pattern fluorescent proteins with the potential again to investigate energy transfer from these regions to others.

- Further work could also include more analysis of the chlorosome species. Similar measurements to those conducted in this work could be applied to different species to systematically analyse them to compare species against one another and to observe degrees of heterogeneity in other species. Using the SNOM system the fluorescence lifetimes of these samples can also be addressed in the future work to see if they vary with the size of the structures or with the heterogeneity within the populations.

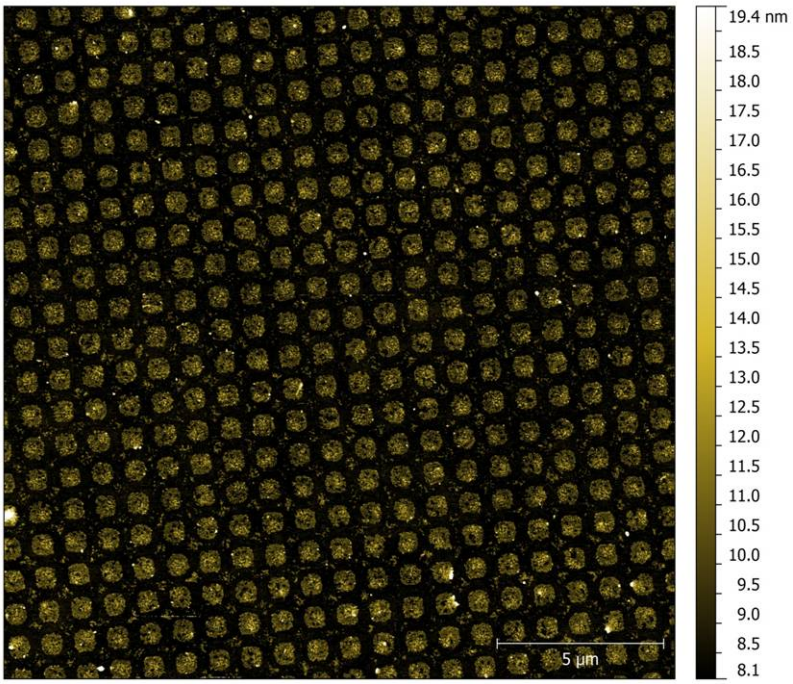

Figure 8.5.1: μCP grid of YFP formed from an AFM calibration grid, acquired with the AFM.

Furthermore with the larger chlorosomes of the species it may be possible to analyse the fluorescence lifetime across the structures opening the possibility of seeing energy transfer in complexes up.

8.6 Bibliography

[1] C. Stoll E. Albrecht T. Quate C Binning, G. Gerber. Atomic Resolution with Atomic Force Microscopy. *Surface Science*, 189/190:1–6, 1987.

[2] E Born, M. Wolf. *Principles of Optic : 7th Edition.* Cambridge University Press, 1999.

[3] D Heinzelmann, H. Pohl. Scanning near-field optical microscopy. *Applied Physics A*, 59:89–101, 1994.

[4] V. Rasmussen, A. Deckert. New dimension in nano-imaging: breaking through the diffraction limit with scanning near-field optical microscopy. *Analytical Bioanalytical Chemistry*, 381(1):165–172, 2005.

[5] J. Michel B. Bosshard H. Delamarche E. Bernard, A. Renault. Microcontact Printing of Proteins. *Advanced Materials*, 12(14):1067–1070, 2000.

[6] H. Stutz R. Delamarche E. Foley, J. Schmid. Microcontact Printing of Proteins Inside Microstructures. *Langmuir*, 21:11296–11303, 2005.

[7] E. Oscarsson S. Quist, A. Pavlovic. Recent advances in microcontact printing. *Analytical and bioanalytical chemistry*, 381:591–600, 2005.

[8] C. Ruiz, S. Chen. Microcontact printing: A tool to pattern. *Soft Matter*, 3:1–11, 2007.

[9] P. Bruinink C. van der Werf K. Olsen J. Timney J. Huskens J. Hunter C.N. Subramaniam V. Otto C. Escalante, M. Maury. Directed assembly of functional light harvesting antenna complexes onto chemically patterned surfaces. *Nanotechnology*, 19:1–6, 2008.

[10] A. Zhao Y. Tas N. Huskens J. Hunter N. Subramaniam V. Otto C Escalante, M. Lenferink. Long-Range Energy Propagation in Nanometer Arrays of Light Harvesting Antenna Complexes. *Nano letters*, 10:1450–1457, 2010.

[11] C. Tiefenauer L. Sorribas, H. Padeste. Photolithographic generation of protein micropatterns for neuron culture aplications. *Biomaterials*, 23:893–900, 2002.